POLITECNICO DI TORINO

Master's degree course in

Ingegneria Energetica e Nucleare

Master's Thesis

Replicability study of the DEMO4 format of the REMOTE project at the Fjellbygda

Relator

prof. Massimo Santarelli

Candidate

Aberto Ferrarese

Co-Relator:

PHD prof. Paolo Marocco

Tronder Energi Tutor:

Bernhard Kvaal

Academic Year 2020/2021

Index

Figures Index

Table Index

Abbreviations

ACC	Accumulation of H2
AUD	Australian Dollar
BAT	Baettery
CAPEX	Capital Expenditure
CNY	Chinese Yuan
EL	Electroliser
EU	European Union
EXT	Externals
FC	Fuel Cell
FPL	Future Partial Load
GPS	Grid Penetration Rate
IEA	International Energy Agency
INR	Indian Rupia
IPCC	International Panel for Climate Change
LCOE	Levelized Cost of Energy
OPEX	Operation and maintenance Expenditure
PPL	Present Partial Load
PEMEL	Polimeric Membrane Electrolyser
PEMFC	Polimeric Membrane Fuel Cell
REP	Replacement
RES	Renewable Energy Sources
TMY	Tipical Meteorological Year
USD	United State Dollar

Abstract

The rapid rise in temperatures due to the greenhouse effect is increasingly stimulating the scientific community to look for new ways of meeting energy needs through the production of energy from renewable sources with zero emissions. The management of the energy produced by these sources, especially the excess energy produced during periods of high resource availability and low demand, represents a challenge that is as urgent and interesting as minimising losses in energy distribution and making energy available even in the most remote places. Solutions to these issues are necessary in order for everyone to be able to meet their needs in societies that demand more and more energy (especially in electrical form) and that realised the necessity of a sustainable use of natural resources. The aim of this thesis is to make a contribution in this sense, acting in collaboration with the Norwegian company Tronderenergi, by defining the possibility of reproducing in a new fictitious remote site in northern Norway, a solution for the production and storage of energy from renewable sources on the model devised by the European, Polito led, REMOTE project, which is being carried out in Rye through its first test in these days. In particular, hydrogen production and the use of lithium batteries are identified as methods for storing excess energy production, and solar photovoltaics and wind power are identified and evaluated as production methods for systems at high latitudes. Simulations were carried out by defining the objective function algorithm on MATLAB software and solving the optimization problem using the Particle Swarm Optimization algorithm already available as built in MATLAB function. Since the study is undertaken in the context of evaluating the convenience of installing the system for off-grid energy production rather than expanding the capacity of an existing hypothetical 1.5MW grid, the minimization of the energy price (LCOE) has been used as objective function to provide the optimal plant sizing. The main purpose of the plant will be therefore to cover the load hypothetically required by users during every hour of the year. The achievement of this aim has been explored through the adoption of various formats that include in some cases also the intervention of the aforementioned network (considering it both as a source and as a possible purchaser of the excess energy produced) up to considering the case of complete independence from the grid (format originally envisaged by the REMOTE project). The study was carried out by considering different reference years for the calculation of the potential energy extractable from renewables and by considering 2 different load scenarios. These differed in the amount of maximum demand required by referring to a current load demand and one assessed as an increase in energy demand. In order to demonstrate the impact at the level of greenhouse gases emissions, the results showed the quantity of emissions avoided thanks to the adoption of this system and the energy produced by it rather than the use of energy available on the grid produced by the national energy mix. In particular, the results for the country of analysis (Norway, with a national mix that is already almost entirely renewable) and that of an average EU country were differentiated. The results also include the values of waste heat energy from the use of the fuel cell available for hypothetical uses not explored in this thesis.

1. GENERAL CONTEXT AND PURPOSE OF THE PROJECT

1.1. EUROPE INTEREST IN HYDROGEN

Interest in hydrogen in Europe is growing every year and this small but powerful molecule is being referred to as one of the keys to achieve the energetic, economic and sustainable transition required in our time.

The main demonstration of these expectations on hydrogen, which has already demonstrated its flexibility of use in many areas, and a sign of the increasingly rapid maturation of the technologies and solutions associated with it, is the fact that the year 2020 was a decisive year in determining the fate of hydrogen in Europe. Indeed, in July 2020, the European Commission presented to the European Parliament, the European Council and the European Committees of Regions and Economic and Social Affairs the document "*A hydrogen strategy for a climate-neutral Europe*" [1], more commonly called "*Hydrogen Strategy*". In November of the same year, the "*European Clean Hydrogen Alliance*" as launched, bringing together a wide range of economic, industrial, political and social players to implement the hydrogen strategy in its various phases, particularly in the industrial sector.

These milestones represent the EU's awareness of the centrality of hydrogen and its stance in making Europe a leader in the production, management and application of this element, which can be defined as a resource, an energy vector and a raw material for a more sustainable and cleaner society. Thus, this movement in the field of hydrogen precedes and is a fundamental element in the objective expressed by the first European law on climate presented by the Commission in March 2020 and approved by the European Council a year later than the presentation of the Hydrogen Strategy (June 2021).

The Hydrogen Strategy envisages three main steps for the development of the hydrogen sector in Europe, defined in three clearly defined time periods:

I. *The Kick-start phase (2021-2025)*

This is where the foundations of the European hydrogen economy and legislation are laid. At the end of the kick-start phase, 1 million tonnes of clean hydrogen will be produced per year and at least 6 GW of electrolyser capacity will have been installed. To reach these targets, projects that demonstrate the scalability of hydrogen and sufficiently mature projects will be considered, such as European Clean Hydrogen Alliance projects, pre-registered IPCEIs, Hydrogen Valleys, blending, first pipelines and pilot storage projects. In addition, research, development, demonstration and projects that support commercialisation, scale-up and increased European competitiveness will be prioritised. Finally, projects in line with National Energy and Climate Plans (NECPS) and submitted under the Recovery and Resilience Facility (RRF) will contribute to a significant increase in hydrogen production and demand.

To facilitate this, states aid rules will be relaxed, allowing up to 100% support from the European Commission and Member States. Here, EU legislation will need to be adapted to recognise and facilitate the important role of hydrogen, while removing barriers and obstacles to its uptake.

II. *The Ramp-up phase (2025 – 2035)*

The ramp-up phase will aim to achieve commercial competitiveness of hydrogen. Large-scale storage, hydrogen backbones and so-called Hydrogen Valleys will be implemented, supported by appropriate measures to stimulate supply and demand.

Regulatory support for hydrogen technologies will be implemented, especially from an economic point of view, such as tariffs, auctions/quotas, investment support and tax relief, to be supported by Guarantees of Origin (GO).

III. *The market growth phase (2035 – 2050)*

In this phase, hydrogen will continue to replace fossil fuels, aiming at the conversion of most natural gas pipelines and further integrating the European hydrogen system. Efforts will be made to achieve a transparent and liquid hydrogen market, and pricing will be largely governed by supply and demand mechanisms.

Like grid integration, the market will require regulation, replacing the regulation defined in the previous two steps, which will have become obsolete in the meantime.

Therefore, the study presented below fits perfectly into step 1 by exploring the scalability of an already successful hybrid P2P solution to meet local needs, with hydrogen storage as its strong point.

1.2. THE STUDY

The study at the heart of this thesis comes from the Norwegian company Tronder Energi's need to evaluate the economic viability of reproducing a format for on-site energy production through a hybrid system that uses fully renewable sources to meet the growing energy needs associated with a hypothetical Norwegian site rather than meeting this increased demand through the expansion of an existing energy distribution grid.In fact, recent studies and successes in the field of the design and construction of standalone hybrid systems for small human settlements that are difficult to reach by traditional infrastructures (or reachable at high cost) have led to the consideration of the possibility of satisfying the new loads by integrating the grid with a system that fully exploits the available renewable sources and stores the possible peaks of direct electricity production in the form of hydrogen and power in lithium batteries.

This study was naturally inspired by the existing plant installed at the Rye test site, also in Norway, designed and built by a group of partner companies coordinated and directed by the Politecnico di Torino and Tronder Energi. The plant in question, called DEMO4, is one of the four plants whose installation has been planned and designed as part of the wider European REMOTE project, winner of the *EUSEW award* at the Sustainable Energy Week in 2020.

The study is therefore an important point for the company to evaluate the commercial potential and elasticity of the solutions identified in the REMOTE project so that it can be proposed as the best possible solution for sites with different needs. The simulations of the operation of the system will in fact be carried out on the basis of a fictitious site that is as likely as possible to represent a small industrial village in the north of Norway whose energy needs have increased in recent years to the point where it is necessary to supplement the availability of energy currently guaranteed by the local grid (max capacity of the grid 1.5 MW).

The fact that a grid is already in place makes this project different from previous studies of the REMOTE format, which identified the need to make an isolated site energy independent in order to solve the difficulties users had in meeting their energy needs, which were met by expensive and polluting solutions. The prerogative of these sites was therefore the absence of a connection to a medium-high electricity distribution network, which in this case is instead supposed to be available in the area, although with a finite capacity.

The solution proposed here, as an evolution of DEMO4 (which aimed to avoid expanding the grid by connecting submarine cables to meet the loads on Froan Island), seeks to exploit the advantage of such a grid in order to amortise the costs of setting up the system, feed green energy into the national circuit by selling it, and study the possibility of revenue in the medium to long term.

Projects such as this represent not only a challenge from an engineering and economic point of view, but also and above all contribute to creating a local community that is more aware of the ways in which energy can be produced and used in a circular manner, since it is hoped that all possibilities for exploiting the energy produced directly and indirectly in its forms will be considered. We are of course referring to the electrical energy produced directly by the plant but also to the thermal energy present as waste energy produced by the operation of the fuel cell and the energy stored in chemical form thanks to the storage components and the compounds derived from them. The DEMO 4 set-up from which we take our inspiration also provides the readiness for modification to exploit the chemical energy as such, present in the form of the hydrogen produced, which lends itself as a raw material for a wide range of uses.

The study presented below consists of several main phases:

1) Identification of the characteristics of the site
2) Collection of meteorological data concerning the site
3) Collection of the technical characteristics of the technologies used
4) Updating of economic data concerning the technologies used
5) Identification of the main economic parameters for buying and selling energy from and to the grid
6) Collection of climate-changing gas emission data for energy produced according to national energy mixes
7) Identification of the different plant operating modes
8) Simulation of different scenarios
9) Conclusion and evaluation of the feasibility and advantages/disadvantages of the project itself.

The Site

The site referred to in the study is a fictitious site that mimics the characteristics of a typical remote site in northern Norway. The very name of the site with the Norwegian word “Fjellbygda” meaning ‘mountain village’ is intended to emphasise its nature as a small, very isolated community.

Since the site is in any case on Norwegian territory, the intention was to make the most of the natural resources available in that particular area, trying to avoid as much as possible relying on sources that are considered renewable but which are nonetheless sources of climate-changing gases (e.g. biomass, which is widely available in Norway). This makes the results of our study even more flexible and generalisable, since we are not tied to resources that are too characteristic of the area but rather common in sites in the same latitude range. For this reason, DEMO4 of the REMOTE project was used as a model, which takes solar and photovoltaic sources into account.

An important role in defining the producibility of technologies (especially photovoltaic technologies) is also played by the temperature of the surrounding environment. Since the efficiency of a photovoltaic panel also depends directly on the temperature of the cell during operation, relatively low temperatures in the latitudes concerned will be an advantage for the system and will not limit its efficiency.

However, the solution does have some limitations since it is assumed that fixed panels will be installed that do not follow the optimum direction to achieve the maximum possible output hour by hour during the day. In addition, other limitations related to photovoltaics derive from the fact that the latitudes at which the system is supposed to be built do not guarantee uniform or almost uniform solar periods during the course of the year, but rather host a very high variation in the amount of solar hours present on different days of the year. This will greatly limit the possibility of relying on photovoltaic technology during the period of lack of daylight hours (winter periods) in which the few hours of daylight available will certainly not be able to meet demand (unless fields of solar panels with a nominal capacity disproportionately large in relation to the load to be met are installed).

One can therefore already imagine how solar power cannot be used on its own in sites with such characteristics and how it is only a support technology for the main one, wind turbines.

Precisely in relation to these major limitations in the use of the most common technologies for the exploitation of renewable energy, this study is particularly important for the evaluation of the key role played by storage technologies, i.e. the lithium battery and hydrogen production, which are also present in this case as in the set-up envisaged by DEMO4 for Froan. In particular, certain advantages resulting from the environment guarantee easier management of storage, especially as regards hydrogen production. The low temperatures of the site ensure that storage is relatively easy, even at relatively low pressure, without the need for large gas refrigeration plants, and provide a safety advantage in that it is very difficult to create situations conducive to ignition.

Linked to the use of conversion technologies upstream and downstream of hydrogen production and the nature of the site, a particular advantage can be identified that at sites with warmer temperatures would have less power in place. Reference is made, in fact, to the availability of waste heat energy that is produced during the operation of the FC.

System layout

The system considered is entirely analogous to the DEMO4 format with the only addition of the possibility of connection to the grid. This introduces an extra degree of freedom into the system which, as we shall see, opens up different scenarios for energy management whether there is a surplus of energy produced or a production deficit to be covered.

Analysing it from a functional point of view, we can define the system as consisting of 5 macro-groups of technologies:

1) Production Group (RES): whose purpose is to produce the energy for covering the load and exploiting the available natural energy resources. It includes the following technologies
   - Photovoltaic Plant
   - Wind Power Plant

2) Storage group (STORAGES): whose purpose is to store the excess energy produced during the hours when there is a high availability of renewable resources and low demand from the load and vice versa to cover the load during the hours when the availability of renewable resources is not able to directly satisfy the load. They include:
   - Hydrogen accumulator (ACC)
   - Lithium-ion battery (LV)

3) Support group (EXTERNALS): the purpose of which is to compensate in the event of deficits, exactly as in the case of the storages group. Actually, this groupe (whose only component is the electric grid) could be assimilated as a storage with maximum availability equal to the capacity of the grid and always available. However, it is treated differently from the other storage components in that it is not a component of the DEMO4 system to be tested, but constitutes an active economic actor because the energy exchange with it is always directly linked to a corresponding flow of money.

4) Load group (LOAD): whose purpose is the passive one of energy acceptor and acts as the main determinant for the dimensionality of the system

5) Conversion and transport group: whose purpose is to ensure the conversion of direct current into alternating current and alternating current into direct current, to take account of energy conversion efficiencies and to ensure the transfer of energy within the system by connecting all the various components. They include:
   - AC/DC converters
   - Conversion modules (CONV)
   - PEMFC fuel cell stacks (FC)
   - Electrolytic cell stacks (Electrolyzer) PEMEL type (EL)
   - AC BUS

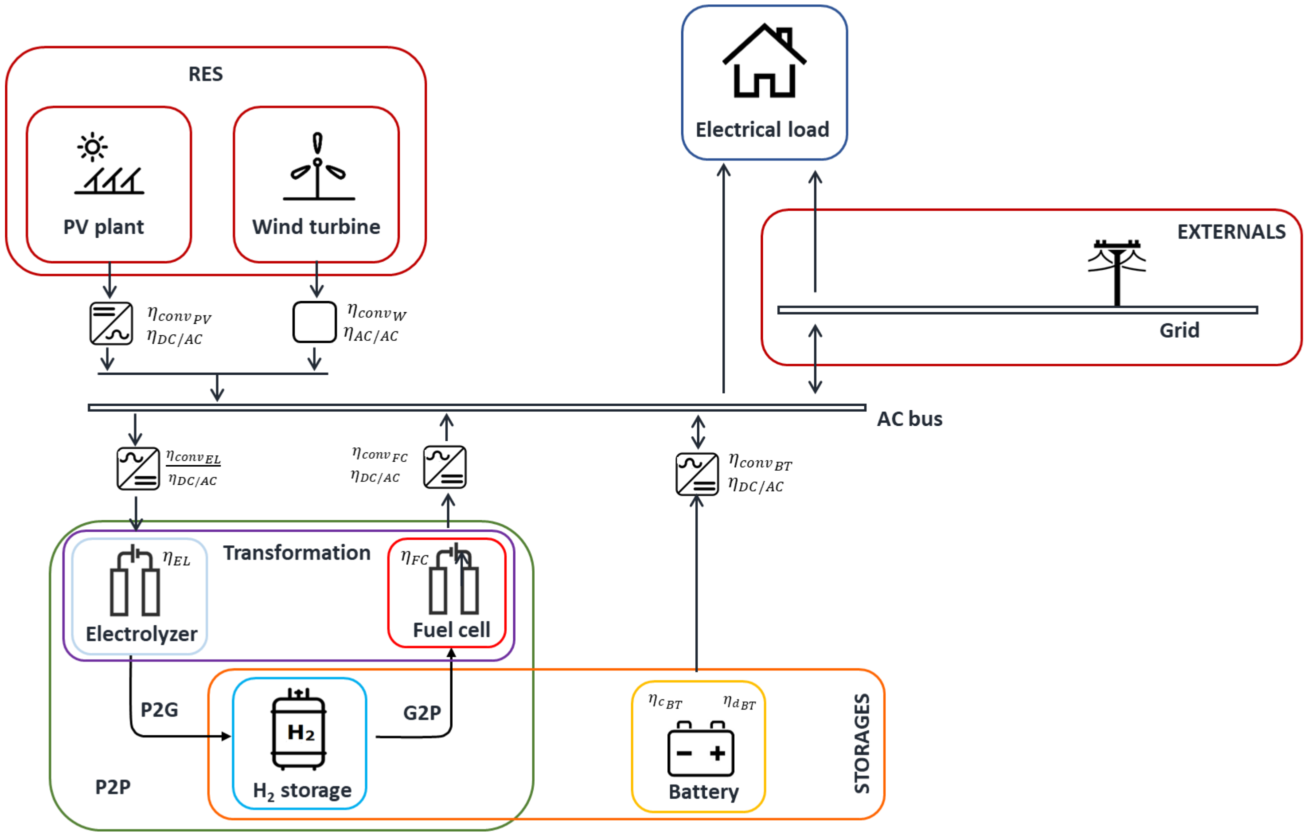

Figure 1 Schema dei componenti che costituiscono il sistema integrato di studio, modifica dell'originale soluzione ipotizzata dall'applicazioen di DEMO4

2. COLLECTION OF INPUT DATA

The data sources used for the study are different depending on the type of data and can be divided into:

- Sources for data related to the load to be satisfied and to the capacity of the energy infrastructure already in place (distribution grid)
- Sources for data on the technical characteristics of energy production technologies (photovoltaic panels and wind turbines)
- Sources for data on the calculation of the energy producibility of the plant
- Sources for data on the economic character of the energy and technologies involved
- Sources for data on the environmental impact assessment expressed as tonnes of CO2 not emitted into the atmosphere compared to the case fully served with grid energy produced with the national energy mix

The data set of the energy requirements to be met was provided directly by *Tronder Energi* in order to reproduce a plausible simulation of the loads required by a site with the above-mentioned characteristics at the present time. These data sets were then used in the study process to simulate a short to medium term projection of the required loads. This was possible thanks to indications obtained from direct comparison with the company. Similarly, estimates of the capacity of the network assumed to be already present on the site were provided directly. However, it should be specified that, as this infrastructure is an element that has been taken into account for the exploration of the benefits of its integration in the management of the load and energy produced by the system being already present, but of which there is no interest in considering it as an option for the solution of the supply problems, no modifications or estimates have been made that would lead to its variation over the time domains concerned. Indeed, one of the main purposes of the project, as already stated several times, is to estimate the convenience of using a hybrid system rather than expanding the network.

On the other hand, the sources that have enabled us to go on to determine the technological characteristics of the energy production systems, i.e. photovoltaic panels and wind turbines, are the data sheets of the technologies already used in the design of DEMO4. However, given the preliminary nature of the study, the choice was not based on optimising the performance of the technologies, but on the choices made previously for DEMO4. Should the simulations prove to be advantageous, it would therefore be appropriate to identify whether better technologies than these are available on the market. These considerations should be kept separate from the economic assessment of the CAPEX and OPEX costs associated with the technologies, which are treated and defined differently as explained below.

Regarding the third type of sources, a first attempt to consider sources that collect data from direct measurements on the ground via data collection stations was considered. However, the Norwegian databases consulted did not guarantee complete hourly coverage throughout the year. In addition, not all the data needed for the assessment of the parameters of interest for the study was present. For this reason, we relied on the data sets provided by the open-source gis database made available by the European Union called PVGIS.

In order to give greater robustness to the results obtained, several reference time domains were considered, based on data sets of real years, and on data sets representing an average meteorological year representative of the last 10 years.

Unfortunately, a very important and fundamental consideration must be made here: global warming is bringing about serious and rapid changes in the climatic and therefore meteorological behaviour of different areas of the planet. In recent years, this phenomenon has become increasingly significant, and its rapid evolution could be a source of uncertainty as to the conclusions reached by this study. This uncertainty, however, is not necessarily to be understood in a negative way with regard to the particular site in object, since the repercussions on the atmospheric component that represents the main source of renewable energy for our system – the wind – cannot be foreseen a priori. While it is true that the greater energy accumulated overall in the stratosphere (and in particular in the troposphere) generates more massive and violent effects in the transfer of air masses, it is not certain that the new currents that can be identified in the seasonal behaviour will bring greater availability of wind energy to the specific site, just as it is not certain that they will limit it.

It is therefore advisable that the results of the following study are periodically updated in order to ensure their robustness or alternatively to allow the identification of a favourable rather than unfavourable trend.

As far as the sources for the economic parameters are concerned, we can still make a distinction with regard to the nature of the data of interest. We will therefore have:

- Resources for the determination of an update of technology costs with respect to those considered for the DEMO4 project currently operating for testing in Rye
- Resources for determining the price of energy in order to determine the economic flows of buying and selling with the network.

In the first case, a bibliographic research was carried out (the details of which will be reported in the dedicated paragraph) separately for each type of technology involved.

In the second case, on Tronderenergi's instructions, the open source databases made available by the company NordPool were used.

To be taken into account is the fact that, especially with regard to the energy price data, reference was made to the year 2017, which was indicated by Tronder Energi as representative for the behaviour of hourly energy prices for the last 10 years. It is therefore emphasised that the differentiation in the solutions attributable to different time domains is due solely to the differentiation in the input data relating to the renewable energy resources available in the different years considered.

Finally, reference is made to the data source used to assess the average emissibility attributable to 1KW generated through the national energy mixes for Norway and a fictitious country assumed to be representative of an average EU country. These coefficients have been taken from the opensource databases of the IEA (International Energy Agency) with reference to recent pre-pandemic years.

Here we would like to emphasise the care taken by the operator to avoid considering the last 2 years as reference years or contributing to the creation of reference time domains. The contingent emergency situation linked to the outbreak of the Sars pandemic Covid2 represents a highly anomalous event that would lead to a very significant disruption of the results and would make the study unrepresentative of the normal conditions under which the system would operate. This is related not so much to the unreliability of the meteorological data, which are totally independent of the health conditions of anthropogenic societies, but rather to the energy market prices and the coefficients representing the average emission levels attributable to the average KW generated by the national energy mix. These parameters are in fact intrinsically linked to market trends, to variations in supply and demand, to geopolitical balances and thus to events that determine the behaviour of anthropogenic societies, such as a pandemic on a global scale.

Let us therefore analyse the input data sets considered for this study.

2.1. LOAD

The load datasets as mentioned above were provided directly by Tronder Energi and refer to the energy requirements recorded at sites they observed that fall within the latitudes indicated and for which it is not possible to provide more details due to confidentiality issues. The model year referred to is the latest available before the pandemic, i.e. 2019.

The load data provided included several items which could be grouped under 2 main macro headings:

- Loads at the end of the network referred to as Partial Principal Loads: this consists of the grouping of load items located at the end of the network beyond which the region is no longer supplied by the local distribution network.

- Loads along the grid denominated as "Partial Secondary Loads": consists in the grouping of the point loads distributed along the last stretch of the grid connecting the last node to the end where the Partial Principal Loads are present.

After a brief dimensional analysis, in agreement with Tronder Energi, it was decided to neglect the Partial Secondary Loads in order to concentrate on the analysis and satisfaction of the Partial Principal Loads which we will refer to from here on by treating them with the simple name of Partial Loads or Load.

For the purposes of this study, it was not necessary to treat the various items relating to Partial Loads individually, since the main purpose is to evaluate an estimate of the LCOE that takes into account the total energy production that simply depends on the total demand shown.

The graph in Figure 2 shows the load profile referred to in the study and its subdivision into the various load items.

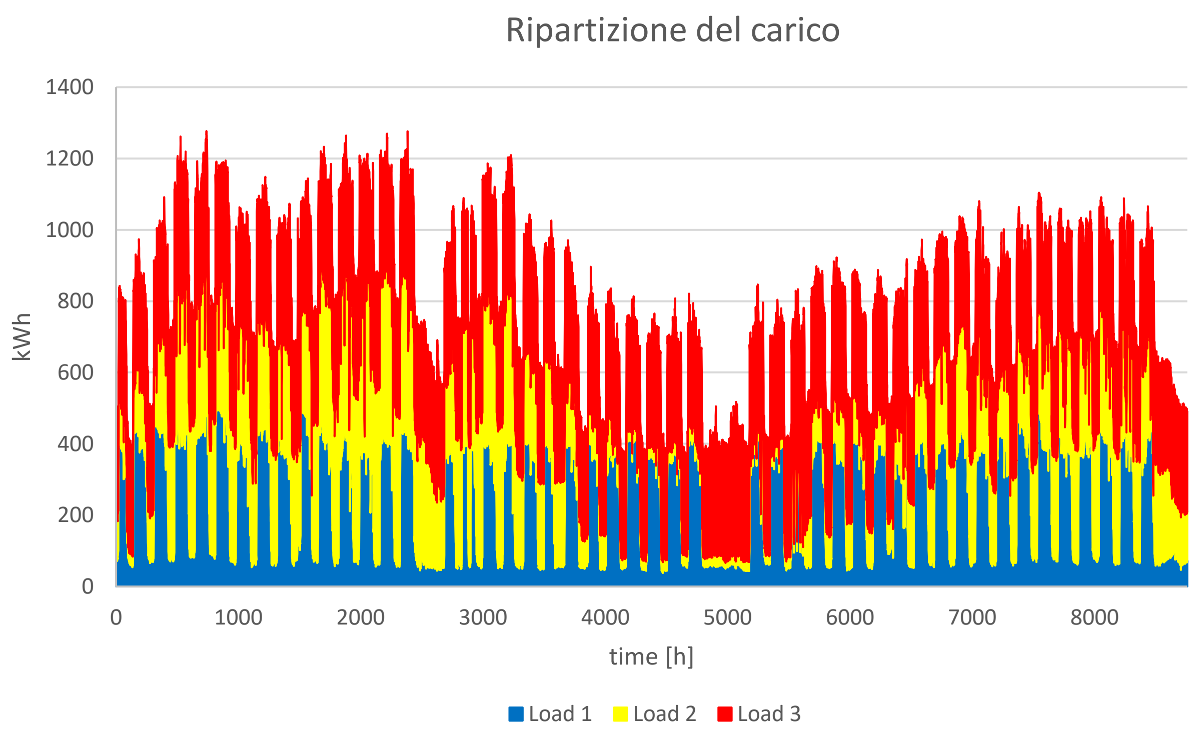

Figure 2 Trend of the total hourly load currently present (referring to the year 2019) divided into its three sub-loads. Source: Tronder Energi

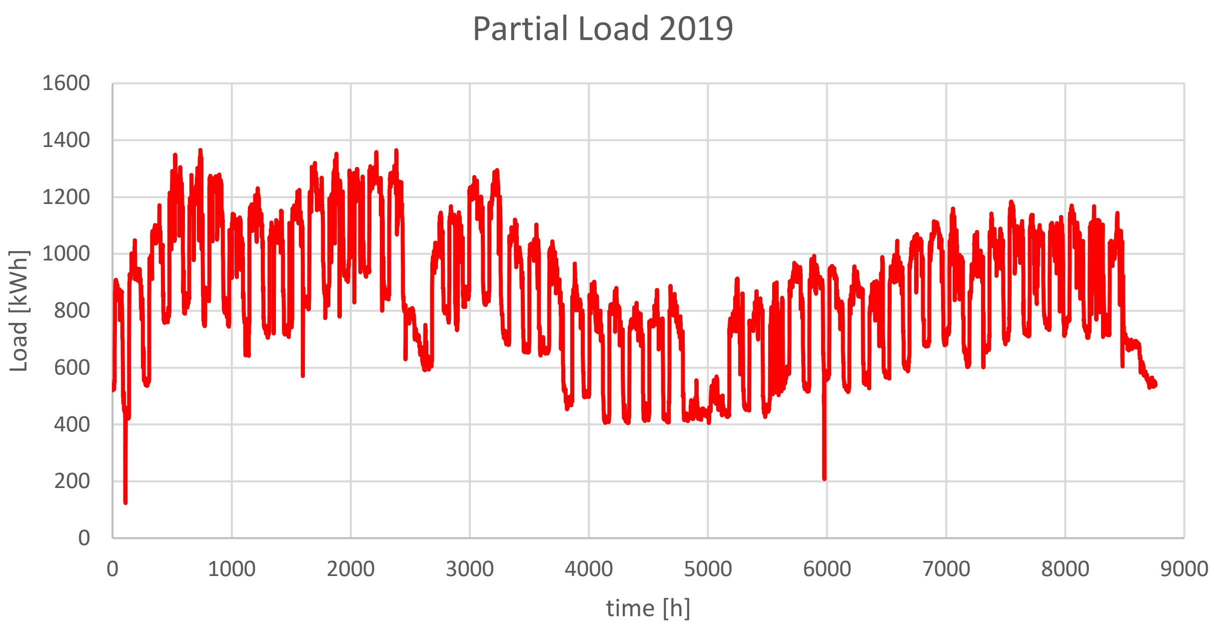

Figure 3 Hourly trend of the currently existing total load (referring to the year 2019). Source: Tronder Energi

The load data thus defined represent both an input data set directly used in the objective function for the calculation of the LCOE and the basis for the determination of a second load data set modelling a future load scenario. The method of determining this new set is defined in detail in the methods section but in general it can be considered as a linear projection of the current load due to a coefficient determined by the proportion between the maximum load currently required and the estimated maximum load required in the future. This estimate has been kindly provided by Tronder Eenergi and refers to a future projection of 2/5 years. The trend is shown below.

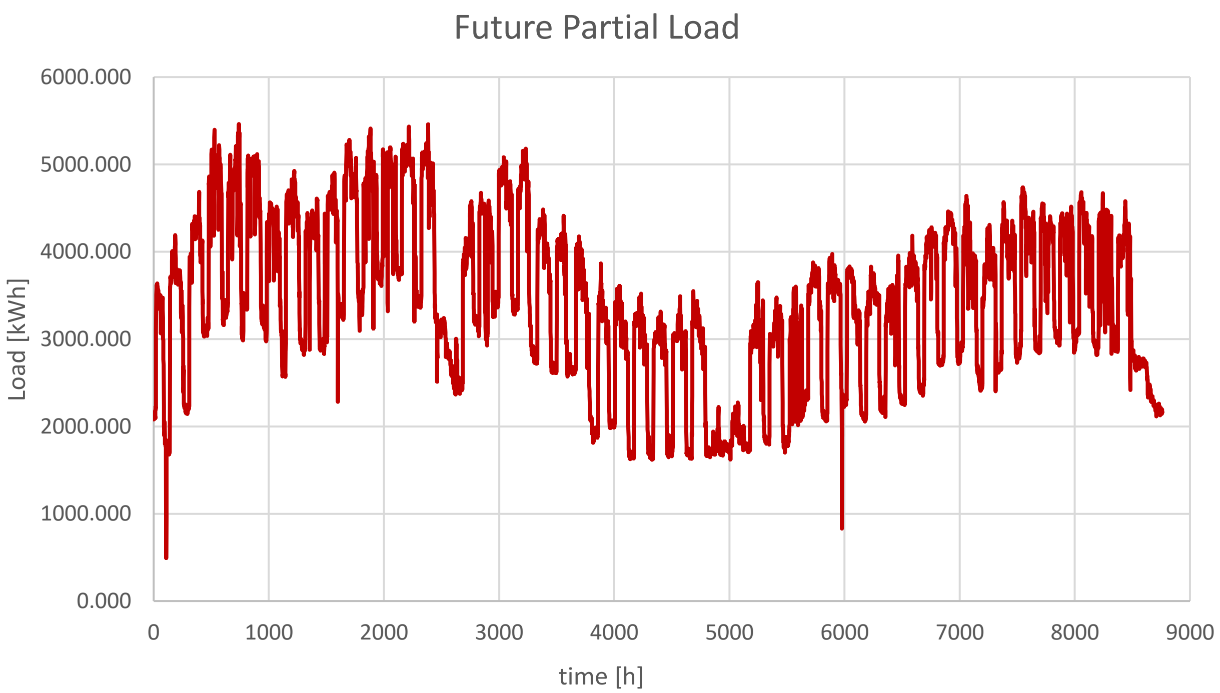

Figure 4 Hourly trend of the total load to be met that is assumed to exist in the future.

It follows that we will refer to the two types of load by calling them differently and in particular we will have:

- Present Partial Load (PPL)
- Future Partial Load (FPL)

2.2. PHYSICAL CHARACTERISTICS OF THE SITE

The site of interest where the system is supposed to be installed must be identified geographically in order to use the longitude and latitude data to determine the producibility of the solar panels and to identify the wind speed data series (as described in more detail in the following paragraphs) and to determine the conformation of the land in order to be able to attribute the most plausible roughness and albedo coefficients possible.

This information was obtained in part through a qualitative survey carried out remotely by analysing satellite images, in part it was provided directly by Tronder Energi as the client of the study, and in part it was obtained from the outputs provided by the open source database PVGIS (to which reference will be made in more detail in the following paragraphs) which also makes available, for example, the altitude of the site.

Figure 5 Panoramic photo of the hypothetical solution application site. Resource: Google Earth

Reference is made to a height of 310m above sea level for the altitude of the site. On the other hand, as can be appreciated from the Figure 4 obtained through a search on Google Heart, Reference is made to a height of 310m above sea level for the altitude of the site. On the other hand, as can be appreciated from the **Errore. L'origine riferimento non è stata trovata.**obtained through a search on Google Heart, it is possible to attribute to the land surrounding the urban area where the system would probably be installed the properties associated with a surface:

- homogeneous
- smooth
- not very reflective
- not inclined

In fact, it is possible to identify the presence of a superficial portion covered by lake water and of a rather deep strip of deforested land that does not pose particular obstacles to wind currents in any direction. This morphology therefore allows us to choose the roughness coefficient τ (necessary for processing the wind data) from those indicated in the following Table 1.

Table 1 Soil roughness classes [2]

Roughness class	Roughness index [τ]	Type of terrain
0	0.0002	Water surface, open sea without waves
0.5	0.0024	Completely open flat land with a smooth surface (mowed lawns, landing strips, ...)
1	0.03	Open cultivable areas without constructions or with few low obstacles
1.5	0.055	Cultivable areas with few medium-sized buildings
2	0.1	Cultivable areas with few medium-sized buildings and hedges
2.5	0.2	Arable land with medium-sized buildings and tree vegetation
3	0.4	Villages and forests
3.5	0.8	Large cities with high buildings
4	1.6	Large cities and metropolises with skyscrapers

In addition, the type of land used for the construction of solar fields has to be classified so that the best albedo coefficient can be chosen for processing the data sets of the radiation incident on the panels. In Table 2 the reference albedo coefficients indicated in the regulations UNI 8477 are given

Table 2 Albedo coefficients in relation to soil type. Source: UNI 8477

Surface	Albedo Coefficient [ρ]
Fresh or frozen snow	0,75
Watery surfaces	0,07
Soil (clay, marl)	0,14
Dirt roads	0,04
Coniferous forest in winter	0,07
Asphalt	0,10
Woodland in autumn	0,26
Concrete	0,22
Dead leaves	0,30
Green grass	0,26
Bitumen roofs and terraces	0,13
Dark surfaces of buildings	0,27
Crushed stone	0,20
Light surfaces of buildings	0,60

In this case, the coastal strip is free and covered in green grass during the summer period (i.e. the one in which the presence of radiation is mainly concentrated). However, one has to take into account both the interaction between the dark surfaces of the panels and those of the surrounding environment, partially formed by coniferous forest and partially by watery surface, which although far away can slightly affect the final albedo value. For this reason, a precautionary condition was chosen, reducing the coefficient for green grass to 0.2, which corresponds to that associated with bare earth.

A more accurate assessment of the albedo coefficient should have taken into account the fact that for a long part of the year the soil is covered by a considerable layer of snow and ice. However, since this period also corresponds to the period of lowest irradiation, it was considered reasonable to keep the coefficient constant throughout the year.

In the following Table 3 the coefficients chosen among those listed above to process the meteorological data that depend directly on the topography of the area and the characteristics are therefore given.

Table 3 Summary of coefficients related to soil characteristics

AMBIENTAL COEFFICIENTS		
Soil roughness coefficient (for Flat surf)	τ	0.14
Albedo coefficient (for Bare soil)	ρ	0.2

2.3. ENERGY SOURCES

This section presents the meteorological data series for the subsequent determination of the energy produced by the exploitation of renewable sources.

SOLAR

The data that allow us to evaluate the nominal producibility of the photovoltaic system we are going to install comes from the European open source GIS database of meteorological data PVGIS. This database can be easily accessed using the commands in the various sections of the tools available on the website. Below are the screenshots of the tool to which reference is made for the supply of the data series of interest for this study.

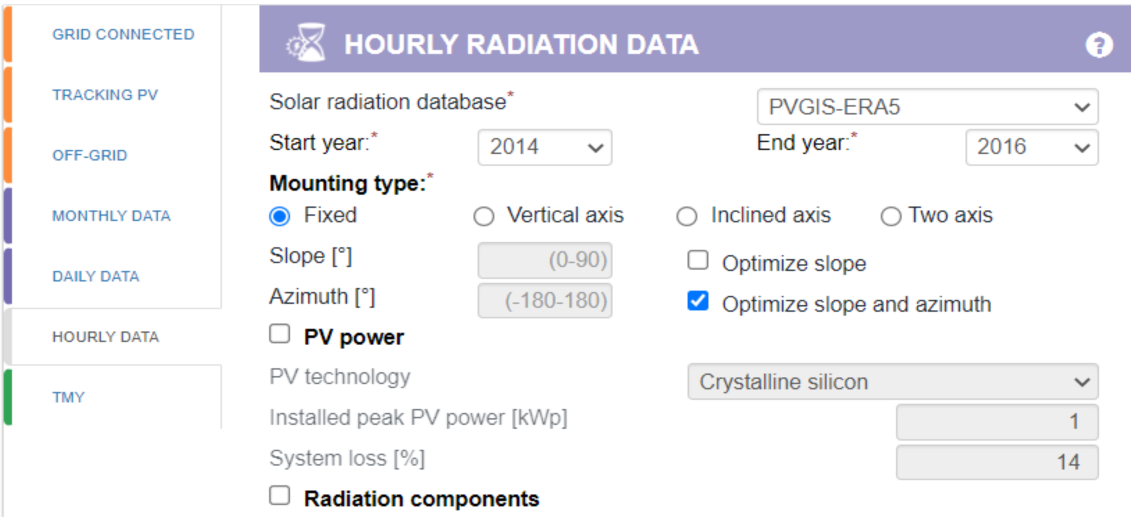

Figure 6 Screenshot of PVGIS tool for collecting hourly irradiance data

The extraction of the series of interest passes through the identification on the tool of the coordinates relative to the place of interest (the value of which cannot be provided for confidentiality reasons) which can be carried out by entering them manually in the appropriate boxes or through the use of the graphic interface (an example of which is shown below in Figure 7) from which general information on the intensity of radiation can already be obtained a priori thanks to the chromatic gradation applied to the map, ranging from blue for areas with lower incidence and red for areas with higher incidence.

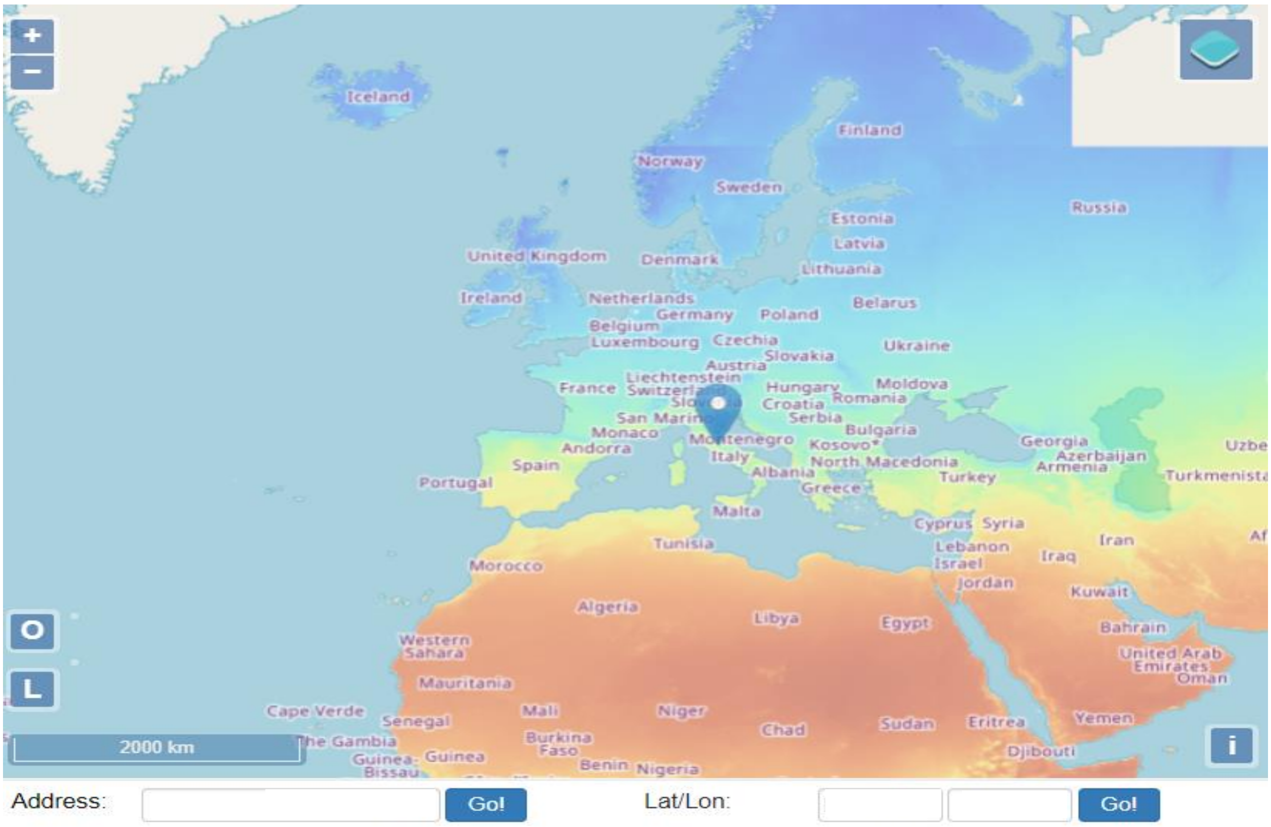

Figure 7 Screenshot of the PVGIS tool that allows you to manually identify the coordinates of the site

The data series required to determine the nominal producibility of our solar panels are of two types, which differ mainly in terms of both the reference time base and the type of data provided by the database:

1) Typical Meteorological Year (TMY) series: i.e. data series relating to a meteorological year considered to be characteristic, already identified by the database and composed of data from the most reliable months belonging to some annual series stored in the database. The time span from which the data were taken to make up the series we use is the most recent available on the GIS and ranges from 2007 to 2016. To obtain it, it was sufficient to go to the TMY section of the tool and select the desired period from those available in the drop-down menu and download the excel file containing the series. The screenshot of the tool referred to for this series is as follows.

   In particular, the Table 4 shows in more detail the composition of the TMY giving an indication of the actual year referred to for each month of the typical meteorological year.

   This year is taken into consideration as a reference year to generate the most probable response of the analysed system. As we will then see in the results section, the weather series related to it will ultimately provide the most cautious case among those investigated.

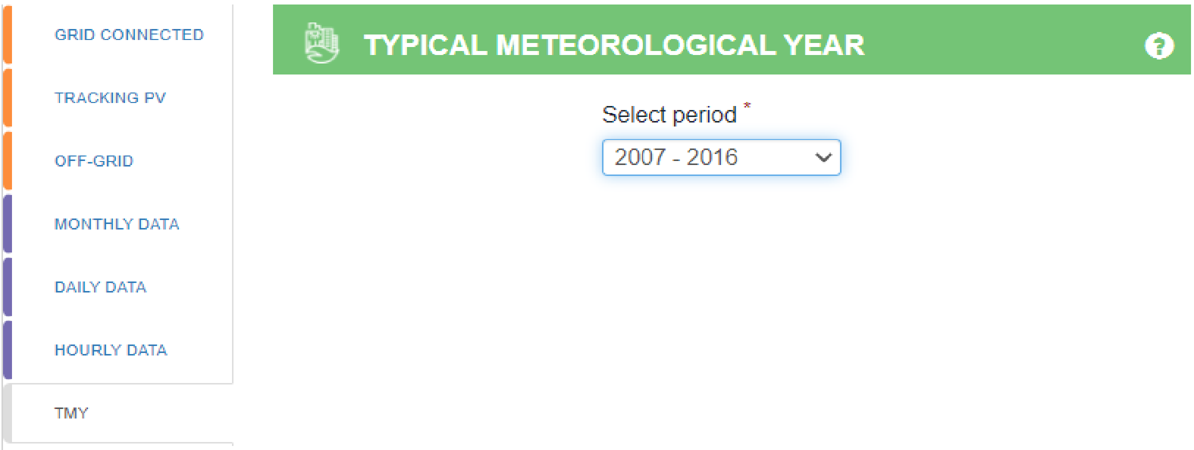

Figure 8 Schermata del tool per l'approvvigionamento dei dati meteorologici riferiti al "Typical Meteorological Year" (TMY)

Table 4 Composition of the TMY time domain

DATA ORIGIN	
Month	***Year***
January	2007
February	2009
March	2007
April	2009
May	2009
June	2016*
July	2009
August	2014
September	2007
October	2016*
November	2014
December	2011

**leap year*

The types of data relating to solar energy declined in its components provided by the TMY tool are those reported in Table 5

Table 5 List of variables provided by the PVGIS database for the reference year TMY

SOLAR ENERGY VARIABLES FOR TMY DATA SERIE			
T_{2m}	2-m air temperature	$°C$	
G_{th}	Global horizontal= Global irradiance on the horizontal plane	W/m^2	
G_{bn}	Direct normal= Beam/direct irradiance on a plane always normal to sun rays	W/m^2	
G_{dh}	Diffused horizontal= Diffused irradiance on the horizontal plane	W/m^2	
IR_h	Infrared horizontal	W/m^2	NU[1]

[1] Not Used

and whose annual trends are shown in the graphs Figure 9, Figure 10, Figure 11. In the last cell of Table 5 data sets that were not used for the purposes of this analysis were identified.

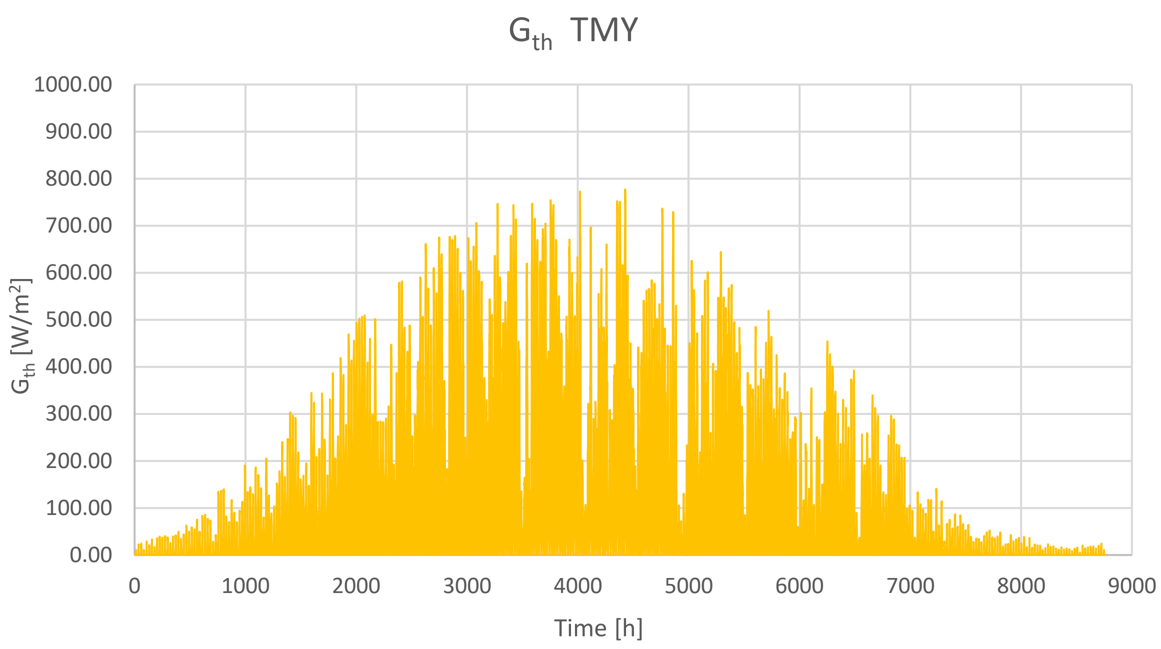

Figure 9 Hourly series of the total solar radiation component assessed on a horizontal plane (G_{th}) with temporal reference to TMY. Resource: PVGIS https://ec.europa.eu/jrc/en

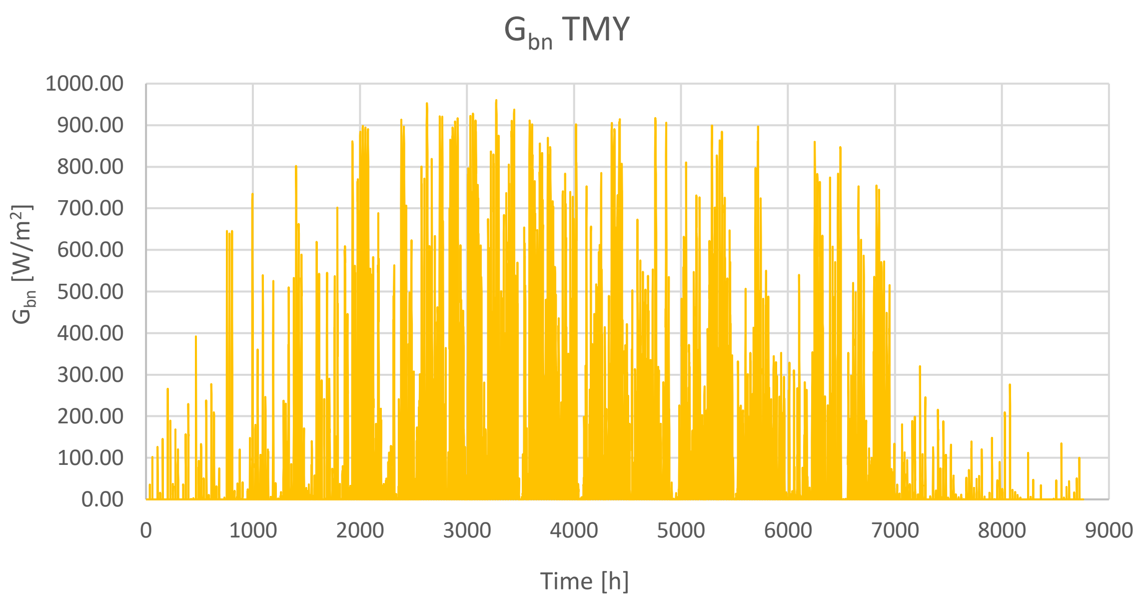

Figure 10 Hourly series of the normal incidence component of the solar radiation (G_{bn}) with temporal reference to TMY. Resource: PVGIS https://ec.europa.eu/jrc/en

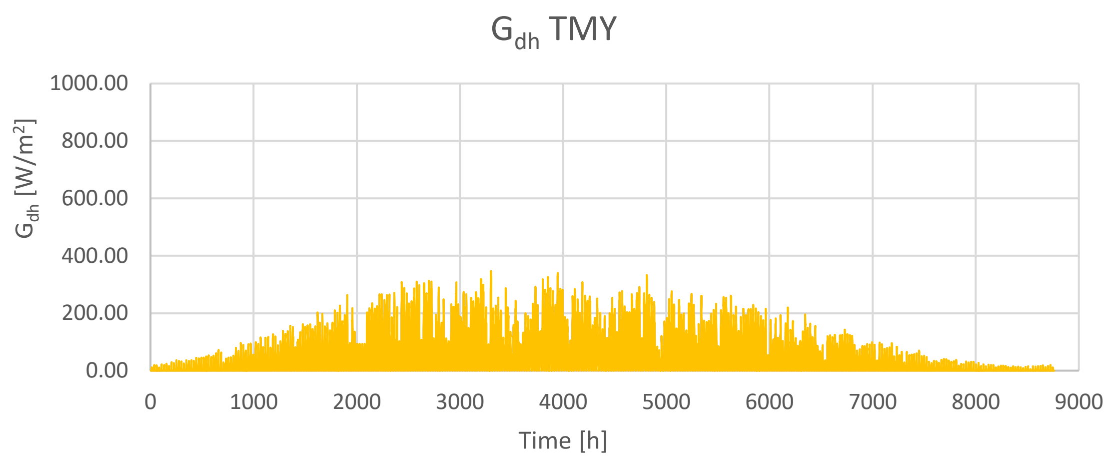

Figure 11 Hourly series of the diffuse component of the solar radiation detected on the horizontal plane (G_{dh}) with temporal reference to TMY. Resource: PVGIS https://ec.europa.eu/jrc/en

Given the high latitudes of the site, the seasonal pattern of the various components of incident radiation is evident. These are larger in the summer period, when there are many hours of daylight, and almost zero in the winter period. It is also clear that the prevailing component is the direct radiation incident normal to the panel plane.

As explained later in the section "3. METHODS" In order to calculate the producibility of the panels, it is essential to have the hourly average T recorded a few metres above ground. In this case the T is that determined at 2m and its annual trend is shown in the following graph

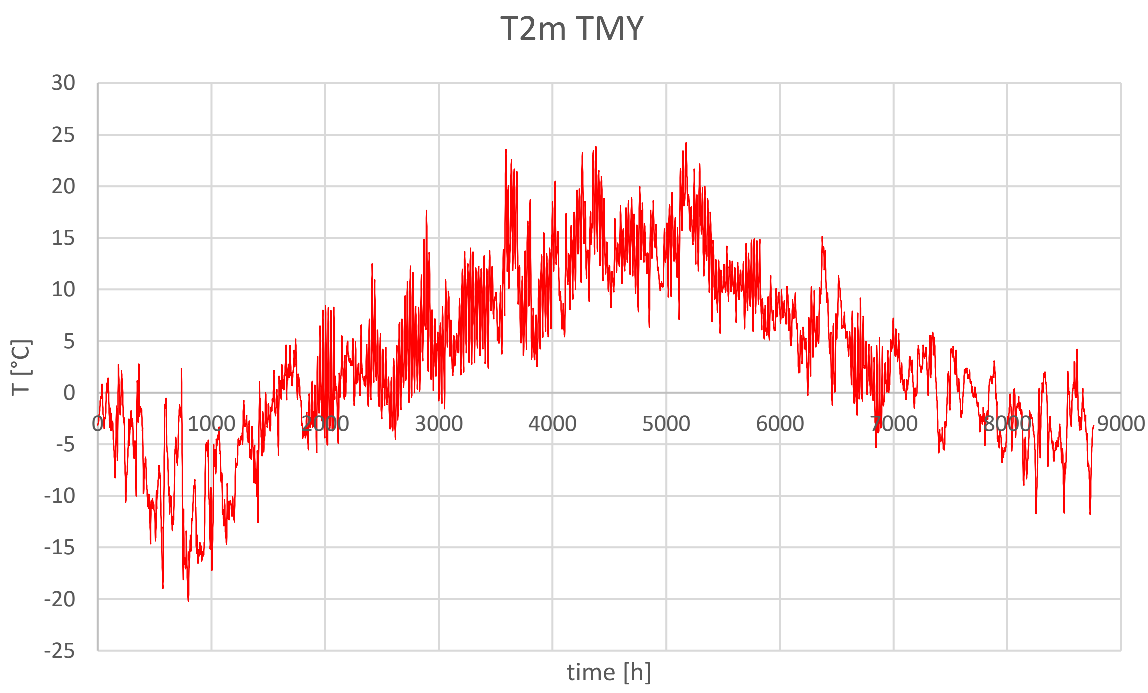

Figure 12 Time series of temperature data at 2m above ground referred to the TMY time domain. Resource: PVGIS https://ec.europa.eu/jrc/en

There is again a seasonal trend in T, mainly linked to the amount of light and dark hours at the site. During the winter, in fact, when radiation is low or almost zero, the coldest temperatures are recorded, in some cases reaching -20°C. Some peaks in the summer season, on the other hand, reach +25°C, resulting in a maximum temperature range of 45°C. This factor must be taken into account when choosing technologies whose life cycle will also be affected by the thermal stresses identified here.

2) Data series from real years: these were considered to provide a comparison with the results from the use of TMY series in order to represent the real trend of meteorological data throughout the year and thus take into account the possibility of particular events that cannot be predicted. The use of these data series also allows us to appreciate, although not entirely transparently, the effect that global warming might have on the local climate. Indeed, while the TMY (as shown in Table 4) is made up of 60% of data from years prior to 2010, the actual years considered are 2014 and 2015, which are 5 years far from 2010. It would be very interesting in the near future, with the data available, to see what changes would result from analysing series belonging to contemporary years in order to identify a trend.

The choice of the real years to which this type of series refers derives from the availability of the series themselves on PVGIS. In fact, only data from years up to and not beyond 2016 are available in an open source manner. However, for the sake of consistency in the comparison, it was considered better to exclude 2016 as it is a leap year. As a result, we have two sets of data referring to real years:

- Series referring to 2014
- Series referring to 2015

each of which is analysed individually.

In this case, too, the data were obtained using PVGIS tools. In this regard, reference is made to Figure 6.

Contrary to what is available in the case of the series referred to TMY, the "Hourly Data" tool also allows the identification of a series of parameters related to the optimal orientation of the panels, namely:

- Azimuth angle (ϕ): intended as the angle of the panel orientation taking south as reference direction and spacing the angle towards west.

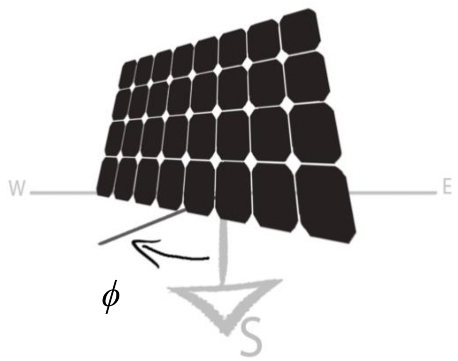

Figure 13 Diagram showing the angle of Azimuth ϕ of the panel. Resource: PVGIS https://ec.europa.eu/jrc/en

- Slope angle (β): also known as tilt angle, intended as the angle between the horizontal plane parallel to the ground and the plane containing the panel surface

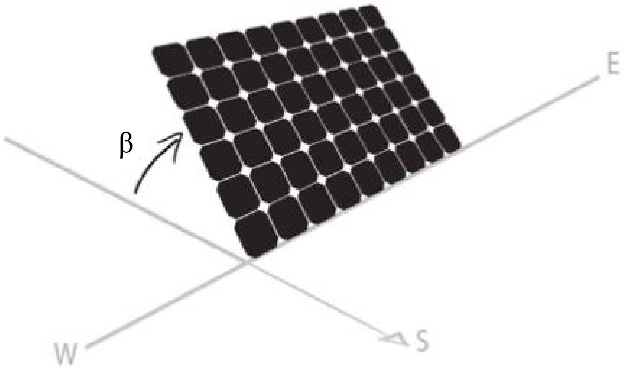

Figure 14 Diagram showing the slope angle β of the panel. Resource: PVGIS https://ec.europa.eu/jrc/en

.

The values of these angles provided by PVGIS are shown in the following Table 6

Table 6 Values associated with the positioning of the solar panel plane

SOLAR PANEL'S PLANE ANGLES		
Slope or Tilt (optimum)	β	45°
Azimuth (optimum)	ϕ	7°

It should be emphasised that the optimal angle data obtained using this tool were also used for processing the TMY series data. In addition, it was necessary for the use of this tool to indicate the type of panels used in relation to the possibility or otherwise of having mechanisms for rotation and/or variation of inclination (tracking system). Since these mechanisms are not present in the panel models used in this study, reference was made to the "Fixed" type.

As indicated in the figure, the database referred to among those available on PVGIS is PVGIS-ERA5, which does not make available data obtained from satellite images (due to the unavailability of the latter for high latitudes) but is made up of reanalysis-based solar radiation data. This choice was made by following the indications for the optimal use of the database given in the "*PVGIS users Manual*" section of the website. As a demonstration of this, the map below shows the geographical areas in which it is advisable to refer to a particular database:

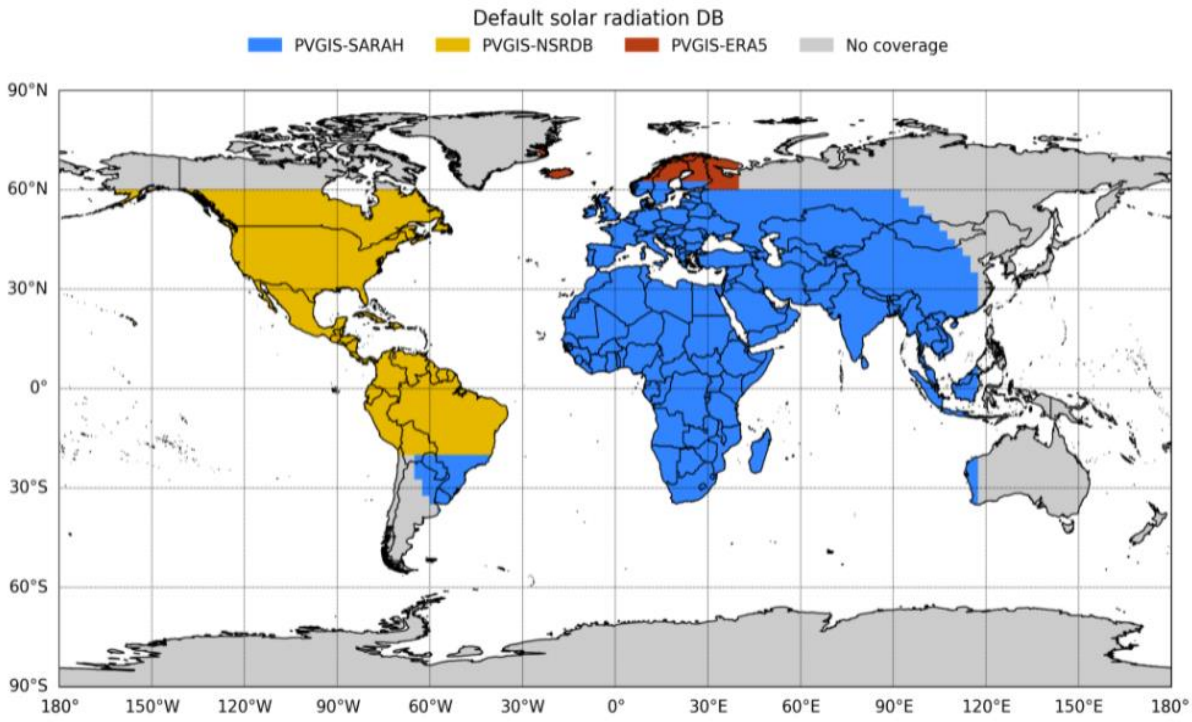

Figure 15 Map of the geographical areas covered by the different databases to which PVGIS provides access. Resource: PVGIS https://ec.europa.eu/jrc/en

The types of data provided by the 'Hourly Data' tool related to solar energy in its components are different from those provided by the TMY tool and are those reported and described in Table 7

Table 7 List of variables provided by the PVGIS database for the series referring to the actual years 2014 and 2015

SOLAR ENERGY VARIABLES FOR REAL YEARS DATA SERIES			
T_{2m}	2-m air temperature	*°C*	
G_t	Global in-plane= Global irradiance on the inclined panel's plane	*W/m^2*	ICNR[2]
G_b	Direct in-plane= Beam/direct irradiance on the inclined panel's plane	*W/m^2*	ICR[3]
G_d	Diffuse in-plane=Diffused irradiance on the inclined panel's plane	*W/m^2*	ICR
G_r	Reflected irradiance on the inclined panel's plane	*W/m^2*	ICR NU[4]
H_{sun}	Sun height	°	NU

In the last column of Table 7 data sets that were not used for the purposes of this analysis were identified. It should also be noted that, unlike in the case of the TMY tool, the datasets relating to total incident, direct diffuse and reflected radiation do not refer to the horizontal plane but rather to the plane identified by the optimal tilt and azimuth angles shown in Table 6. Therefore, as will be better described in the section "3.METHODS" the processing of the data series referring to real years will be slightly different from that of the TMY series (at least for the first passages where some particular assumptions have to be done).

[2] If Components Not Requested
[3] If Component Requested
[4] Not Used data

The following graphs present the trends of the input data series shown in Table 7 separately for the 2014 and 2015 series and excluding the series provided by PVGIS but not used:

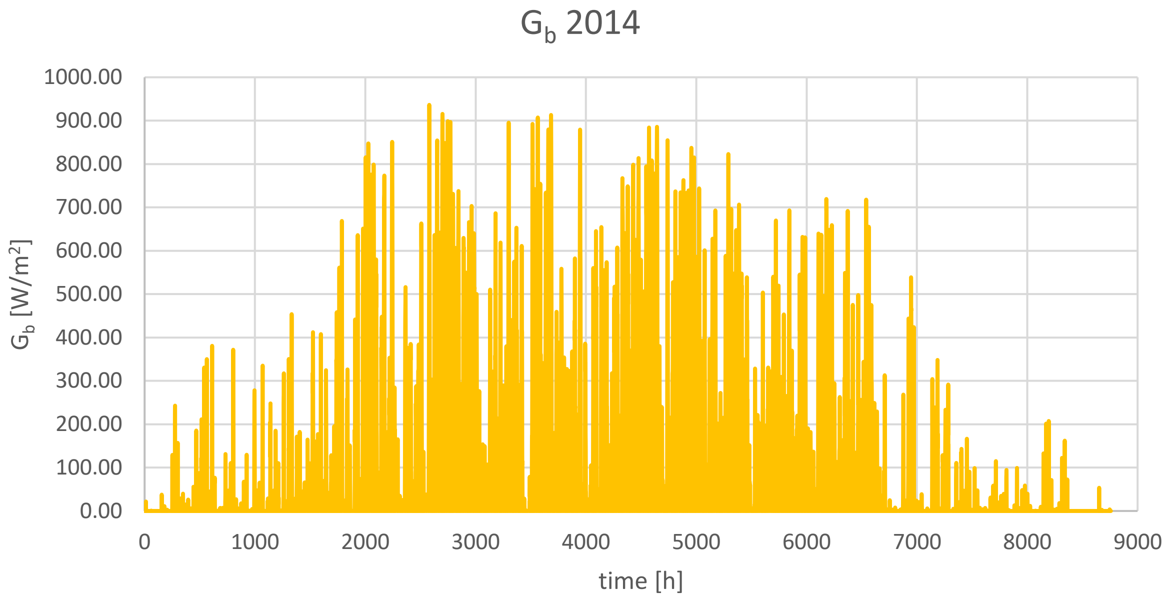

Figure 16 Hourly series of the direct component (G_b) of solar radiation, incident on the inclined plane of the panel and referred to the real time domain of the year 2014. Source: PVGIS https://ec.europa.eu/jrc/en/pvgis

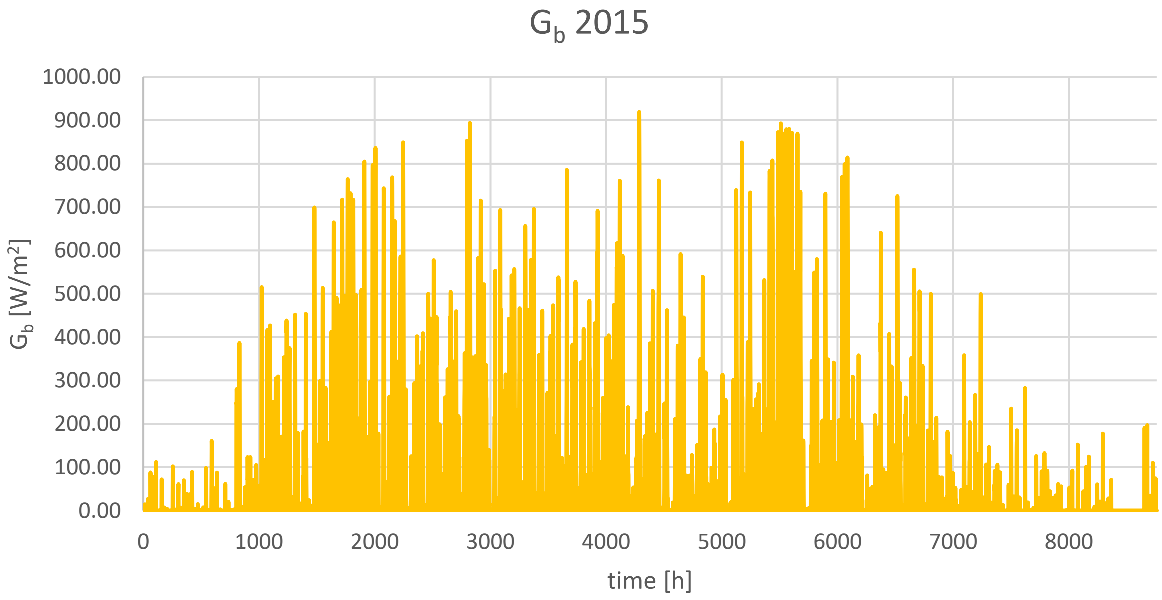

Figure 17 Hourly series of the direct component (G_b) of solar radiation, incident on the inclined plane of the panel and referred to the real time domain of the year 2015. Source: PVGIS https://ec.europa.eu/jrc/en/pvgis

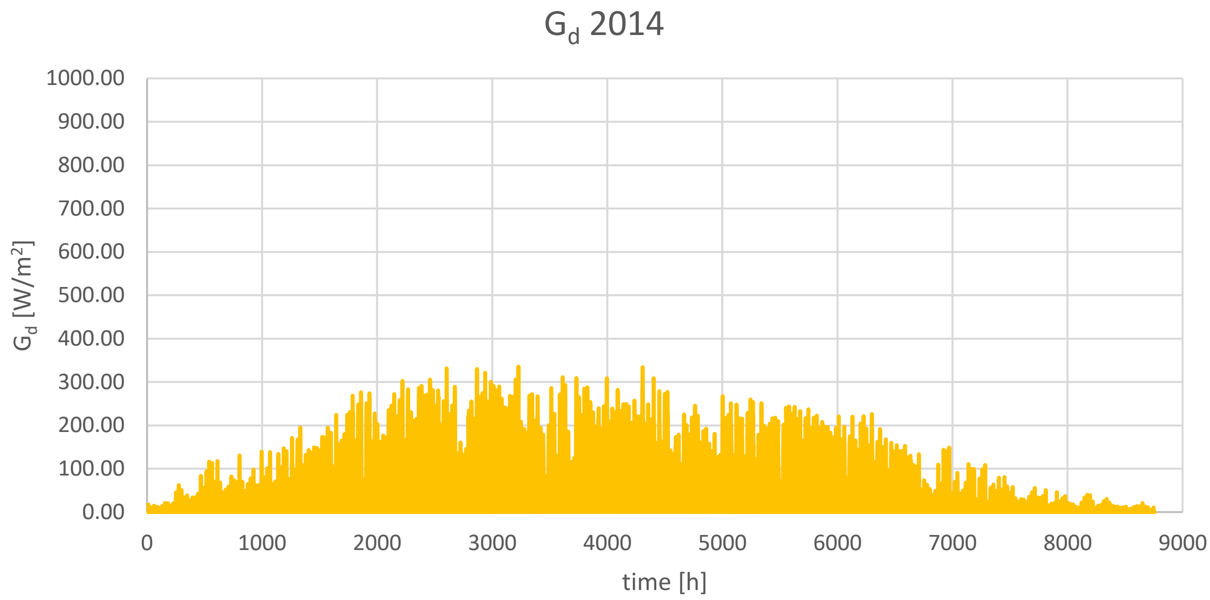

Figure 18 Hourly series of the diffuse component (G_d) of solar radiation, referring to the real time domain of the year 2014. Source: PVGIS https://ec.europa.eu/jrc/en/pvgis

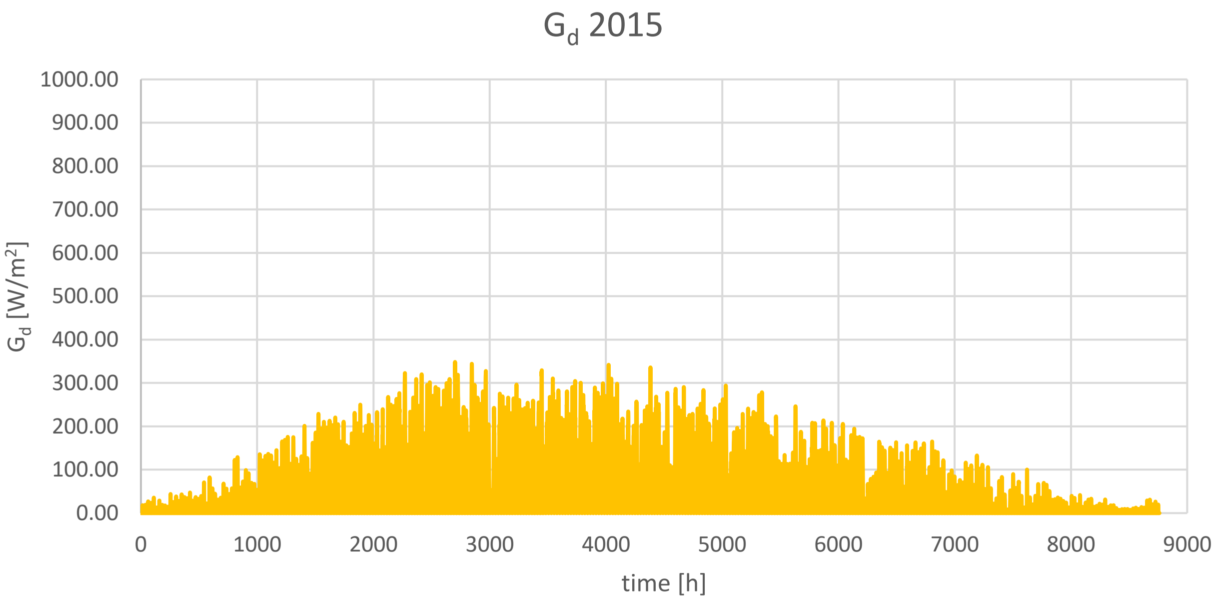

Figure 19 Hourly series of the diffuse component (G_d) of solar radiation, referring to the real time domain of the year 2015. Source: PVGIS https://ec.europa.eu/jrc/en/pvgis

The same comments as for the TMY time domain apply to the radiation graphs related to real years. In particular, a comparison can be made here between the $G_b(t)$ of 2014 and 2015, which differ in their behaviour for a short time between 4000 and 5500 hours. Here, in fact, a lower amount of incident radiation is recorded for 2015, which is similar to the trend of the same type of component recorded in TMY during the same period. This factor could make some difference in the producibility value of solar technologies by bringing the series for 2015 and TMY to similar values.

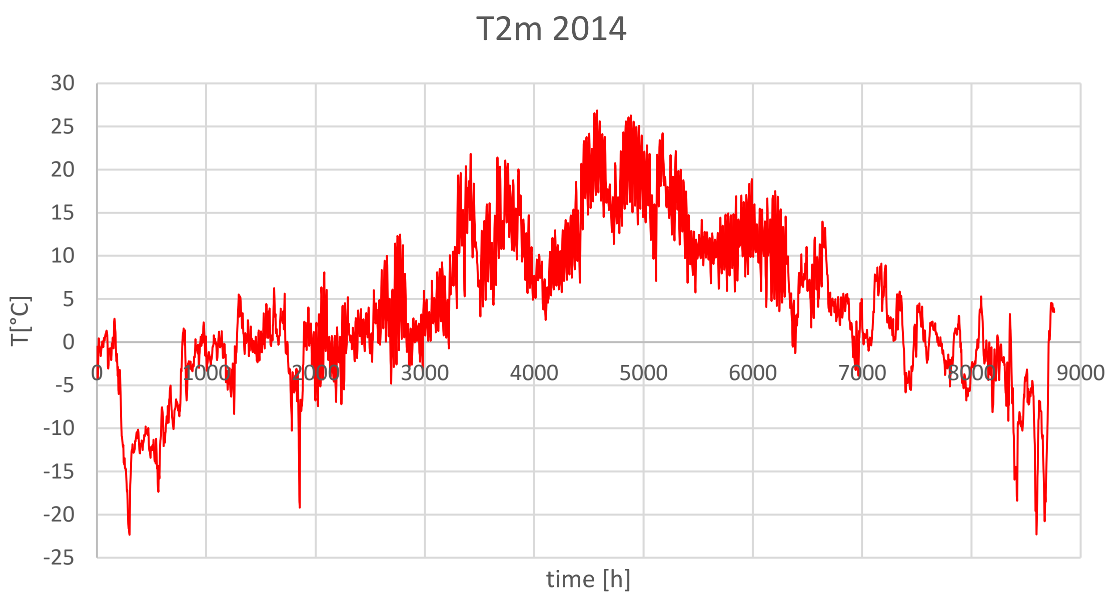

Figure 20 Serie oraria dei dati della Temperatura rilevata all'altezza di 2m da terra riferita al dominio temporale reale 2014. Risorsa: PVGIS https://ec.europa.eu/jrc/en/pvgis

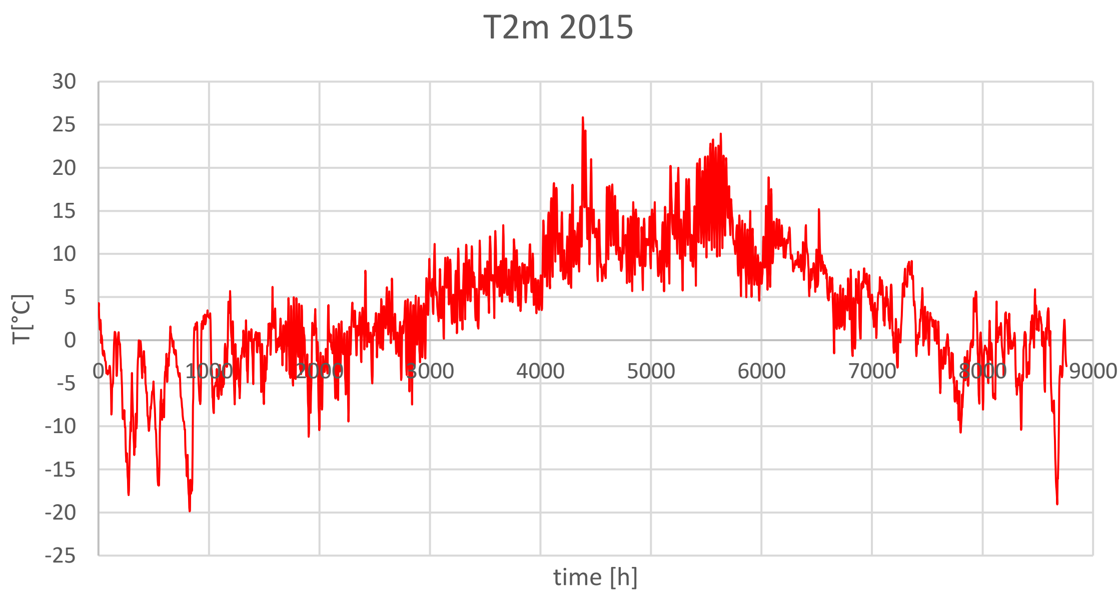

Figure 21 Serie oraria dei dati della Temperatura rilevata all'altezza di 2m da terra riferita al dominio temporale reale 2014. Risorsa: PVGIS https://ec.europa.eu/jrc/en/pvgis

Comparing the T(t) series, we immediately notice that the average T(t) for 2015 is higher than that for 2014. This could be an effect of the warming of the local climate, although no other data are available to support this theory.

Finally, we would like to mention here that the time references with which the PVGIS data have been provided are expressed according to the "Coordinated Universal Time", which must therefore be referred to the "Central Europe Time" in order to allow the couplings between the different data series. The reference longitude of -15° has been used for this purpose.

WIND

The wind speed datasets from which the producibility of the turbines can be calculated are classified in the same way as the solar radiation datasets since the source is the same. Indeed, PVGIS also provides the data series for wind speed at a height of 10m above the ground.

We will therefore have again the series:

- Wind TMY: which refers to the typical meteorological year as described in the previous paragraph in Table 4
- Wind Real Years: which are 2 sets of data related to the 2 real years already taken into account for the radiation data, which are 2014 and 2015.

The provisioning of these data is done simultaneously with that of the solar series by downloading the data in the same .csv file generated by the PVGIS tools (respectively "TMY" tool and "Hourly data" tool).

The graphs Figure 22, Figure 23, Figure 24 represent respectively the 3 sets of wind speed data evaluated at 10m height.

Again, there is a slight difference between the 2014 series and the other two series, which are much more similar. In fact, the data for 2014 are much more homogeneous and higher in certain precise time periods. In any case, the clear difference between the series and the radiation series is noticeable. Since they are almost totally independent of seasonality, they will be crucial for energy coverage, especially in the winter months.

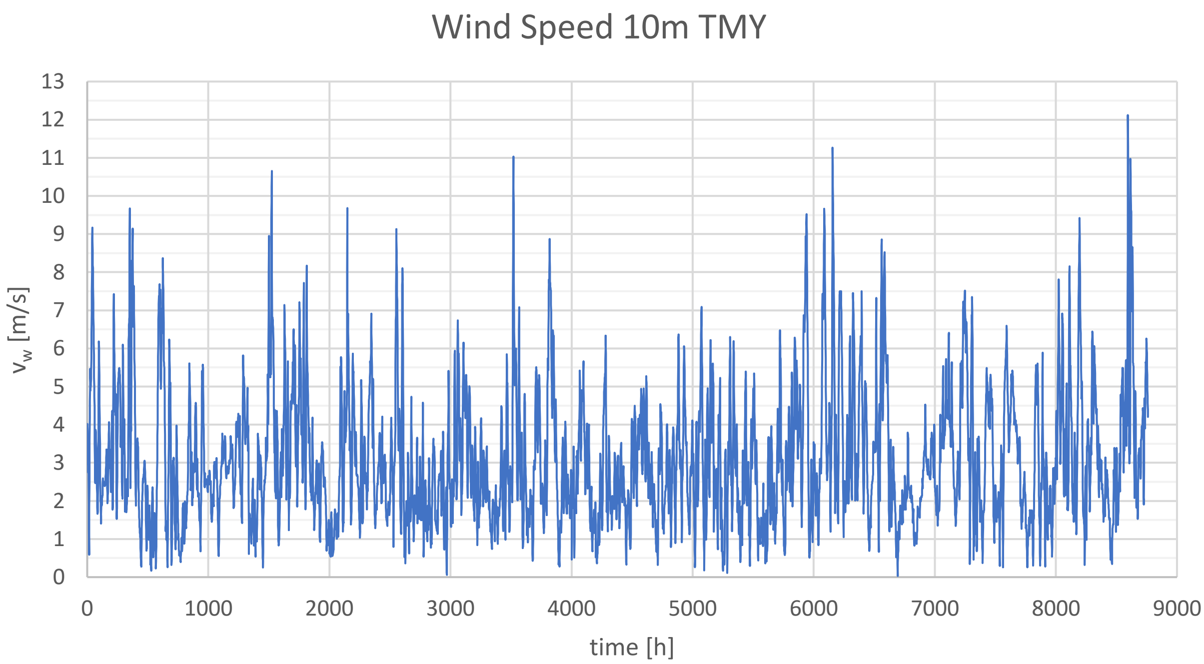

Figure 22 Hourly series of wind speed (v_w) data measured at a height of 10m above ground referred to the TMY time domain Resource: PVGIS https://ec.europa.eu/jrc/en/pvgis

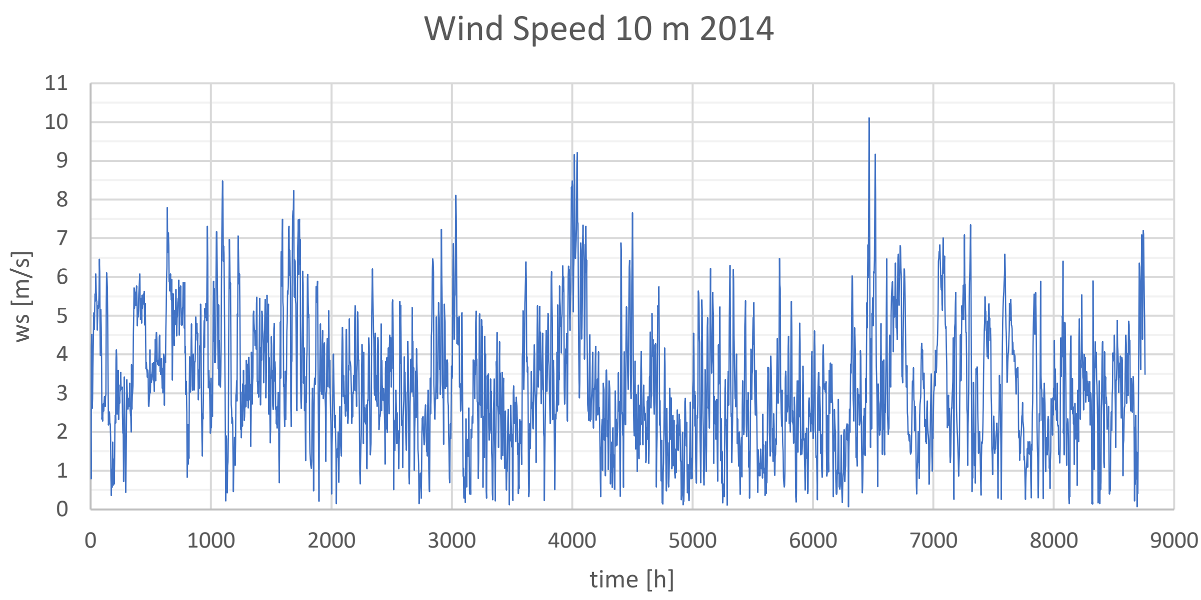

Figure 23 Hourly series of wind speed (v_w) data measured at a height of 10m above ground referred to the 2014 real time domain. Resource: PVGIS https://ec.europa.eu/jrc/en/pvgis

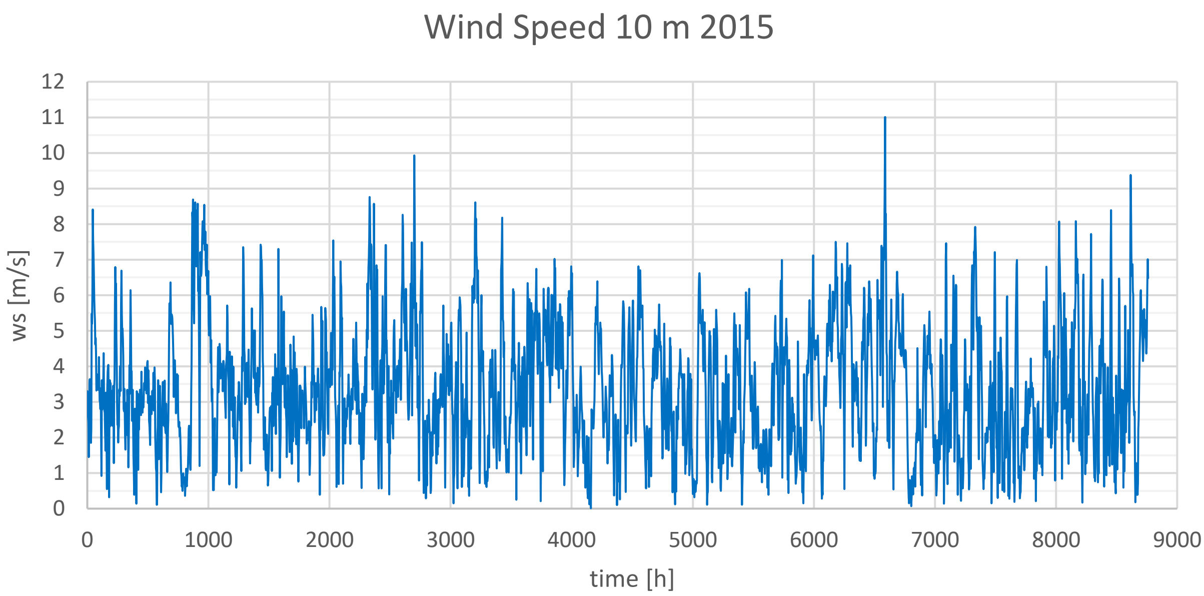

Figure 24 Hourly series of wind speed (v_w) data measured at a height of 10m above ground referred to the 2015 real time domain. Resource: PVGIS https://ec.europa.eu/jrc/en/pvgis

In addition, the "TMY" tool also provides information on the direction of the wind that is shown in Figure 25 so that to the reader can be given generic information on the best orientation direction in which to install the turbines.

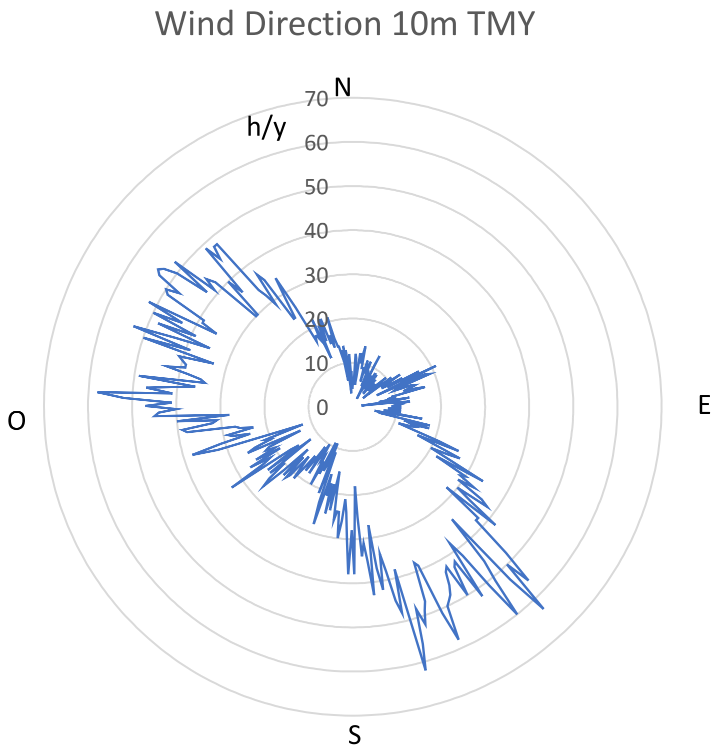

Figure 25 Frequency of the direction where wind is going assessed for currents at a height of 10m above ground and in reference to the year TMY. Source: PVGIS *https://ec.europa.eu/jrc/en/pvgis*

2.4. TECHNIC CHARACTERISTICS OF PRODUCTION TECHNOLOGIES

As previously stated, no particular new assumptions have been made with respect to energy production technologies, which are mainly:

- Photovoltaic panels
- Wind turbines

In fact, the same technologies were assumed as those used for the DEMO4 prototype under study in Rye. Let us take a closer look at them by collecting the data of interest from their data sheets.

TWINPEAK 2 MONO SERIES SOLAR PANELS

The panels used are the same ones that were chosen for the implementation of the DEMO4 prototype. They are produced by the company REC and are of monocrystalline type with a maximum efficiency of 19.8%. Below, in Figure 26, a diagram of the top view of the panel taken from the technical data sheet [3], [4] is shown, and, again from the technical data sheet, the Table 8 show the main technical data characterising the panel in the operating conditions of our case study.

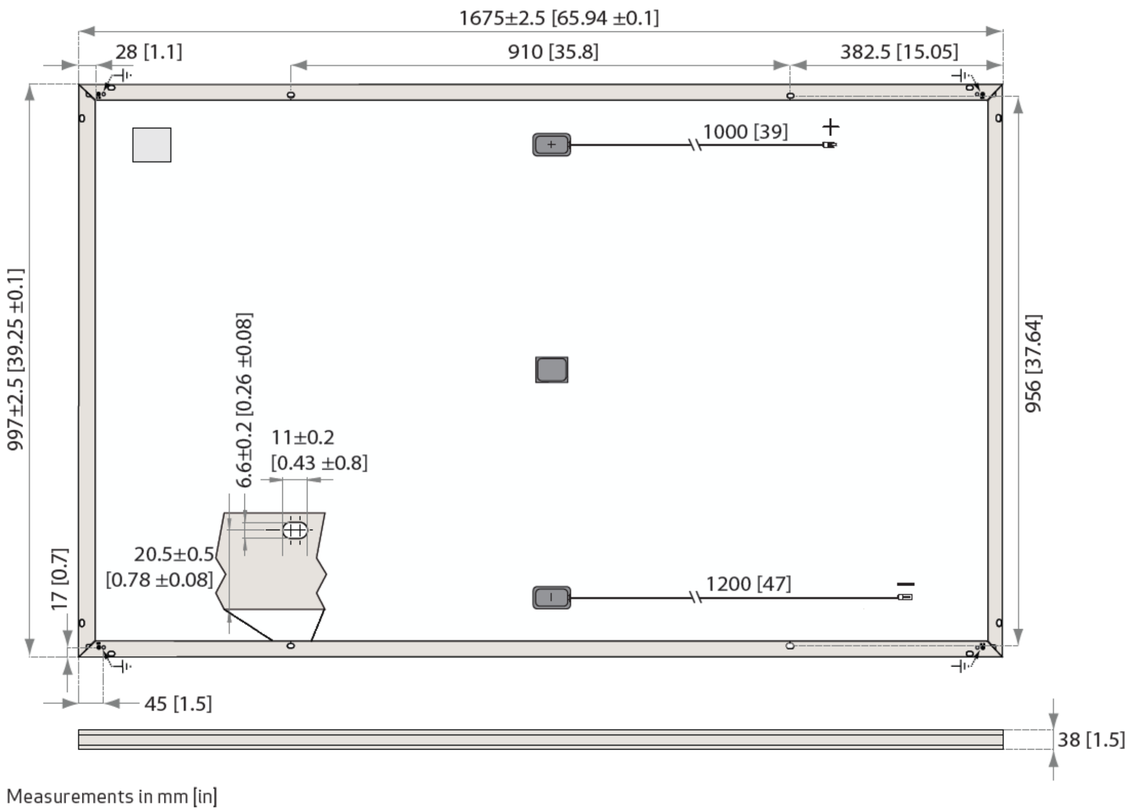

Figure 26 Technical sketch showing front and side views of the Twin Peak 2 Mono Series panel. Source: Twin Peak 2 Mono Series data sheet [3], [4]

Table 8 Twinpeak2 Single-series panel data sheet [3], [4]

GENERAL DATA	
Cell type	120 half-cut mono-Si p-type PERC cells 6 strings of 20 cells in series
Glass	3.2 mm solar glass with anti-reflection surface treatment
Backsheet	Highly resistant polyester polyolefin construction
Frame	Anodized aluminum
Junction box	3-part, 3 bypass diodes, IP67 rated in accordance with IEC 62790
Cable	4 mm² solar cable, 1.0 m + 1.2 m in accordance with EN 50618
Connectors	Stäubli MC4 PV-KBT4/PV-KST4 (4 mm²) in accordance with IEC 62852, IP68 only when connected
Origin	Made in Singapore

MAXIMUM RATINGS	
Operational temperature	-40 ... +85°C
Maximum system voltage	1000 V
Design load (+)	snow 3600 Pa (367 kg/m²)+
Maximum test load (+)	5400 Pa (550 kg/m²)*
Design load (-)	wind 1600 Pa (163 kg/m²)+
Maximum test load (-)	2400 Pa (244 kg/m²)*
Max series fuse rating	25 A
Max reverse current	25 A

+ Calculated using a safety factor of 1.5

* See installation manual for mounting instructions

TEMPERATURE RATINGS*	
Nominal Operating Cell Temperature (NOCT)	44.6°C (±2°C)
Temperature coefficient of P_{MAX} [γ]	-0.37 %/°C
Temperature coefficient of V_{OC}	-0.28 %/°C
Temperature coefficient of I_{SC}	0.04 %/°C

*The temperature coefficients stated are linear values

MECHANICAL DATA	
Dimensions	1675 x 997 x 38 mm
Area	1.67 m²
Weight	18.5 kg

ELECTRICAL DATA @ STC Product code*	RECxxxTP2M						
Nominal Power – PMAX (Wp)	**300**	**305**	**310**	**315**	**320**	**325**	**330**
Watt Class Sorting – (W)	-0/+5	-0/+5	-0/5	-0/5	-0/5	-0/5	-0/5
Nominal Power Voltage – VMPP (V)	33	33.3	33.5	33.7	33.9	34	34.3
Nominal Power Current – IMPP (A)	9.11	9.17	9.26	9.36	9.45	9.56	9.62
Open Circuit Voltage – VOC (V)	38.3	38.8	39.1	39.6	40	40.3	40.8
Short Circuit Current – ISC (A)	10.01	10.04	10.07	10.1	10.13	10.15	10.19
Panel Efficiency (%)	18	18.3	18.6	18.9	19.2	19.5	19.8
Values at standard test conditions (***STC air mass AM 1.5, irradiance 1000 W/m², temperature 25°C***), based on a production spread with a tolerance of PMAX, VOC & ISC ±3% within one watt class. At a low irradiance of 200 W/m² at least 95% of the STC module efficiency will be achieved. *Where xxx indicates the nominal power class (PMAX) at STC indicated above.							

Note that the last cell of Table 8 defines the Standard Conditions to which reference was made to evaluate the cell parameters and to which reference will be made in the “METHODS” section when calculating the relevant parameters.

Another assumption made was that of using the same panel loss coefficient (indicated with f_{PV}) for these panels as that used for modelling DEMO4 at Rye, which also corresponds to that used by default by the PVGIS “Hourly data” tool in the event that a calculation of the power supplied by the panels is also requested from the database (an option which, however, was not used in this study since the calculation of the nominal producibility for each hour was calculated autonomously following the relations which are reported in the “MET” section).

Similarly, reference will be made to a nominal peak power class of the panels equal to that of the modules used for Rye, i.e. 320Wp.

Table 9 shows in a more concentrated manner the data that will be useful for determining the producibility of the solar sector of the production system.

Table 9 summary table of data selected for photovoltaic panel characterisation

TWINPEAK2 MONO SERIES		
f_{PV}	14%	
NOCT	44.6	°C
γ	-0.37%	1/K
$P_{PV_{rated}}$	86400	Wp
$T_{cell_{STC}}$	25	°C
G_{STC}	1000	W/m²

Note that P_PV_rated refers to the peak power of the reference system, which is the one used by DEMO4 (270 modules x 320Wp)[5], while T_cell_STC refers to the cell temperature under standard conditions and G_STC refers to the maximum incident radiation power per unit area.

WIND TURBINE VESTAS V27/225

The model of the turbine chosen as the module for the wind component of the system is also the same as that used for DEMO4. It is a turbine designed and manufactured by the manufacturer VESTAS model 27 with a maximum rated power of 225kW.

In Table 10 are the characteristics taken from the technical data sheet [6].

Table 10 Dati relativi alla scheda tecnica tella turbina Vestas V27/225 [6]

GENERAL		
Manufacturer	Vestas	
Model	V27/225	
Rated power	225	kW
cut in wind speed	3	m/s
rated wind speed	14	m/s
cut off wind speed	25	m/s
Power control	Pitch	

ROTOR		
Diameter	27	m
Swept area (surface)	573	m^2
N blades	3	
Density power 1	392.7	W/m^2
Density power 2	2.5	m^2/kW
Weight	2.9	ton
maximum rotor speed	43	rad/min

GEAR BOX		
stages	2	
gear ratio	25	

TOWER		
h	33.5	m
Weight	9-12	tons

NACELLE		
Weight	7.9	tons

GENERATOR		
Connessione alla rete	Double wound evelizedt 480	
Type	ASYNC	
number	1	
maximum speed	1008	rpm
Voltage	400-800	V
Manufacturer	Siemens, AEG, ABB	

The characteristic power curve of the turbine is also shown both as a graph and as a series in Figure 27 and *Table 11*.

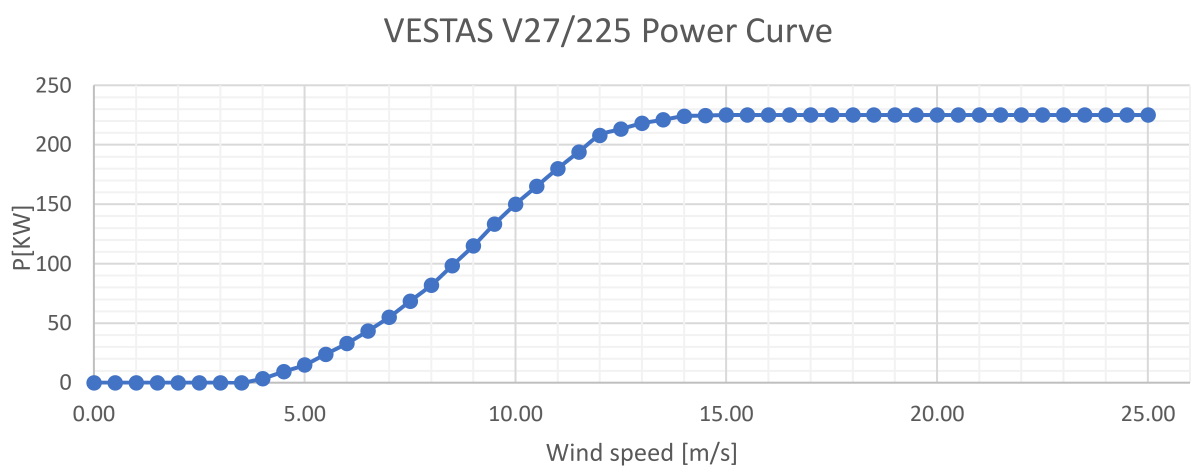

Figure 27 Power curve of the Vestas V27/225 wind turbine. Source: Turbine data sheet [6] *https://it.wind-turbine-models.com/turbines/9-vestas-v27*

Table 11 Vestas V27/225 turbine power curve

Power curve VESTAS V27/225	
v_w [m/s]	**P [KW]**
0.00-3.50	0
4.00	3.52
4.50	9.26
5.00	15
5.50	24
6.00	33
6.50	43.52
7.00	55
7.50	68.5
8.00	82
8.50	98.5
9.00	115
9.50	133.26
10.00	150
10.50	165
11.00	180
11.50	194
12.00	208
12.50	213.22
13.00	218
13.50	221
14.00	224
14.50	224.52
15.00-25.00	225

The choice of a small-to-medium sized turbine thus provides great flexibility at the time of installation both in terms of positioning the technology in the area and in terms of the power to be actually installed as dictated by the system optimisation results.

2.5. TECHNICAL CHARACTERISTICS OF THE OTHER SYSTEM COMPONENTS

Since the purpose of this work is to investigate in a general way the feasibility of a technological transfer from a site with certain characteristics to a different one, it has not been necessary to identify any particular technical characteristics for the transformation technologies (PEMEL and PEMFC) nor for the storage technologies (Battery and Hydrogen Tank) other than those shown in the following table, which are independent of the manufacturing origin. If desired, the reader should refer to the case modelled for DEMO4 [5], which proposes the storage and transformation technologies that would be installed in a more than plausible manner in the hypothetical realisation of this project.

The data we are now going to list in Table 12, Table 13, Table 14, Table 15 (referring to generic technologies) were however also re-used in an identical way to those used for the preliminary implementation of the DEMO4 project.

PEMFC

Table 12 Technical data on PEMFC [5]

PEMFC		
Minimum power	0.1	% of nominal power
Maximum power	1	% of nominal power
η_{FC}	0.471	

PEMEL

Table 13 Technical data for PEMEL [5]

PEMEL		
Minimum power	0.1	% of nominal power
Maximum power	1	% of nominal power
η_{EL}	0.58	

HYDROGEN STORAGE TANK

Table 14 Technical data referring to H2 tank [5]

H_2 TANK		
Minimum p	3	bar
Maximum p	28	bar
Minimum SOC	0.11	
Maximum SOC	1	

BATTERY

Table 15 Battery-related technical data[5]

BATTERY	
Minimum SOC	0.2
Maximum SOC	1
η_{charge}	0.11
$\eta_{discharge}$	1

2.6. ECONOMIC DATA ON TECHNOLOGIES

Since the objective function of the optimisation is the LCOE, the choice of economic parameters to be attributed to the different technologies is of fundamental importance. Since the values of mainly CAPEX and OPEX that were used for the DEMO4 modelling referred to the state-of-the-art technologies of more than 5 years ago, it was necessary to update them.

This update was performed in a precise manner, technology by technology, by carrying out bibliographical research that would first of all guarantee an overall view of the state of the art of the various technologies available and then concentrate on the best ones and those most commonly used for modelling or creating systems similar to the one in discussion.

The difficulty of such research is highlighted here, especially with regard to the supply of data on transformation technologies. This is mainly due to two factors:

- *The relative youth of the technologies*: which implies rapid variations in terms of both technological improvements and the amount of investment costs.

- *The rarity of cases in terms of use similar to ours of these technologies:* which are very often still used in experimental projects or even only for preliminary studies and in any case almost always relative to loads of a more modest entity (speaking of the uses that can be traced back to that of this project, which in any case represent a non-preponderant percentage of all the uses explored to date).

This testifies to the fact that research in this field is very active and still holds enormous potential that needs to be explored.

After the selection of 91 relevant studies published between 2015 and 2021 related to the different technologies, their analysis led to the identification of cost updates which are shown in the summary Table 16 which also provides a comparison with the old data used for DEMO4 modelling. The new data referred to for the study all relate to a period of time that reflects that of the studies analysed, i.e. from 2015 to 2020.

In general, at least 4 terms have been defined for each technology:

- CAPEX: Investment cost related to the technology referred to as normalised CAPEX, i.e. expressed in €/KW of installed power.

- OPEX: Variable Operation and Maintenance Costs of the technology. Sometimes expressed as normalised values like CAPEX, sometimes expressed as a percentage of the investment cost per year.

- REPLACEMENT COST: These were identified for those technologies whose lifetime was shorter than that of the system assumed to be 20 years. In this case the cost was always referred to as a percentage of the investment cost.

- LIFETIME: not directly intended as cost data but included in the economic data section as it is decisive for the need to replace certain technologies over the life of the system.

The table summarising the economic data assumed to characterise the entire system is then reported. It shows both the life of the entire system and the coefficients used to discount the cost of the components over the 20 years.

The table summarising the exchange coefficients from the different currencies in € at the time the cost was determined is also shown. This is because many of the studies analysed reported CAPEX or OPEX data in the currency of the country or geo-political-economic area of reference.

Table 16 Economic data referring to the different technologies making up the system

COMPONENT		lifetime [y]	CAPEX		Reference Size [KW]	OPEX		Replacement [%CAPEX]
Battery	old	10 [5]	550 [5]	€/kWh	-	10 [7]–[9]	€/kWh/y	50 [5]
	updated	15 [7], [10]–[12]	380 [11]	€/kWh				100 [12], [13]
H_2 Tank	old	35 [5]	470 [5]	€/kg	-	2[5]	%CAPEX/y	nn*
	updated							
PEMEL	old	5 [5]	4600[5]	€/KW	-	3[5]	% CAPEX/y	35.00[5]
	updated	10 [14]–[17]	1188 [18]	€/KW	5000 [18]	2 [14], [15], [19]	% CAPEX/y	33 [19]
PEMFC	old	5 [5]	3947[5]	€/KW	10[5]	3[20]–[24]	%CAPEX/y	26.67[5]
	updated	10 [20], [25], [26]	1419-2075[20], [24], [27]	€/KW	1224-192 [27]			100[24]
PV system	old	25[28]–[37]	1453	€/KW	-	2 [32], [36], [38], [39]	%CAPEX/y	nn*
	updated		890 [31], [39], [40]	€/KW				
PV inverter	old	10 [5]	93 [5]	€/KW	-	4[5]	€/kW/y	86[5]
	updated	12[7], [41]	58[42]	€/KW		6[41]	€/kW/y	83[41]
Wind Turbine	old	25[43]–[45]	1175 [5]	€/KW	-	3[43], [46]–[50]	%CAPEX/y	nn*
	updated		1154[49]	€/KW				

Table 17 Economic parameters concerning the entire system

COMPLETE SYSTEM		
	value	**unit**
SYSTEM CHARACTERISTICS		
Lifetime	20	years
ECONOMIC PARAMETERS		
es	2 [5]	%
ii_nom	7 [5]	%

Table 18 Currency conversions used to convert currencies from bibliographic sources of origin to the amount in €

monetary conversion							
year	**USD**	**CNY**	**INR**	**AUD**	**£**		**€**
2014	1						0.76
2017	1						0.88
2020	1						0.88
2021	1					=	0.83
		1					0.13
			1				0.01
				1			0.61
					1		1.17

It should be noted that, for the processing technologies PEMEC and PEMFC, reference values for size have been identified and associated with them the relative costs of CAPEX and OPEX. This is because, as will be explained in more detail in section “3.METHODS” , they are associated to cost functions that allow the variation of CAPEX and OPEX according to the installed size. The coefficients characterising these cost curves will be obtained from the reference data shown in the table. Table 16.

2.7. GRID-RELATED ECONOMIC DATA

Since integration with the grid is the main difference between the DEMO4 model and the one in the following study, it is of fundamental importance to illustrate the economic data characterising the exchange of energy between the system and the grid.

In the following paragraph we will limit ourselves to illustrate the components of the cost or of the eventual revenues, referring once again to the section “METHODS” for the definition of how they have actually been evaluated and how they have been taken into account in the optimization system.

The energy cost component is made up of various items that can be grouped under 3 main headings:

- POWER cost: which aims to assess the cost associated with energy starting from its market value. This component will therefore be the only variable (in our case on an hourly basis) and will contribute according to the amount of power purchased from or sold to the grid.

- cost related to NETWORK SERVICES: which mainly includes the costs of transport along the network and a fixed fee on a consumption basis that is charged to the consumer.

- cost related to NETWORK CONNECTION AUTHORISATION: which consists of a single cost item related to an annual fee for network connection authorisation.

Generally, the first 2 cost items must then be increased by VAT. However, as reported in “METHODS” for some cases of users such as ours, which is identified as a business activity, VAT can be deducted and therefore not accounted for the purpose of evaluating the energy price.

Table 19 therefore shows the values of the constant price components with a small description of their meaning on the side.

Table 19 Cost items considered related to interaction with the network

VOICES OF COST		Definition	Value	Unit	Comments
POWER	**Power price**	Variable, hourly spot prices	-	€/MWh	Market price of energy which varies hour by hour (reference year: 2017)
	VAT 25 %	Power price*0.25	-	€/MWh	
GRID ENERGY BASED	**Energy price**	constant	18.50	€/MWh	cost of transporting energy (depending on the sizes of the customers)
	Consumer tax	constant	16.69	€/MWh	from government
	VAT 25 %	(Consumer tax + Energy Price) *0.25	8.80	€/MWh	
GRID YEARLY BASED	**Grid fee Basic**	constant	270.00	€/year	

As can be seen, there are no values under Power Price because, as indicated, the value of the market price varies over time. In this case, an hourly data set was considered for consistency with the other data sets that will be included as input in the optimisation algorithm. The series of spot prices was provided directly by Tronder Energi, which in turn relied on the Norwegian energy market management company [Nord Pool](https://www.nordpoolgroup.com/) to source them.

Tronder Energi also identified a particular year to which to refer for the data series, which was 2017. This was due to the fact that 2017 was a standard year in terms of rainfall on Norwegian territory and this directly affected the energy price development as the Norwegian energy mix consists of more than 80% hydropower generation.

From this same data set, the incomes generated by the sale of any surplus generation on the grid will then also be assessed (see section “3”). In order to process the data for the calculation of these incomes, it will be necessary to take into account a fixed fee that must be paid for the authorisation by the electricity company to feed energy into the grid. This fee consists of 1.2 €/MWh.

The data set referred to is therefore shown in the graph Figure 28.

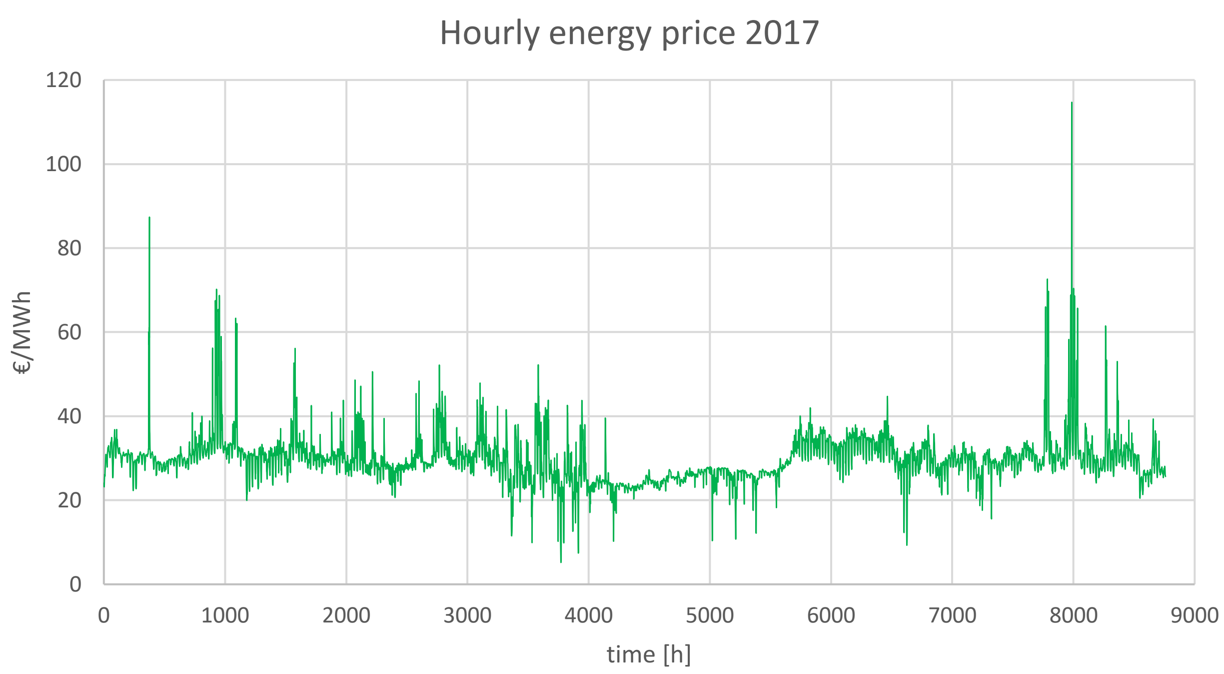

Figure 28 Hourly series of electricity market price developments in Norway for the year 2017. Source Tronder Energi/Nord Pool https://www.nordpoolgroup.com/

It should be noted that the data serie shown in the graph Figure 28 represents only the variable component of the total cost, i.e. the market price of energy. The real costs or incomes resulting from it will be explained in more detail in the section “3.METHODS”.

2.8. CLIMATE-AFFECTING IMPACT ASSESSMENT DATA

In this study, we also want to highlight the impact on the emission of climate-changing gases of adopting such a solution. It is expected that in a landscape similar to the Norwegian one, where almost the entire energy mix is composed of renewables, the impact does not represent a switch in terms of emissions but confirms the validity of such a system as a technology capable of implementing the technological development of areas in a context of environmental protection and sustainability.

The Norwegian energy mix, however, is an extremely virtuous case on the international scene, which is very different from the average conditions of an energy mix in an average European country, for example.

The following graphs Figure 29, Figure 30, Figure 31 support this statement. These were taken from the data series made available on the International Energy Agency's website and refer to the evolution of the composition of the Norwegian energy mix and electricity production over the last 20 years and the European average over the same period.

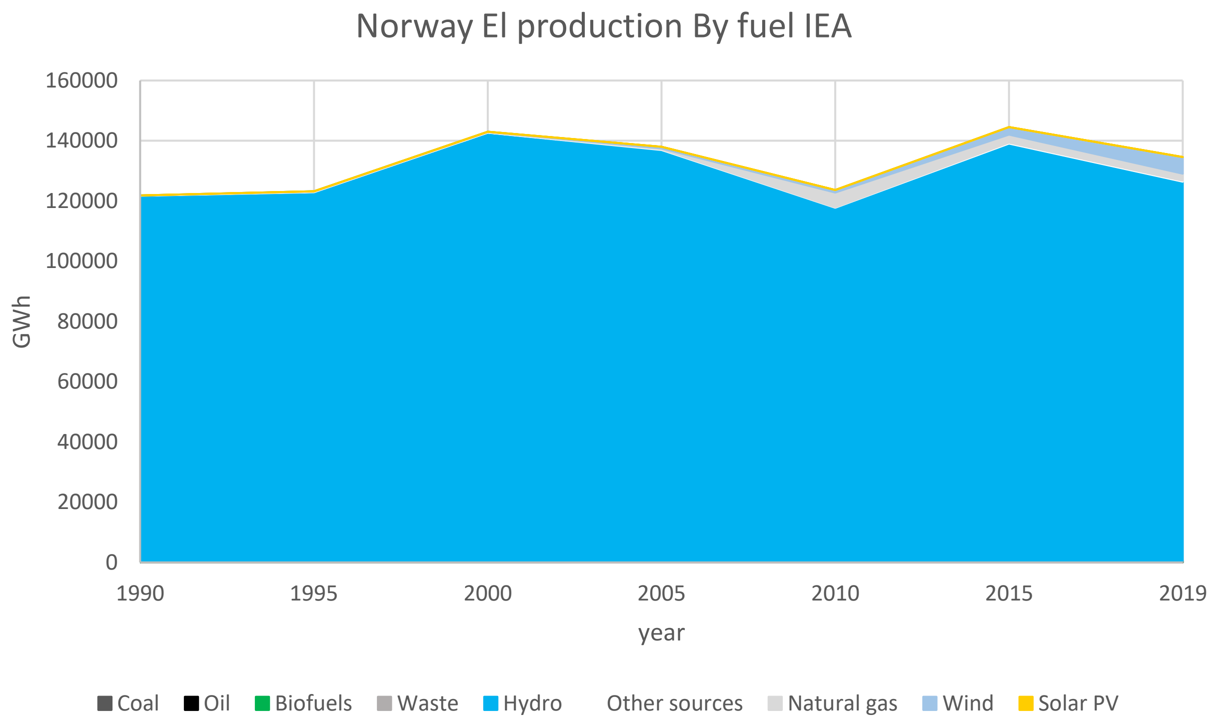

Figure 29 Composition of Norway's national energy mix for electricity production from 1990 to 2019. Source: IEA https://www.iea.org/

It can be seen that the behaviour of the graphs is very different both in terms of the composition of the mix and the electricity production trend. In the first case, it can be seen that Norway, which has a tradition of renewable energy and in particular hydroelectric power, is diversifying its energy mix by introducing an increasingly large share of wind power. This is the reason for the country's huge investments in the construction of on-shore and, above all, off-shore wind farms, of which Tronder Energi's activity is one example.

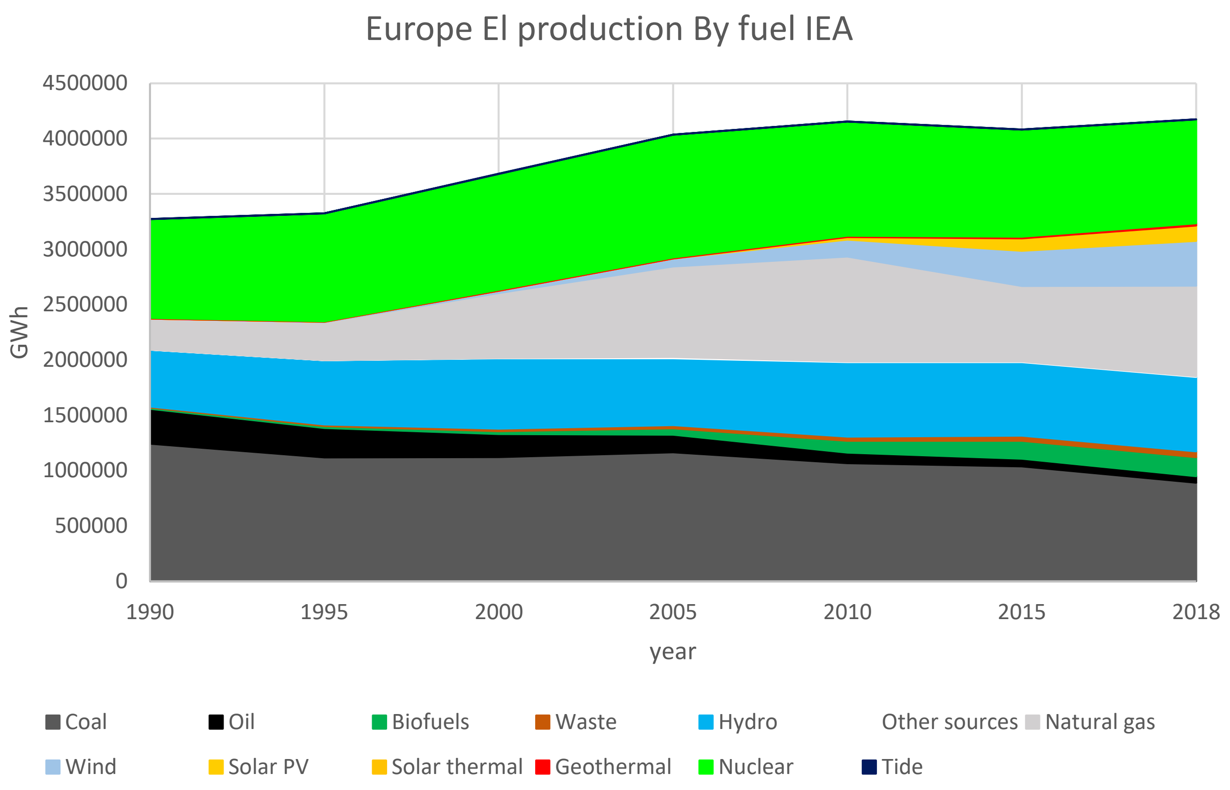

Figure 30 Composition of the European energy mix for electricity production from 1990 to 2018. Source: IEA https://www.iea.org/

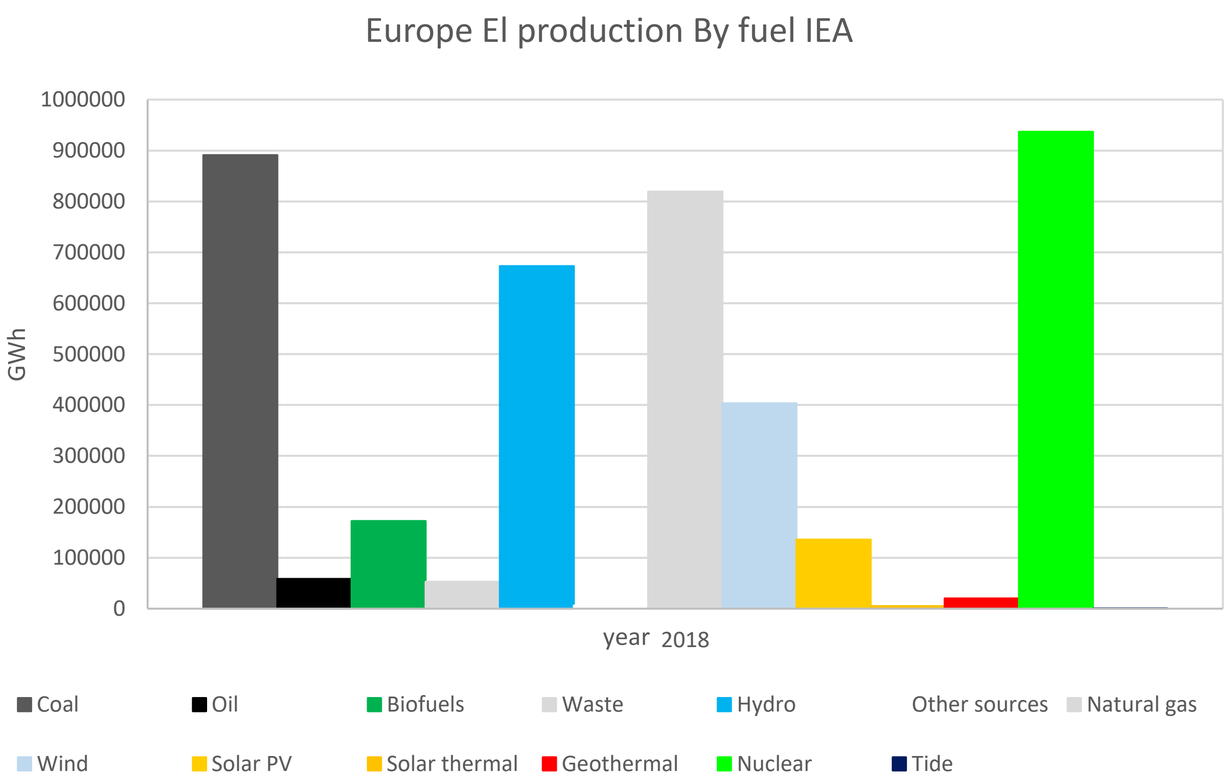

Figure 31 Composition of the European energy mix for power generation in 2018. Source: IEA https://www.iea.org/

In the second case, however, it is shown how a Europe that mainly produces electricity from fossil fuels is very slowly moving in the direction of replacing coal and oil to the benefit of natural gas and, especially in the last decade, of the various types of renewable sources, among which wind power plays the dominant role. However, it should be noted that, for example, the reduction in the use of oil products has been almost totally replaced by new biofuels which, although they are renewable, are not a solution in terms of reducing emissions as they are still products based on carbon chains. The graph omits the last few years, due to lack of available data, where the effects of the completion of decarbonisation and denuclearisation implemented by the German energy policy plan would be clearly visible. In any case, the high dependence on fossil fuels, especially coal, is clearly visible, mainly in Eastern European countries.

In addition, it should be noted that, while Norway continues to maintain its production values substantially unchanged, Europe is experiencing an increase in production linked to an increase in demand that is rooted in the increasingly technological and therefore energy-intensive substrate of the societies of the various countries (both the more economically advanced and the less so).

These graphs can then be translated in terms of impact on emissions by grouping energy sources according to their contribution to CO_2 emissions producing Figure 32, Figure 33, Figure 34, Figure 35.

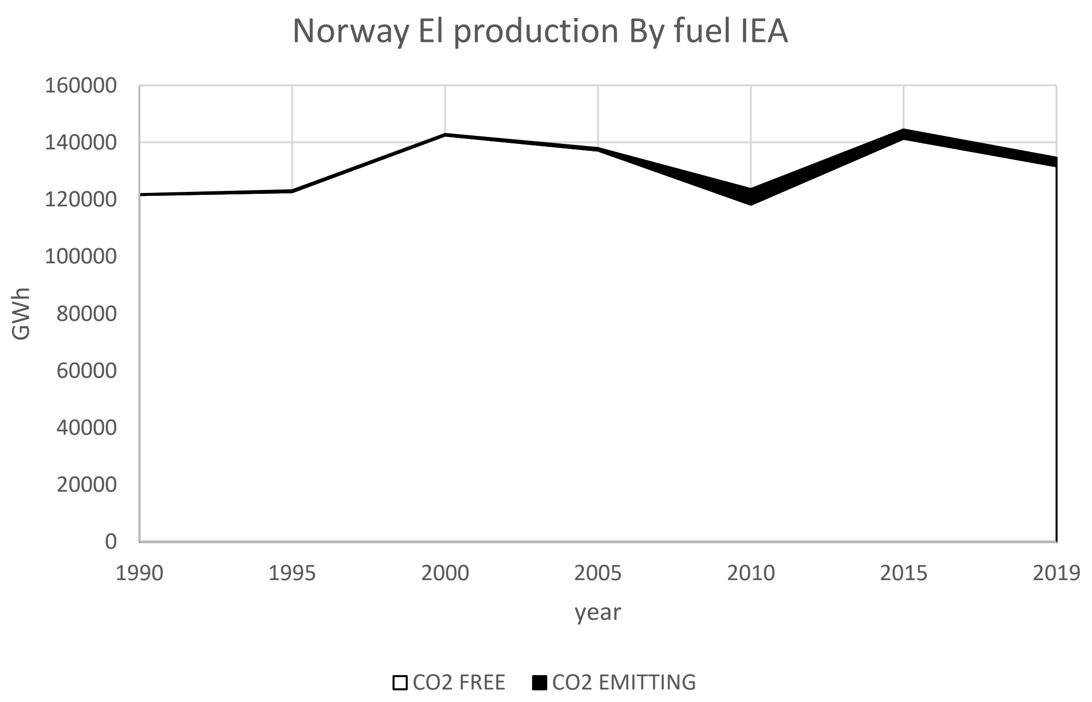

Figure 32 Breakdown of Norway's national energy mix for electricity production from 1990 to 2019 according to CO_2 emitting and clean fuels.

Although Norway's use of emitting sources is increasing slightly (due to the fact that the use of natural gas is also increasing), the amount of emitting sources is derisory compared to the average in Europe (which therefore also takes into account particularly virtuous countries) and in 2018 barely reaches 50% of the entire mix (related only to the production of electricity), despite the fact that a series of measures have already been taken in some individual states as a result of COP21 of Paris in 2015 [51].

It will therefore be possible to demonstrate how a solution such as the one proposed by this study can at least limit emissions, bringing considerable benefits in the environmental sphere, and in particular contribute to the decarbonisation desired and searched for in such a determined way by the European Union and by extension by the international community to try to limit the greenhouse effect and therefore the rise in temperatures with all the consequences that this entails.

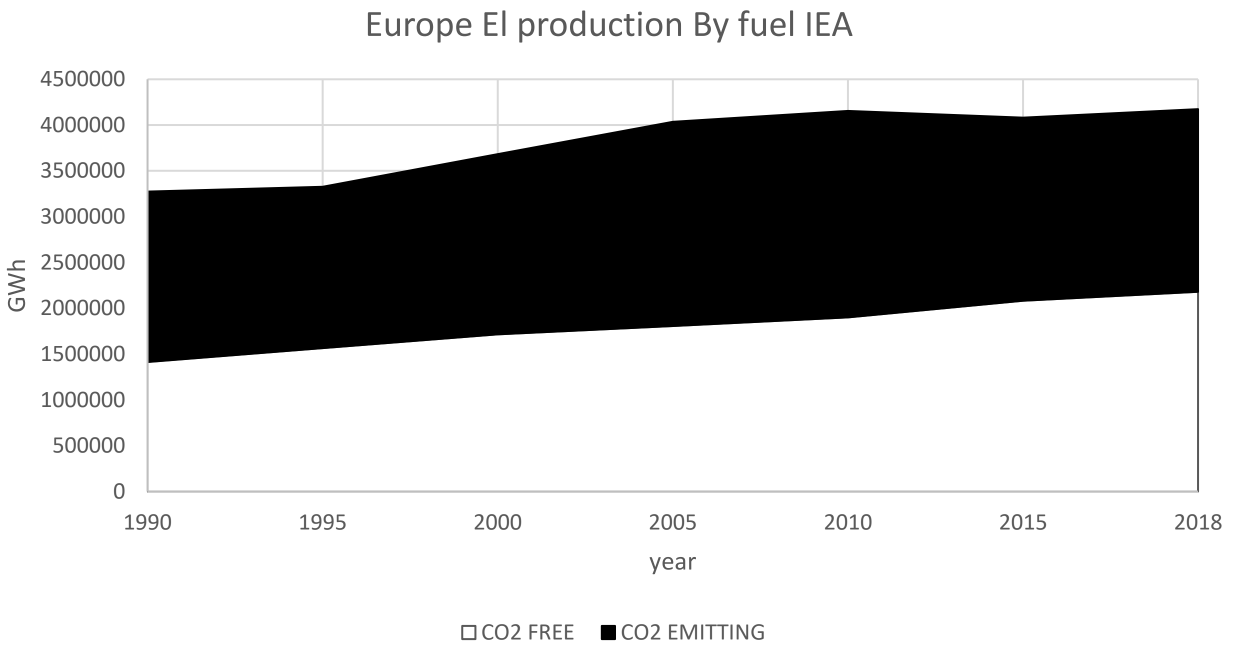

Figure 33 Breakdown of the European energy mix for electricity production from 1990 to 2018 according to CO_2 emitting and clean fuels.

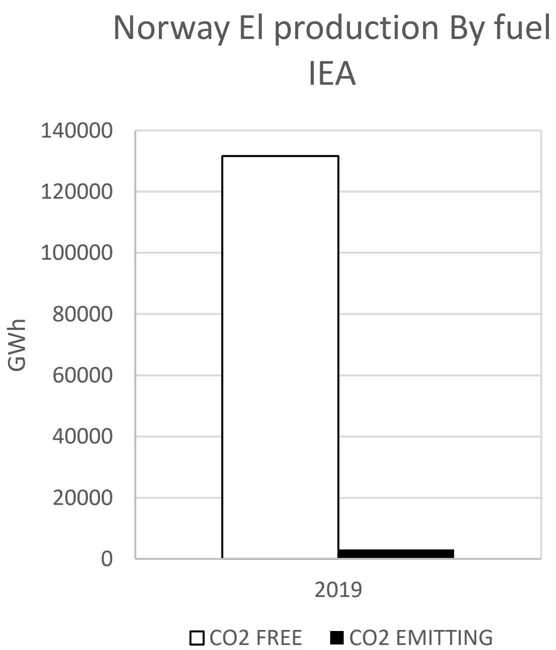

Figure 34 Breakdown of Norway's national energy mix for electricity production in 2019 according to CO_2 emitting and clean fuels.

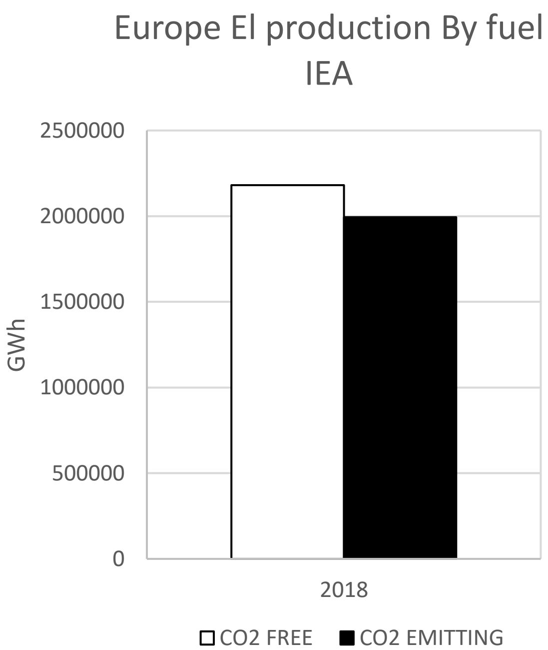

Figure 35 Breakdown of the European energy mix for electricity production in 2018 according to CO_2 emitting and clean fuels.

To evaluate these benefits, it was necessary to develop a methodology that would allow us to identify the savings in terms of emissions. In order to do this, we first considered the problem of which type of emissions to observe and take as reference. From the practice and the evidence we are going to show, it was decided to take CO2 emissions as a reference.

This conclusion was reached by associating to the energy mixes shown in the previous graphs Figure 29, Figure 30 the emissions of different types of atmospheric pollutants that cause climate change, indicated as the main ones by the International Panel for Climate Change, and comparing their entities.

These substances are:

- CO_2
- CH_4
- N_2O

Table 20 summary table of emission coefficients given by the IPCC and associated with the different categories of fuels given by the IEA. [52]

IEA FUEL	IPCC FUEL DENOMINATION	CO_2			CH_4			N_2O			Unit
		Default	Lower	Upper	Default	Lower	Upper	Default	Lower	Upper	
Coal	Anthracite	98300	94600	101000	1	0.3	3	1.5	0.5	5	Kg/TJ
	Coking Coal	94600	87300	101000	1	0.3	3	1.5	0.5	5	Kg/TJ
	Other Bituminous Coal	94600	89500	99700	1	0.3	3	1.5	0.5	5	Kg/TJ
	Sub-Bituminous Coal	96100	92800	100000	1	0.3	3	1.5	0.5	5	Kg/TJ
	Lignite	101000	90900	115000	1	0.3	3	1.5	0.5	5	Kg/TJ
	Brown Coal Briquettes	97500	87300	109000	1	0.3	3	1.5	0.5	5	Kg/TJ
	Coke Oven Coke and Lignite Coke	107000	95700	119000	1	0.3	3	1.5	0.5	5	Kg/TJ
	AVERAGE	**98443**	**91157**	**106386**	**1**	**0.3**	**3**	**1.5**	**0.5**	**5**	Kg/TJ
Oil	Crude Oil	**73300**	**71100**	**75500**	**3**	**1**	**10**	**0.6**	**0.2**	**2**	Kg/TJ
Biofuels	Wood/Wood Waste	112000	95000	132000	30	10	100	4	1.5	15	Kg/TJ
	Other Primary Solid Biomass	100000	84700	117000	30	10	100	4	1.5	15	Kg/TJ
	Charcoal	112000	95000	132000	200	70	600	4	1.5	15	Kg/TJ
	Biogasoline	70800	59800	84300	3	1	10	0.6	0.2	2	Kg/TJ
	Biodiesel	70800	59800	84300	3	1	10	0.6	0.2	2	Kg/TJ
	Other Liquid Biofuels	79600	67100	95300	3	1	10	0.6	0.2	2	Kg/TJ
	Landfill Gas	54600	46200	66000	1	0.3	3	0.1	0.03	0.3	Kg/TJ
	Sludge Gas	54600	46200	66000	1	0.3	3	0.1	0.03	0.3	Kg/TJ
	Other Biogas	54600	46200	66000	1	0.3	3	0.1	0.03	0.3	Kg/TJ
	Municipal Wastes (biomass fraction)	100000	84700	117000	30	10	100	4	1.5	15	Kg/TJ
	AVERAGE	**80900**	**68470**	**95990**	**30.2**	**10.39**	**93.9**	**1.81**	**0.669**	**6.69**	Kg/TJ
Waste	Municipal Wastes (non-biomass fraction)	91700	73300	121000	30	10	100	4	1.5	15	Kg/TJ
	Industrial Wastes	143000	110000	183000	30	10	100	4	1.5	15	Kg/TJ
	AVERAGE	**117350**	**91650**	**152000**	**30**	**10**	**100**	**4**	**1.5**	**15**	Kg/TJ
Hydro		0	0	0	0	0	0	0	0	0	Kg/TJ
Other sources		0	0	0	0	0	0	0	0	0	Kg/TJ
Natural gas	Natural Gas	**56100**	**54300**	**58300**	**1**	**0.3**	**3**	**0.1**	**0.03**	**0.3**	Kg/TJ
Wind		0	0	0	0	0	0	0	0	0	Kg/TJ
Solar PV		0	0	0	0	0	0	0	0	0	Kg/TJ

The association of emissions was done through the use of different emission coefficients for each altering substance and for each fuel type. These coefficients are also provided in a table in [52] from which an extraction is given in the Table 20.

Due to the specificity of the headings in the IPCC document, it was necessary to group several fuels representing specific components of the IEA macrocategory under one heading. Finally, in order to be able to associate a coefficient to each macrocategory of the IEA, not having specific data on the weight of the different components for each macrocategory, the arithmetic average of the coefficients of the subcategories provided by the IPCC [52] was carried out. They can be read in the highlighted rows of the Table 20 and represented in Figure 36, Figure 37.

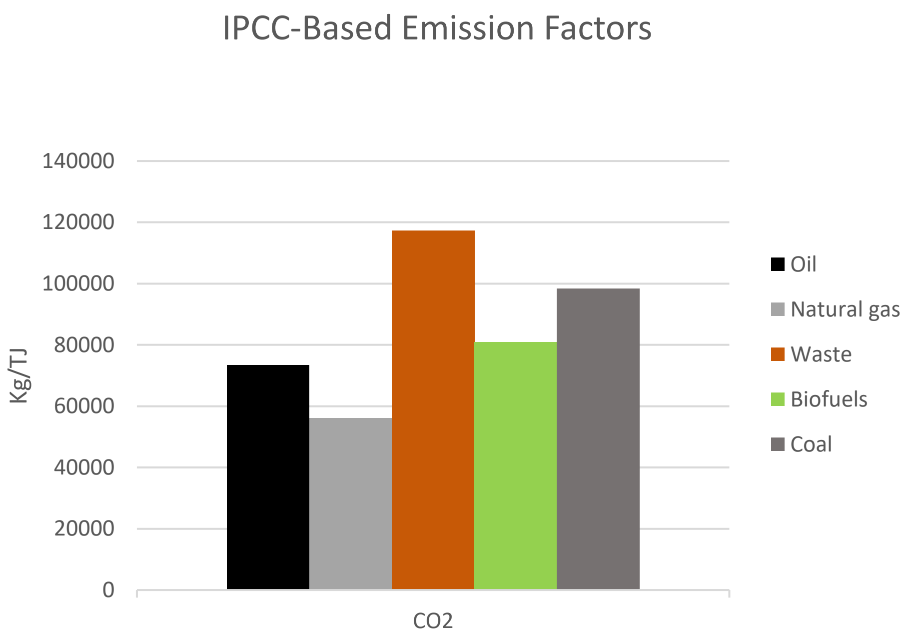

Figure 36 CO_2 emission factors per IEA fuel

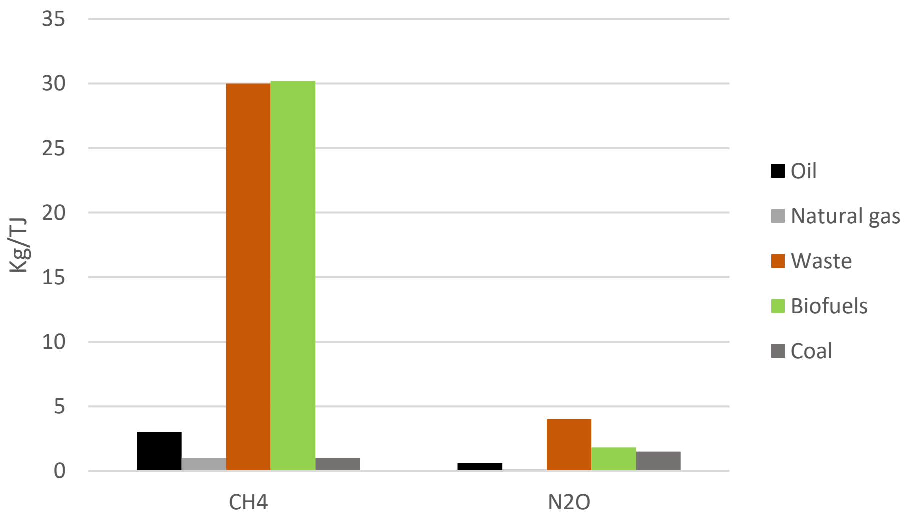

Figure 37 CH_4 and N_2O emission factors per IEA fuel

Combining these factors with the two 20-year series of energy mixes and normalising them for the total amount of electricity produced emission series for the three different pollutants per KWh of electricity produced in Norway and in an average European country respectively come out, which are shown in Figure 38, Figure 39.

As can be seen, the values of both N_2O and CH_4 are orders of magnitude lower than those of CO_2. Therefore, with reference to CO_2, we will identify the improvements in the climate-altering gas that is released in a more massive way and therefore represents an upper bound below which we will certainly find the values for N_2O and CH_4.

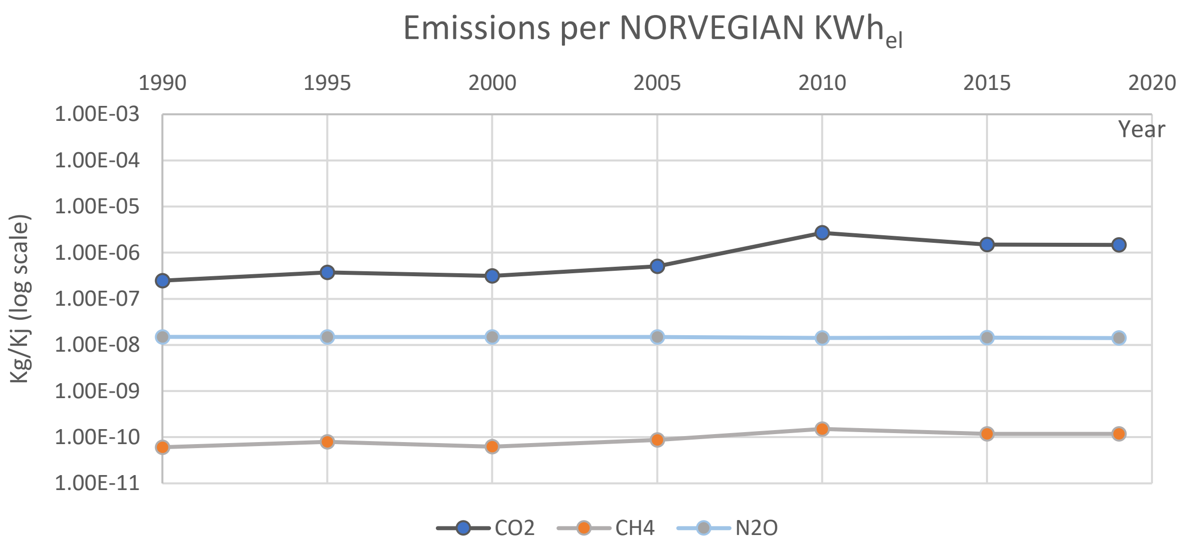

Figure 38 Pollutant emissions generated from the production of 1kWhel using Norway's national energy mix, 1990 to 2019

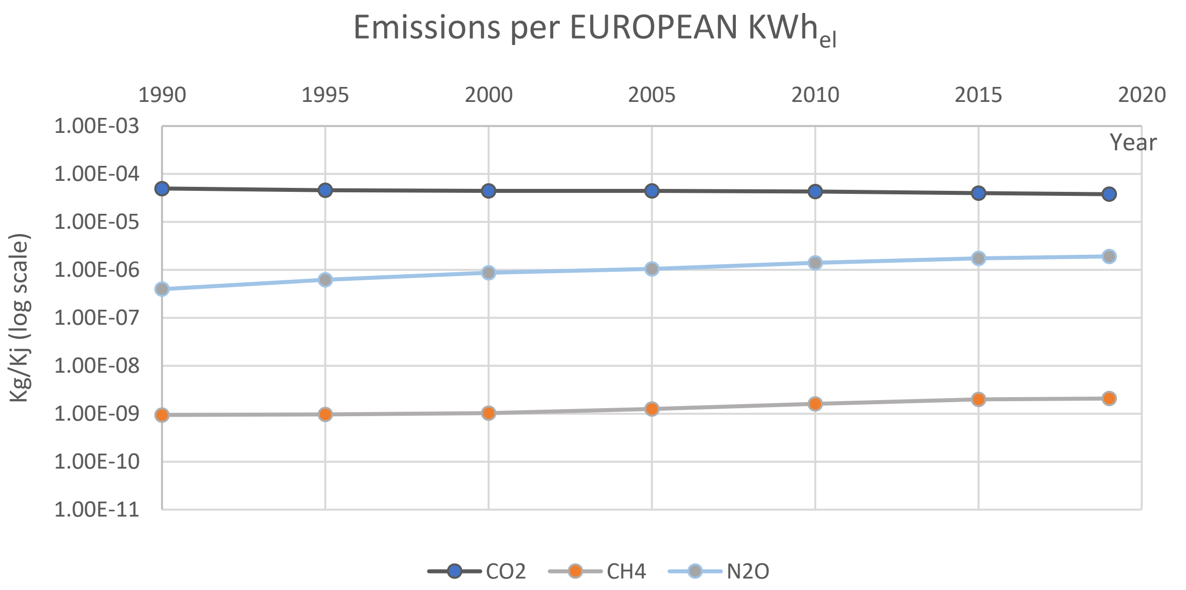

Figure 39 Pollutant emissions generated by the production of 1kWhel using the European energy mix, 1990 to 2018

Finally, it is pointed out that despite its virtuousness, Norway is still experiencing an increase in emissions (Figure 38) in the electricity production sector. This means that a solution such as the one proposed in this study would also benefit the Norwegian system.

3. METHODS

In this section we will first of all identify the way in which the problem has been tackled, i.e. the type of problem we have been faced with and the mathematical tool used to solve it.

Since, as we shall see, this is an optimisation problem, we shall identify the way in which the objective function has been defined and, therefore, the existing connections between the various components of the system and the various operating modes in which the latter may be found.

We will then be able to define the set of case studies to be analysed and implemented with simulations using PSO.

This done , we will finally illustrate all the operations and physical-mathematical relations suitable for the manipulation of the data collected as specified in the previous paragraph in order to produce the input data sets for the algorithm and therefore for the calculation of the value of the objective function.

3.1. PROBLEM AND OPTIMISATION ALGORITHM

The problem to be solved was, as already illustrated, to find the optimal solution for the installation of an electricity generation and storage plant as an alternative to the extension of the medium-sized distribution grid.

In order to compare the two solutions, the Levelized Cost of Electricity (LCOE) parameter was used, which includes both the cost of energy as such and the cost of investment and maintenance of the structure.

It was therefore a question of facing an optimisation problem in which the objective was to reach the minimum value of the objective function, i.e. the function that describes the LCOE.

In order to solve this problem, two main operations had to be carried out:

- Determine the structure of the objective function
- Choice and determine the optimisation algorithm to be used to identify the optimum of the objective function.

In this paragraph we will illustrate the choices made for the second point, while in the following paragraph we will indicate in detail how the objective function was modelled.

Since the software used for the elaboration of the data was MATLAB, we wanted to make use of one of the built-in algorithms provided by the software. Among the various proposals, the one used was an algorithm attributable to the category of heuristic optimisation algorithms called Particle Swarm Optimisation (PSO), which can be translated as "optimisation with swarms of particles" inspired by the movement of natural swarms.

The class of heuristic optimisation methods, in fact, involves the search for the optimum in a more intuitive way rather than based on a robust methodology that allows the exact identification of the solution (as can be implemented for example by a gradient method). This way of proceeding from attempt to attempt, but in an intuitive manner, following patterns that often follow behaviour observed in nature, makes it possible to reach the result more quickly than a more structured method. However, the use of heuristic methods, precisely because they are not deeply structured, does not provide a guarantee that the result identified actually corresponds to the absolute optimum existing in the objective function.

A greater guarantee on the results identified with the use of PSO comes from the fact that it is in particular a meta-heuristic method, which means that it does not make any specific assumptions about the problem and allows the exploration of very large solution spaces. This is because a meta-heuristic method is made up of a number of algorithms which are themselves heuristic in nature and which allow the main algorithm to be more robust and reliable by avoiding it always falling back on finding local minima rather than absolute minima.

The PSO optimises a problem using a population of candidate solutions (called "particles") that move in the search space on the basis of simple formulae, which take into account their current speed of movement, their knowledge of the fitness space (i.e. the best solution they have explored up to that point) and shared knowledge (i.e. the best general solution identified). The algorithm weighs these three components (inertia, cognitive and social) and uses small random jittering to minimise the possibility of trapping in local minima.

The PSO algorithm is called in the MATLAB environment through the following line of code:

```
[x,fval,exitflag] = particleswarm(fun,nvars,lb,ub,options)
```

in which the following elements can be identified:

`x`= vector containing the variables with which the optimum of the objective function was obtained.

`fval`= value of the objective function identified by the algorithm.

`exitflag`= numerical value describing the algorithm output conditions.

`fun`= field in which the objective function is called and defined.

`nvars`= definition of the number of input variables of the objective function and which are to be taken into account for variation from the PSO.

`lb`= lower limits of the search range of the algorithm, i.e. lower limits of the values that the different variables of the objective function can take.

`ub`= upper limits of the search range of the algorithm, i.e. upper limits of the values that the different variables of the objective function can take.

`options`= field in which some more specific options of the algorithm are indicated, such as the possibility of graphically printing the optimum of the successive iterations in order to graphically see the convergence of the algorithm, or parameters to define the three components of the algorithm: inertia, cognitive and social.

The only options defined in this system were:

- *Quantity of particles in the swarm*: 300 particles
- *Activation of the plotting of the optimums:* for the graphical detection of convergence, an example of which is given in Figure 40
- *Determination of the operating parameter* `MinNeighborsFraction`: 0.75

which are unchanged from those chosen for the optimisation of the DEMO4 objective function.

There are 2 ways to define the end of the optimisation process and therefore the exit from PSO:

- Achievement of a maximum number of consecutive iterations, identified through the `MaxStallIterations` variable with a default value of 20, in which the results of the objective function do not produce a relative error greater than a certain tolerance chosen and identified by the `FunctionTolerance` option set by default equal to 1e-6.

- Reaching a maximum number of iterations regardless of the tolerance reached. This number of iterations is identified by the `Maxiterations` variable whose default value is 200*n_var where n_var is the number of variables of the target function. It follows that for us `MaxIterations = 1200.`

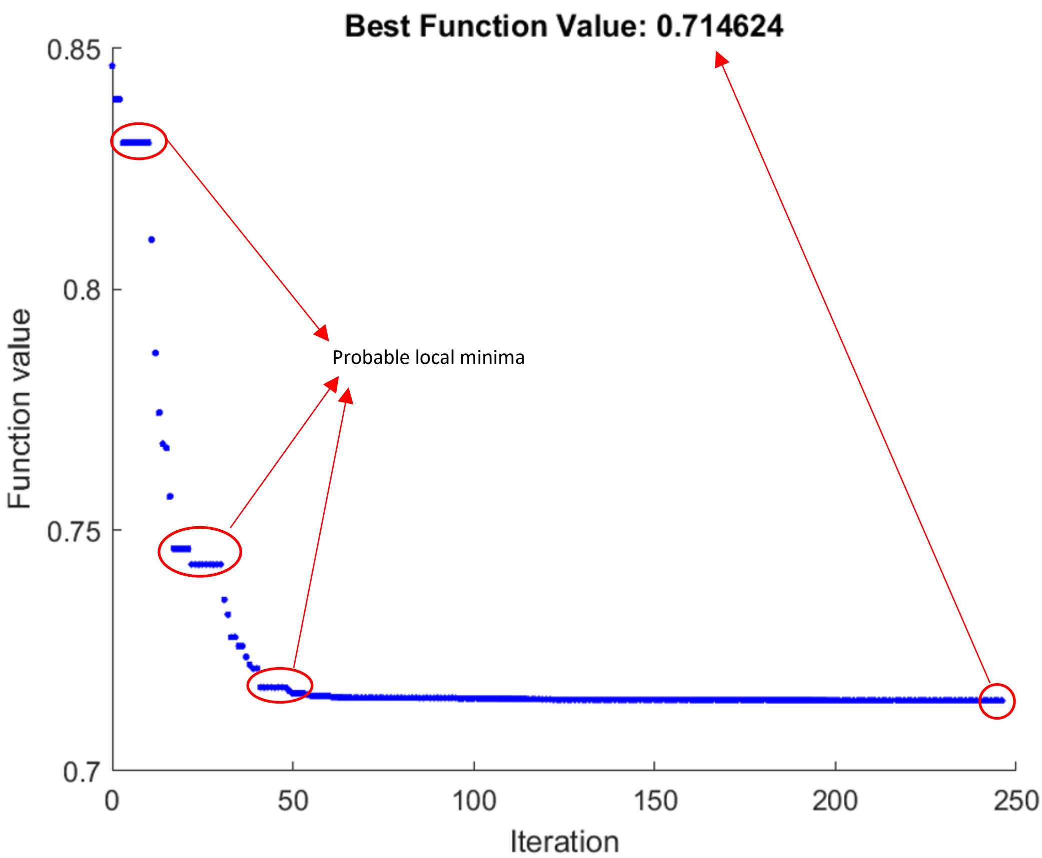

Figure 40 Example of convergence of the results of the objective function during the search for the optimum by PSO

Since, as mentioned above, a heuristic method does not guarantee 100% correctness of the solution for each optimisation attempt made, we were forced to identify a methodology to ensure the reliability of a solution. This methodology consisted in carrying out the optimisation of the objective function defined by the same series of input data a number of times necessary to obtain for at least 3 times the minimum solution identified among the different attempts.

3.2. OBJECTIVE FUNCTION AND CASES OF OPERATION OF THE SYSTEM

In this section, the objective function whose optimums are to be found with the PSO algorithm, is described. The different operating conditions under which the system was tested, i.e. the different cases of system configuration that have been considered as case studies in this work, are also explained.

As anticipated, the objective function will be the one for calculating the LCOE. This prerogative can only be satisfied by a way of structuring the function that takes into account the processing of two main groups of data sets which together also constitute the input variables or constants of the function:

- Series of physical-energy data for determining and assigning the load coverage mode. These include:
    - Annual hourly output series of the solar plant
    - Annual hourly output series of the wind plant
    - Annual hourly load series (PPL, FPL)
    - Coefficients for constraint of operability of storage and processing technologies

- A set of technical and economic data to determine the costs of the technologies used and the energy flows between the production-storage-load system and the grid and their evolution over the system's lifetime.
    - Annual hourly series of the purchase price of energy from the grid
    - Annual hourly series of the selling price of energy to the grid
    - Series of technical and economic data of the different technologies making up the system (CAPEX, OPEX, Replacement cost, lifetime)
    - Coefficients for discounting the value of the investment

Among the input data needed to complete the objective function we have:

- Definition of maximum network capacity
- Definition of the GPS_target parameter or "Grid Penetration Share"_target which corresponds to the maximum percentage of load that can be satisfied throughout the year by energy purchased directly from the grid. This parameter was created as a natural adaptation to this system of the more general LPSP parameter used in the modelling of the DEMO4 system objective function, which expressed the maximum percentage of load that could not be satisfied throughout the year.

Some of these data are manually inserted directly into the function code, while others are considered as external inputs. To the first group belong mainly constant data that do not represent time series, except for the maximum network capacity and GPS_target that are also considered as external inputs.

We chose to follow this insertion scheme because we wanted to make the code as flexible as possible with regard to its adaptability to different conditions related to the information concerning the installation site. In this way, a hypothetical extraneous user could use the main algorithm quite easily and for a general evaluation of the solutions proposed by the system for a different application site. This eventuality is definitely more probable, or at least more frequent, than that of a user needing to vary the technical-economic data of the technologies, which would rather suggest the exercise of a more detailed type of investigation by the aforementioned user.

It follows that the script with which the objective function is called in the PSO algorithm is as follows:

```
fun_DEMO_h2_BT_GRID(x,v_PV,v_WIND,v_Pl,grid_cap,v_cost,v_price,GPS_target)
```

where:

x = vector of the 6 input variables generated by the PSO algorithm to find the optimum. These variables consist of the power or capacity values attributed to each technology of the system and together they constitute the dimensioning of the system itself. In particular they are:

- P_rated_PV [kW]: rated power of the PV system
- P_rated_wind [kW]: rated power of the wind system
- P_Fcnom [kW]: nominal power of the fuel cell
- P_Elnom [kW]: nominal power of the electrolyzer
- E_ACC [kWh]: capacity of the hydrogen storage
- E_BT [kWh]: capacity of the battery

`v_PV`= vector of the timeseries of a 1kW PV panel producibility

`v_WIND`= vector of the timeseries of a 1kW Wind Turbine producibility

`v_Pl`= load time series vector

`grid_cap`= value of installed grid capacity

`v_cost`= time series vector of costs for energy purchased from the grid

`v_price`= time series vector of prices for energy sales to the grid

`GPS_target`= value of GPS_target

The methods by which these input data are derived from the data acquired from the sources as reported in chapter "2.COLLECTION OF INPUT DATA" will be explained in the following sections of this chapter.

Given the type of input data, we can then proceed to define the actual structure of the function. LCOE is then defined according to a process that is divided into two macro-steps as already identified by the types of inputs involved and listed above:

- STEP I: Identification of the size of the energy flows between the different components of the system so that the GPS_target is respected. These are defined on the basis of the way in which the system is operated, which mainly derives from the availability of energy produced by renewable technologies (PV and WT). These operation cases can be 3:

  - *SURPLUS of production*: system production > load required
  - *NEUTRALITY*: system production = load required
  - *DEFICIT of production*: system production < load required

- STEP II: allocation of costs to any interchange flows with the network, allocation of different investment costs, projection of costs over the 20-year life and their discounting, determination of the LCOE.

In next 2 paragraphs we will further specify the types of operations that are carried out in the two steps by listing the significant output series for both and in particular providing for STEP I examples for each operative situation that could occur.

3.2.1. STEP I

After the arbitrary allocation to the sizing values of the different technologies provided by PSO, the different nominal effective output series that can be provided by the renewable generation technologies are immediately calculated.

These series are then compared in a time-based loop to identify the mode in which the system is operating among the three listed above, which we see in more detail below and of which schematic example representations are given (from Figure 42 a Figure 51) complete with numerical examples to facilitate reading.

To well understand the examples we must state here a anticipation of what will be more accurately presented in the section dedicated to money fluxes. Indeed, it has to be assumed that, because of the regulations of Norway about the management of the energy produced by privates and used by themselves, the energy produced has firstly to be sold to the regional or national grid and then bought back to be used. From here on we'll referred to this mechanism as sell-buyback mechanism and it's shown in Figure 41. This process could be possible until the grid capacity is fulfilled, then here is assumed that the energy produced can be directly used bypassing the regional or national grid.

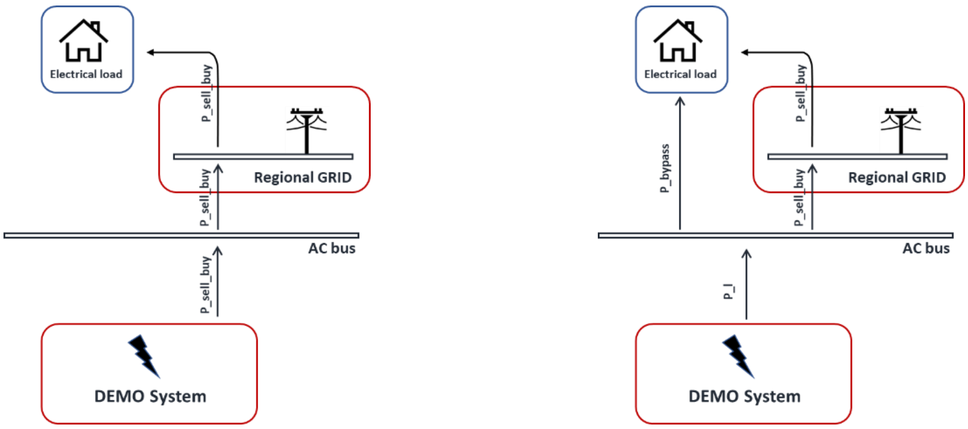

Figure 41 explanation of the sell-buyback mechanism. On the left with enough capacity of the grid to accept all the power produced to be directly consumed on the right the case the capacity is not enough

SURPLUS of production

This situation occurs when production is greater than the actual amount of load required. In this case, therefore, what is defined as SURPLUS is excess production, which can be managed in 3 different ways listed below according to the priorities imposed in the code:

- *Accumulation in storage technologies* (if capacity is available): in this case priority is always given to the use of the battery as it represents the technology with the fastest and most flexible response capacity. In case the battery capacity does not allow the storage of all the SURPLUS, H2 production and accumulation is used with the necessary activation of the Electrolyser.
- *Sale to the grid* (only in grid-connected cases if capacity is available)
- *Curtailment of excess production*: which is the extreme solution and the least advantageous both from an energy and economic point of view

The logic with which SURPLUS is managed is detailed in the Figure 42 while the different management cases are shown in the numerical examples associated with the schemes Figure 43, Figure 44, Figure 45, Figure 46, Figure 47.

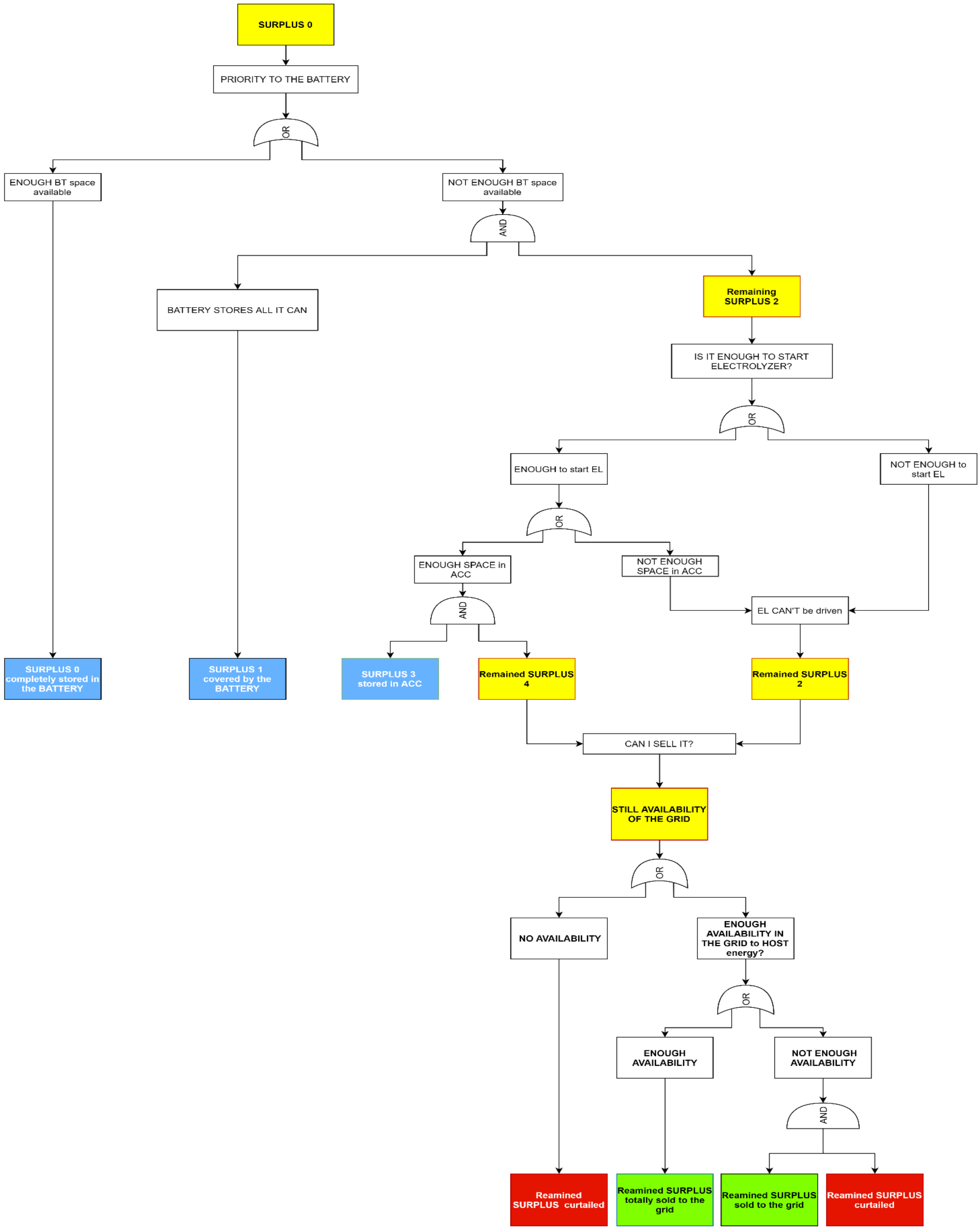

Figure 42 logic scheme of the surplus management

CASE 1: Surplus/ Enough Space in Storage /Load≤Grid_cap_max

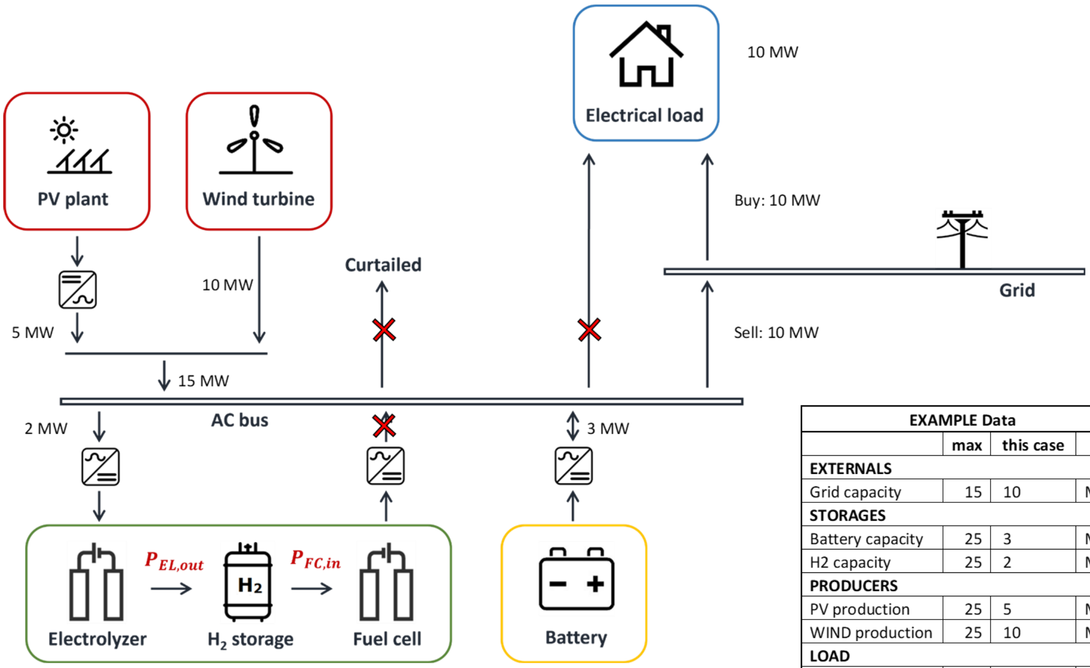

EXAMPLE Data			
	max	this case	
EXTERNALS			
Grid capacity	15	10	MW
STORAGES			
Battery capacity	25	3	MW
H2 capacity	25	2	MW
PRODUCERS			
PV production	25	5	MW
WIND production	25	10	MW
LOAD			
Load required	40	10	MW

Figure 43 Surplus management scheme and related numerical example if there is enough storage space to accept all the surplus and enough grid availability to sell and buy back the energy produced and directly consumed

CASE 2: Surplus/ NOT Enough Space in Storage/Enough Grid/Load≤Grid_cap_max

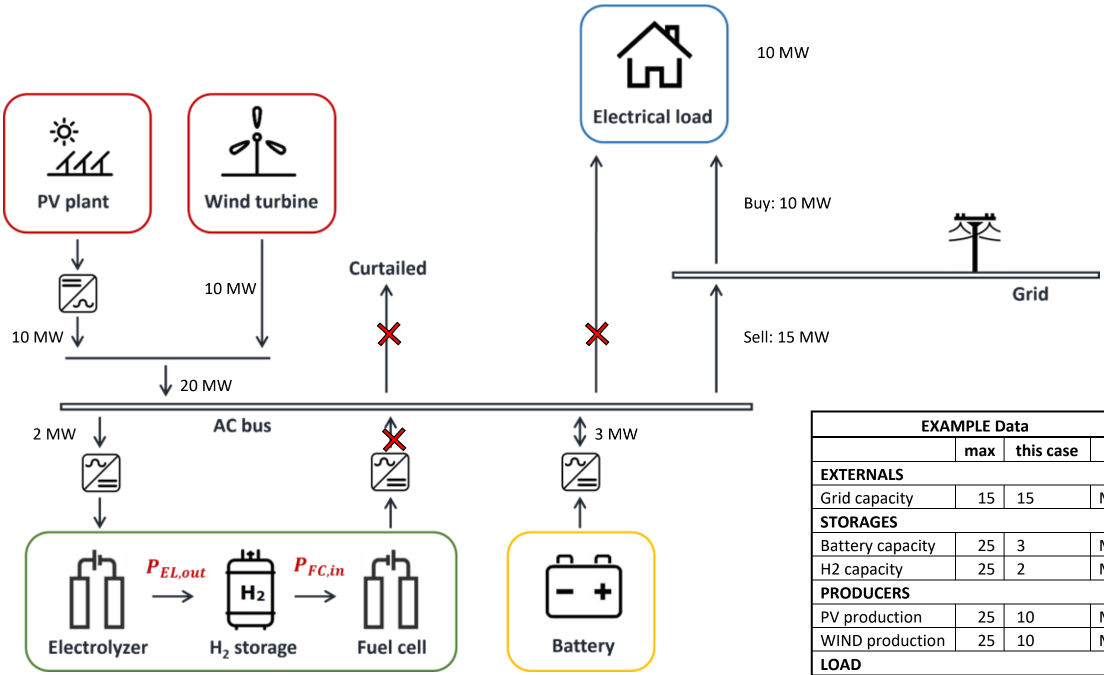

EXAMPLE Data			
	max	this case	
EXTERNALS			
Grid capacity	15	15	MW
STORAGES			
Battery capacity	25	3	MW
H2 capacity	25	2	MW
PRODUCERS			
PV production	25	10	MW
WIND production	25	10	MW
LOAD			
Load required	40	10	MW

Figure 44 Surplus management scheme and related numerical example in case there is NOT enough storage space to host all the surplus and there is enough grid availability to sell and buy back the energy produced and directly consumed and sell all the non-storageable surplus

CASE 3: Surplus/ NOT Enough Space in Storage/NOT Enough Grid/Load≤Grid_cap_max

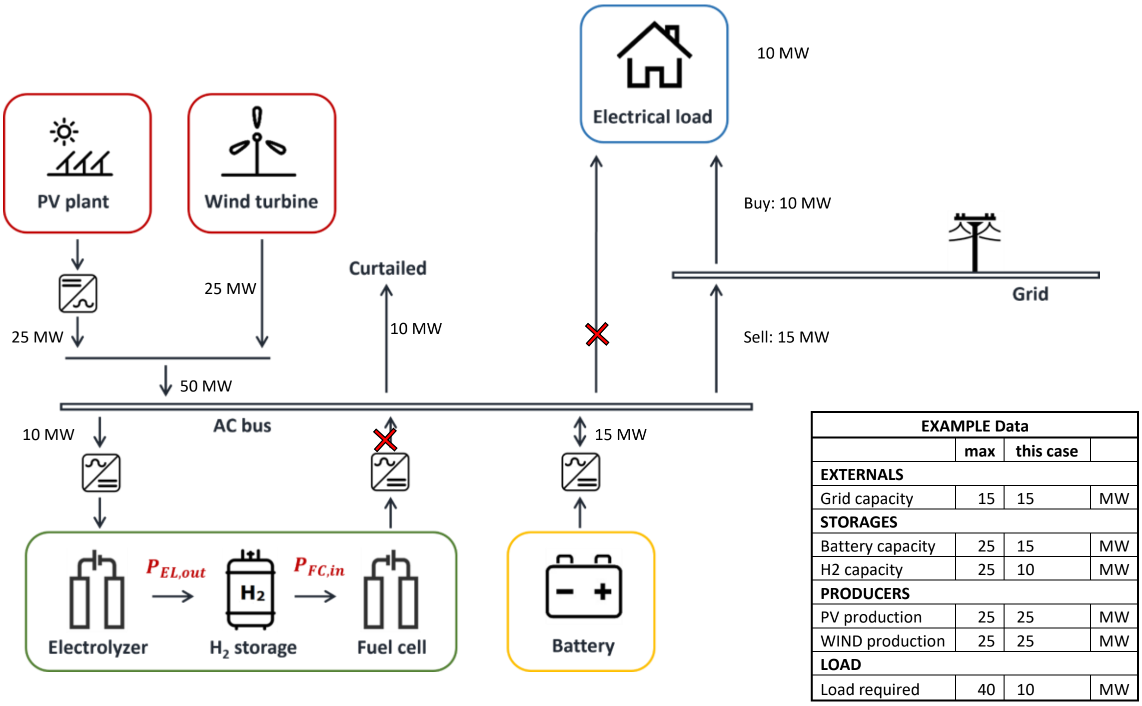

EXAMPLE Data			
	max	this case	
EXTERNALS			
Grid capacity	15	15	MW
STORAGES			
Battery capacity	25	15	MW
H2 capacity	25	10	MW
PRODUCERS			
PV production	25	25	MW
WIND production	25	25	MW
LOAD			
Load required	40	10	MW

Figure 45 Surplus management scheme and related numerical example in case there is NOT enough storage space to contain all the surplus, there is enough grid availability to sell and buy back the energy produced and directly consumed but not to sell all the non-storageable surplus that has to be partially curtailed.

CASE 4: Surplus/ Enough Space in Storage/Load>Grid_cap_max

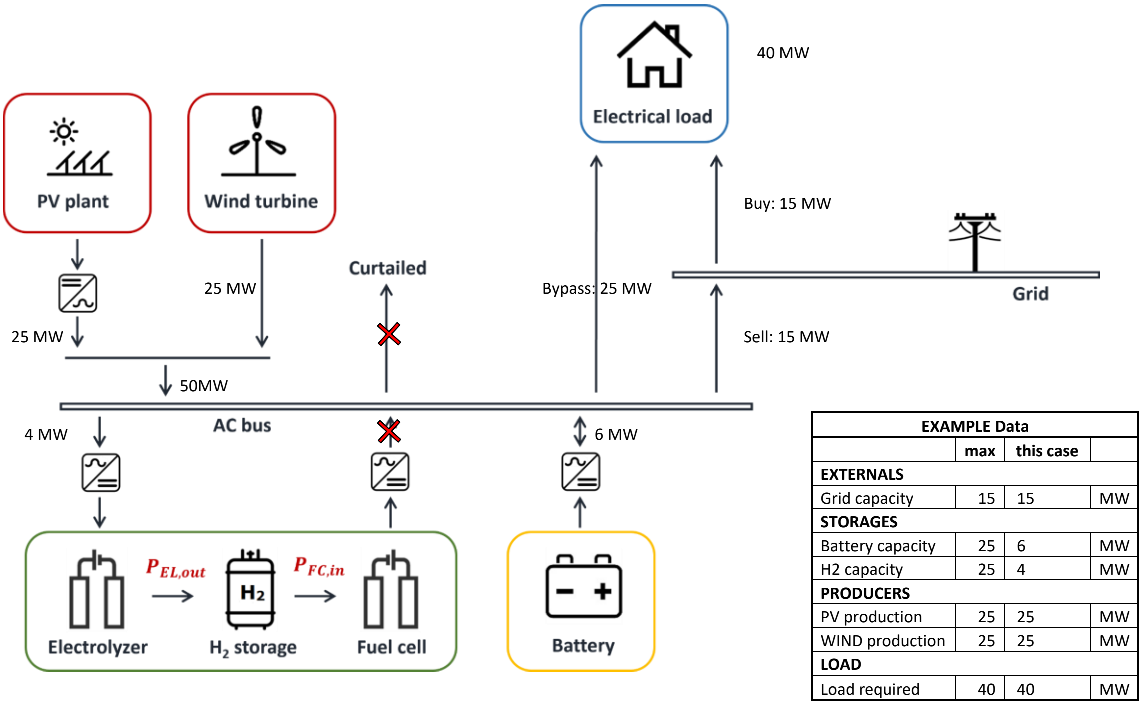

EXAMPLE Data			
	max	this case	
EXTERNALS			
Grid capacity	15	15	MW
STORAGES			
Battery capacity	25	6	MW
H2 capacity	25	4	MW
PRODUCERS			
PV production	25	25	MW
WIND production	25	25	MW
LOAD			
Load required	40	40	MW

Figure 46 Surplus management scheme and related numerical example where there is enough storage space to accept all the surplus and NOT enough grid availability to sell and buy back the energy produced and directly consumed, a proportion of which will bypass the grid and arrive directly at the load.

CASE 5: Surplus/ NOT Enough Space in Storage /Load>Grid_cap_max

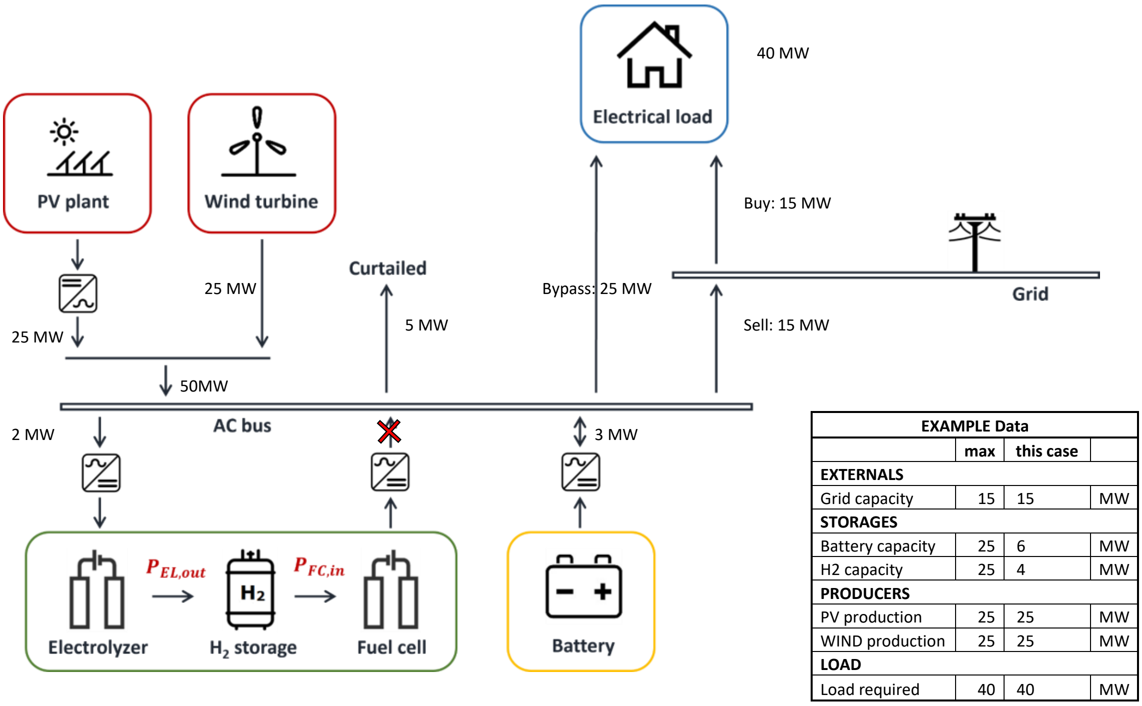

EXAMPLE Data			
	max	this case	
EXTERNALS			
Grid capacity	15	15	MW
STORAGES			
Battery capacity	25	6	MW
H2 capacity	25	4	MW
PRODUCERS			
PV production	25	25	MW
WIND production	25	25	MW
LOAD			
Load required	40	40	MW

Figure 47 Surplus management scheme and related numerical example in the case where there is NOT enough storage space to contain all the surplus and NOT enough grid availability to: sell and buy back the energy produced and directly consumed of which a portion will bypass the grid and arrive directly at the load; sell the non-storageable surplus which is completely curtailed.

System Neutrality

This situation has no particular need of explanation as it simply involves the case where the amount of production covers exactly the amount of load required. As can be intuitively understood, this is the rarest situation in which the system finds itself. From an economic point of view, moreover, it does not represent an advantage for the system if we consider the format of integration with the network. This is because, as we will see later, the system is bound to sell the production destined for direct consumption first to the network (up to its saturation) and then buy it back, which is disadvantageous since the revenues from the sale are less than the costs of purchase.

DEFICIT of production

A DEFICIT occurs when the system production in that hour is not sufficient to cover the requested load directly. The production shortfall is therefore defined as a DEFICIT and its management can involve 2 ways which, as in the case of SURPLUS, are reported here hierarchically according to the priority assignment provided for in the code and the logical scheme of which is reported in Figure 48:

- *Exploiting energy stored in storage technologies*. In this case too, the technology that is given priority is the battery, again because of its versatility and speed of response. In the event of demand not being met by the battery, the energy reserve stored as H2 is then exploited with the necessary activation of the PEM Fuel Cell. It is reported in particular the fact that in this last case, the FC could actually deliver more energy than it needs to cover the surplus only, condition summarized in the inequality:

$$DEFICIT < (Max\ energy\ deliverable\ by\ BAT + Min\ energy\ derivable\ by\ PEMFC)$$

This is due to the operational constraints imposed on PEMEL and PEMFC, which cannot operate below a certain power threshold and which is therefore associated with the minimum amount of energy that can be stored or produced by these transformation technologies respectively. It follows that in these cases there is also the question of managing this quantity of energy, which is produced in a constrained manner but which is not totally used to cover the DEFICIT, which is lower than it.

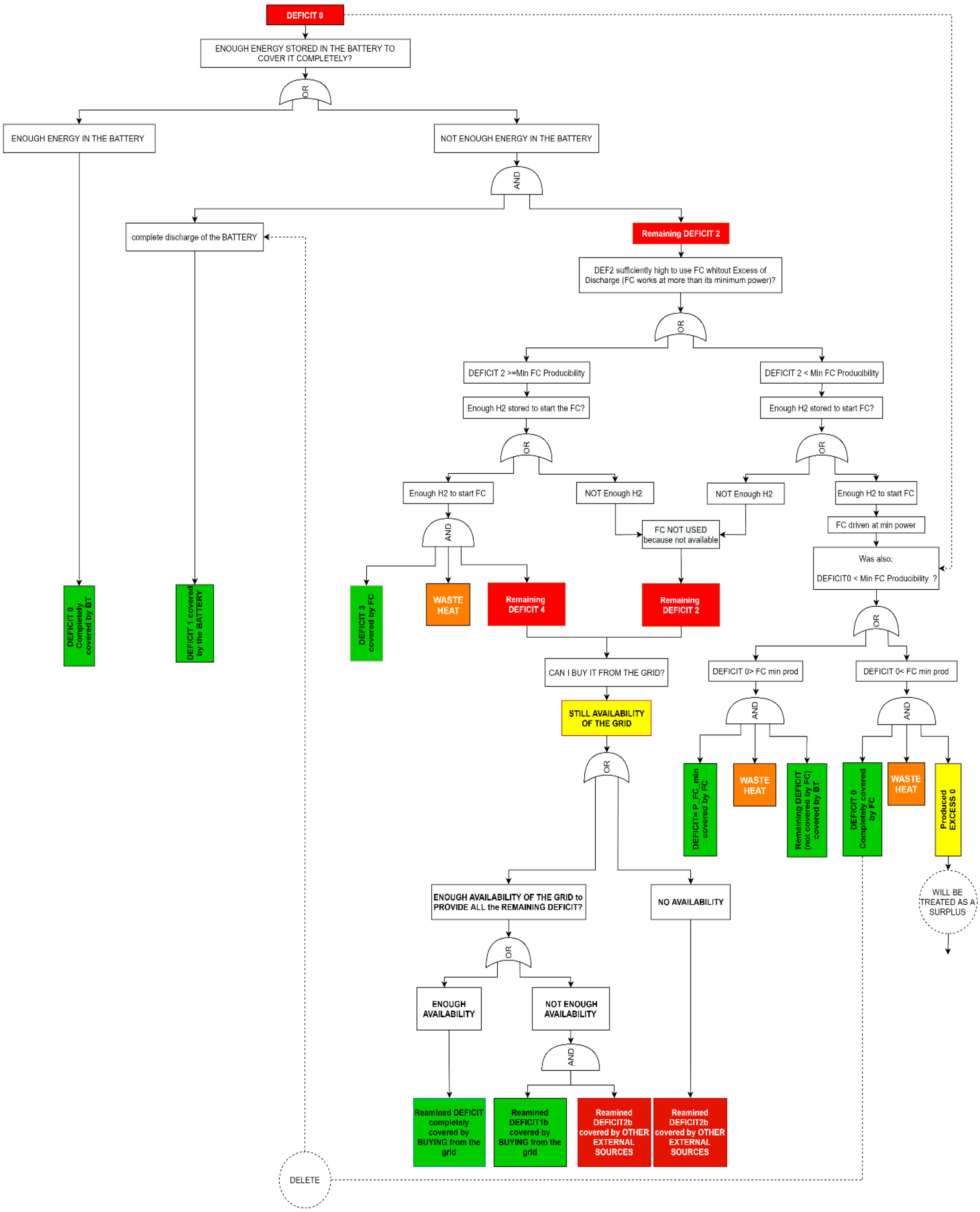

Figure 48 Logic scheme of the deficit management

There are two possible alternatives for managing it, which can be implemented depending on the characteristics of the starting deficit (which must always be greater than the minimum energy that can be delivered by the battery at that moment):

- $DEFICIT > Min\ energy\ deliverable\ by\ PEMFC$: In this case, the code provides for a change of priority by first imposing the choice of hydrogen storage, which is exploited at minimum power by the PEMFC operating at its minimum power, and then the conclusion of coverage by the battery. In this way, no excess production is generated in the management of the DEFICIT.

- $DEFICIT < Min\ energy\ deliverable\ by\ PEMFC$: In this case too, the code imposes the cancellation of the prescribed hierarchy, but definitively excludes the intervention of the battery, limiting itself to using the energy stored in the form of hydrogen through the operation of the PEMFC at the minimum available power. In this second case, however, an overproduction of energy is also generated, which must in turn be managed for the DEFICIT. Unlike what was assumed in the case of DEMO4, it was decided to treat this excess exactly like any other surplus, thus giving the system the possibility of re-stocking it, selling it to the grid or dispersing it. This is because of the size of the flows which, being already greater in the current case than in the DEMO4 application, will be even greater in the case of future load.

- *Purchase from the grid* (only in grid-connected cases and depending on grid availability)

Again, the different management cases are shown in the numerical examples associated with the schemes Figure 49, Figure 50, Figure 51.

CASE 1: Deficit/Enough Storage/Load≤Grid_cap_max

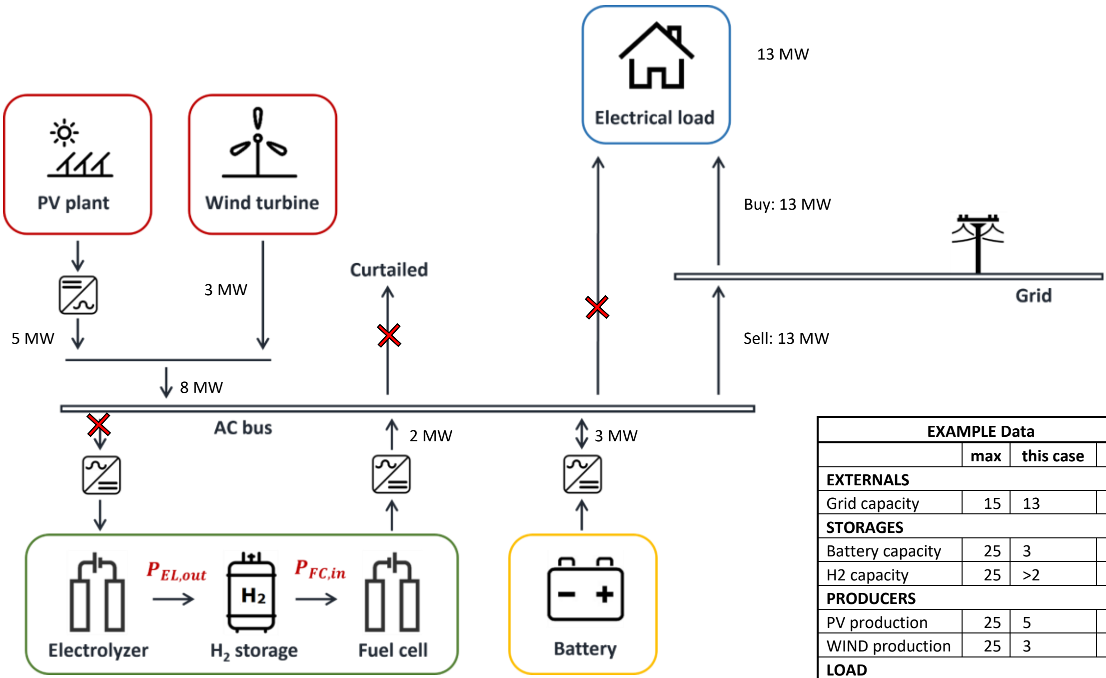

EXAMPLE Data	max	this case	
EXTERNALS			
Grid capacity	15	13	MW
STORAGES			
Battery capacity	25	3	MW
H2 capacity	25	>2	MW
PRODUCERS			
PV production	25	5	MW
WIND production	25	3	MW
LOAD			
Load required	40	13	MW

Figure 49 Deficit management scheme and related numerical example in case there is enough availability in the storage to complete the load coverage and there is enough grid availability to sell and buy back all the energy coming from the grid system for the load.

CASE 2: Deficit/Enough Storage/Load>Grid_cap_max

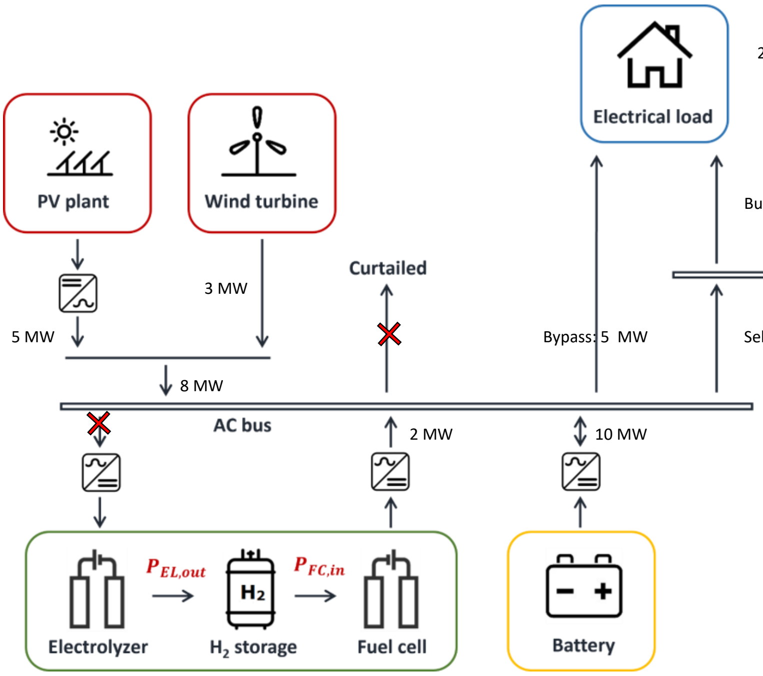

EXAMPLE Data			
	max	this case	
EXTERNALS			
Grid capacity	15	15	MW
STORAGES			
Battery capacity	25	10	MW
H2 capacity	25	>2	MW
PRODUCERS			
PV production	25	5	MW
WIND production	25	3	MW
LOAD			
Load required	40	20	MW

Figure 50 Deficit management scheme and related numerical example in the case where there is enough availability in storage to complete load coverage but NOT enough grid availability to sell and buy back all the energy coming from the system to the load, part of which will then bypass the grid and arrive directly at the load.

CASE 3: Deficit/NOT Enough Storage/Load≤Grid_cap_max

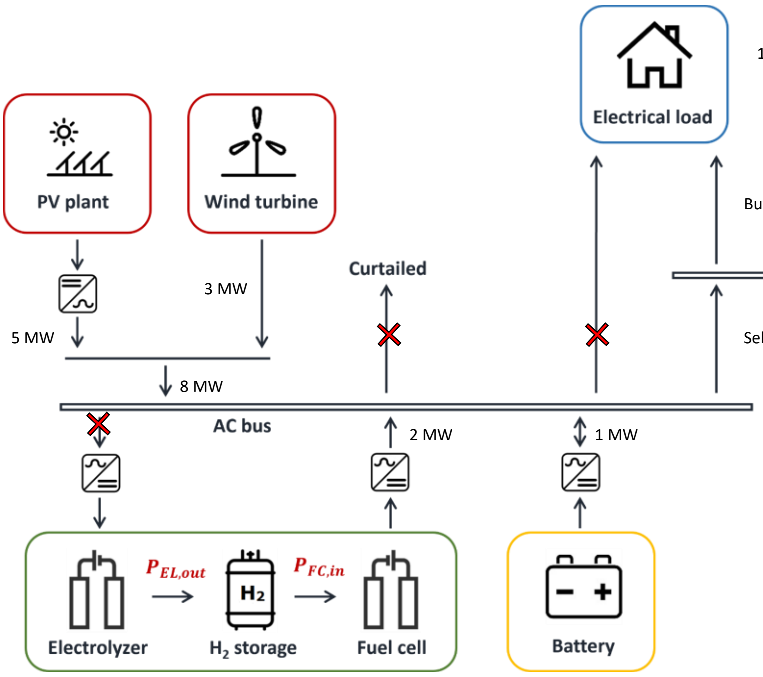

EXAMPLE Data			
	max	this case	
EXTERNALS			
Grid capacity	15	15	MW
STORAGES			
Battery capacity	25	1	MW
H2 capacity	25	2	MW
PRODUCERS			
PV production	25	5	MW
WIND production	25	3	MW
LOAD			
Load required	40	15	MW

Figure 51 Deficiency management scheme and related numerical example in the case where there is NOT enough availability in storage to complete the load coverage but there is enough grid availability to sell and buy back all the energy from the system for the load and provide the missing coverage.

It is necessary to consider the fact that, as mentioned at the beginning of this paragraph, in both cases of surplus and deficit, the energy supplied by the system, whether it comes directly from the production section or from both the production and storage sections, must by law be first sold to the grid and then bought back by the system for use. This process referred to as SELL-BUYBACK can be carried out as long as the network capacity is not saturated. In case the flows from the system exceed the available network capacity the excess can by-pass the SELL-BUYBACK process and thus be used internally without the allocation of costs from buying and selling.

This particular assumption in the modelling actually represents a simplification compared to a real system where it should be instead taken into account a difference between the local network, the medium distribution network and the AC BUS network that connects the different elements of the system. In the model presented here, it is assumed that the BUS AC network is the only local network to which all the technologies in the system and the load on one side and the network on the other are connected, which is why the case of network bypass can be assumed (thing that does not represent the reality of the facts because it excludes the presence of a local network). However, for a study that is intended as a first general approach to solving the problem, this configuration is valid.

In simulations subsequent to those reported in this thesis and which will go into more detail in order to provide Tronder Energi with even more realistic results, the assumption made here of the merging of the local and system grids (and the consequences we will see in stage 2 respectively to the definition of the economic actors) will be overcome and defined in more detail.

The main output parameters of the first stage which will then be used for the second stage are therefore:

Table 21 Main output parameters from the hourly energy management section of the objective function (STEP 1)

Pl_GRID	Powerload_grid	Load amount covered by energy bought by the grid	kWh	Vector (h)
P_BUS_GRID	Power_BUS(side)_Grid	Power at AC BUS level (not accounting for the transformation losses) on the way to be sold to the grid	kW	Value*
P_sell_buy	Power_sell_buy	Power that occupies partially or totally the capacity of the grid because of sell-buyback operation which means amount of energy to be sold and re-bought before its use	kW	Value*
GPS	Grid Penetration Rate	Actual GPS obtained by the simulation	%	Value
*They are values changing at each loop step (which means at each hour)				

We want to underline that the GPS parameter listed in Table 21 is not the parameter defined as GPS_target but it is actually the GPS value calculated in the particular solution and that, to make the result valid, it must be equal or less than GPS_target. It is therefore the control and validation parameter of the whole simulation carried out with the input dimensions assumed at each cycle of the PSO. In fact, the condition for the registration of the final value of the LCOE (final output of the second stage and therefore of the whole function) is bound to the validity of the GPS as it is demonstrated below by reporting the last lines of code of the target function:

```
If GPS>GPS_target || LCOE<=0 || GPS<0
  LCOE=NaN;
end
```

As regards the way in which these parameters are assessed, refer to the next section [3.4.3] of this chapter.

3.2.2. STEP 2

With the processes implemented in the second stage, we arrive at the final parameter expression of the objective function, namely the LCOE. Four main steps can be identified:

I. Determination of

- investment costs attributable to the year of installation (CAPEX)
- O&M costs (OPEX)
- replacement costs if necessary

related to the technologies as dimensioned in the specific PSO step. The intermediate variables that describe them are:

Table 22 Objective function parameters containing investment and cost data associated with the first year of system life for each system component

c_capex_PEM_fc_system	cost_capex_PEM_fuelcell_system	normalized CAPEX of the fuel cell system evaluated through the cost function	€/kW	value
c_capex_el_system	cost_capex_Electrolyser_system	normalized CAPEX of the PEMEL evaluated through the cost function	€/kW	value
CAPEX_wind_pw	CAPEX_wind_power	CAPEX for the WT	€	value
CAPEX_PV_tot_pw	CAPEX_PV_total_power	CAPEX for the PV	€	value
CAPEX_inv_pw	CAPEX_inverter_power	CAPEX for the inverter	€	value
CAPEX_el_pw	CAPEX_electrolyzer_power	CAPEX for the PEMEL	€	value
CAPEX_PEM_fc_pw	CAPEX_PEM_fuelcell_power	CAPEX for the PEMFC	€	value
CAPEX_h2_tank_pw	CAPEX_h2_tank_power	CAPEX for the H2 TANK	€	value
CAPEX_bat_pw	CAPEX_battery_power	CAPEX for the BAT	€	value
v_OPEX_wind_0	vector_OPEX_wind_firstvalue	OPEX for the WT in the installation year	€	value
v_OPEX_PV_0	vector_OPEX_PV_firstvalue	OPEX for the PV in the installation year	€	value
v_OPEX_inv_0	vector_OPEX_inverter_firstvalue	OPEX for the inverter in the installation year	€	value
v_OPEX_el_0	vector_OPEX_electrolyzer_firstvalue	OPEX for the PEMEL in the installation year	€	value
v_OPEX_PEM_0	vector_OPEX_PEMFC_firstvalue	OPEX for the PEMFC in the installation year	€	value
v_OPEX_h2_tank_0	vector_OPEX_h2_tank_firstvalue	OPEX for the H2 TANK in the installation year	€	value
v_OPEX_bat_0	vector_OPEX_battery_firstvalue	OPEX for the BAT in the installation year	€	value

v_REP_wind_0	vector_REPLACEMENT_wind_firstvalue	REPLACEMENT cost evaluated for the WT in the installation year	€	value
v_REP_PV_panels_0	vector_REPLACEMENT_PV_firstvalue	REPLACEMENT cost evaluated for the PV in the installation year	€	value
v_REP_inv_0	vector_REPLACEMENT_inverter_firstvalue	REPLACEMENT cost evaluated for the inverter in the installation year	€	value
v_REP_el_0	vector_REPLACEMENT_PEMEL_firstvalue	REPLACEMENT cost evaluated for the PEMEL in the installation year	€	value
v_REP_PEM_fc_0	vector_REPLACEMENT_PEMFC_firstvalue	REPLACEMENT cost evaluated for the PEMFC in the installation year	€	value
v_REP_h2_tank_0	vector_REPLACEMENT_h2_tank_firstvalue	REPLACEMENT cost evaluated for the H2 TANK in the installation year	€	value
v_REP_bat_0	vector_REPLACEMENT_battery_firstvalue	REPLACEMENT cost evaluated for the BAT in the installation year	€	value

Note that the only 2 normalised CAPEX values in the table Table 22 which have been determined internally to the objective function refer to the PEMEL and PEMFC transformation technologies, i.e. the youngest technologies. In fact, as already mentioned above, for these two technologies it was very difficult to find an univocal price for the order of magnitude to which our system refers, and therefore cost functions were used which, inserted within the objective function, evaluate each time the nominal normalised capex for the technologies pertaining to the size in use. How these functions have been determined will be shown in the next section of this chapter [3.4.2].

II. Determination of the costs and revenues associated with the energy flows of exchange with the grid when present and available and their combination to generate a net value of annual cost/revenue attributable to the action of buying and selling energy with the grid. The evaluation of the single hourly flows is directly done during the different steps of the hourly loop that determines the entities of the different energy and power flows between the different technologies and is combined with the variables of the first 3 rows of the table Table 22. The determination of the annual net value is carried out outside this loop.

We would like to open a small parenthesis here to specify how the economic actors have been defined in this particular study to enable the reader to interpret as appropriately as possible what is meant by revenues and what is meant by costs. As properly defined in the illustration of STEP I we refer to the BUS AC network as the network connecting the storage and production system, the loads, and the external network. This simplification, which has led to neglecting the definition of the intermediate local network, has resulted in the following 2 economic actors being identified:

- SEMI-AUTONOMOUS USER/AUTONOMOUS USER: this player consists of the set of loads, the production and storage system and the AC BUS network. It follows that the following economic flows are considered for it:

Table 23 Summary of economic items of expenditure and income associated with the economic actor "SEMI-AUTONOMOUS/AUTONOMOUS USER".

EXPENDITURES	REVENUES
Technology investment costs	Sale of energy to the grid if present and available
Operation and maintenance costs	
Costs of connecting and transporting energy in the medium distribution network	
Costs of purchasing electricity from the grid if present and if available	

It is therefore evident that energy flows that remain internal to this actor are not considered either for the calculation of expenditure or for the calculation of earnings. No economic flow is associated with them. We are talking in particular about:

  - Bypass flows of the SELL-BUYBACK mechanism
  - Flows related to the storage of surplus production

- ENERGY MANAGEMENT COMPANY OWNING THE MEDIUM DISTRIBUTION GRID: which is not always present and for which the following economic flows are defined as the natural counterparts of those defined for users

Table 24 Summary of economic items of expenditure and income associated with the economic player "GRID"

EXPENDITURES	REVENUES
Costs of purchasing electricity from the semi-autonomous user	Sale of energy to the semi-autonomous user
	Transport and authorisation fees for the connection and exchange of both incoming and outgoing energy

It follows that the final variable that for each year counts the net value among the following 3 types of economic flows

- Net from SELL-BUYBACK mechanism
- Net expenditure on energy purchases to cover the DEFICIT
- Net gains from the sale of energy from a SURPLUS of production

is taken into account in the objective function in a split between net costs and net incomes as follows:

Table 25 Parameters of the objective function associated with the economic flows related to the economic actor "Semi-autonomous/semiautonomous users".

cost_GRID	costs_Grid	total economic outcomes in the year due to interaction with the grid	€	value
rev_GRID	revenues_Grid	total economic incomes in the year due to interaction with the grid	€	value

III. Determination of the discount coefficients and discounting of all the cost and gain items OPEX, REPLACEMENT and GRID over the life of the system (in our case assumed to be 20 years) and of the load coverage. The calculation methods are always reported in the last section of this chapter while the intermediate variables defined at the end of this step are those reported in Table 26 .

Table 26 Annual series on a 20-year basis showing the investment, maintenance and replacement costs associated with each system component and updated

v_OPEX_wind_pw	vector_OPEX_wind_power	OPEX for the WT actualized year per year	€	Vector (y)
v_OPEX_PV_pw	vector_OPEX_PV_power	OPEX for the PV actualized year per year	€	Vector (y)
v_OPEX_inv_pw	vector_OPEX_inverter_power	OPEX for the inverter actualized year per year	€	Vector (y)
v_OPEX_el_pw	vector_OPEX_electrolyzer_power	OPEX for the PEMEL actualized year per year	€	Vector (y)
v_OPEX_PEM_fc_pw	vector_OPEX_PEMFC_power	OPEX for the PEMFC actualized year per year	€	Vector (y)
v_OPEX_h2_tank_pw	vector_OPEX_h2_tank_power	OPEX for the H2 TANK actualized year per year	€	Vector (y)
v_OPEX_bat_pw	vector_OPEX_BATTERY_power	OPEX for the BAT actualized year per year	€	Vector (y)
v_REP_wind_pw	vector_REPLACEMENT_wind_power	REPLACEMENT cost evaluated for the WT actualized year per year	€	Vector (y)
v_REP_PV_panels_pw	vector_REPLACEMENT_PV_power	REPLACEMENT cost evaluated for the PV actualized year per year	€	Vector (y)
v_REP_inv_pw	vector_REPLACEMENT_inverter_power	REPLACEMENT cost evaluated for the inverter actualized year per year	€	Vector (y)
v_REP_el_pw	vector_REPLACEMENT_PEMEL_power	REPLACEMENT cost evaluated for the PEMEL actualized year per year	€	Vector (y)
v_REP_PEM_fc_pw	vector_REPLACEMENT_PEMFC_power	REPLACEMENT cost evaluated for the PEMFC actualized year per year	€	Vector (y)
v_REP_h2_tank_pw	vector_REPLACEMENT_h2_tank_power	REPLACEMENT cost evaluated for the H2 TANK actualized year per year	€	Vector (y)
v_REP_bat_pw	vector_REPLACEMENT_BATTERY_power	REPLACEMENT cost evaluated for the BAT actualized year per year	€	Vector (y)
v_cost_GRID	vector_costs_(from the)Grid	total cost comin from interactions with the grid	€	Vector (y)

		actualized year per year		
v_rev_GRID	vector_revenues_(from the)Grid	total revenues comin from interactions with the grid actualized year per year	€	Vector (y)
v_L_system_pw	vector_LOAD_system_power	total load covered by the system actualized year per year	kWh	Vector (y)

IV. Determination of the Net Present Values associated with each component and determination of the value of the objective function (LCOE). The variables referred to are shown in Table 27

Table 27 Objective function parameters containing the Net Present Values (NPV) associated with each system component and used to determine the LCOE

NPV_wind	NetPresentValue_wind	€	value
NPV_PV	NetPresentValue_PV	€	value
NPV_inv	NetPresentValue_inv	€	value
NPV_el	NetPresentValue_electrolyzer	€	value
NPV_fc	NetPresentValue_fuelcell	€	value
NPV_h2_tank	NetPresentValue_h2_tank	€	value
NPV_bat	NetPresentValue_bat	€	value
NPV_grid	NetPresentValue_grid	€	value
NPV_tot	NetPresentValue_tot	€	value
L_system_pw	L_system_power	kWh	value
LCOE	LevelizedCostOfEnergy	€/kWh	value

3.3. STUDY CASES

Now that the structure of the objective function has been fully defined and the technical-economic relations between the various components have been described in detail (even if only qualitatively), we can go on presenting the various case studies that have been investigated.

Since the fundamental break with the DEMO4 modelling was the introduction of grid integration, we wanted to investigate in depth the effect this had on the LCOE by studying the solutions produced by the PSO for a range of different GPS_targets. This describes a range of situations from "being able to fully rely on the availability of maximum grid capacity throughout the year" (GPS_target=100%) to the "complete absence of the possibility to use the grid" (off-grid case, GPS_target=0%). This range of possibilities was then translated by assuming GPS_targets decreasing each time by 10% starting from the case of complete availability arriving to the case of complete unavailability.

The series of simulations thus defined was then reproduced three times in order to investigate the variation of the solutions according to the variation of the type of meteorological data series. In fact, as we have seen, the latter are structured differently as they are associated with two different types of time series (TMY and RealYear).

Finally, in order to try to understand the incidence of a possible size effect of the technologies, but above all as required by Tronder Energi, the series defined as above were repeated with reference to the 2 different load series presented in the chapter 2"COLLECTION OF INPUT DATA" (PPL, FPL). This distinction was in fact absolutely necessary in order to investigate a solution to the problem posed by the company, which was that of an increase in load not followed by an increase in the availability of energy from the grid (which is not yet the case of today but will occur in the future).

So, the series of simulations carried out are shown in Table 28 which is a table with multiple inputs.

Table 28 Table summarising the simulations carried out, which make up the totality of the case studies tackled

		RES TIMESERIES			
		TMY	2014	2015	
LOAD TIMESERIES	PRESENT (2019)	100%	100%	100%	GPS_target
		90%	90%	90%	
		80%	80%	80%	
		70%	70%	70%	
		60%	60%	60%	
		50%	50%	50%	
		40%	40%	40%	GPS_target
		30%	30%	30%	
		20%	20%	20%	
		10%	10%	10%	
		0%	0%	0%	
	FUTURE	100%	100%	100%	GPS_target
		90%	90%	90%	
		80%	80%	80%	
		70%	70%	70%	
		60%	60%	60%	
		50%	50%	50%	
		40%	40%	40%	GPS_target
		30%	30%	30%	
		20%	20%	20%	
		10%	10%	10%	
		0%	0%	0%	
		GPS_target		GPS_target	

As we can then see in the section 4 ."RESULTS" the simulations carried out are actually slightly less than those reported in the table because it will be impossible in the case of future load to cover the load with only the grid availability.

For the sake of brevity, from now on we will refer to the simulation we want to talk about by giving the references of the 3 input coordinates of the Table 28 according to the following writing:

SIM_RES"*name of the RES timeserie*"**_L**" 'P' *for PPL* or 'F' *for FPL*"**_GPS**"*value of GPS_target*"

For example, to indicate the simulation carried out with the res belonging to 2015, the future load series and GPS_target=30% we will have the following identification code:

"SIM_RES2015_LF_GPS30"

3.4. EQUATIONS AND METHODS FOR DATA PROCESSING

In this section we are going to illustrate all the mathematical procedures that have allowed us to work out:

- data obtained from the sources mentioned in chapter 2."**Errore. L'origine riferimento non è stata trovata.**" in order to make them inputs for the objective function
- the input data within the objective function for the calculation of the LCOE
- data necessary for the determination of emissions both at the state of the art and when the system is installed

3.4.1. SET OF INPUTS FOR THE OBJECTIVE FUNCTION

As we have seen, the objective function mainly needs 5 sets of data, of which:

- 1 relativa al carico da soddisfare (v_Pl_year)
- 2 data sets derived from meteorological data taken from PVGIS:
  - Normalised hourly output of a photovoltaic panel (v_Ps_year_PV)
  - Normalised hourly output of a wind turbine (v_Ps_year_WIND)
- 2 datasets on energy price as part of its purchase and sale with the grid:
  - Hourly cost of purchased energy (v_cost)
  - Hourly price of energy sold (v_price)

Let us therefore see how these series have been defined one by one.

Power required from the load in the future (v_Pl_year(*future*))

The definition of the power required by the load in the time series referring to the present (2019) does not need to be modified from that provided by Tronder Energi and in fact has already been reported in the section " LOAD" del capitolo "2.COLLECTION OF INPUT DATA" and is visible in Figure 2, Figure 3 both in disaggregated and aggregated mode for the different load components. Reference is made to the maximum load that can be demanded in its current state with Pl_max_p having a value of $2MW_{el}$.

On the other hand, the load series referring to the future conditions under which the site will be located was not provided and therefore had to be calculated. Tronder Energi did, however, provide us with an estimate of the maximum rated power required by the load defined as Pl_max_f of approximately $8MW_{el}$.

It was therefore decided to derive the series referring to future time by means of a linear projection of the load through the determination of the proportionality coefficient existing between the maximum loads that can be demanded. This coefficient will then be defined as:

$$c_l = \frac{Pl_{max_f}}{Pl_{max_p}} = 4 \tag{1}$$

Applying this coefficient to the time series for 2019, we will have:

$$v_{Pl_{year}}(t_f) = c_l \, v_{Pl_{year}}(t_{2019}) = 4 \, v_{Pl_{year}}(t_{2019}) \tag{2}$$

The comparison between the two series demonstrating the reciprocal proportionality is shown in Figure 52

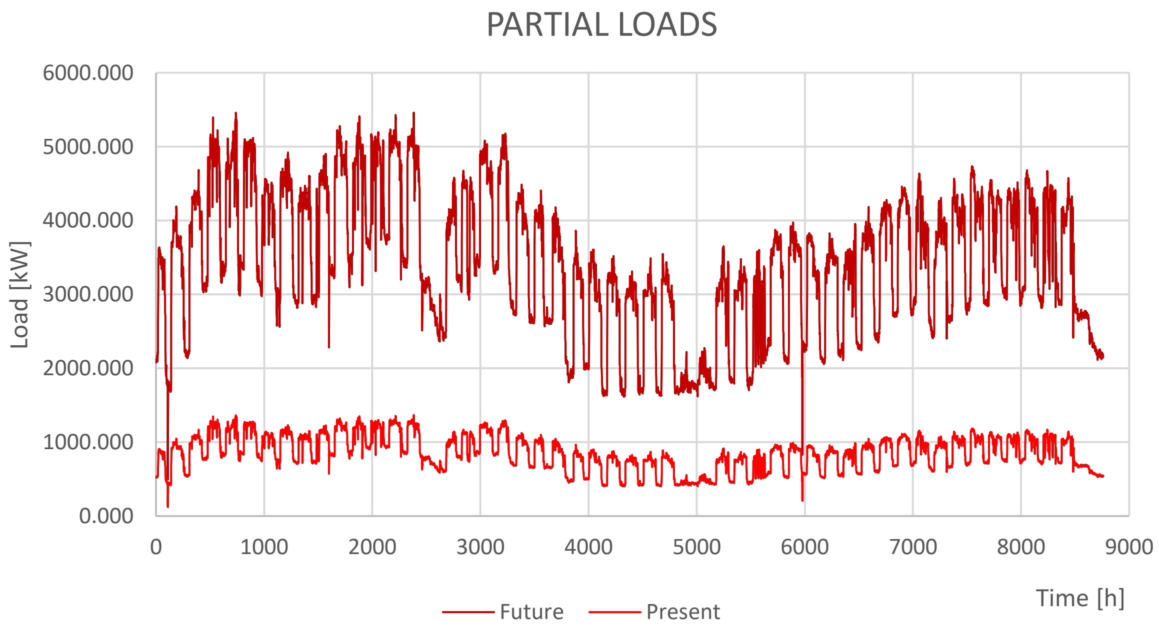

Figure 52 Comparison of load series referring to present (2019) and future time

Power supply over the year from pv (v_Ps_year_PV)

Below we are going to illustrate a series of formulas and equations that we will have to imagine applied to the input data sets presented in the chapter "SOLAR" [0] and not to a single value.

In Figure 53 the main steps for calculating the series are summarised schematically v_Ps_year_PV.

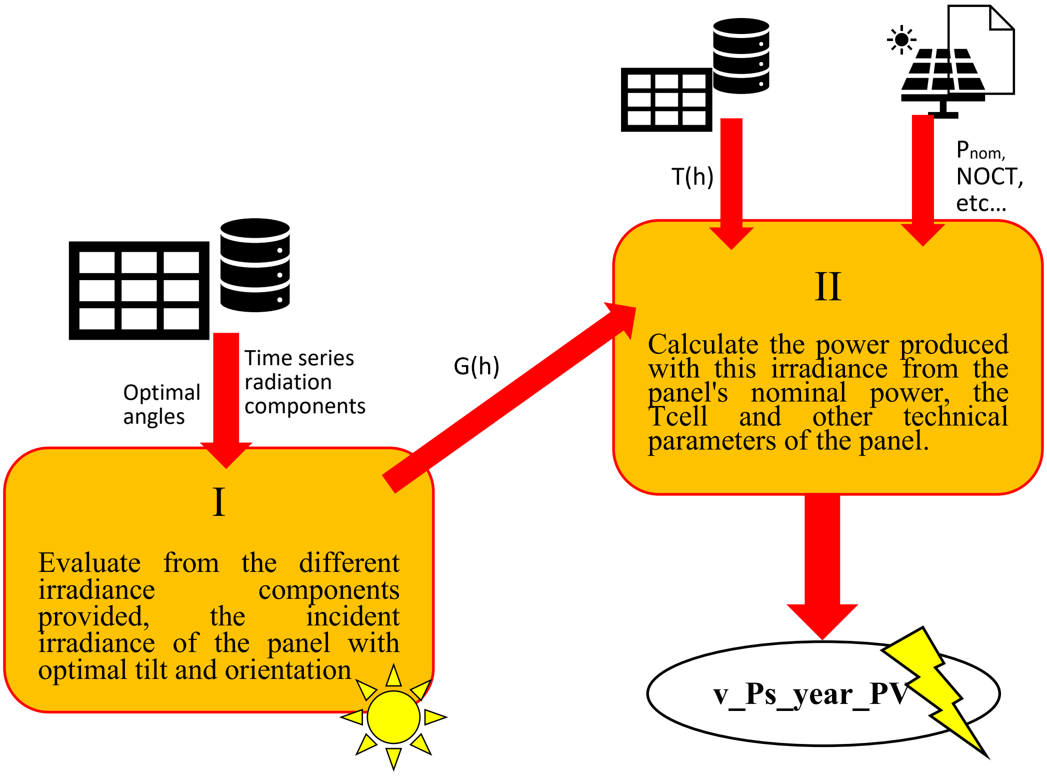

Figure 53 Logic diagram for managing the input data relating to solar radiation for calculating the producibility of the PV system

Before performing any calculations, it was essential, here as in all the files provided by PVGIS, to translate the time defined in UTC into the CET time to which it refers. This was done by simply moving the UTC time back by one hour:

$$\text{CET hour} = \text{UTC hour} + 1\text{h} \tag{3}$$

Having done this, the first step was to identify the irradiance incident on our panels so that we could then calculate the extracted power.

However, since the calculation of incident radiation is a function of a series of solar angles, before going into its definition, let us summarise the different solar angles and their definition and behaviour throughout the year, using *Figure 54* and *Table 29 and the formulas that follow them.*

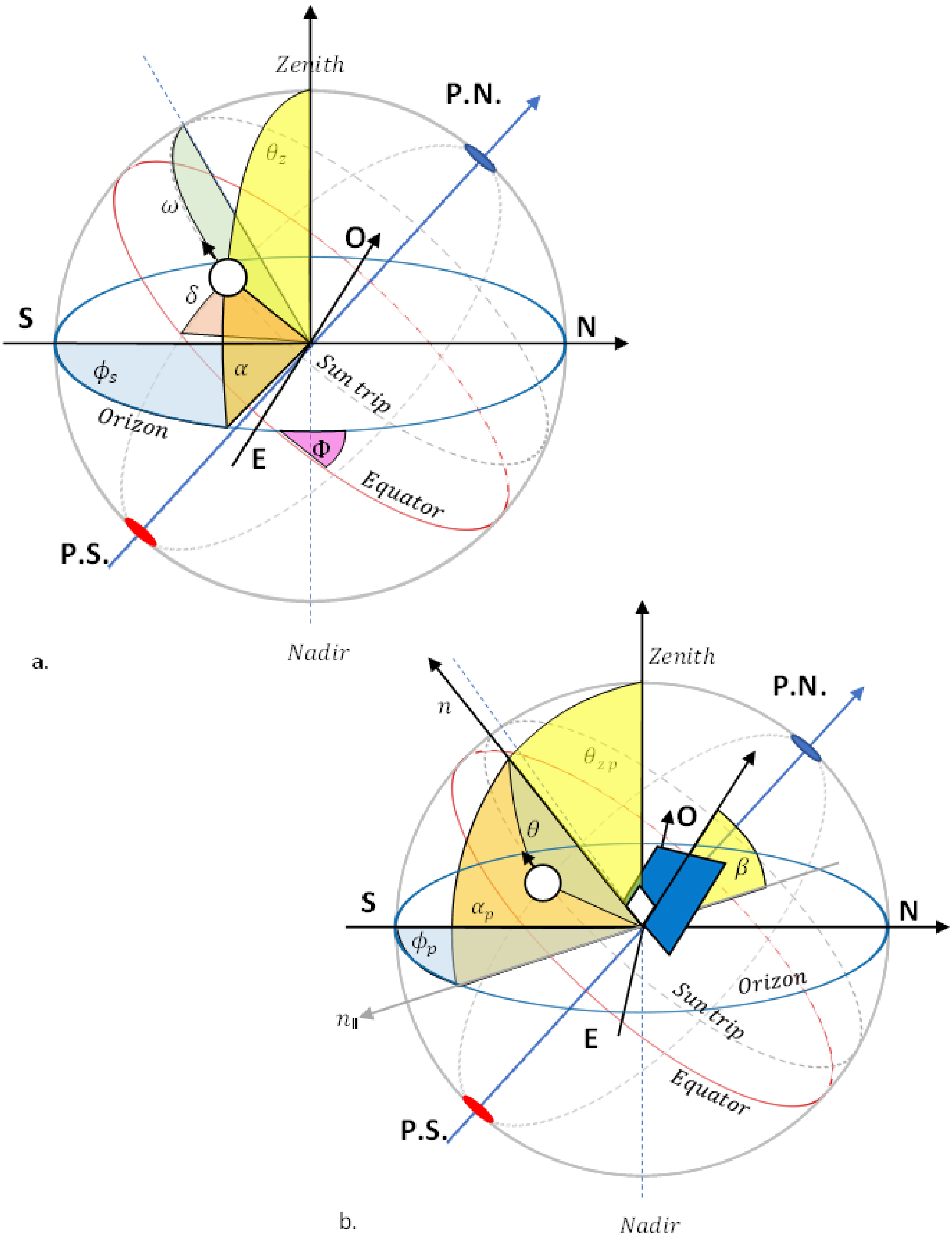

Figure 54 Solar angle diagrams relating to: a. Reference point on the horizontal plane; b. Inclined surface of the photovoltaic panel

Table 29 Definition of the solar angles referred to the reference point at the centre of the horizontal plane enclosed by the horizon line and those referred to the inclined plane to which the surface of the solar panel belongs, shown graphically in Figure 54

Symbol	Name	Definition
α	*Solar elevation*	Angle between the horizon plane and the direction of the incident solar beam (complementary to θ_z)
α_p	*Panel's heigh*	Angle between the plane of the horizon and the normal to the plane of the panel (complementary to β)
β	*Slope or Tilt angle*	Angle of inclination of the panel otherwise defined as the zenith of the panel, i.e. the angle between the normal of the panel and the normal of the ground plane (optimum from PVGIS)
ϕ_p	*Panel's Azimuth*	Angle between the projection of the normal to the plane of the panel on the reference plane and the south direction (optimum from PVGIS)
ϕ_s	*Sun's Azimuth*	angle between the projection of the sun's position on the horizon and the south direction
θ	*Incidence angle*	Angle at which the beam strikes the panel plane in relation to the panel normal.
θ_z	*Zenith*	Angle formed by the direction of the sun's ray and the normal to the reference plane enclosed by the horizon line
θ_{zp}	*Panel's Zenith*	Angle formed by the direction of the normal to the plane of the panel and the normal to the reference plane enclosed by the horizon line (takes the same value as β)
δ	*Solar declination*	Angle of incidence of the sun's rays with respect to the line of the equator
ω	*Hour angle*	Angle of the sun with its culmination point at a given time assessed along the solar trajectory

Mathematically, these angles are defined as follows:

Solar declination (δ(n))

The declination can be derived by applying the approximated Cooper formula, which is function of the day of the year n as follows:

$$\delta = 23.45 \cdot sin\left(360 \cdot \frac{284 + n}{365}\right) \tag{4}$$

Its graphical representation as a function of n is given in Figure 55

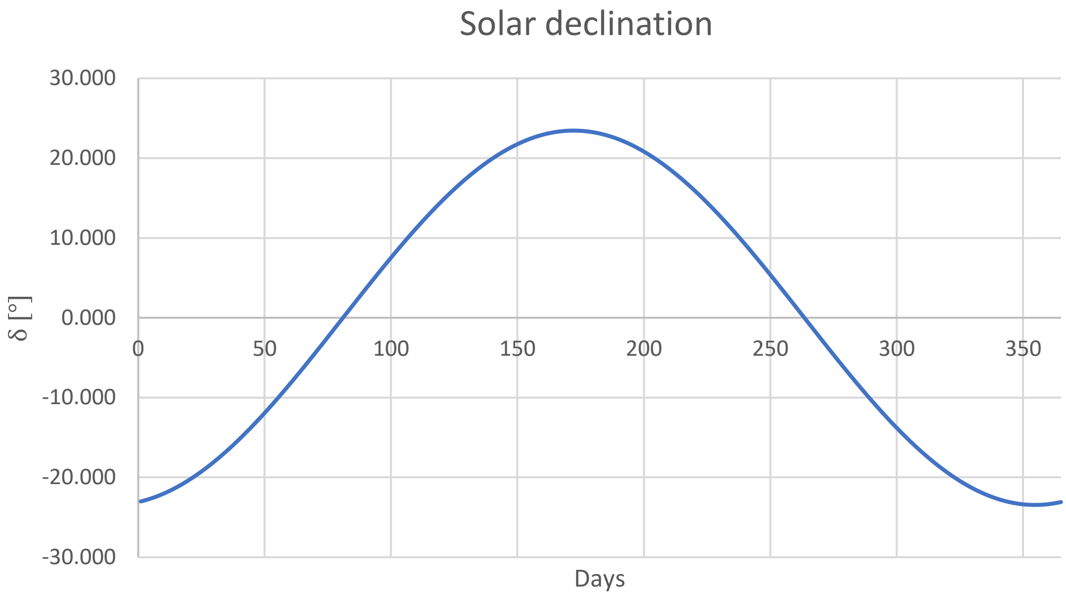

Figure 55 Declinazione solare associata al sito in questione

<u>*Hour Angle*</u> <u>(ω)</u>

The hour angle was instead assessed as:

$$\omega = (h - h_{culm}) \cdot \frac{360}{24} \tag{5}$$

where h corresponds to the standard time, i.e., the time given by local clock and h_{culm} is the noon time, i.e., the time given by local clock when the sun is at its highest point above the horizon (crosses the local meridian).

The term h_{culm} is given by:

$$h_{culm} = 12 + \frac{L_{loc} - L_{ref}}{15} - \frac{EOT}{60} + DST \tag{6}$$

where L_{loc} is the longitude of the observer's meridian, L_{ref} is the longitude of the meridian for the local time zone, EOT (in minutes) is the equation of time and DST is the daylight-saving time (equal to 1 when in force and 0 otherwise). It begins for European Union members on the last Sunday in March and ends on the last Sunday in October. Liechtenstein, Andorra, Monaco, San Marino, Switzerland, Norway and the Vatican City also follow the same rules.

The EOT is the Equation of Time which represents the deviation of solar time from the reference time indicated by a clock. In fact, due to the combination of the axis' iclination and the eccentricity of the Earth's orbit, the passage of time assessed according to the sun's trajectory (which is affected by the planet's different speeds and therefore varies) and the constant time assessed by a clock have a variable deviation over the year. It can be evaluated according to [53] as:

$$EOT = 2.292\,(7.5\ 10^{-3} + 0.1868\ \cos B - 3.2077\ \sin B\ - 1.4615\ \cos 2B - 4.089\ \sin 2B)\ [\text{min}] \quad (7)$$

with

$$B = (n-1)\frac{360}{365} \quad (8)$$

with n always the number of the day of the year, and its behaviour is represented in Figure 56

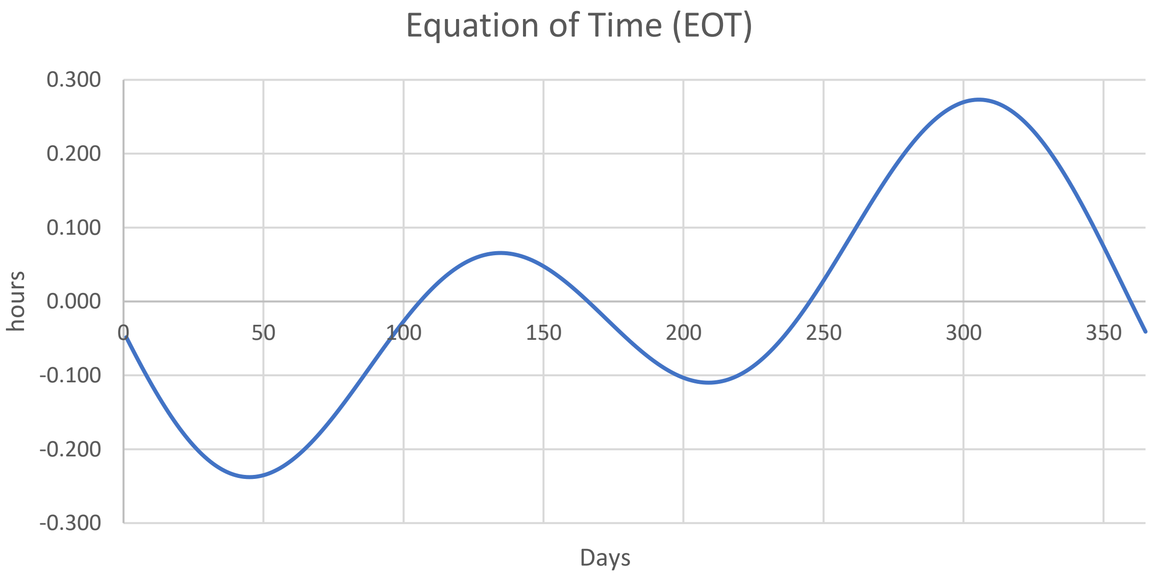

Figure 56 Rappresentazione grafica dell'equazione del Tempo (EOT)

And so, having defined h_{culm} and EOT the trend of the hour angle can be evaluated and is represented in Figure 57

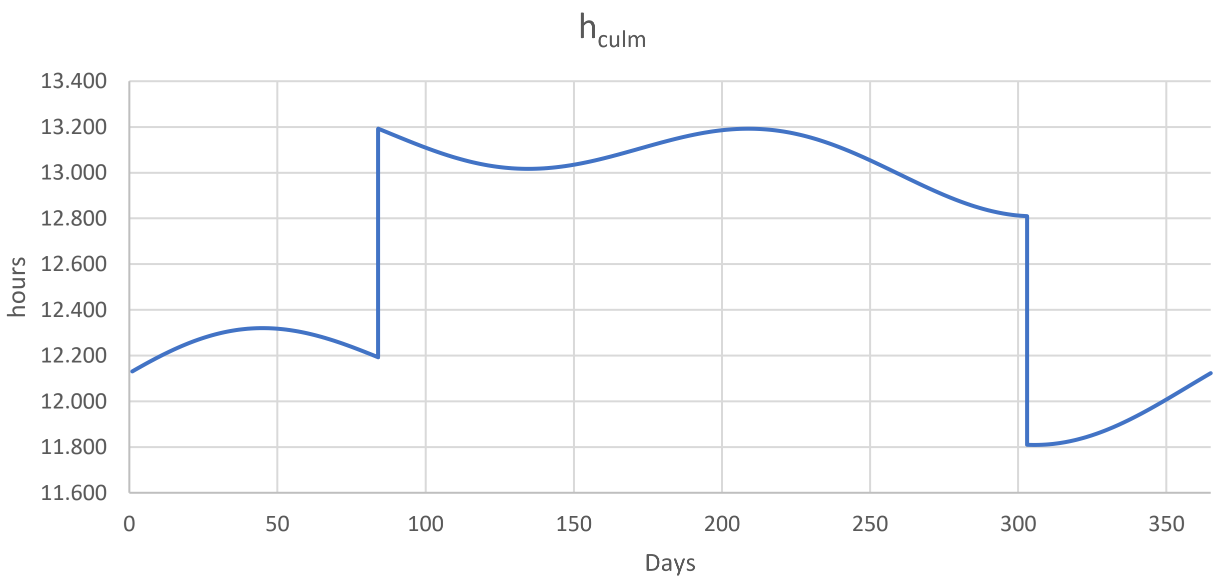

Figure 57 Orario di culminazione durante il corso dell'anno per il sito in questione

Zenith (θ_z)

The zenith angle (θ_z) parameter was defined as:

$$cos(\theta_z) = cos(\Phi) \cdot cos(\delta) \cdot cos(\omega) + sin(\Phi) \cdot sin(\delta) \qquad (9)$$

where Φ is the latitude. As can be seen from Figure 54 negative values of $cos(\theta_z)$ indicate times when the sun is below the horizon line. Thus this angles are not considered significant for the calculation of the total incident irradiance and therefore are discarded. This means that at times when $cos(\theta_z)$<0 the irradiance is assumed to be zero. It should be noted that this assumption neglects the contributions made by diffuse radiation, which is present in the time span just before dawn and just after sunset.

Solar Azimuth (ϕ_s)

The following expression was employed to assess the solar azimuth angle

$$cos(\phi_s\,) = \frac{cos(\theta_z) \cdot \sin(\Phi) - \sin\,(\delta)}{sin(\theta_z) \cdot \cos(\Phi)} \qquad (10)$$

Angolo di incidenza (θ)

Finally, the angle of incidence was evaluated by applying the following relationship:

$$cos(\theta) = \cos(\beta) \cdot cos(\theta_z) + \sin(\beta) \cdot sin(\theta_z) \cdot \cos(\phi_s - \phi_p) \qquad (11)$$

Note that, since $cos(\theta)$ depends on θ_z , the values of $cos(\theta)$ will not be calculated for the hours for which $cos(\theta_z) < 0$. This is always because this condition expresses a position of the sun below the horizon line.

At this point, having defined in detail all the solar angles necessary to calculate the total irradiance, we can define how it can be calculated:

$$\begin{cases} G(t) = G_b(t) + G_d(t) + G_r(t) & if\ cos(\theta_z(t)) \geq 0 \\ G(t) = 0 & if\ cos(\theta_z(t)) < 0 \end{cases} \qquad (12)$$

namely

$$\begin{cases} G(t) = G_{b,n}(t) \cdot cos(\theta(t)) + G_{d,h}(t) \cdot F_{c,s} + G_{t,h}(t) \cdot \rho_g \cdot F_{c,g} & if\ cos(\theta_z(t)) \geq 0 \\ G(t) = 0 & if\ cos(\theta_z(t)) < 0 \end{cases} \qquad (13)$$

where $G_{b,n}$ (in kW/m^2) is the direct normal irradiance which is defined as the energy associated with a direct ray impinging on a plane that is always normal to it (i.e. not a horizontal plane, but one that is normal moment by moment to the direction of the ray), $G_{d,h}$ (in kW/m^2) is the diffusive irradiance over the horizontal surface, $G_{t,h}$ (in kW/m^2) is the total irradiance over the horizontal surface, ρ is the ground albedo, $F_{c,s}$ is the collector-sky view factor, $F_{c,g}$ is the collector-ground view factor. The irradiance thus assessed refers to the radiation incident on the plane of the photovoltaic panel..

The terms $F_{c,s}$ and $F_{c,g}$ express respectively the portion of the sky and the portion of the ground visible from the surface of the panel, which are used to weigh the relevance of diffuse radiation (assessed on the horizontal plane) and that coming from the environment (and therefore also of "rebound" from the ground). They were determined in the following way:

$$F_{c,s} = \frac{1+\cos(\beta)}{2} = 0.85 \tag{14}$$

$$F_{c,g} = 1 - F_{c,s} = \frac{1-\cos(\beta)}{2} = 0.15 \tag{15}$$

It is necessary here to make a clarification on the input data for the series of actual years (2014 and 2015). As mentioned in section [0] referred to the sources, the irradiance values provided by PVGIS referred to the irradiance calculated directly on the panel plane.

However, since:

- As indicated in Table 7, it is not possible to discharge all radiation components and the total incident radiation at the same time
- The sum of the components did not exactly give the value of the total incident radiation (fact verified by the calculations)
- there is no indication of the actual relationship between the total incident radiation and the components supplied as given by PVGIS

it was decided to treat the component series and the total irradiance series as if they had been provided in the same way as those for TMY. As a result, the assumptions summarised in Table 30. These assumptions were nevertheless considered valid, as they underestimated the reported value of the incident normal radiation by a few watts and therefore placed the series under reasonably conservative conditions.

Table 30 Summary of assumptions made regarding the consideration of the types of radiation components provided by PVGIS for the time domains consisting of the actual years 2014 and 2015

From PVGIS		Assumed	Unit
G_t	=	G_{th}	W/m^2
G_b		G_{bn}	W/m^2
G_d		G_{dh}	W/m^2

In Figure 58, Figure 59, Figure 60 the 3 series of total incident irradiance calculated as follows for the different time domains considered are reported.

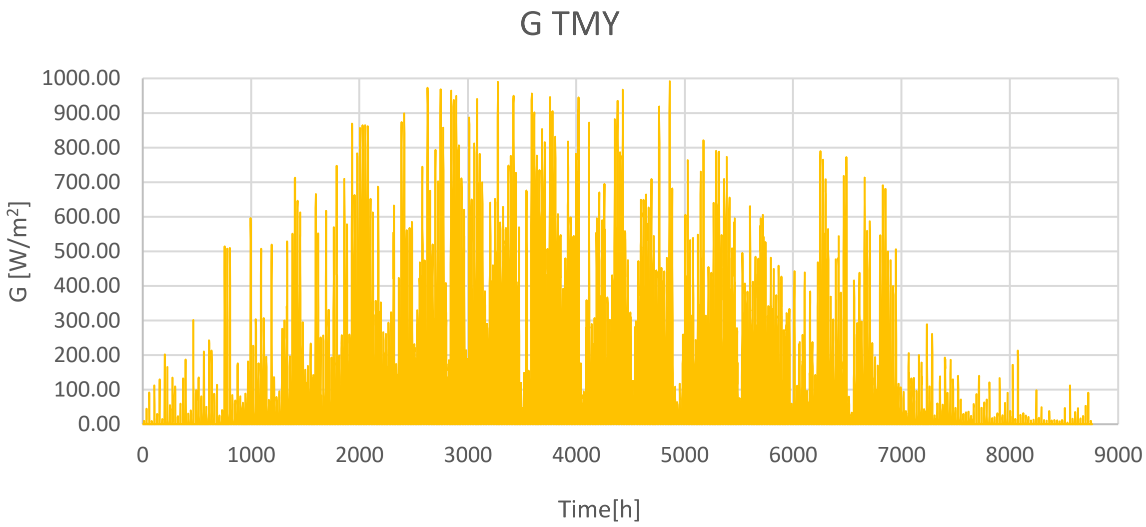

Figure 58 Annual series of the total irradiance G incident on the plane of the PV panel referred to the time domain TMY

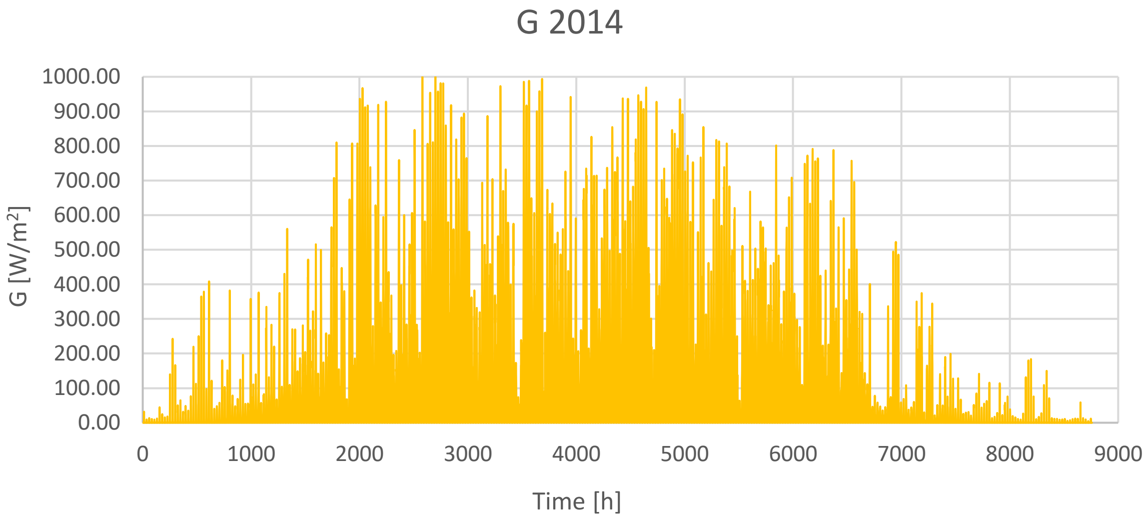

Figure 59 Annual series of the total irradiance G incident on the PV panel plane referred to the time domain 2014

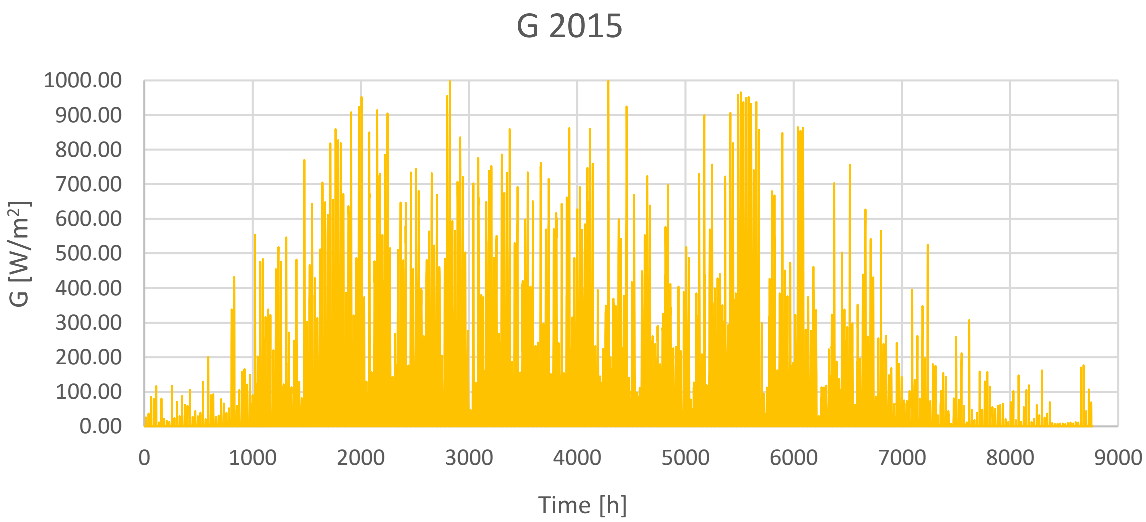

Figure 60 Annual series of the total irradiance G incident on the PV panel plane referred to the time domain 2015

Once the value of the incident series has been defined, it is possible to evaluate the series that express the power produced by a photovoltaic system of a given nominal power. Obviously, in our case the nominal power referred to is the reference power of 1KW.

The PV power production is defined as:

$$P_{PV}(t) = (1 - f_{PV}) \cdot P_{PV,rated} \cdot \frac{G(t)}{G_{STC}} \cdot \left(1 + \gamma \cdot \left(T_{cell} - T_{cell,STC}\right)\right) \tag{16}$$

Where:

- G_{STC} is the incident radiation at standard test conditions (equal to 1 kW/m2)
- $P_{PV,rated}$ is the rated PV power (in our case assumed 1kW)
- T_{cell} is the PV cell temperature (in °C)
- $T_{cell,STC}$ corresponds to the PV cell temperature at standard test conditions (equal to 25°C)

And the other coefficients are those already defined in the data sheet (see chapter [0])

In order to calculate the power, it can be seen that it is necessary to know the value of T_{cell}. The cell temperature T_{cell} can be expressed as follows:

$$T_{cell} = T_a + \frac{G(t)}{800} \cdot (NOCT - 20) \tag{17}$$

Where T_a is the ambient temperature (which for us is the T_{2m} given by PVGIS). The series of the T_{cell} are reported in Figure 61, Figure 62, Figure 63.

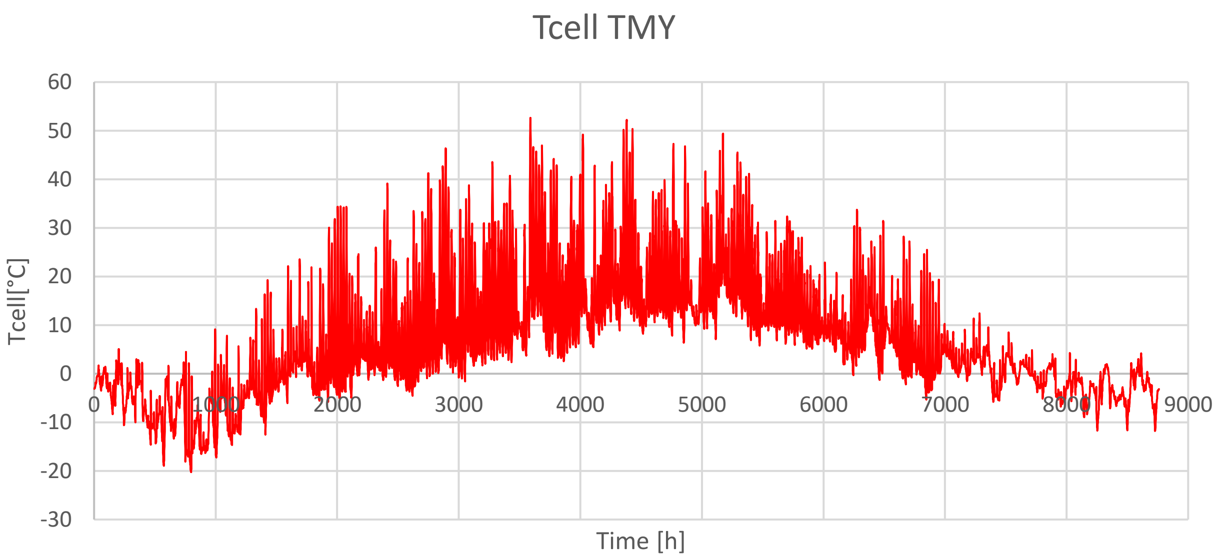

Figure 61 Annual series of cell temperature (T_{cell}) of the photovoltaic panel referred to the TMY time domain

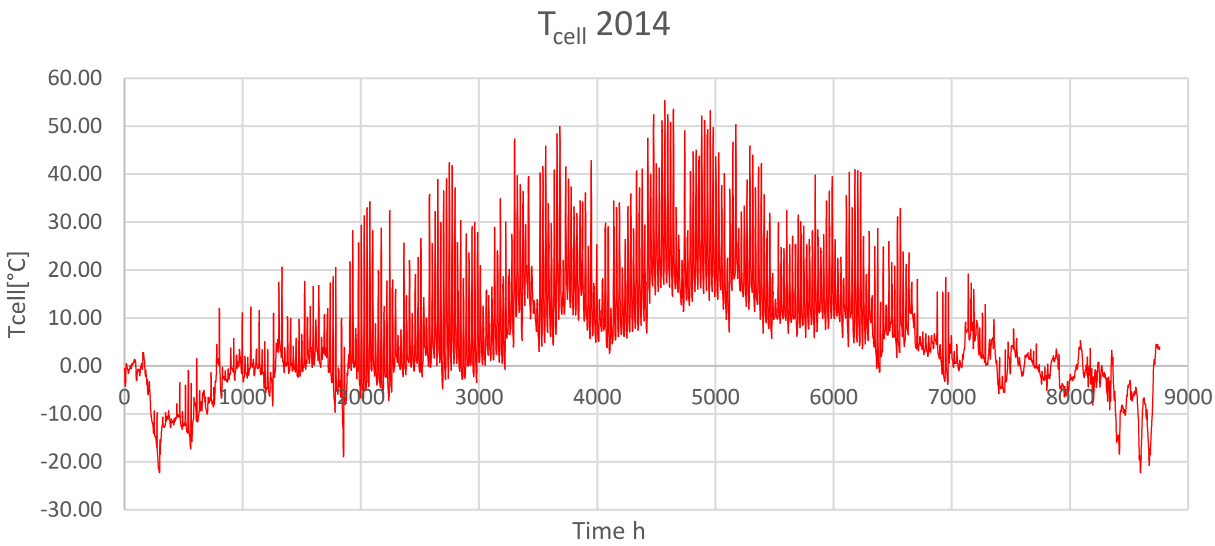

Figure 62 Annual series of cell temperature (T_{cell}) of the photovoltaic panel referring to the time domain 2014

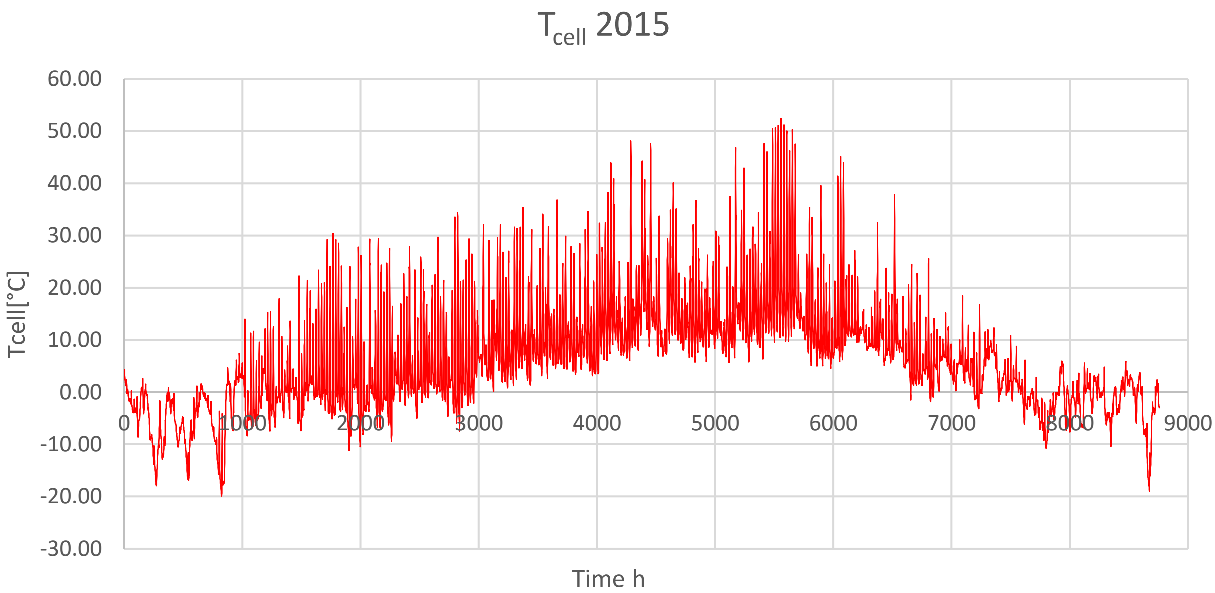

Figure 63 Annual series of cell temperature (T_{cell}) of the photovoltaic panel referring to the time domain 2015

Therefore, the relation can be rewritten in the following form:

$$\text{v\_Ps\_year\_PV} = P_{PV}(t) = G(t) \cdot (1 - f_{PV}) \cdot \left(1 + \gamma \cdot (T_{cell} - 25)\right) \tag{18}$$

The resulting series are reported in figures Figure 64, Figure 65, Figure 66.

As expected, due to the similarities in the direct irradiance values, the producibility trends of the 2015 and TMY time series are also very similar.

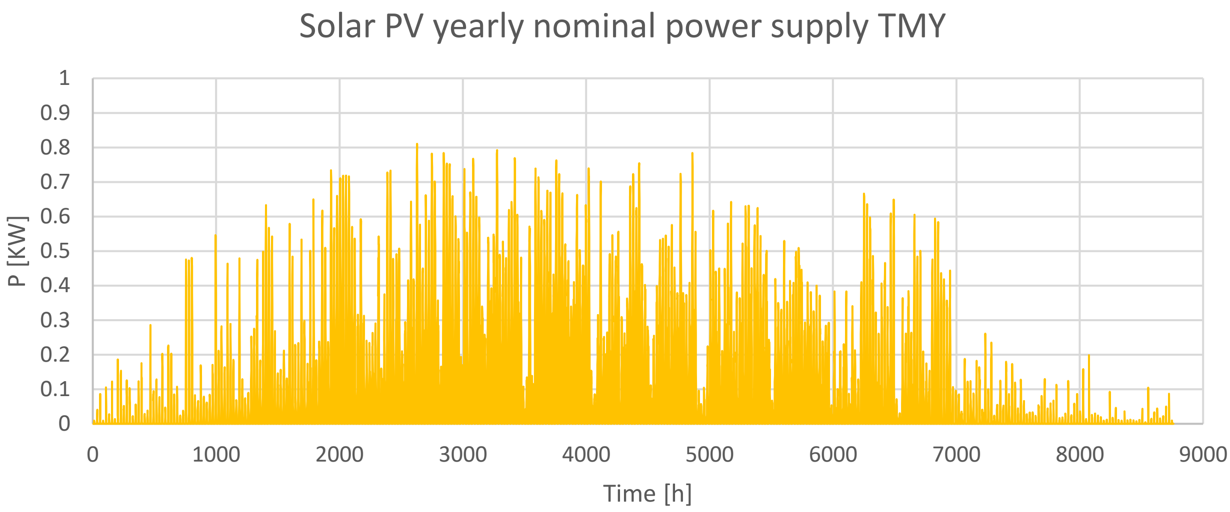

Figure 64 Annual serie of the producibility of a panel with a peak power of 1KW referred to the time domain TMY

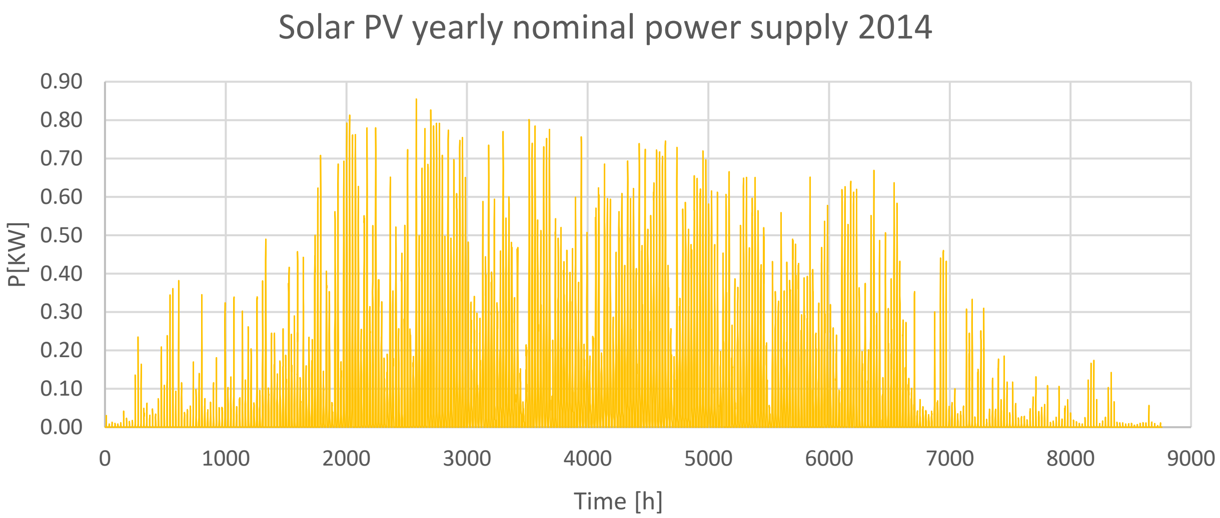

Figure 65 Annual serie of the producibility of a 1KW peak power panel referring to the time domain 2014

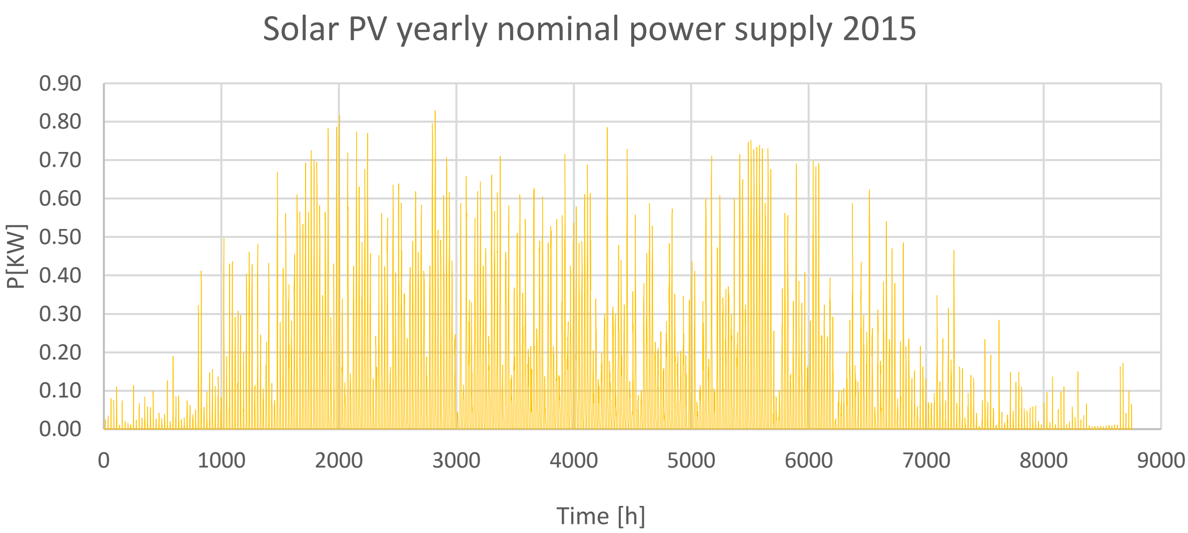

Figure 66 Annual series of the producibility of a panel with a peak power of 1KW referred to the time domain 2015

Power supply over the year from wind turbine (v_Ps_year_WIND)

The third set to be supplied to the target function is the normalised producibility of the chosen turbine, the technical characteristics of which have been given in chapter [0].

As with the PV in Figure 67 is reported a general outline of the steps for processing the data set provided by PVGIS.

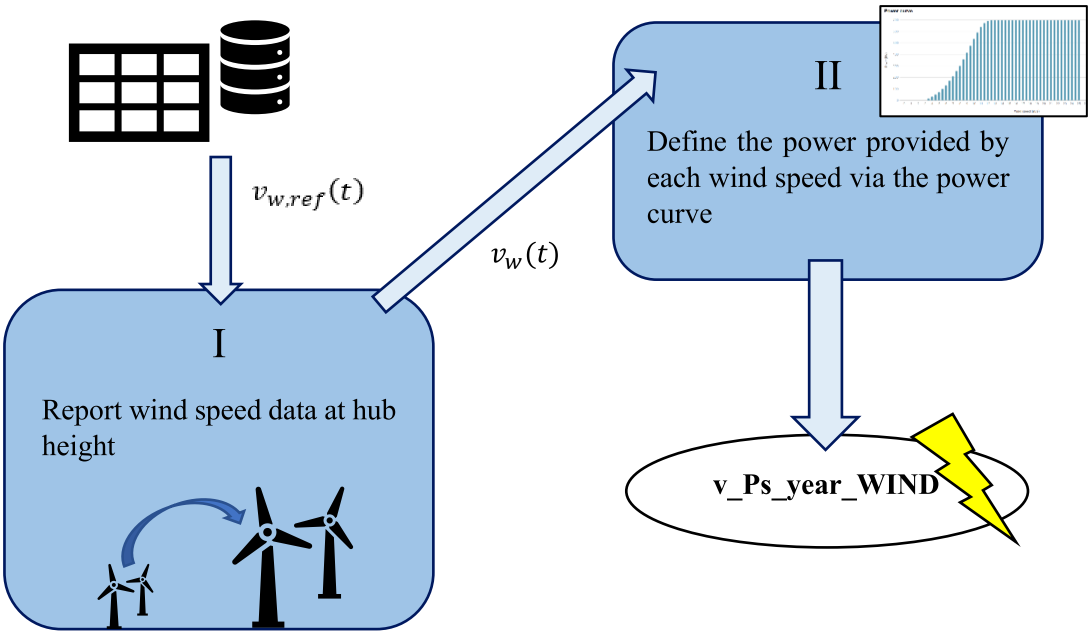

Figure 67 Logic diagram for the management of input data relating to wind speed for the calculation of the wind plant's producibility

The first step is therefore to use an expression that takes into account the roughness coefficient τ defined in chapter [2.2], the wind speed at the reference height at the hub height of the turbine used. Indeed, wind speed data are available for a certain reference height from PVGIS. The relation used to do that is the following:

$$v_w(t) = v_{w,ref}(t) \cdot \left(\frac{h_t}{h_{ref}}\right)^{\tau} \tag{19}$$

where:

- $v_{w,ref}$ is the wind speed measured at the reference height (from PVGIS)
- h_{ref} corresponds to the reference height (for us 10m)
- h_t is the turbine height

In Figure 68, Figure 69, Figure 70 the series of velocities at hub height obtained for the 3 time domains analysed are shown.

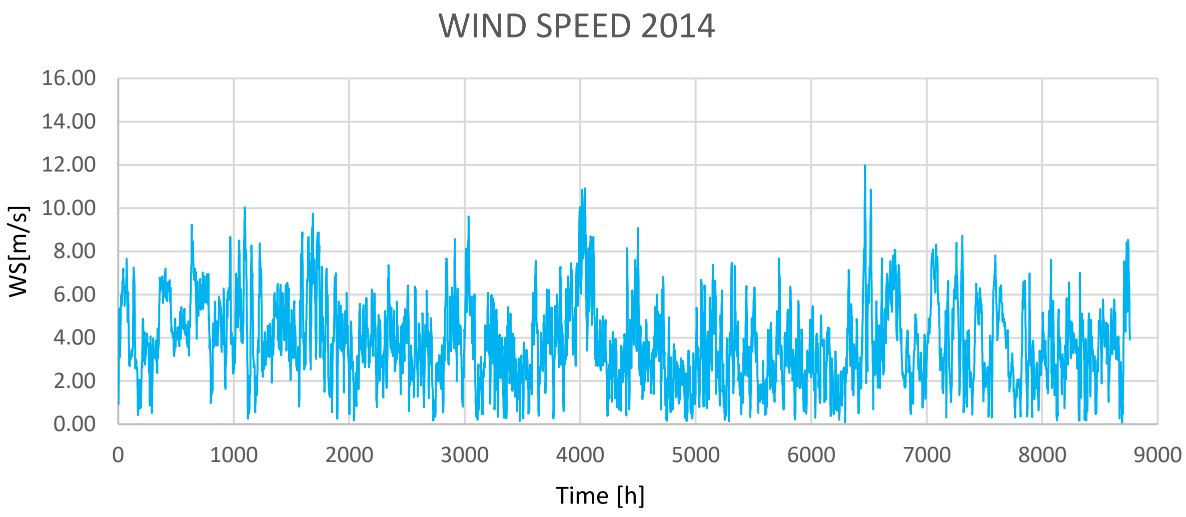

Figure 68 Annual series of wind speeds reported at hub height (33.5m) for the time domain 2014

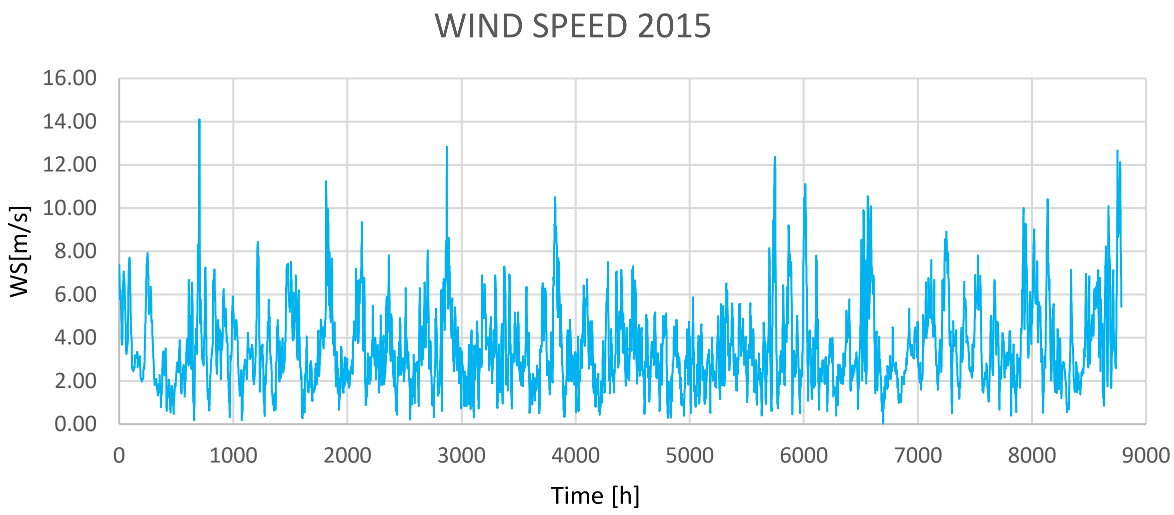

Figure 69 Annual series of wind speed reported at hub height (33.5m) referring to the 2015 time domain

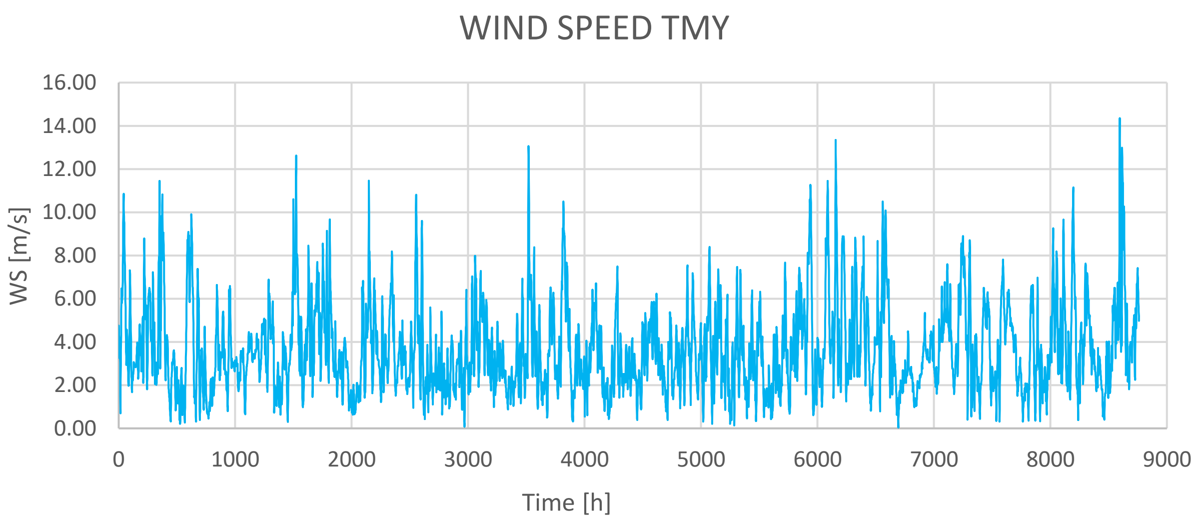

Figure 70 Annual series of wind speed reported at hub height (33.5m) referred to time domain TMY

Once the series of speeds relative to the effective height of the hub has been defined , the corresponding power value shown on the characteristic power curve of the turbine (also shown in chapter [0] among the technical data of the turbine) is associated hour by hour with each speed. This operation has been carried out by means of a simple code implemented on Matlab, the script of which is shown in the APPENDIX A.

In Figure 71, Figure 72, Figure 73 the final series of v_Ps_year_WIND for the 3 reference time domains for turbines with a nominal power of 225kW are shown (see data sheet and power curve [0]). The actual input series to the objective function will first be normalised by dividing by the nominal power of the turbine.

For the sake of completeness Figure 74 the relative frequency of the hub-height speeds recorded in the series superimposed on the turbine power curve is then shown. From this graph it can be seen very clearly that the highest frequencies fall in ranges where the turbine fails to extract the nominal power. It would therefore be worth investigating whether it would be better to replace the turbine model with another with a power curve shifted more towards low speeds. It can be seen that the TMY series is the one most affected by this power curve characteristic.

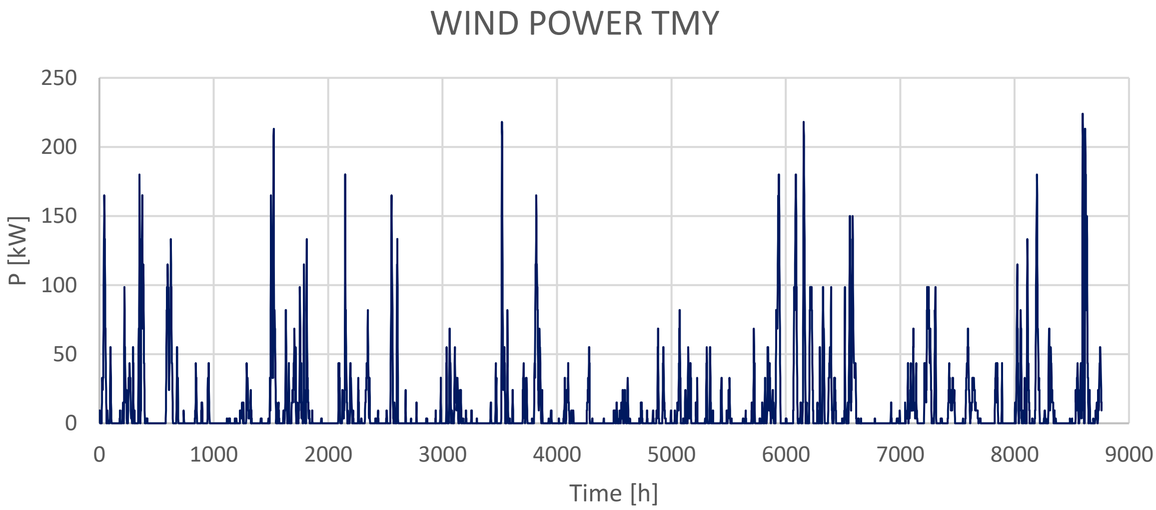

Figure 71 Annual series of power produced by a Vestas V27/225 turbine in the TMY time domain

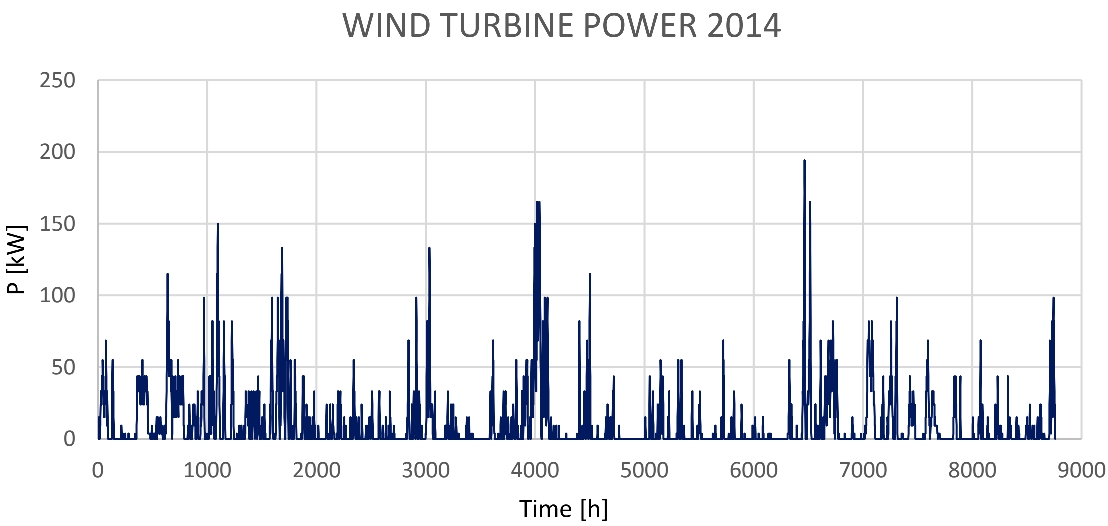

Figure 72 Annual series of power produced by a Vestas V27/225 turbine referring to the time domain 2014

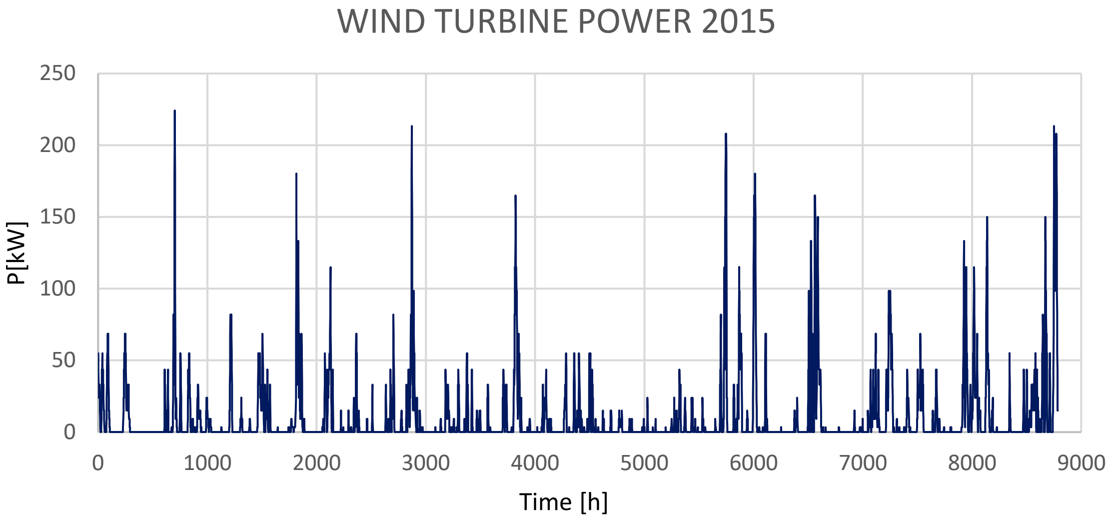

Figure 73 Annual series of the power produced by a Vestas V27/225 turbine referred to the time domain 2015

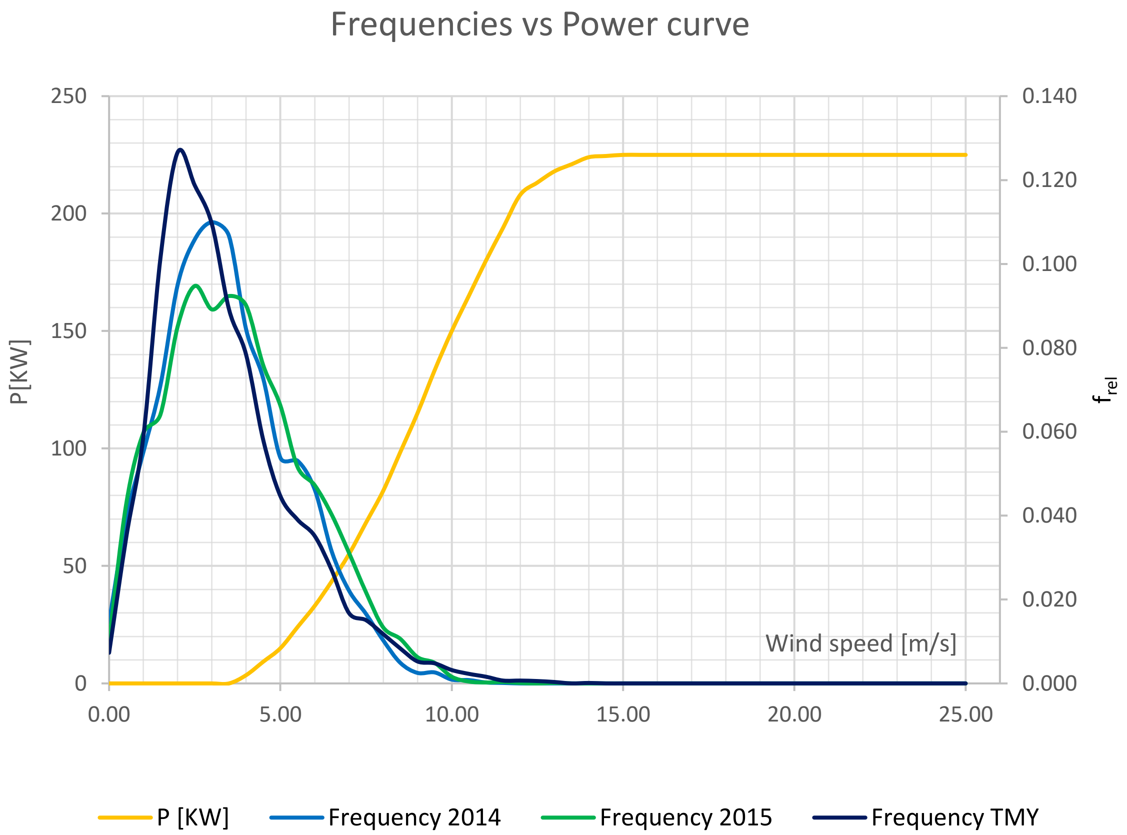

Figure 74 Comparison of the Vestas V27/225 turbine power curve with relative wind speed frequency curves on an annual basis

Cost and price of electricity (v_cost, v_price)

The last two sets of data that need to be processed before being entered as inputs into the objective function are the sets that characterise the economic flows during the purchase and sale of electricity from/to the grid when present and available.

The two series differ in the fact that one describes how much the semi-autonomous user would pay for electricity at a given time of the year (cost of energy) while the other describes the revenue he would get from selling it to the grid.

Both series are calculated from the spotprices series shown in chapter [2.7]. From them we will proceed in 2 different ways for the 2 series:

- *Cost of energy* (v_cost): It is made up of the sum of 3 main components, 2 of which are constant and one variable (energy market price). Referring to Table 19 we'll have:

$$v_{cost} = (Power\ price(t) + Power\ price \cdot VAT) + (Consumer\ tax\ +\ Energy\ Price) + (Consumer\ tax\ +\ Energy\ Price) \cdot VAT\ [€/MWh] \tag{20}$$

  which means

$$v_{cost} = (Power\ price(t) + Consumer\ tax\ +\ Energy\ Price) \cdot (1 + VAT)\ [€/MWh] \tag{21}$$

  Since for commercial operators of load sizes of the order of MW and above the application of VAT can be avoided, we can ultimately write for our system:

$$v_{cost} = Power\ price(t) + Consumer\ tax + Energy\ Price\quad [€/MWh] \tag{22}$$

- *Price of energy* (v_price): It consists of the sum of only two components, one of which is the time-varying market price of energy, while the other is a constant tax that must be paid for the occupation of part of the network capacity. The constant value of this tax, here called occupation_tax, has been reported in Table 19. The price for calculating the revenue from the sale of energy to the grid will then be defined as:

$$v_{price} = Power\ price - occupation\ tax\ [€/MWh] \tag{23}$$

It follows that the two series will have the same behaviour except for a constant represented by the sum of the constant components that characterise them. In Figure 75, Figure 76, Figure 77, Figure 78, Figure 79 the 2 time series are shown and then also their daily, weekly, monthly averages diversified by daytime and night time period to highlight their short and long term behaviour.

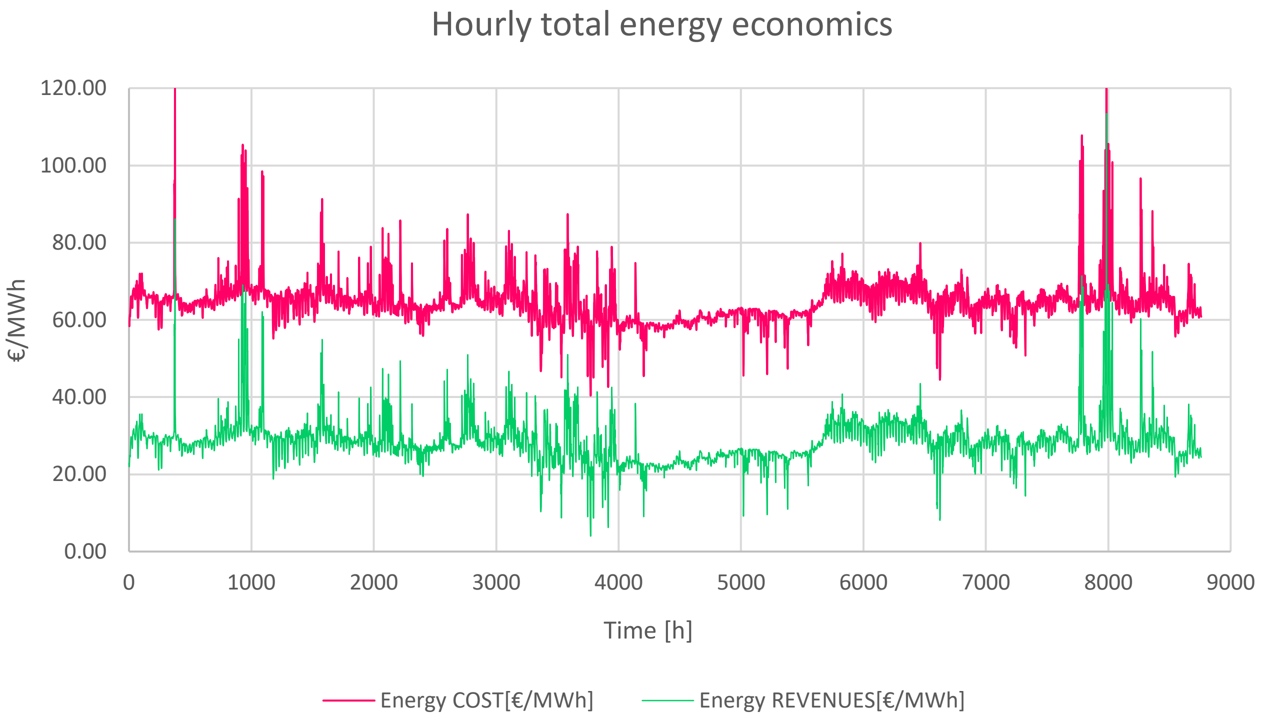

Figure 75 Time series of the cost of energy if purchased from the grid and the revenue from its sale to the grid (reference year 2017)

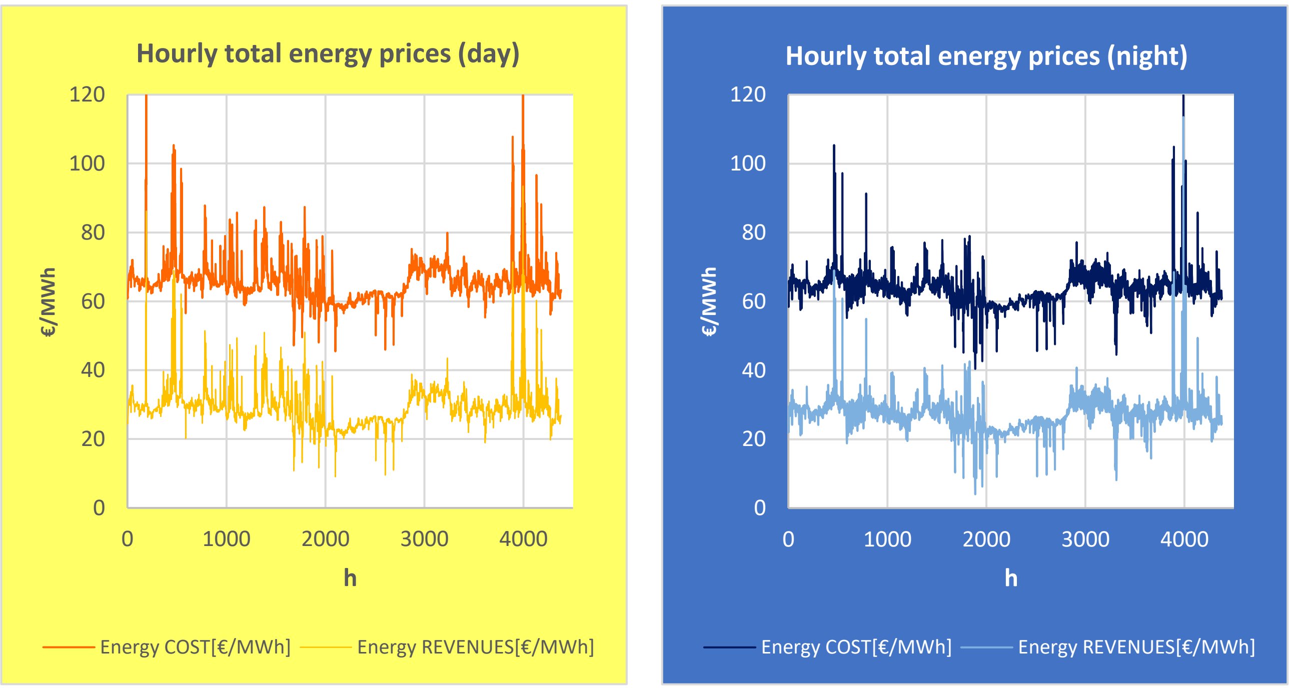

Figure 76 Daytime (left) and night-time (right) time series of the cost of energy if purchased from the grid and the revenue from its sale to the grid (reference year 2017)

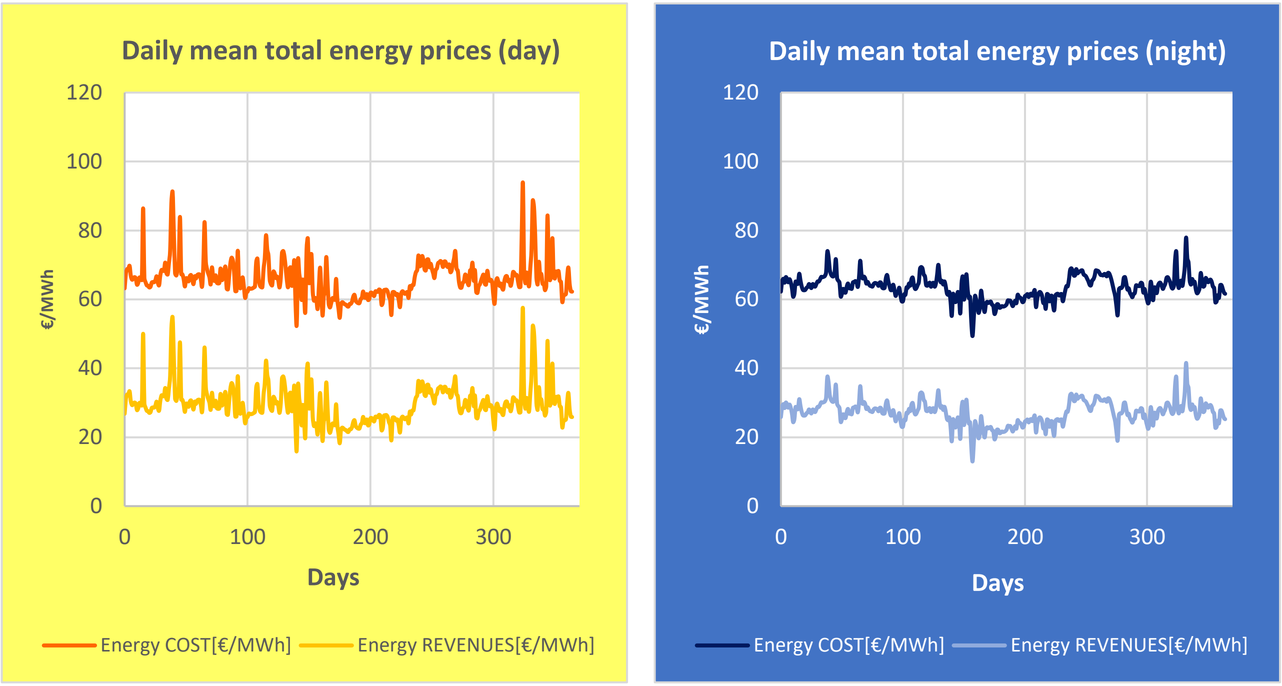

Figure 77 Series of daily daytime (left) and nighttime (right) averages of the cost of energy if purchased from the grid and the revenue from its sale to the grid (reference year 2017)

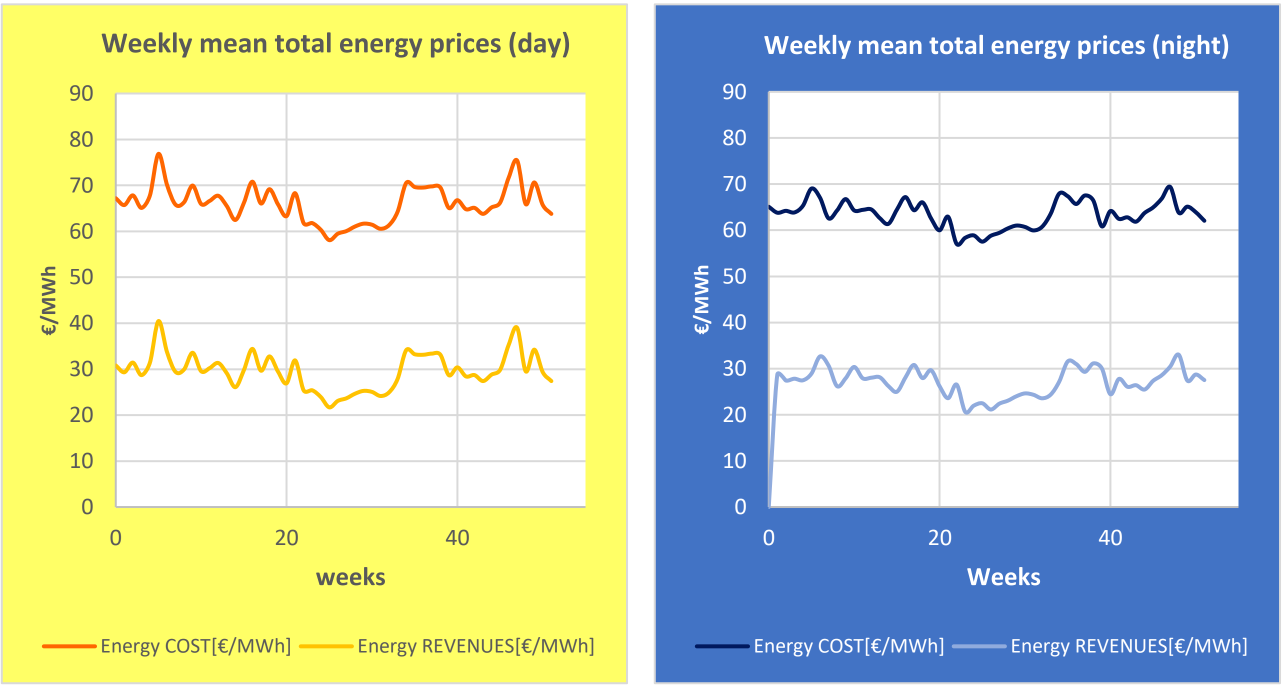

Figure 78 Series of weekly daytime (left) and nighttime (right) averages of the cost of energy if purchased from the grid and the revenue from its sale to the grid (reference year 2017)

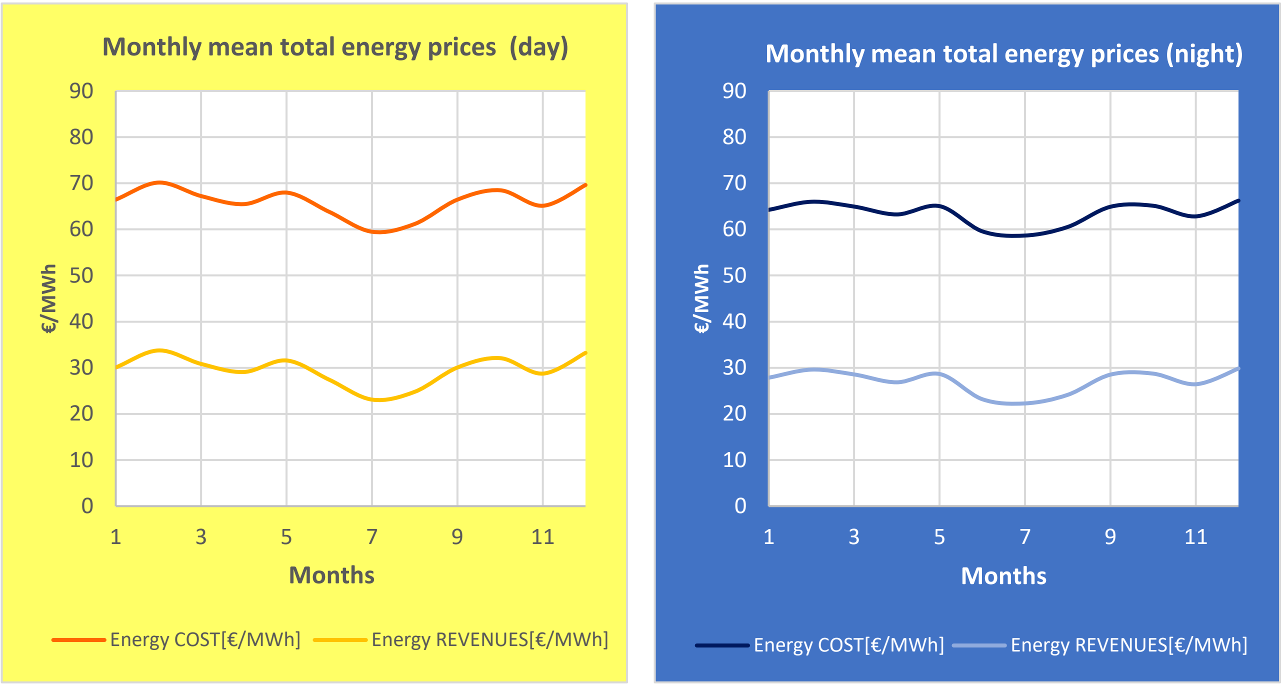

Figure 79 Series of monthly daytime (left) and nighttime (right) averages of the cost of energy if purchased from the grid and the revenue from its sale to the grid (reference year 2017)

These graphs show that there is no significant difference between the price/cost in night and day, apart from the fact that fluctuations are smaller at night. On the other hand, the difference between the situation in the summer and winter months is very clear. This is due to 2 main factors:

- the decrease in demand in the summer period (where there is also a decrease in load)
- the abundance of the primary resource that is used in Norway for electricity production - water. Although rainfall may be more frequent in the winter months, the low temperatures cause the water to solidify, building up water reserves that melt in the spring and summer months and can be used in hydroelectric power plants.

3.4.2. COST FUNCTIONS OF PROCESSING TECHNOLOGIES (PEMEL & PEMFC)

As mentioned in the chapter [2.6] the innovative and not fully mature character of these types of technologies made it difficult to find reliable and precise data referring to machines of the sizes used here. For this reason it was necessary to construct, starting from the data collected, cost curves that relate the size and investment value of the technology per unit of installed power (CAPEX [€/kWh]).

The relationship that has been used to describe these cost curves is the following which links them together:

- cb: costo normalizzato rispetto alla taglia di riferimento
- ca: costo normalizzato riferito alla taglia di interesse
- Sa: taglia di interesse
- Sb: taglia di riferimento
- f: coefficiente caratteristico utilizzato come esponente del rapporto tra le taglie e determinante la forma della curva di costo

$$\frac{c_a}{c_b} = \left(\frac{S_a}{S_b}\right)^f \tag{24}$$

On the basis of the data from the different sources analysed, the following were determined:

- reference sizes
- normalised costs referring to the reference size
- coefficient to be used as exponent

let's see the two cases:

PEMEL CAPEX cost curve

From the source [18], found during the bibliographic search of the normalized costs of PEMEL, results Figure 80:

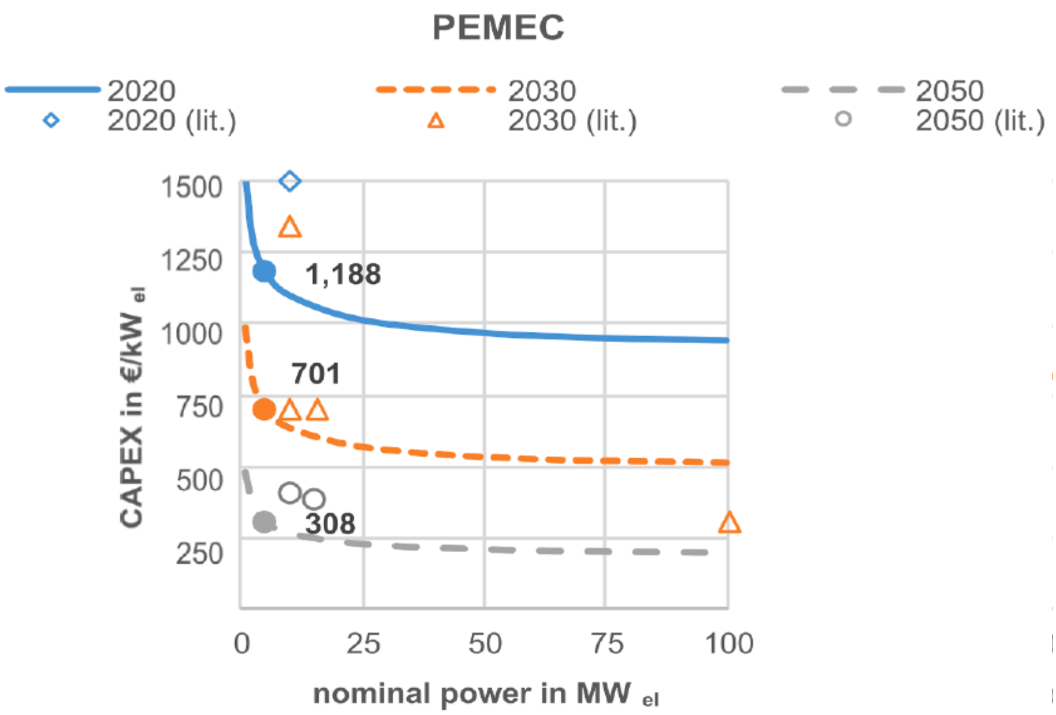

Figure 80 Curve di costo per la determinazione del CAPEX di un elettrolizzatore in base alla taglia. [18]

Therefore, was made an attempt to reproduce the equation describing the cost curve referred to the year 2020, using 2 points extrapolated from the graph of this curve to evaluate the coefficient f. This latter was then used to re-write the cost function, taking as reference cost and size those of the highlighted point in Figure 80. In Figure 81 the points chosen on the graph are shown and the reference point is defined as 'ref' while the other arbitrary point (easily identifiable in red) is called auxiliary and denoted 'aux'.

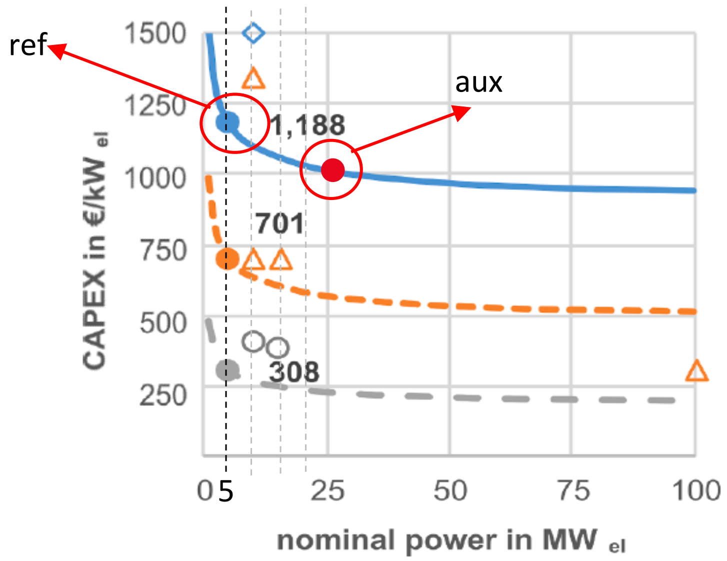

Figure 81 Cost curves for determining the CAPEX of an electrolyser by size with references for analytical reproduction of the curve for 2020.

The coefficient could therefore be identified by the following inverse formula:

$$f = \frac{\log\left(\frac{C_{aux}}{C_{rif}}\right)}{\log\left(\frac{S_{aux}}{S_{rif}}\right)} \tag{25}$$

Table 31 then reports the values of the reconstructed curve, the coordinates of the reference and auxiliary points and the general formula of the cost curve referring to the cost and size chosen as the reference with which the curve was constructed.

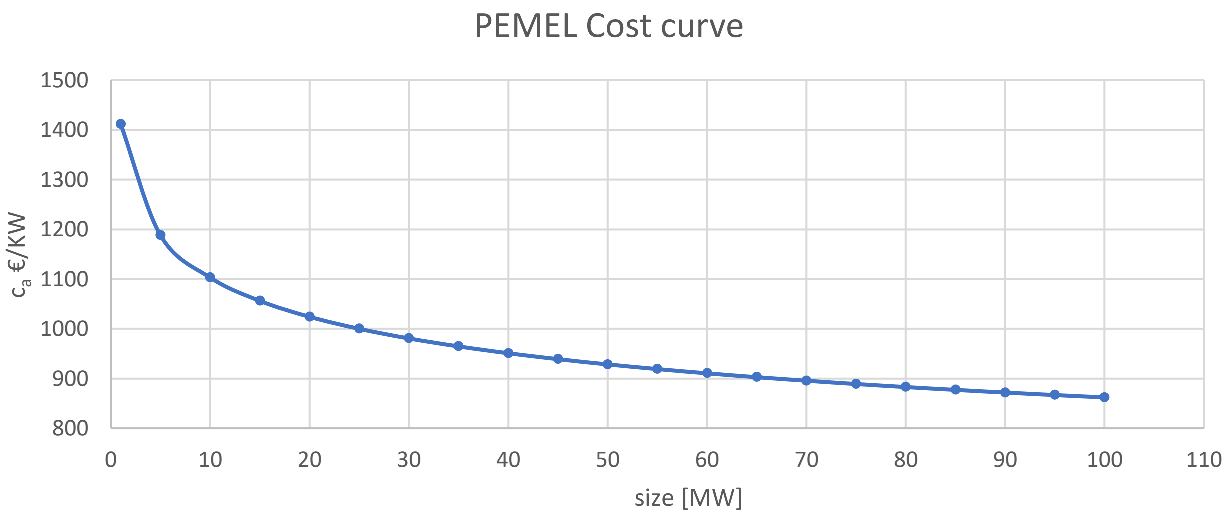

Figure 82 Curva di costo per un elettrolizzatore ricavata a partire dai riferimenti individuati sulla curva dei costi di figura Figure 80 riferita al 2020

Table 31 Curva di costo per la determinazione del CAPEX del PEMEL in base alla taglia

CURVE			
$c_a = 1188\left(\frac{S_a}{5}\right)^{-0.107}$ [€/kW]			
f	**-0.107**	**Size [MW]**	**Cost [€/KW]**
		1	1411
Reference		5	1188
		10	1103
		15	1056
		20	1024
Auxiliery		25	1000
		30	981
		35	965
		40	951
		45	939
		50	928
		55	919
		60	911
		65	903
		70	896
		75	889
		80	883
		85	877
		90	872
		95	867
		100	862

PEMFC CAPEX cost curve

Given the absence of pre-built curves, it was more difficult to identify coefficients describing a cost function for PEMFC. It was constructed by interpolating a set of data from different sources.

In contrast to PEMEL, ways of imposing benchmarks and exponential coefficient f were also attempted. These solutions were then compared with some data from other sources for some dimensions other than the benchmark dimensions in order to find a validation of the model. All these approaches, however, led to resulting curves of poor quality. In Table 32 the attempts made with the sources referred to for the determination of the parameters chosen each time are reported.

Table 32 Summary of attempts to construct the cost curve for determining the CAPEX of the PEMFC carried out

attempt	REFERNECE DIMENSION [MW]	REFERENCE COST [€/KW]	*f*	Observation
I	0.192 [29]	2075 [29]	-0.3 [5]	Coefficient f causes underestimation of cost for large sizes* and overestimates data for small sizes REF SOURCE 2018
II			-0.107 used for PEMEL	Coefficient f causes an overestimation of the cost for large sizes* and underestimates the data for small sizes REF SOURCE 2017
III	1.224 [54]	1419 [54]	-0.3 [5]	Coefficient f causes an underestimation of the cost for large sizes* and overestimates the data for small sizes REF SOURCE 2018
IV			-0.107 used for PEMEL	Coefficient f causes an overestimation of the cost for large sizes* and underestimates the data for small sizes REF SOURCE 2017
*according to [5] for sizes of MW you have cost orders of 1000€/kW				

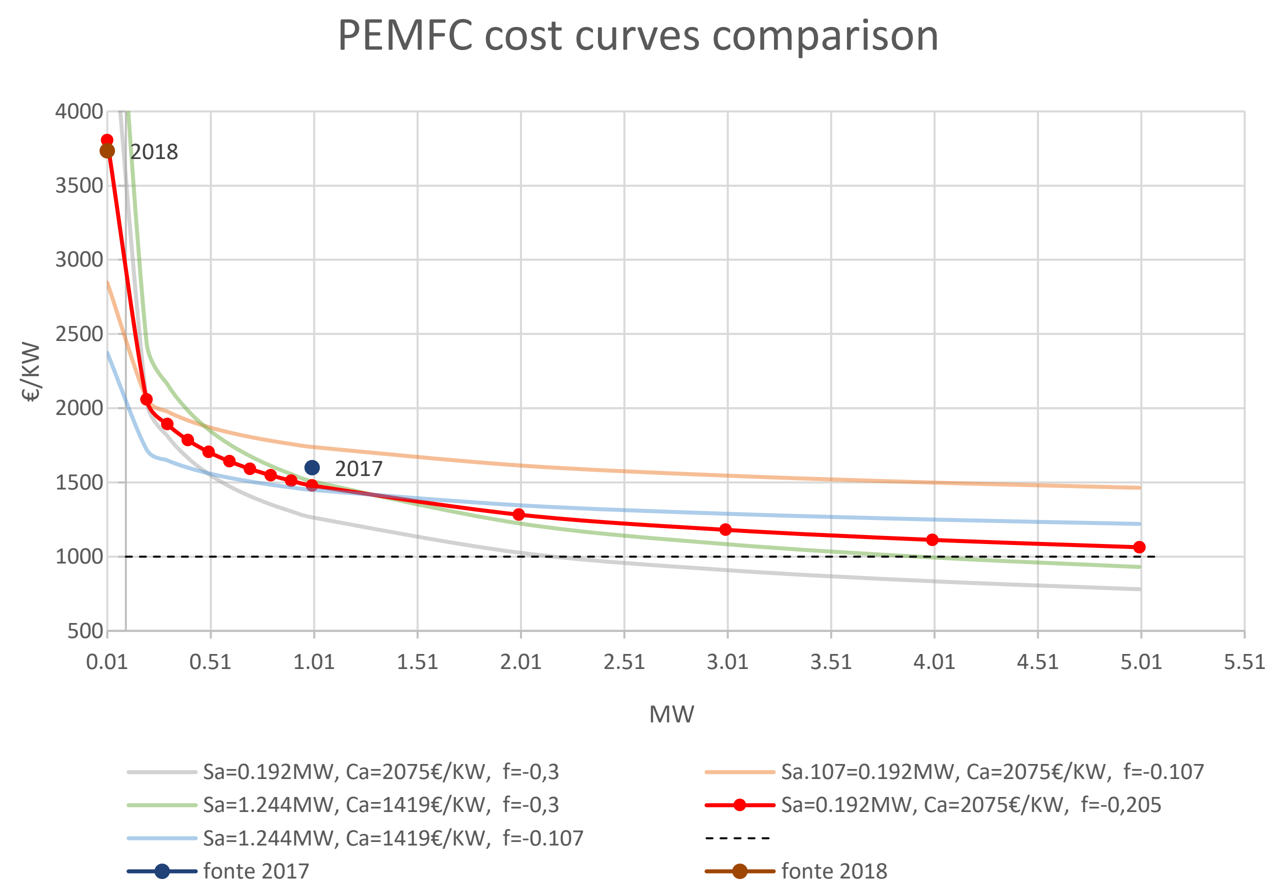

Figure 83 Assumed cost curves for defining the cost of PEMFC by size (in transparency) and the curve ultimately chosen for this purpose (in red)

However, the failures with the curves assumed in Table 32 made it possible to identify 2 more reliable points which were then chosen to make an interpolative reasoning like the one used in the case of PEMEL. Using then the same inverse formula used for the PEMEL we identified the treatment described in Table 33.

In Figure 83 the assumed curves are shown, those in transparency refer to the discarded ones while the one in red is the definitively chosen one. There are also 2 pairs of cost and size coordinates from other sources[55], [56] that show the validity of the curve. With f=-0.205 in fact, extending the curve backwards towards the tens of KW, I find that the curve given by the interpolation is the one that comes closest to the values given by these sources while the other curves are very far from them.

Table 33 Cost curve for determining the CAPEX associated with PEMFC according to its size

CURVE			
$c_a = 2075\left(\frac{S_a}{0.192}\right)^{-0.205}$ [€/kW]			
f	**-0.205**	**Size [MW]**	**Cost [€/KW]**
		0.01	3804
Reference		0.192	2075
		0.2	2058
		0.3	1893
		0.4	1785
		0.5	1705
		0.6	1642
		0.7	1591
		0.8	1548
		0.9	1511
		1	1479
Auxiliery		1.244	1419
		2	1283
		3	1181
		4	1113
		5	1063

3.4.3. FUNDAMENTAL VARIABLES OF THE OBJECTIVE FUNCTION

Given the inherent complexity of the structure of the objective function, the following are the steps for calculating the main variables leading to the:

- validation of the sizing explored by PSO in relation to the assigned GPS_target
- definition of the value of the function or the definition of the value of the LCOE

These two variables are GPS and PCOE respectively.

GPS

The Grid Penetration Share is described and calculated by the following relationship:

$$GPS = \frac{\sum_{t=1}^{T} P_{GRID}(t) \cdot \Delta t}{\sum_{t=1}^{T} P_l(t) \cdot \Delta t} \tag{26}$$

Where:

- $P_{GRID}(t)$ represents the power fournished by the grid at each time step t
- $P_l(t)$ represents the electrical power demand at each time step t

A certain dimensioning is considered valid if it can guarantee the following condition:

$$GPS \leq GPS_{target} \tag{27}$$

LCOE

Let's start with the operational definition of LCOE which is as follows:

$$LCOE = \frac{\sum_i NPV_i}{E_t} \left[\frac{€}{kWh}\right] \tag{28}$$

where:

NPV_i= Net Present Value associated to each technology
E_t= Total energy produced in the entire lifetime of the plant

Let’s then proceed to better define these two types of parameters that define the LCOE.

The NPV is the value associated with a given technology taking into account 3 different cost items which are::

- CAPEX: which assesses the cost of the investment

- OPEX or O&M: which evaluates all the costs associated with the operation and maintenance of the plant during its years of operation

- REPLACEMENT COST: which takes into account the replacement costs of the technologies in correspondence with the replacements made during the lifetime of the entire system.

While the first cost item represents a single, constant component (since it is defined at the time of the investment) and therefore does not need to be discounted, the other two components take into account the contribution of the expenses to be incurred in the years following the year of installation (continuously or discontinuously) and therefore the costs relating to the years following the first must be discounted (hence "Present Value"). The relationship used for discounting these costs is as follows:

$$actualized\ cost = \sum_{n_y}^{sl} cost \cdot \left(\frac{1 + i_{nom}}{1 + es}\right)^{n_y} \quad [€] \tag{29}$$

where:

i_{nom}= nominal discount rate;
es= escalation rate;
n_y=number of the year;
sl=system lifetime;

Thus we'll have:

$$NPOPEX_i = \sum_{n_y}^{sl} OPEX_i \cdot \left(\frac{1 + i_{nom}}{1 + es}\right)^{n_y} \quad [€] \tag{30}$$

$$NPREPLACEMENT_i = \sum_{n_y}^{sl} REPLACEMENT_i \cdot \left(\frac{1 + i_{nom}}{1 + es}\right)^{n_y} \quad [€] \tag{31}$$

And

$$NPV_i = CAPEX_i + NPOPEX_i + NPREPLACEMENT_i \ [€] \tag{32}$$

We would like to point out that the grid is also counted as technology and is associated with an NPV equal to the net of NPGRIDCOSTS and NPGRIDREVENUES which, being repeated every year, also need to be discounted.

$$NPGRIDCOSTS = \sum_{n_y}^{sl} GRIDCOSTS \cdot \left(\frac{1+i_{nom}}{1+es}\right)^{n_y} \quad [€] \tag{33}$$

$$NPGRIDREVENUES = -\sum_{n_y}^{sl} GRIDREVENUES \cdot \left(\frac{1+i_{nom}}{1+es}\right)^{n_y} \quad [€] \tag{34}$$

Where the incomes component is negative because it reduces the cost. So we will have:

$$NPV_{GRID} = NPGRIDCOSTS + NPGRIDREVENUES \quad [€] \tag{35}$$

The other variable that makes up the LCOE is E_t which comprises the sum of all the energy consumed during the lifetime of the system. It corresponds in practice to the cumulative load of the first year plus the same load evaluated for future years but also discounted. That is:

$$E_t = \sum_{n_y}^{sl} E_{t1} \cdot \left(\frac{1+i_{nom}}{1+es}\right)^{n_y} \quad [kWh] \tag{36}$$

with

$$E_{t1} = \sum_{t}^{T} P_l(t) \cdot \Delta t \; [kWh] \tag{37}$$

where $P_l(t)$ is the value of the load at that time of the year evaluated in the year of installation of the system.

3.4.4. DETERMINATION OF SECONDARY RESOURCES

Here we will quickly describe how the value of the waste heat energy produced during the period of operation of the PEMFC, if any, was assessed.

It is assessed simply as the term for losses in the transformation of energy from chemical to electrical energy using the efficiency of the PEMFC:

$$Q_{FC} = P_{ACC} \cdot (1 - \eta_{FC}) \quad [kWh] \tag{38}$$

where P_{ACC} indicates the chemical energy leaving the hydrogen storage tank.

As expressed in the title of this paragraph and as better highlighted in the presentation of the results, we want to look at this energy with a view to circularity and sustainability, considering it not as waste but as a secondary source for which it would be interesting to find some use.

3.4.5. EMISSIONS EVALUATION

The calculation of the emissions saved through the installation of the system was carried out by weighing the load component covered by the network and multiplying it by the emission coefficients evaluated from the IPCC coefficients.

After having gathered under the macro-groups of fuels identified by the IEA the fuels listed by the IPCC as shown in the Table 20, an average emission factor for each pollutant was generated for each fuel macro-group in the following way:

$$e_{IEA\,fuel,i} = \frac{\sum_{j}^{n_{IPCCsubfuels}} e_{IPCC,j,i}}{n_{IPCCsubfuels}} \left[\frac{Kg}{kWh}\right] \tag{39}$$

Which is a simple arithmetic mean where::

- $e_{IEA\,fuel,i}$= emission factor of the fuel categorised by the IEA for the i-th pollutant
- $e_{IPCC,j,i}$= emission factor of the j-th subfuel associated to the IEA macrocategory categorised by the IPCC for the i-th pollutant
- $n_{IPCCsubfuels}$= number of subfuel associated with the IEA macrocategory categorised by the IPCC

Once this is done, a single emission coefficient per pollutant is identified. This coefficient is derived from the weighted average of the coefficients according to the role in the energy mix of the country in question that each fuel has:

$$e_i = \frac{\sum_{fuels}\left(e_{IEA\,fuel,i} \cdot E_{IEA\,fuel}\right)}{\sum_{fuels} E_{IEA\,fuel}} \left[\frac{Kg}{kWh}\right] \tag{40}$$

with $E_{IEA\,fuel}$=produced energy associated to each IEA categorized fuel.

Having thus defined the emission factor for a given pollutant, all that remains is to multiply it by the share of load covered by the grid to find the quantity of emissions EM_i associated with the production of that energy

$$EM_i = e_i \cdot \sum_{t}^{T} P_{l_{GRID}}(t) \cdot \Delta t \;\; [Kg_i\,] \tag{41}$$

4. RESULTS

In this section, the results obtained from the simulations of the various case studies investigated are presented in an analytical and objective manner. For the sake of brevity, the results of every single simulation will not be presented, but an attempt will be made to make the reader understand the main directions that the case studies as a whole indicate as most favourable for the application of the system.

To this end, for the comparison between the results of the same series concerning different GPS_targets, reference will be made mainly to the 2 cases of extreme GPS_targets and the intermediate one (which, as we will see, do not necessarily refer to 100%-50%-0%).

For simplicity, we shall first analyse the results referring to the present load series and then refer the comparison between this and the future series to the paragraph dedicated to the presentation of the results relating to the future load series.

4.1. PRESENT PARTIAL LOAD SIMULATIONS

The main parameter that most effectively represents the results of the simulations, as mentioned several times, is the value of the objective function or LCOE. It is represented in the as a function of the GPS_target we set for each simulation. Here we see very clearly both the relationship between LCOE and GPS_target and between LCOE and the meteorological series associated with the 3 different time domains considered.

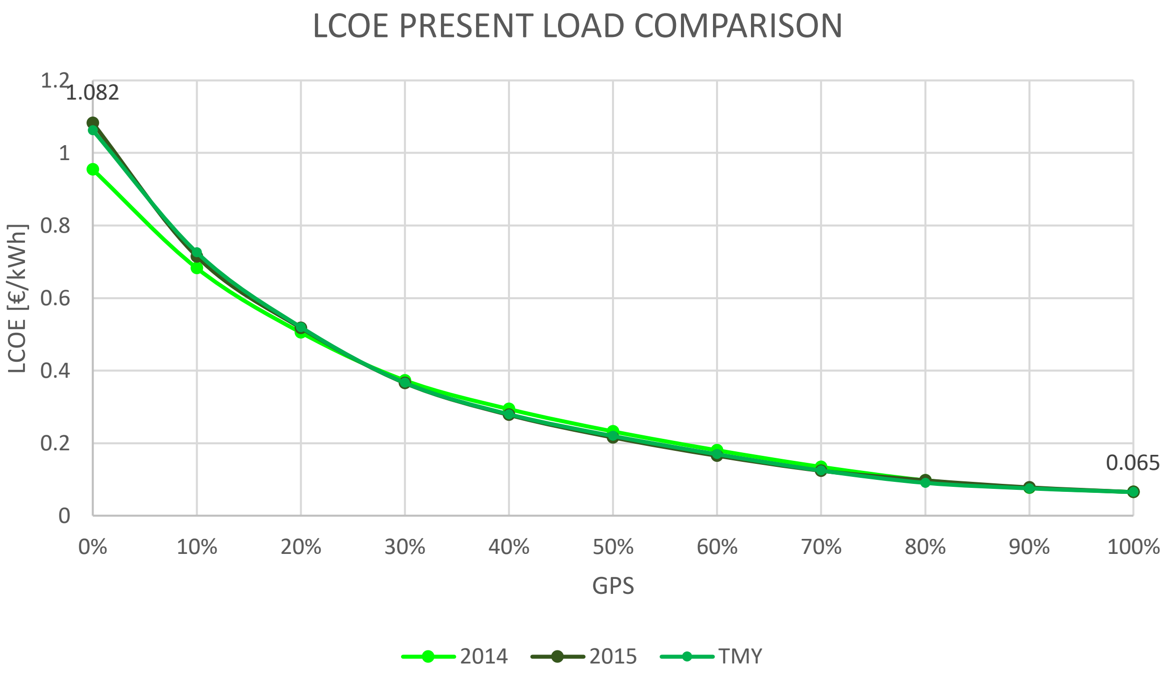

Figure 84 Comparison of LCOE pareto curves defined in relation to PPL for the 3 time domains

As expected, the trend is increasing towards low GPS_target values. The dependence on the latter is therefore strong. This is due to the fact that, as shown in the graphs Figure 94 e Figure 103 if the grid is allowed to intervene completely, the grid alone can cover the full load at all times of the year and is the cheapest source of supply. As a result, limitations on its ability to intervene lead increasingly to a need to rely on the system. This dependence is also very gradual and manages to identify a real pareto curve for the LCOE. This is due to the fact that we did not impose discrete size installations, i.e. we did not seek a dimensioning constrained by the possibility of installing modular technologies with a defined size that should at least cover the load, but rather we focused on the actual power necessary only to meet the deficits.

The dependence on the different time domains is minimal, but it is clear that the main difference is made by the meteorological basis associated with each year. In fact, the curves diverge particularly for low LCOE where the main production actor is the system. Moreover, the two most divergent series are those referring to the actual years 2014 and 2015 and allow us to identify a range in which the LCOE is likely to be found. There is also a close similarity between the curves for the TMY and 2015 series, which represent the upper limit of this range. It does not therefore appear that meteorological data from more recent years are responsible for profound changes in the sizing of the system compared to what would have been theorised in earlier years, although the curve for 2015 is still the least advantageous.

In general, however, there is a jump of more than one order of magnitude in the value of the energy cost compared to the case where the demand is met with grid energy alone. In fact, LCOE goes from a value of 0.065€/KWh for the case GPS_target=100% (case completely covered by the grid) to 1.082€/kWh for the case GPS_target=0% (completely off-gird).

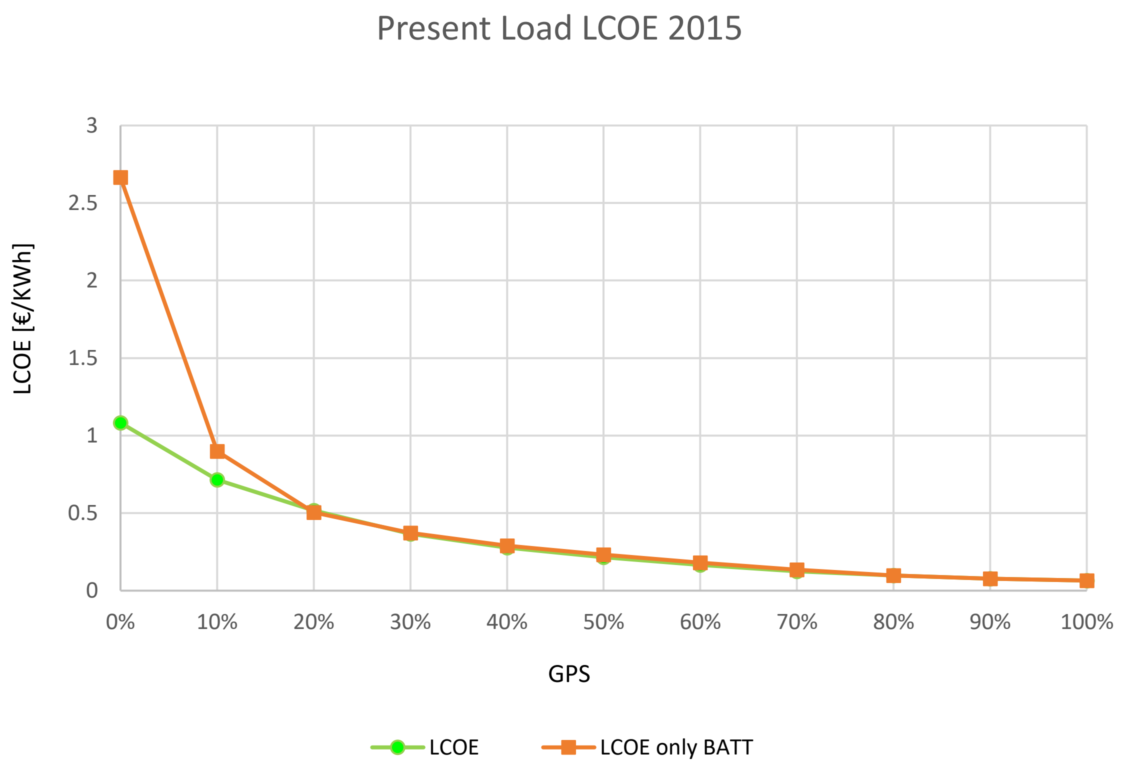

Figure 85 Comparison of the LCOE pareto curve trend calculated considering a hybrid storage, i.e. H2+Battery (in green) and Li-only storage (in orange). Reference time domain: real year 2015

The Figure 85 shows a very interesting feature that constitutes one of the main considerations to which this study leads. In fact, two curves are shown (for the time domain indicated as the worst, i.e. the one referring to 2015) relating to two optimal situations proposed by the optimisation algorithm, namely:

- Case in which only the battery is used for storage management
- Case in which both proposed storage solutions (battery and hydrogen storage) are used

It is clear that the worst solution is the one that only considers the battery as the storage technology. In this case, the cost of energy rises to double that of a hybrid solution.

This behaviour occurs starting from the imposition of the GPS_target at 20% and the fundamental role that hybrid storage plays at these grid dependency values is also very clearly visible in Figure 86 e Figure 89 which show the sizing of the storage technologies.

In particular, they represent the same graph but with different scales so that the absolute relationship between the sizing of the two types of technologies (Battery and Hydrogen) and more precisely in the case of the optimal solution par excellence, i.e. hybrid storage, can be clearly seen. In order to be consistent and to take a precautionary approach, it was decided to show the graphical representations of the series of results related to this and to the sizing of the other components, always relative to the time domain that provides the worst solution, i.e. 2015.

Nel grafico Figure 86 shows how the sizing of the two storage technologies varies considerably. The main explanation for this behaviour is basically linked to the nature of the storage types and their versatility.

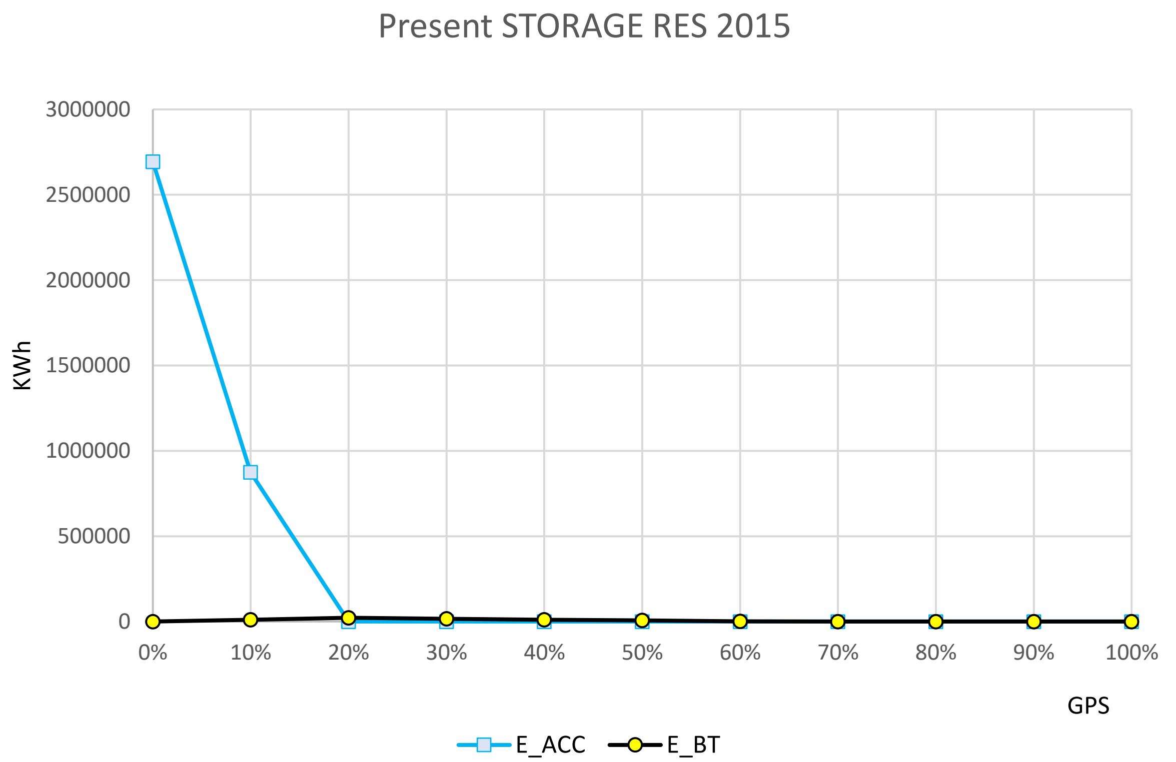

Figure 86 Sizing of the different types of storages according to the GPS_target for the time domain consisting of the real year 2015.

In fact, the battery, as can be seen in Figure 87 is mainly used in a perspective of being able to provide a quick response to the needs of the load unsatisfied by direct production. It therefore represents a technology for short-term storage that is capable of providing a high degree of flexibility and readyness.

Storage with production and accumulation of hydrogen, of which the load status throughout the year is shown in Figure 88, on the other hand, allows for seasonal energy management, guaranteeing the possibility of storing energy that is used even far from the period in which it was stored. This type of management is fundamental because it makes it possible not to lose any production surplus during the year and thus reduce the dimensioning and therefore the costs linked to production technologies. With regard to this storage method, it should be pointed out that even though no constraint has been included to impose a load status at the end of the year equal to that at installation, this constraint is practically independently respected by the proposed solutions as shown in Figure 88.

It follows that the bigger the sizing of the production technologies, the higher the surpluses and therefore the need for long-term storage. This explains the behaviour of the sizing of storage technologies shown at two different scales Figure 89. Here can be clearly seen the change of trend in the sizing of the battery which, if used as the only technology for storage up to low GPS_targets (≈ 20%) (), is being partially replaced by hydrogen storage. Hydrogen storage starts to grow, taking the burden of long-term storage off the battery and leaving it to operate only for balancing small and fast hourly fluctuations. In fact, the size of the battery returns to be the same as in cases with high GPS_targets, where the seasonal management of deficits was left entirely to the grid, for GPS_target =0%

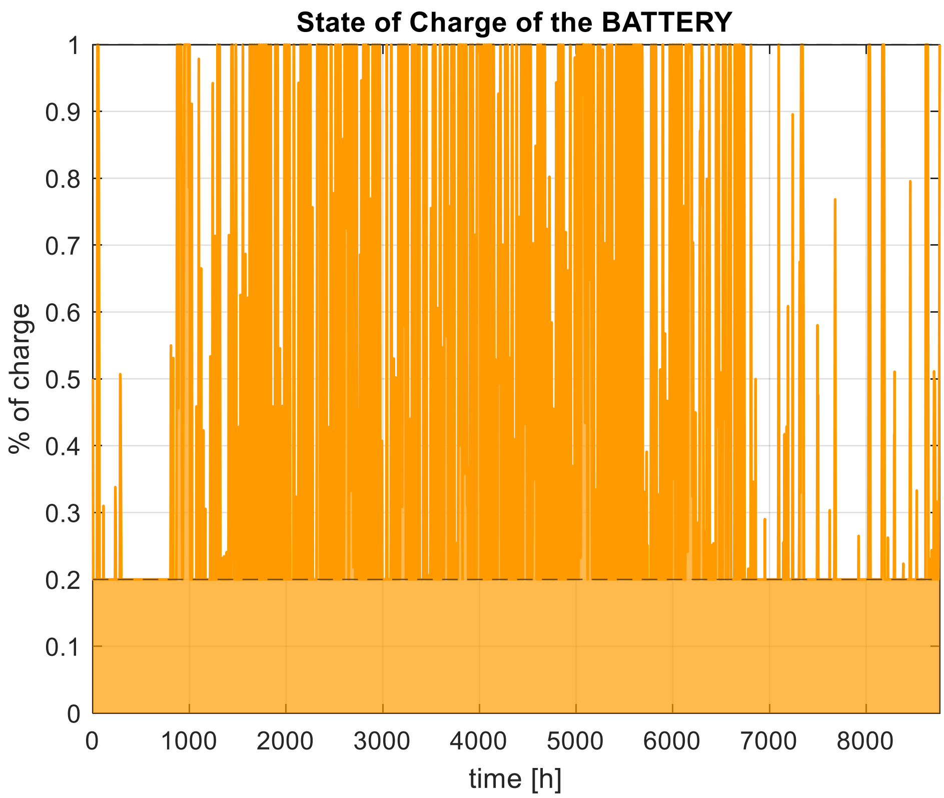

Figure 87 Annual state of charge (SOC) behaviour of the Li-ion battery. The dotted line indicates the minimum charge level (SOC_min) below which the battery cannot be discharged. Reference simulation: SIM_RES2015_LP_GPS0

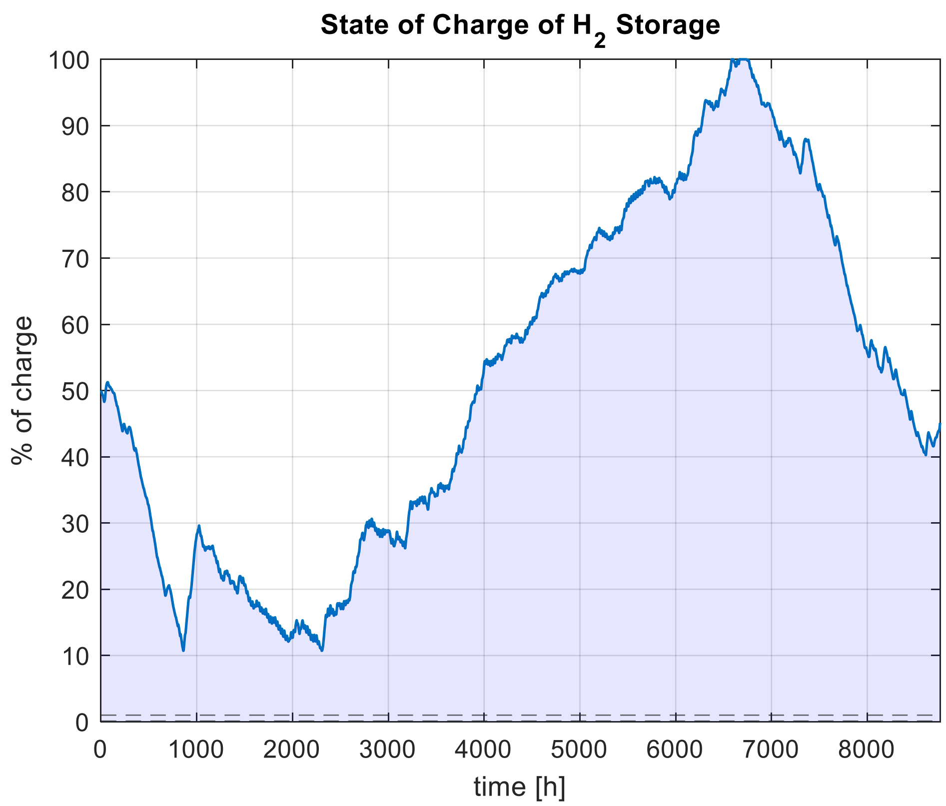

Figure 88 Annual behaviour of the H2 tank state of charge (SOCH). The dotted line indicates the minimum charge level (SOC_h2_min) below which the reservoir cannot be discharged. Reference simulation: SIM_RES2015_LP_GPS0

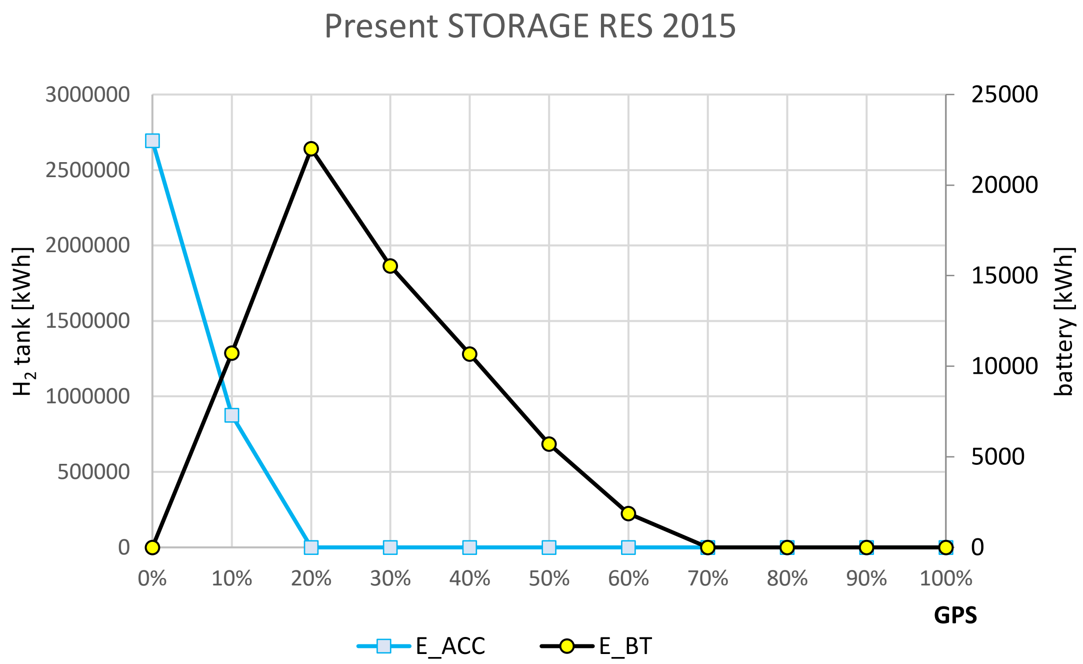

Figure 89 Dimensioning of the different types of storages according to the GPS_target expressed with different reference axes to highlight the relative behaviour of the two technologies that influence each other. Time domain composed of the real year 2015.

Looking more deeply into the behaviour of hydrogen storage in particular, we show in Figure 90, Figure 91, Figure 92, Figure 93 the parameters describing the size of the transformation technologies and their activity over the year.

As they are linked to the presence of hydrogen storage, they only appear at very low GPS_targets (≈ 20%). The size of the two depends very much on the objective of the type of storage under consideration, as well as on the size of the production technologies, on which the surplus values to be managed depend in the first instance, and consequently the size of the technologies for storing this surplus. It is therefore the electrolyser in particular that depends on the size of the production technologies. The electrolyser must guarantee a maximum operating power capable of transforming the surplus at any time to ensure that the hydrogen tank can fulfil its task of seasonal storage.

Indeed, comparing Figure 90 with the graph representing hourly surpluses and deficits Figure 96 it can be seen that the size of the electrolyser is such that it can store most of the surplus that occurs during the year.

While the size of the electrolyser follows this logic, the size of the FC follows much more a logic similar to that of the battery, to which it merely provides support. The size of the FC therefore depends not so much on the amount of surplus or deficit as on the frequency of surplus during the year. The rapid alternation of surpluses and deficits is advantageous because it allows the battery to be active and available during most of the hours of deficit, thus delegating to the FC a supporting role that allows it to complete the coverage of the deficit where the battery does not match all the request mainly because of its size rather than its state of charge.

However, as the availability of hydrogen increases as the GPS_target decreases, it may be possible to reach situations where the availability is so high that hydrogen storage can also play the role of fast deficit manager, which in some cases (as in the 2015 example) leads to the complete replacement of the battery with hydrogen storage. In this way, hydrogen storage assumes a key and fundamental role for hybrid systems with high degrees of autonomy (GPS_target which means 0%).

La Figure 94, which shows us the percentage shares of load fulfilment between the different technologies of production, storage (for hydrogen storage represented by FC) and external for different GPS_target values, allows us to clearly see the two possibilities that are being referred to in case the system is off-grid. The pie chart at the bottom right (time domain real year 2015) shows the solution in which the battery and the PEMFC work together in the same way and thus share the burden of deficit management bringing a higher degree of reliability to the whole system that can count on one in case of problems with the other technology and vice versa. The graph at the bottom left (TMY time domain) shows the solution with only hydrogen storage as the main player, thus proving its key importance: can be done without the battery but not without the hydrogen. The fact that these solutions belong to the two time domains in which the LCOE is the worst shows that one solution over the other does not necessarily entail an economic advantage, even if, for the time domain with the most advantageous LCOE and which is not shown in the figure, the solution adopted is the first one, which is the most advantageous as it brings with it greater reliability of the system.

The difference in the drivers influencing the sizing of the PEMEL rather than of the PEMFC is clearly visible both in Figure 90 where it is possible to see a behaviour always directed towards a sustained growth for the PEMEL and almost asymptotic for the PEMFC, and in Figure 91 where the comparison between the inlets and the outlets of the hydrogen tank shows 2 different trends.

In the first case the continuous growth is well associated with a continuous growth of the size of the production technologies (as shown in Figure 99) while the asymptotic behaviour of the PEMFC follows the constant behaviour of the size and distribution of the deficits along the year (Figure 96).

In the second case, we identify in the shape of the outlets (negative part) the characteristic behaviour of the load while in the inlets we identify a behaviour mainly related to the distribution of the surpluses. In Figure 94 where only the behaviour of the PEMEL is shown, this dependence is even clearer as its activity is more rarefied in the winter months in which, as the contribution of photovoltaic production is lacking, there is a lower frequency of surpluses.

Associated to the activity of the PEMFC shown in detail in Figure 93 , there is also the availability of waste energy (Figure 95), essentially in the form of heat, which could be exploited for uses which have not been considered here. Its availability throughout the year, however, would make it an interesting element for a more in-depth investigation of its use. Moreover, if the trends in surpluses and deficits are analysed in detail separately between night and day (Figure 97, Figure 98) it can be seen that the deficits, and therefore the start-up of the PEMFC, are concentrated at night, which is also the coldest time. From this observation it might even be interesting to consider placing constraints on the system in which the PEMFC works more frequently at night, favouring the use of energy from storage during the latter, which would be accompanied by the production of heat that can be used, for example, for air conditioning, rather than the direct use of the energy just produced.

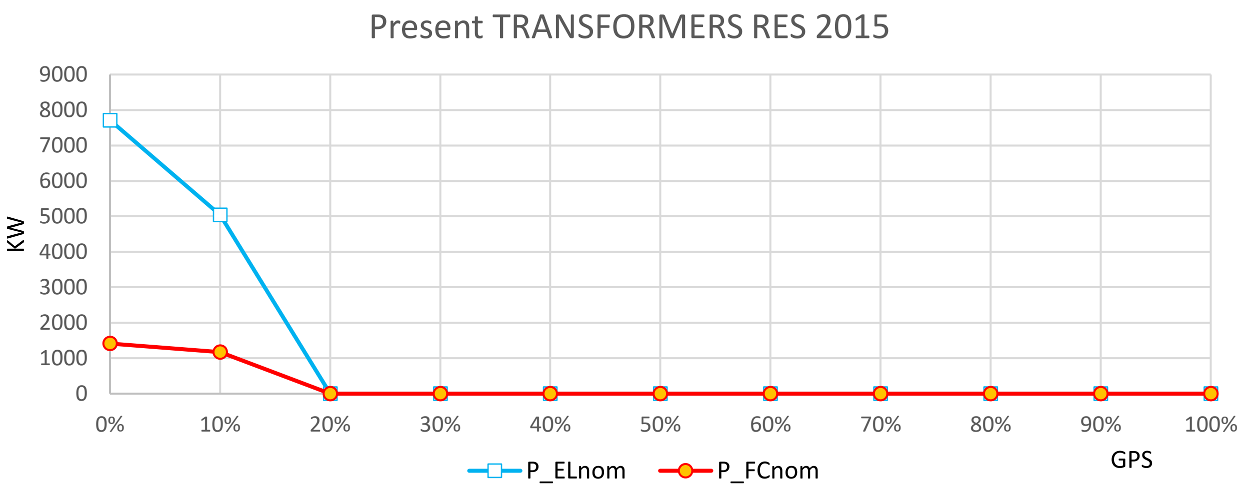

Figure 90 Dimensionamento delle tecnologie di trasformazione P2G (PEMEL) e G2P (PEMFC) in funzione del GPS_target ipotizzato durante le simulazioni per PPL sul dominio temporale composto dall'anno reale 2015

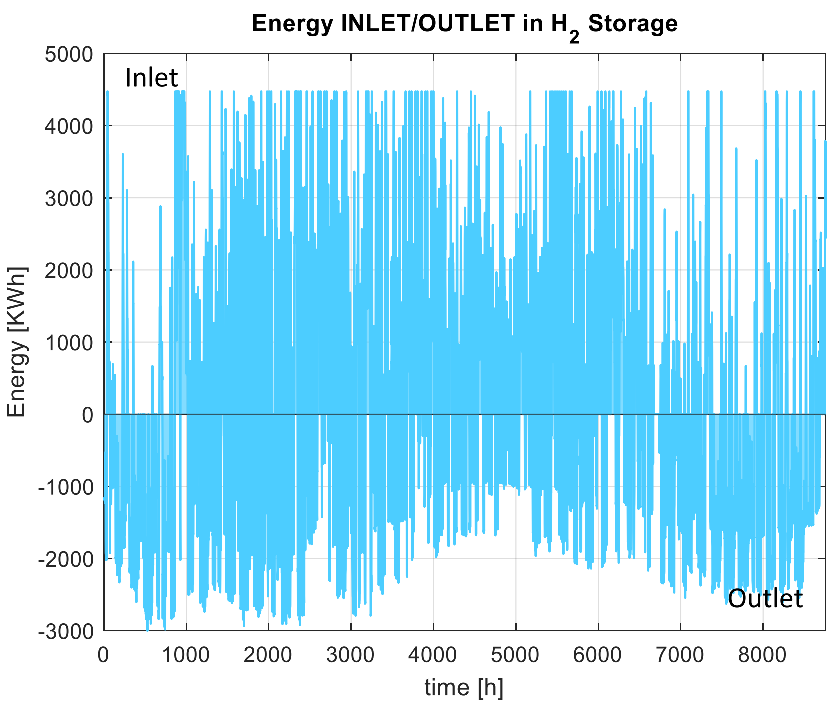

Figure 91 Annual series of energy charged (E>0) and discharged (E<0) into and from the H2 reservoir. Reference simulation: SIM_RES2015_LP_GPS

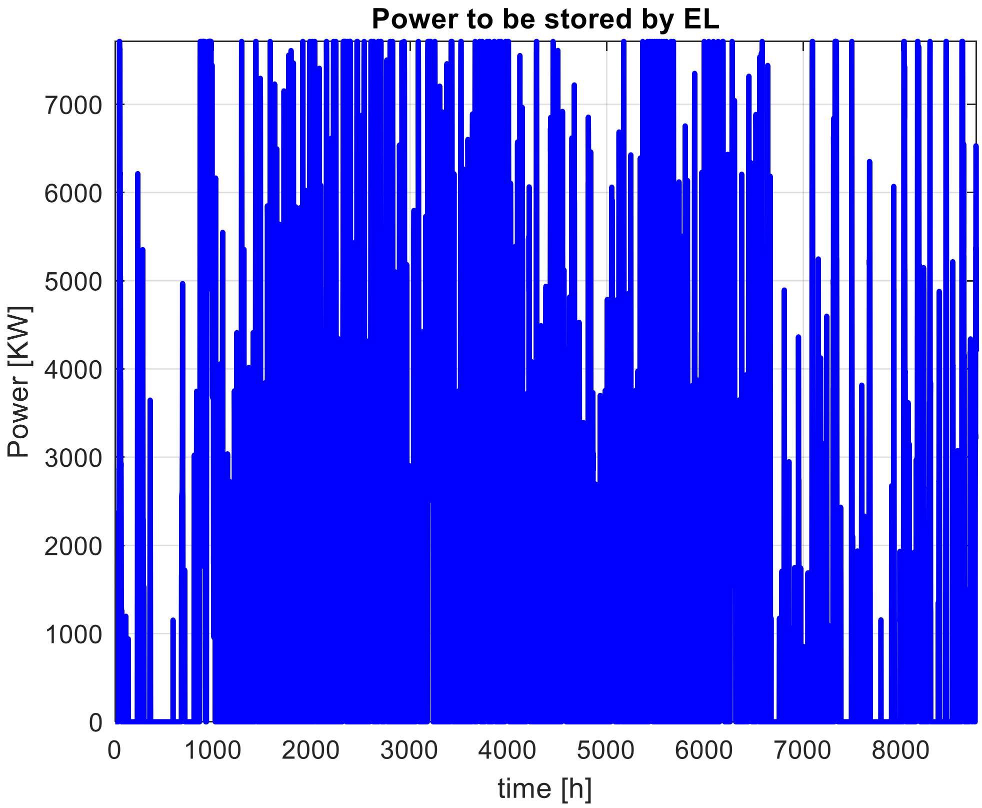

Figure 92 Annual series of energy input to PEMEL to be converted to H2 for reservoir storage during the P2G process. Reference simulation: SIM_RES2015_LP_GPS0

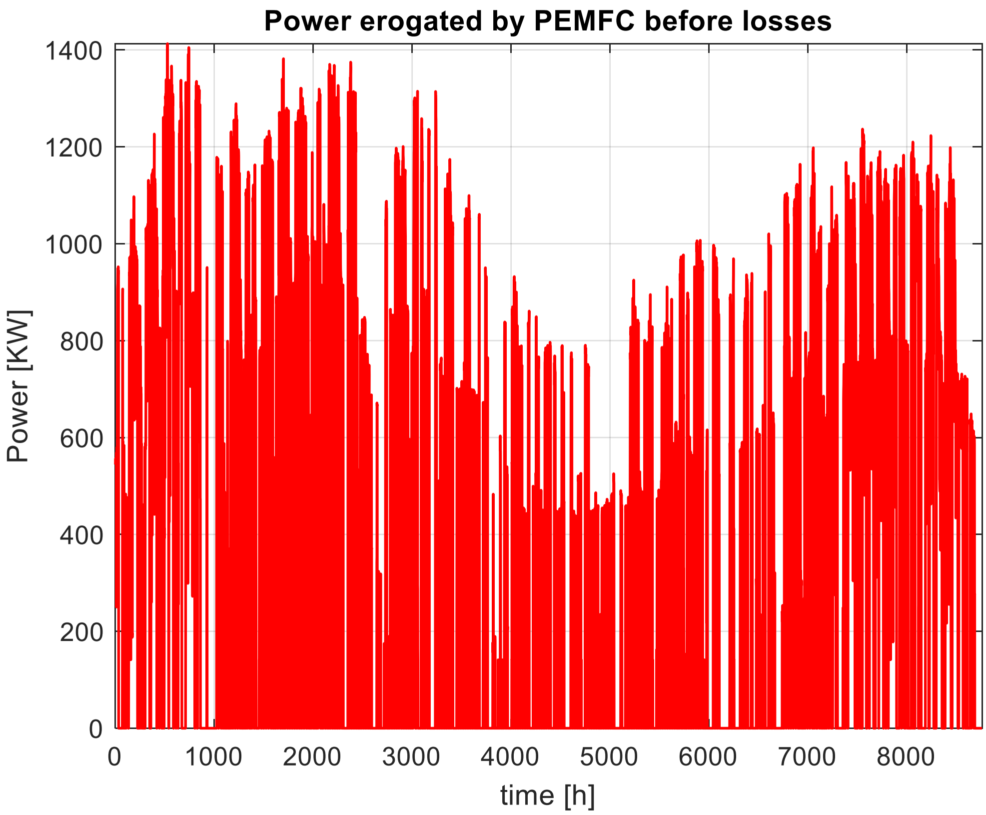

Figure 93 Annual series of energy output from the PEMFC during the G2P process of H2 tank discharge. Reference simulation: SIM_RES2015_LP_GPS0

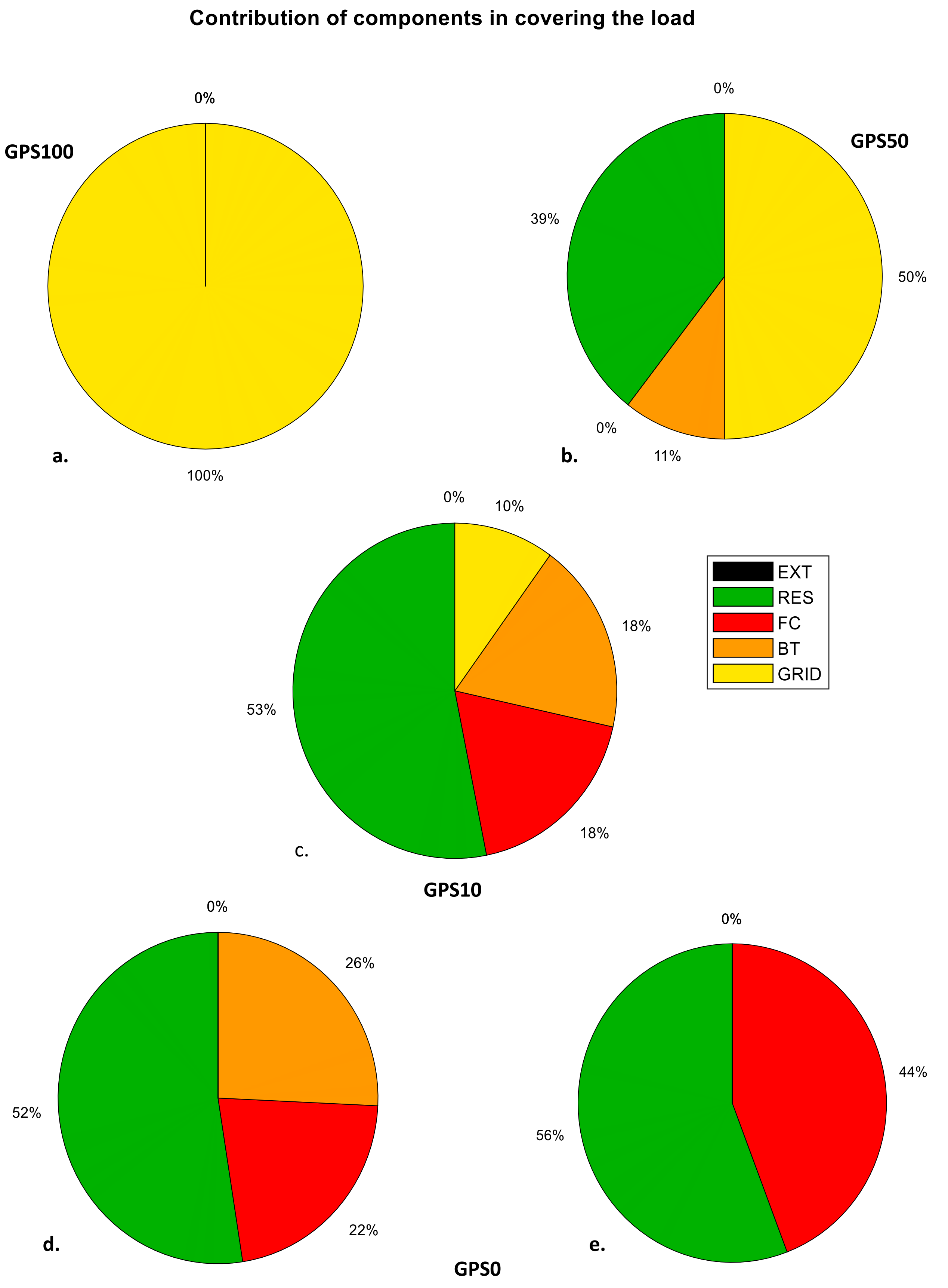

Figure 94 Pie charts showing in relation to 4 different GPS_target values the annual percentage contributions made by each component to load coverage. The graphs refer respectively to the following simulations: a. SIM_RES2015_LP_GPS100; b. SIM_RES2015_LP_GPS50; c. SIM_RES2015_LP_GPS10; d. SIM_RESTMY_LP_GPS0; e. SIM_RES2015_LP_GPS0

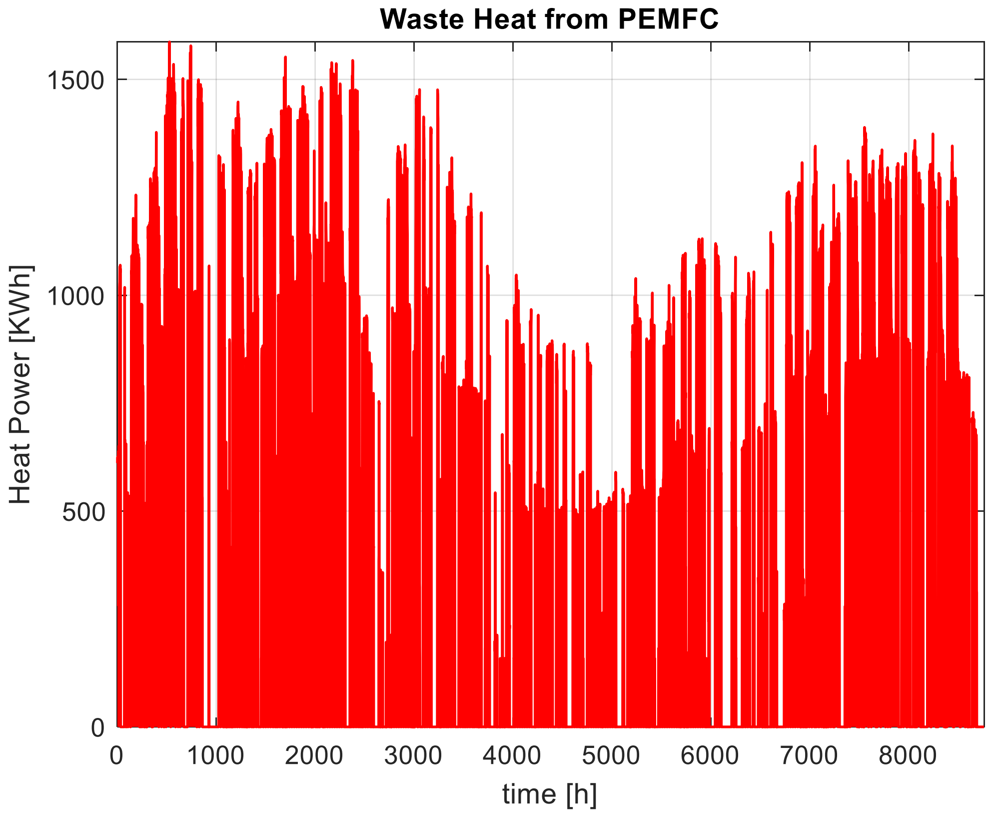

Figure 95 Annual hourly series of the "waste" heat output generated during the use of PEMFC and which can be used for different purposes not analysed in this work. Reference simulation: SIM_RES2015_LP_GPS0

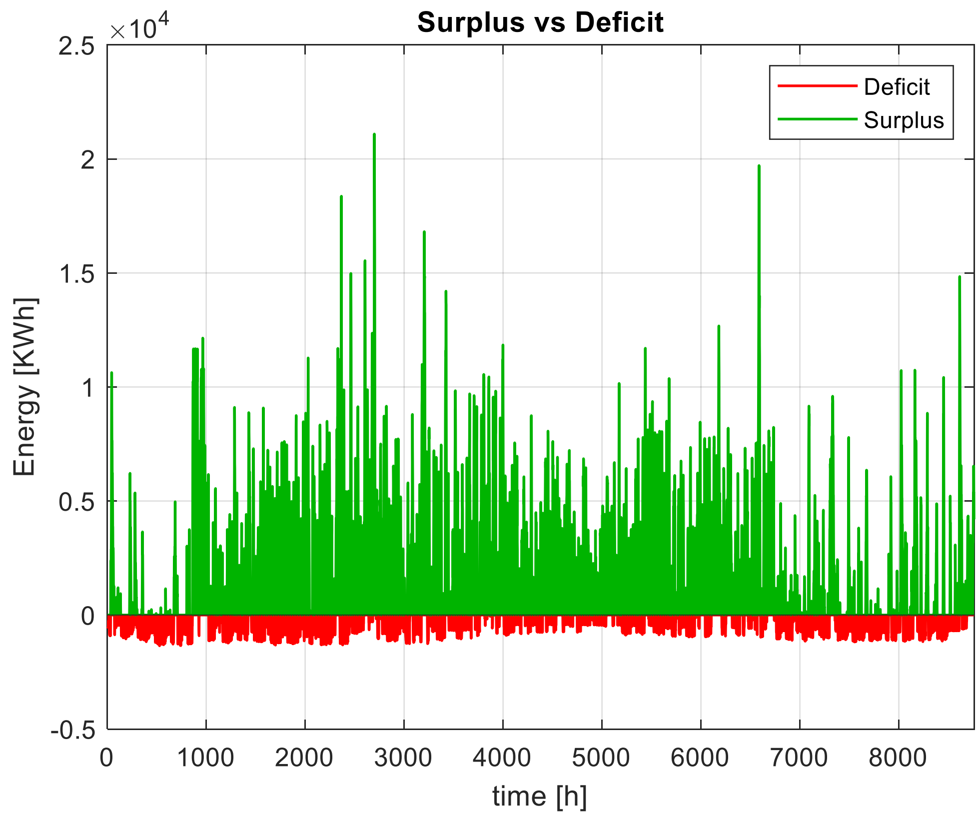

Figure 96 Hourly, annual series of energy available as surplus (E>0) or needed and considered as deficit (E<0). Reference simulation: SIM_RES2015_LP_GPS0

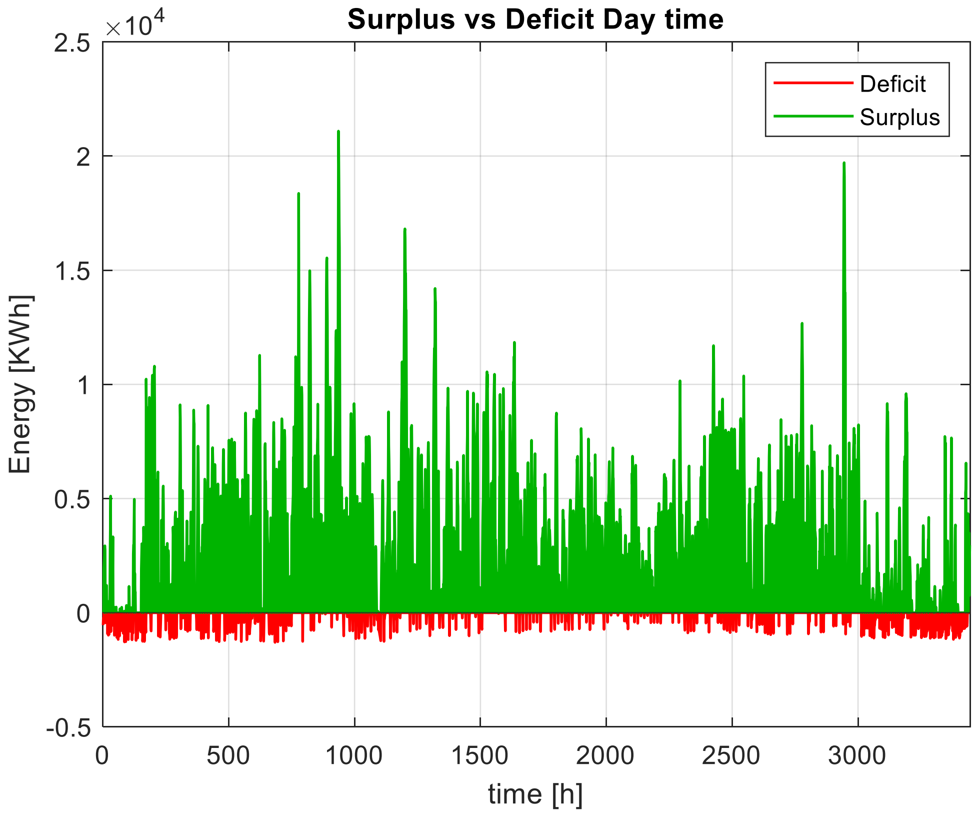

Figure 97 Daytime, annual time series of energy available as surplus (E>0) or needed and considered as deficit (E<0). Reference simulation: SIM_RES2015_LP_GPS0

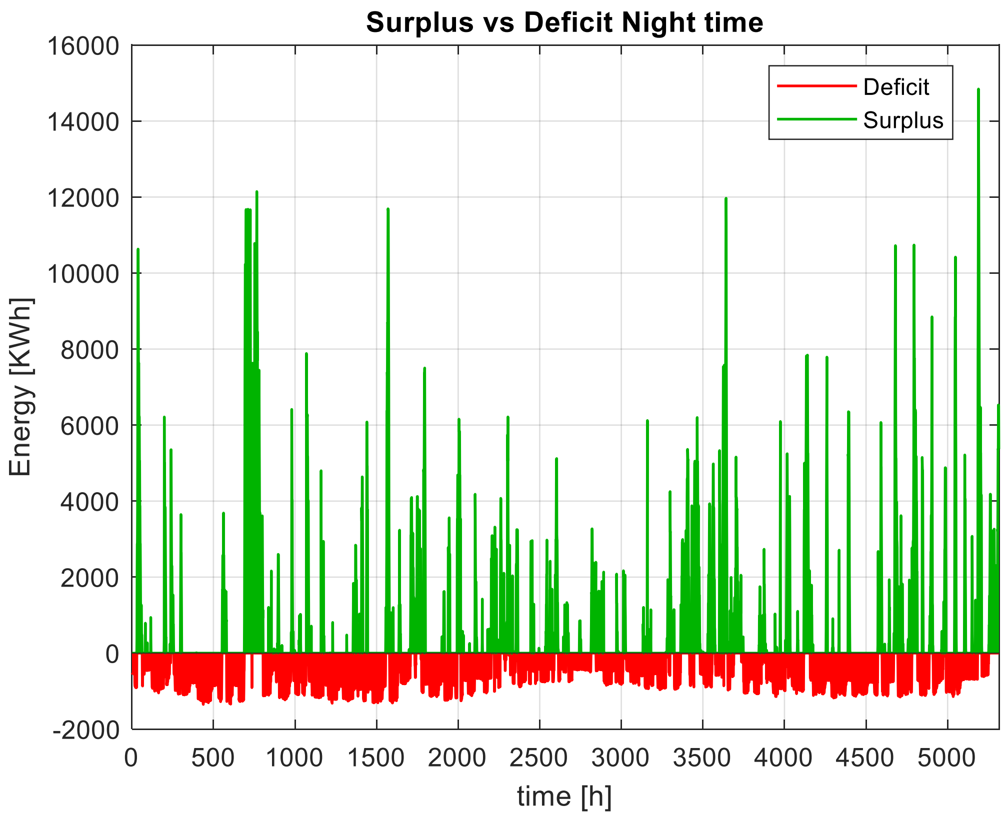

Figure 98 Nighttime, annual time series of energy available as surplus (E>0) or needed and considered as deficit (E<0). Reference simulation: SIM_RES2015_LP_GPS0

The last technologies shown to be sized according to the GPS_target (again in the worst case detected) are production technologies (Figure 99). It is immediately apparent that there is a likely dependency between the growth in wind power sizing and the growth in the use of hydrogen storage. This relationship is effective in that it can be explained by the fact that, as wind turbine is a technology that allows for much less seasonal production than solar PV technology (Figure 71,Figure 72, Figure 73, Figure 100), if sufficiently large, it allows for almost instantaneous coverage with less need for stored energy. This happens especially at the latitudes where we are assuming to operate. At the same time, the required installation of solar power, which guarantees greater reliability, predictability and frequency density in the months of light (Figure 64, Figure 65, Figure 66, Figure 100) makes it possible in those same months (which also correspond to the months with a lower load Figure 101) to use solar energy to cover the load directly, thus dispensing wind powe from the main role it had in the darker months and making it responsible for producing the bulk of the surplus in the summer months. This surplus, having seasonal characteristics, is therefore preferably stored in the hydrogen tank rather than in the battery.

This also explains the asymptotic trend of the solar installation at the lowest GPS_target. In fact, it is only installed to facilitate the coverage of deficits in the summer months.

On the other hand, the sizing behaviour of the two production technologies for lower GPS_target values than the hydrogen storage input is easy to interpret. Indeed, the preponderance of solar installation in this area has 2 co-existing explanations:

- Lower investment cost per kW than wind
- The high GPS_target values allow a wide availability of grid intervention that tends to cover the deficits of the periods that should be covered by the most expensive technology, i.e. wind power. This means that in the dark months, rather than installing wind power or rather than installing long-term storage, the main reliance is on the availability of the grid as can be seen in Figure 101, Figure 102.

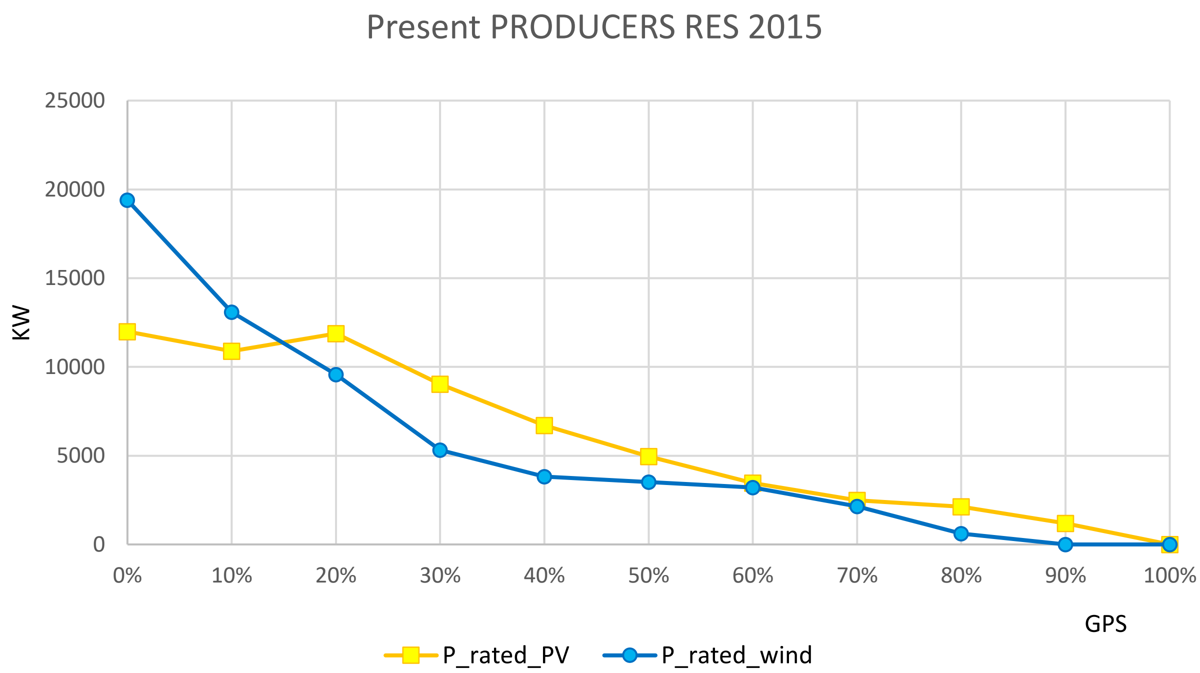

Figure 99 pareto curves of the sizing of renewable generation technologies (WIND &PV plants) referred to different GPS_target values assumed during the simulations in the actual reference year of 2015

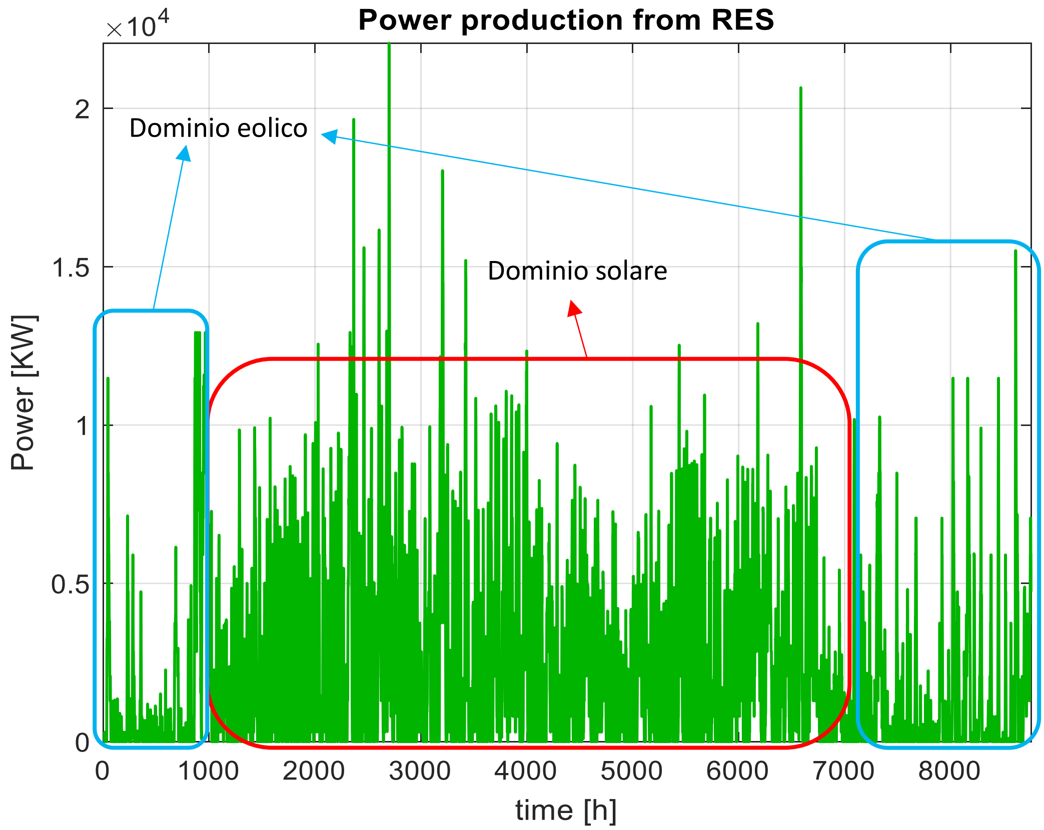

Figure 100 Hourly, annual series of the total power generated by renewable energy plants (PV &WIND). In particular, the time periods in which production by one or the other technology prevails are indicated. Reference simulation: SIM_RES2015_LP_GPS0

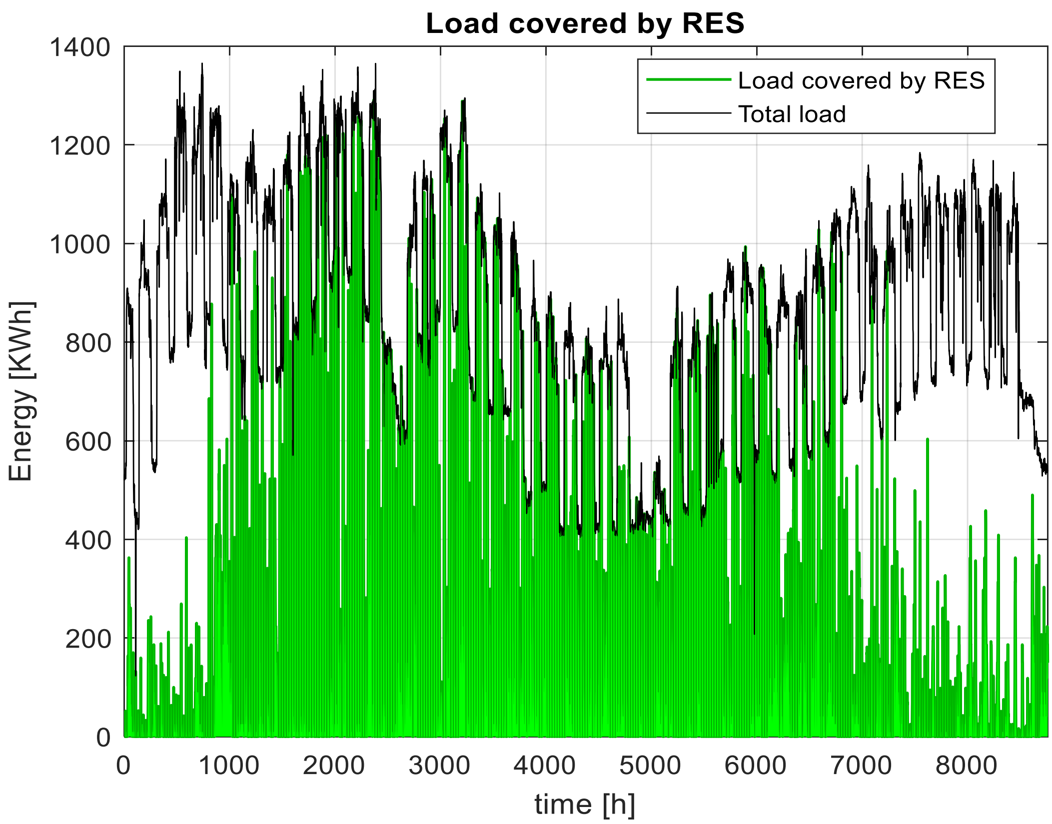

Figure 101 Annual time series of energy produced by renewable energy technologies and used directly for PPL coverage without first being stored. Reference simulation: SIM_RES2015_LP_GPS80

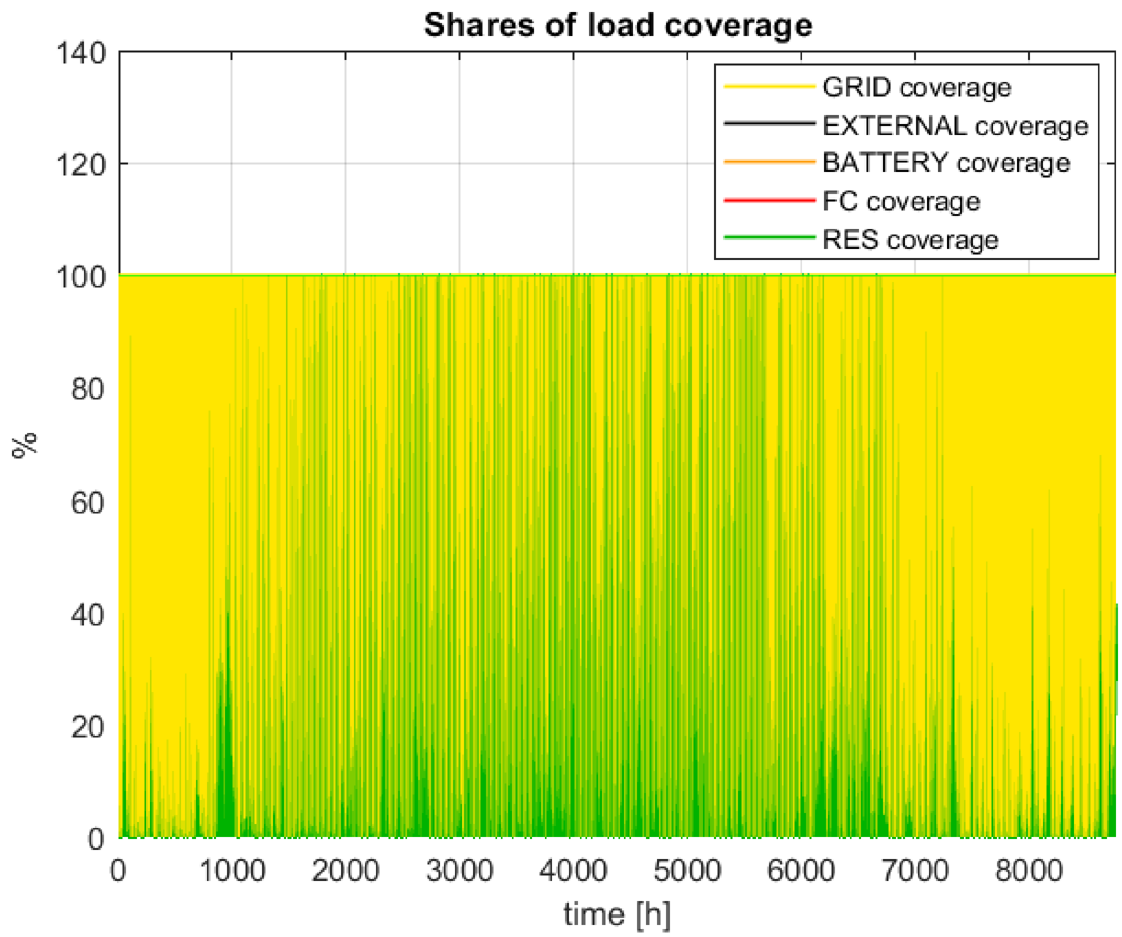

Figure 102 Comparison on an hourly, annual basis of the shares of energy used for PPL coverage from the different available technologies. Reference simulation: SIM_RES2015_LP_GPS80

Finally, let us analyse the results obtained from an economic point of view. Figure 103 shows the shares of the LCOE refferred to the different contributions of each technology. Four graphs are shown in parallelism to Figure 94**Errore. L'origine riferimento non è stata trovata.** ignoring the 10% GPS_target graph.

In general a large portion of the LCOE, which comes to oscillate more or less around 50%, is due to the costs related to production technologies. This was easy enough to predict, since these are the core technologies on which the system is based and on which energy availability depends in the first place.

However, the graph referring to GPS_target=50% is interesting because it shows the high cost-effectiveness of using the grid: for each percentage unit of contribution to the LCOE, there are two units of load coverage (use). We can interpret this comparison as an evaluation of the efficiency of the investment, which is very high. On the other hand, the same efficiency evaluated considering the investment for the installation of the battery and its use is much lower, since each percentage point of investment corresponds to only half a percentage point of use.

However, this efficiency of the battery improves when compared with the efficiency of all hydrogen storage technologies. This is shown by the graph at the bottom left.

Comparing the off-grid cases with and without a battery, we can see that hydrogen storage is always the most expensive item, depending mainly on the tank size. We can also see that the "substitution" of the battery-related cost with hydrogen storage does not vary drastically. This may therefore lead us to think that, for systems requiring approximately the same investment in terms of processing technology, there is a general storage-related cost that is similar to that of each technology used for the same.

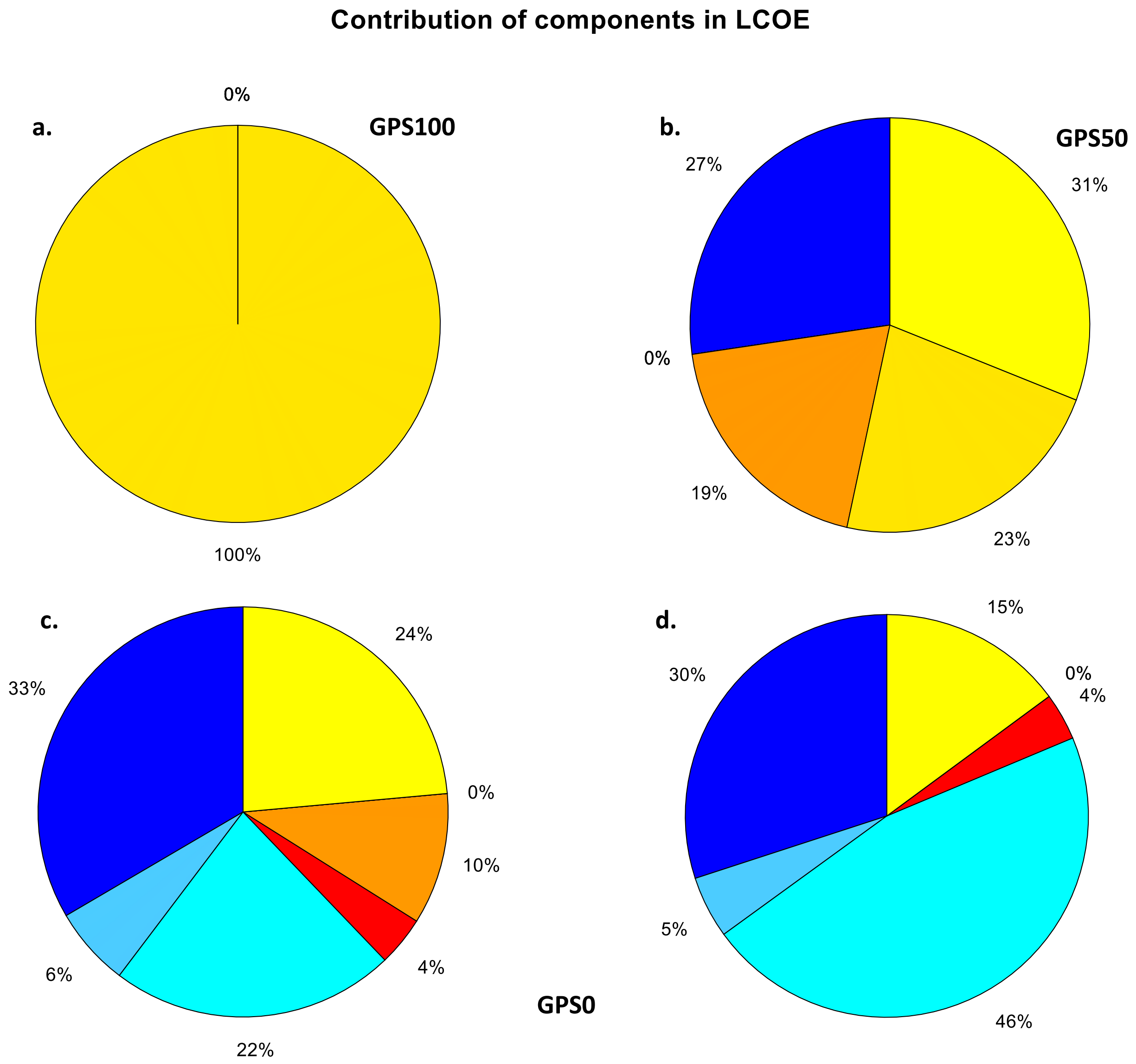

Figure 103 Pie charts showing in relation to 3 different GPS_target values the percentage contributions made by the costs associated with each component in the composition of the LCOE. The graphs refer respectively to the following simulations: a. SIM_RES2015_LP_GPS100; b. SIM_RES2015_LP_GPS50; c. SIM_RESTMY_LP_GPS0; d. SIM_RES2015_LP_GPS0;

Having said that, it is clear that the bulk of the energy cost will come from the investment cost of the system whose behaviour according to the GPS_target is shown in the Figure 104. The reason for the increase near the low GPS_target is the increase in investment in wind and hydrogen storage.

Finally, while the Figure 105 simply shows us the fact that the cost of buying and selling energy for immediate consumption follows the load trend, Figure 106 shows us the period when selling to the network is considered favourable. This coincides with the summer period when the load is lower (which relieves grid occupation for the sell-buyback mechanism) and the surplus is higher. In fact, in the most favourable conditions for the network balance, which occur for GPS_target=10% as shown in Figure 107, , there is a net gain from the exploitation of the network in this period (obviously excluding the costs related to the sell-buyback mechanism).

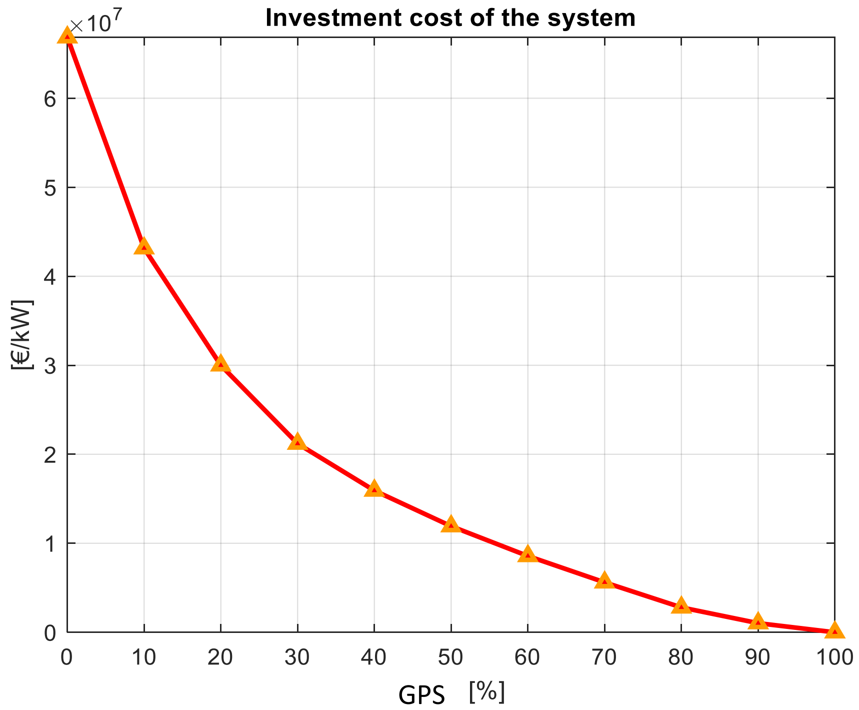

Figure 104 Pareto curve of the investment cost of the whole plant referred to the simulations carried out on the time domain of the real year 2015

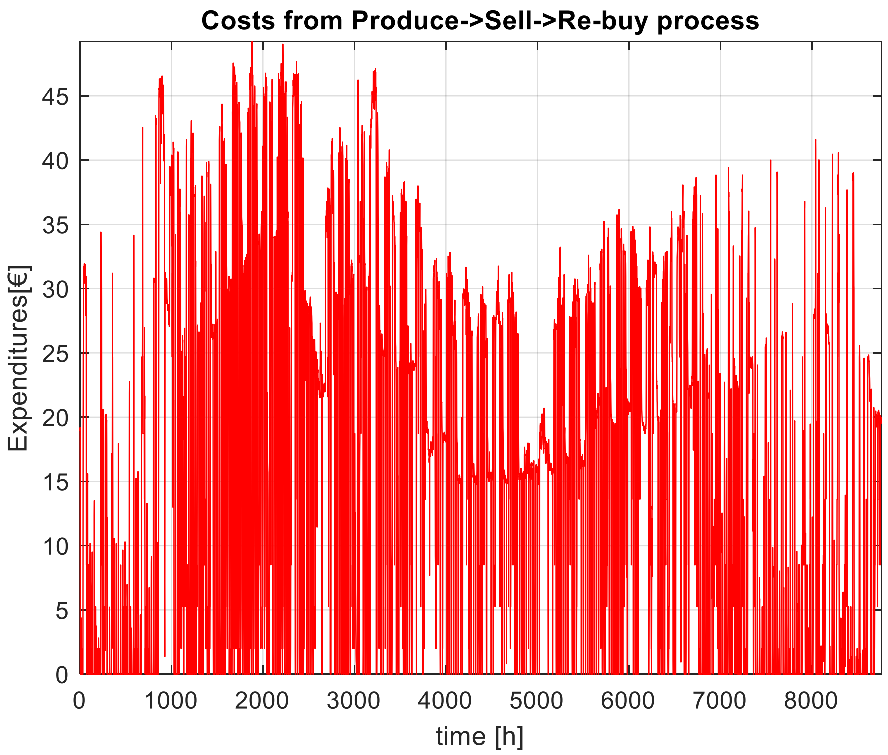

Figure 105 Time series, annual ostium arising from the presence of the network and in particular associated with the sell-buyback mechanism. Reference simulation: SIM_RES2015_LP_GPS50

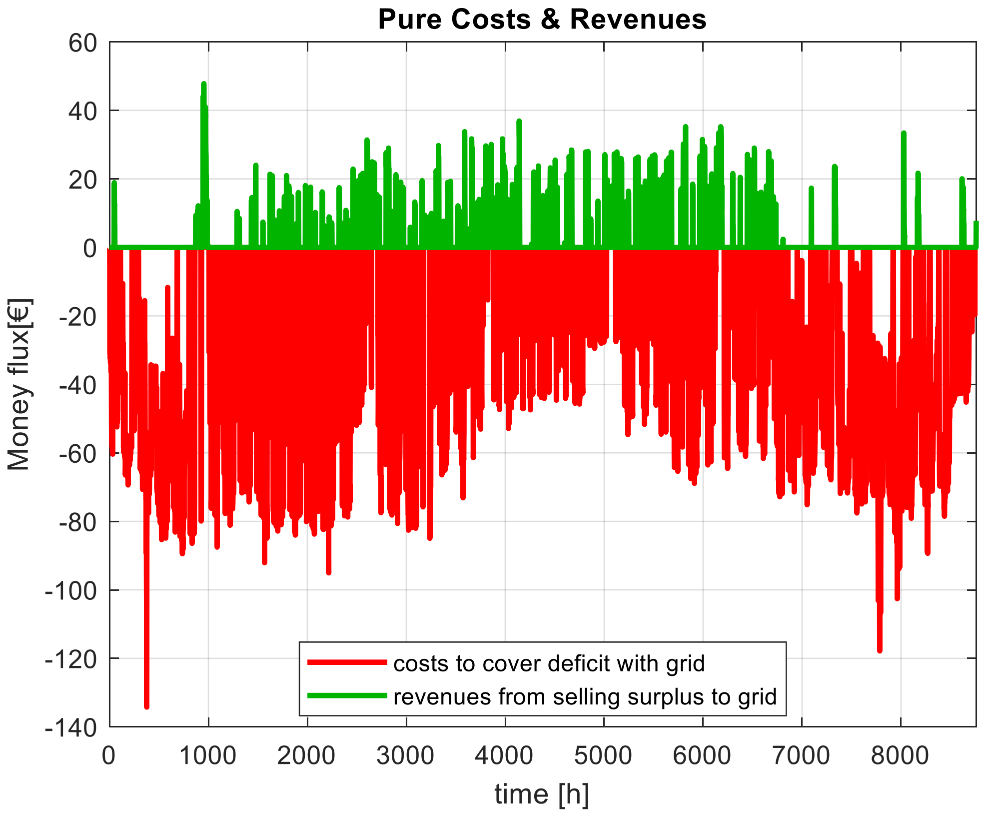

Figure 106 Annual series on an hourly basis of the revenues and costs of selling excess non-storageable energy to the grid and buying energy to help cover the load in the case of a deficit. Reference simulation: SIM_RES2015_LP_GPS50

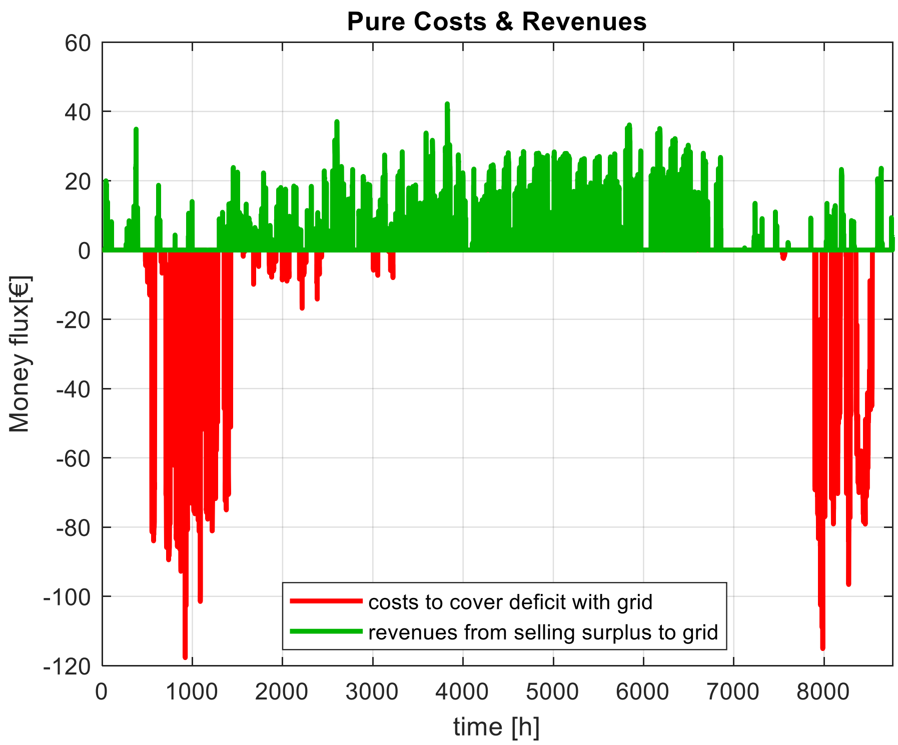

Figure 107 Annual series on an hourly basis of the gains and costs of selling excess non-storageable energy to the grid and buying energy to help cover the load in the case of a deficit. Reference simulation: SIM_RES2015_LP_GPS10

4.2.FUTURE PARTIAL LOAD SIMULATIONS

This paragraph shows the results of the simulations that actually reproduce the regime in which the system will have to operate, i.e. the regime in which the limitations due to the bottleneck caused by the medium distribution network will be effective in all the simulations.

Precisely because of the presence of this bottleneck, indeed, the network, even if operating at full capacity, will never be able to cover 100% of the load. It follows that the simulations that can be carried out cannot, as in the previous case, cover the entire spectrum of GPS_targets, but only from the one corresponding to the maximum possible use of the network to the one describing the off-grid situation.

The purpose of the first simulation was therefore to establish this upperbound for the GPS_target, which was found to be equal to

GPS_target_max=43,52%

The set of possible simulations therefore differs from that presented in the methods section and is as follows Table 34:

Table 34 Summary table of possible simulations referred to FPL compared to those considered in Table 28

	RES TIMESERIES			
	TMY	**2014**	**2015**	GPS_target
FUTURE LOAD	43,52%	43,52%	43,52%	
	40%	40%	40%	
	30%	30%	30%	
	20%	20%	20%	
	10%	10%	10%	
	0%	0%	0%	
	GPS_target			

The results of these simulations will therefore be illustrated below, taking care to highlight in particular only those which bring an element of novelty and/or discontinuity with respect to those obtained from the simulations with the load present which were presented in the previous paragraph.

Figure 108 shows the LCOE trends as a function of the desired GPS_target. One can immediately see the difference between the curves and those resulting with the PPL. However, this difference is only apparent since can be recognised in the constant condition reported by these curves the condition related to GPS_target=0% presented for the present partial load. Indeed, referring to Figure 109 we see that the actual GPS is always GPS=0%. This is because the minimum load is so large compared to that of the network capacity that the network is always totally occupied by the sell-buyback mechanism thus no longer being available for other types of buying and selling with the system.

It follows that the analysis of these cases always corresponds to an analysis of an off-grid configuration that brings with it the disadvantage of being constrained to sell and buy back the produced energy to the grid and therefore to have a net cost attributable to the grid (as shown in Figure 108, Figure 110, Figure 119) that could be avoided by being totally disconnected.

This last effect can be seen very clearly by analysing the LCOE value at GPS_target=0% which is always lower than the value of the previous simulations. In that case, in fact, since the system is supposed to be completely independent from the network and not connected to it in any particular way, all the network costs are saved, which weighed 1% in the composition of the LCOE (as shown in Figure 119).

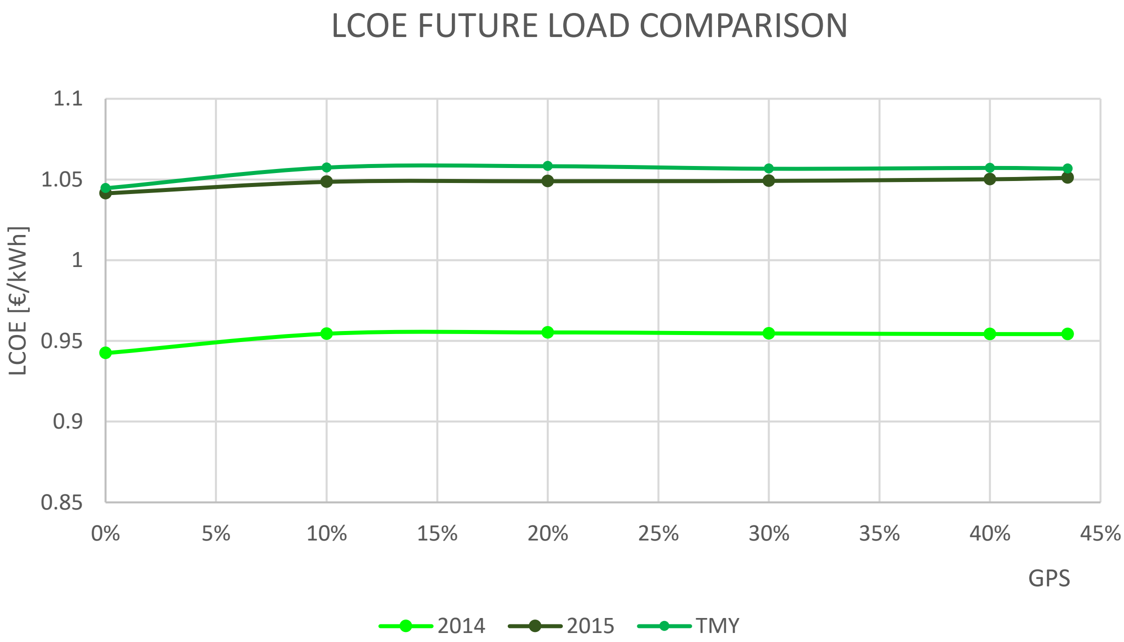

Figure 108 Comparison of LCOE pareto curves defined in relation to PPL for the 3 time domains

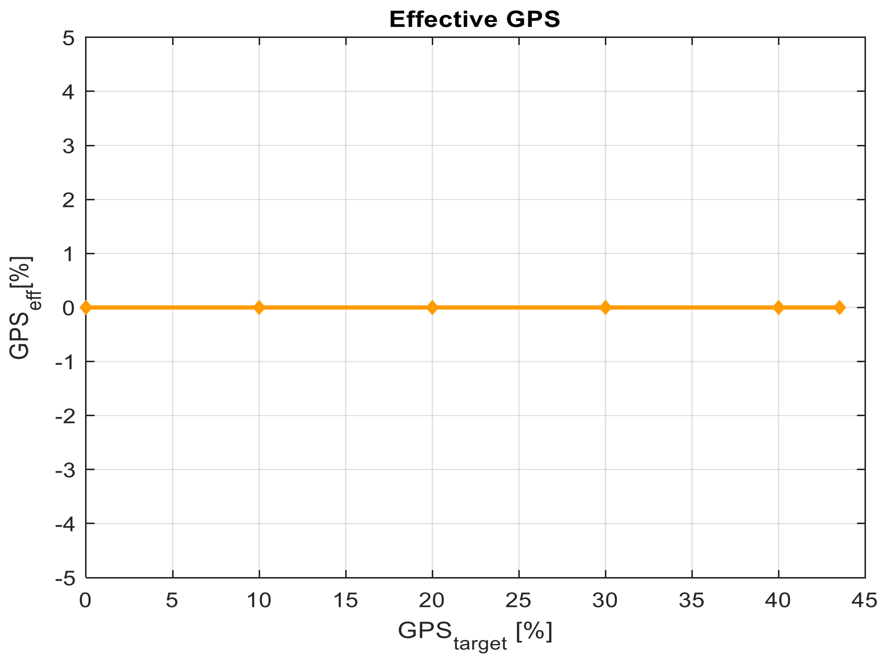

Figure 109 GPS curve actually satisfied in simulations with different GPS_target assumed.

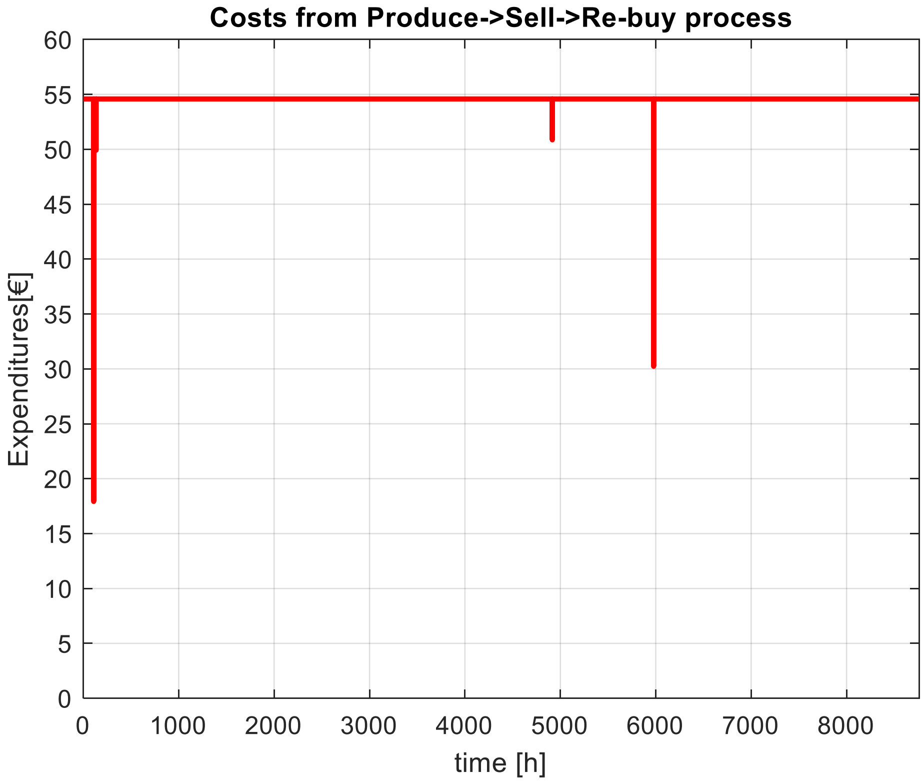

Figure 110 Hourly, annual costs arising from the presence of the network and in particular associated with the sell-buyback mechanism. Reference simulation: SIM_RESTMY_LF_GPS30

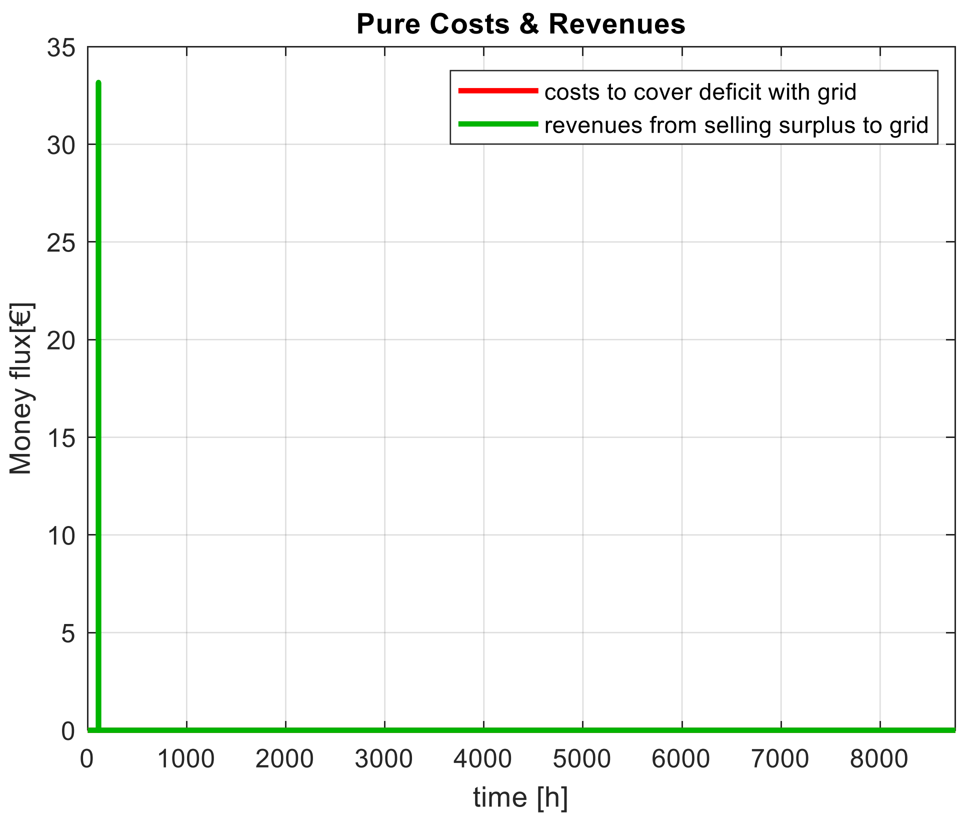

Figure 111 Annual series on an hourly basis of the revenues and costs resulting from the sale of excess non-storageable energy to the grid and the purchase of energy to help cover the load in the event of a deficit. Reference simulation: SIM_RESTMY_LF_GPS30

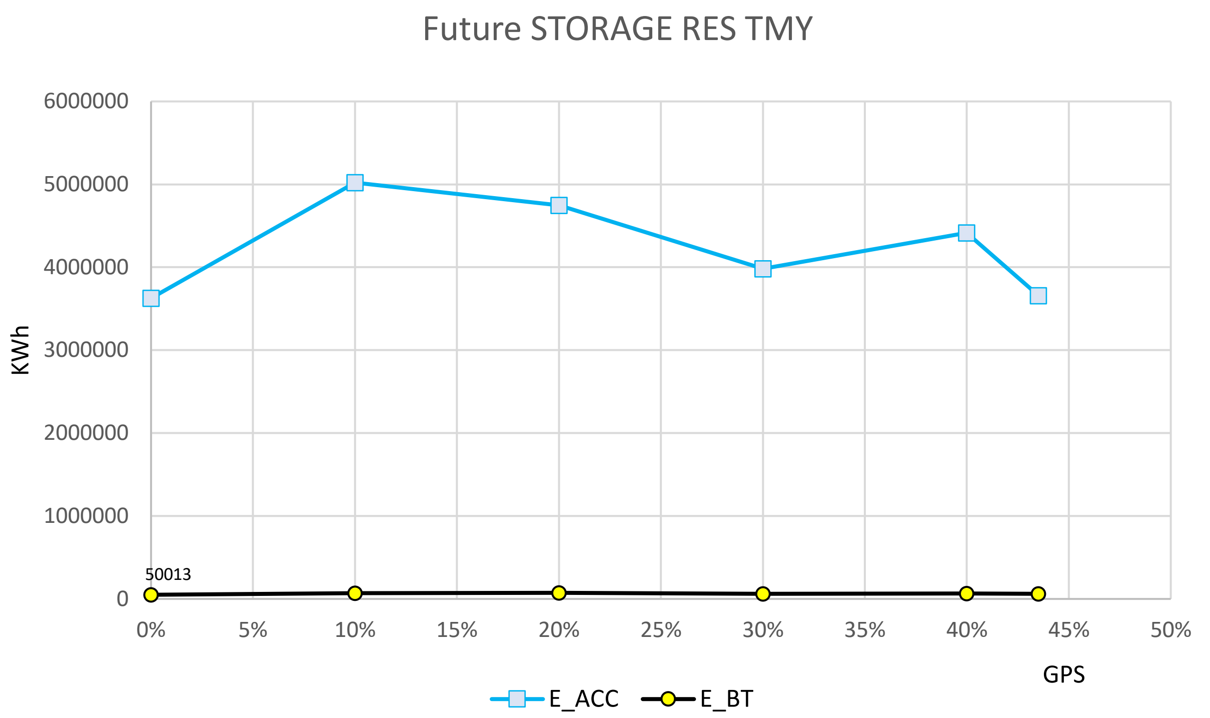

Figure 112 Pareto curve of the sizing of the different types of storages as a function of GPS_target for the time domain consisting of TMY.

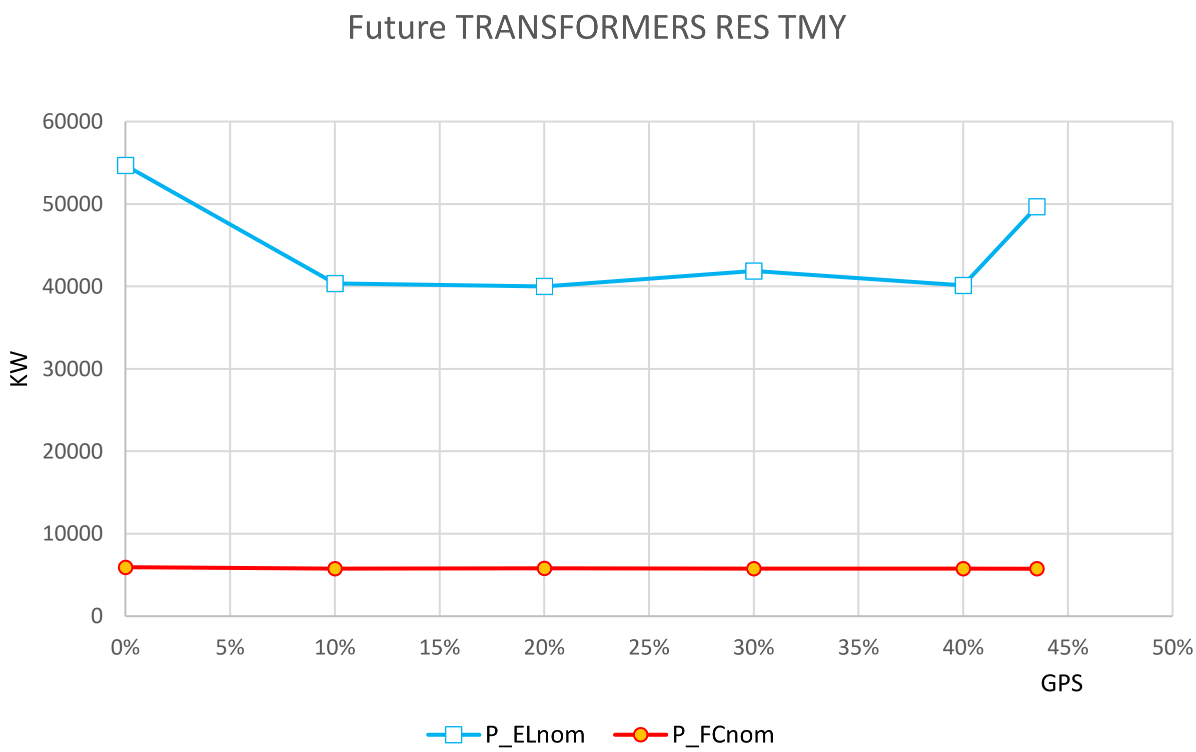

Figure 113 Curva di pareto del dimensionamento delle diverse tipologie di tecnologie per la trasformazione durante i processi di P2G (PEMEL) E G2P (PEMFC) in funzione del GPS_target per il dominio temporale composto dall'anno TMY.

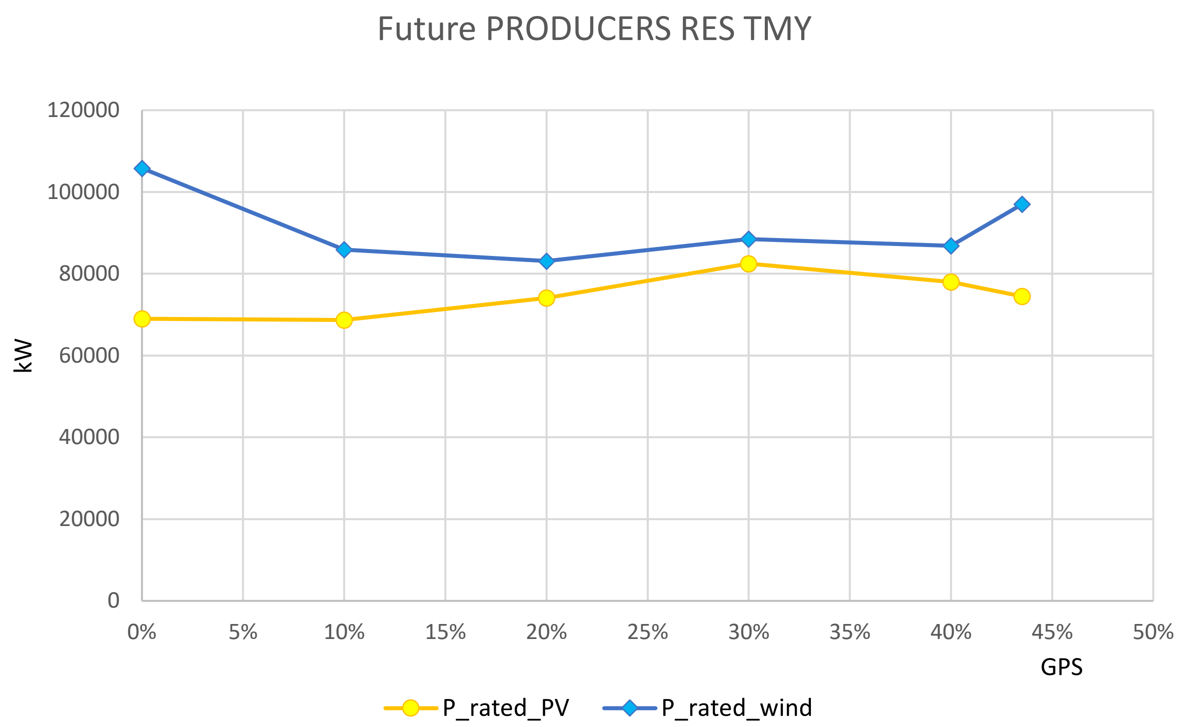

Figure 114 Pareto curve of the sizing of the different types of technologies for production as a function of GPS_target for the time domain consisting of the year TMY.

The graphs Figure 112, Figure 113, Figure 114 showing the sizing of the different technologies confirm the relationships identified for the off-grid situation analysed for the present load with the only difference in the size orders that are adapted to the size of the load to be satisfied.

This confirms the fundamental role played by hydrogen storage in the management of surpluses. As can be seen from Figure 115 , the optimal solutions identified always include the hybrid storage configuration in order to operate a reliable management as described in the previous paragraph.

La Figure 116 gives us further confirmation of this since it can be seen that, given the larger size of the system compared to the previous case, the storage is used to the maximum of its possibility for a long period of the year, solidifying its definition as seasonal storage.

On this point, however, it should be noted that the optimal solution is not able to store all the surplus energy produced. Indeed, especially in the summer period, remains a considerable amount of surplus which, as the system is designed, would be wasted. It would therefore be advisable to better investigate the possibilities of managing the energy produced, either by taking a two-year period as a reference time or by supposing some parallel use for the surplus now curtailed. This second option could be studied by also taking into account the waste energy produced by PEMFC activity, which contrary to that defined above is concentrated in the coldest and darkest periods of the year (see Figure 117, Figure 118)

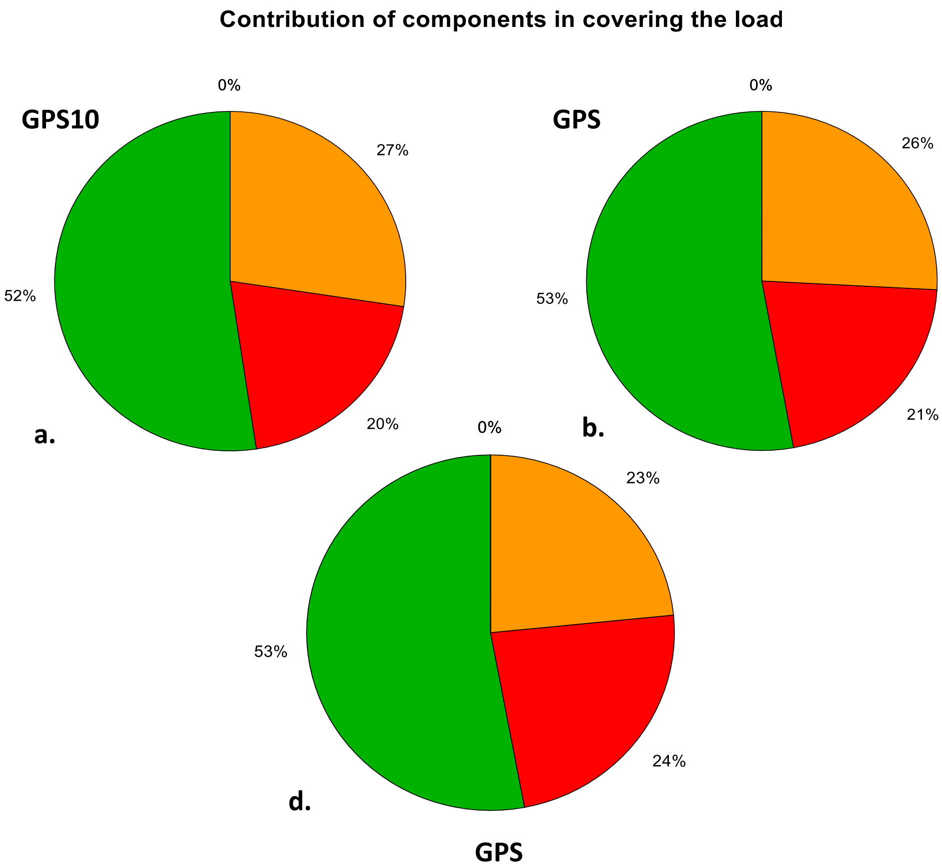

Figure 115 Pie charts showing in relation to 3 different GPS_target values the annual shares by each component to load coverage. The graphs refer to the following simulations respectively: a. SIM_RESTMY_LF_GPS100; b. SIM_RESTMY_LF_GPS50; c. SIM_RESTMY_LF_GPS0;

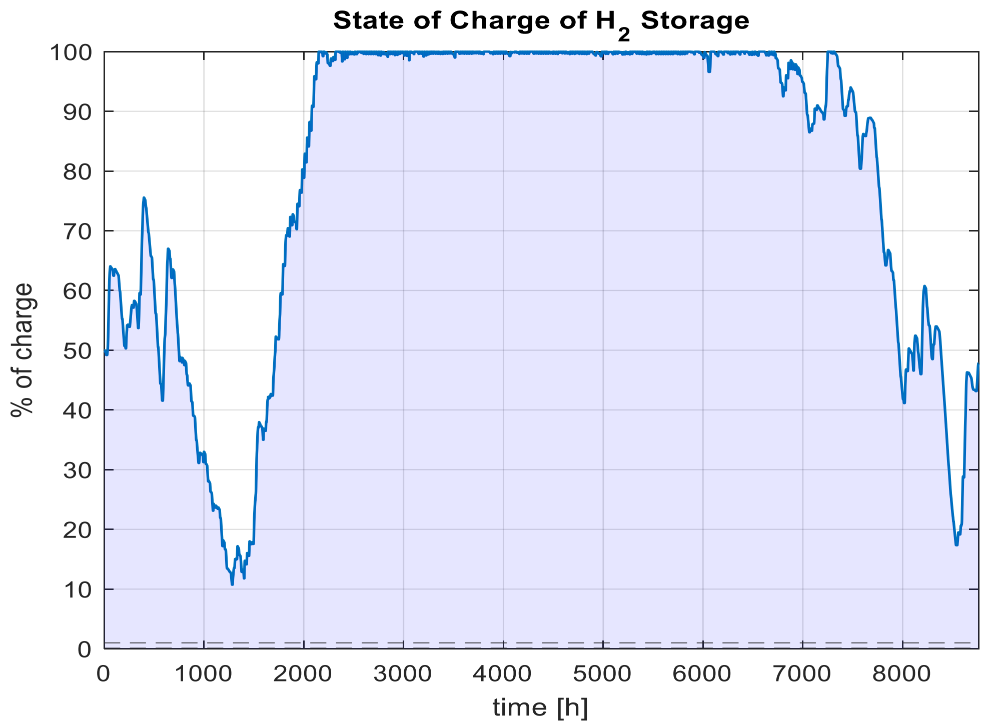

Figure 116 Comportamento annuale dello stato di carica del serbatoio di H2 (SOCH). La linea tratteggiata indica il minimo livello di carica (SOC_h2_min) al di sotto del quale il serbatoio non può essere scaricato. Simulazione di riferimento: SIM_RESTMY_LP_GPS0

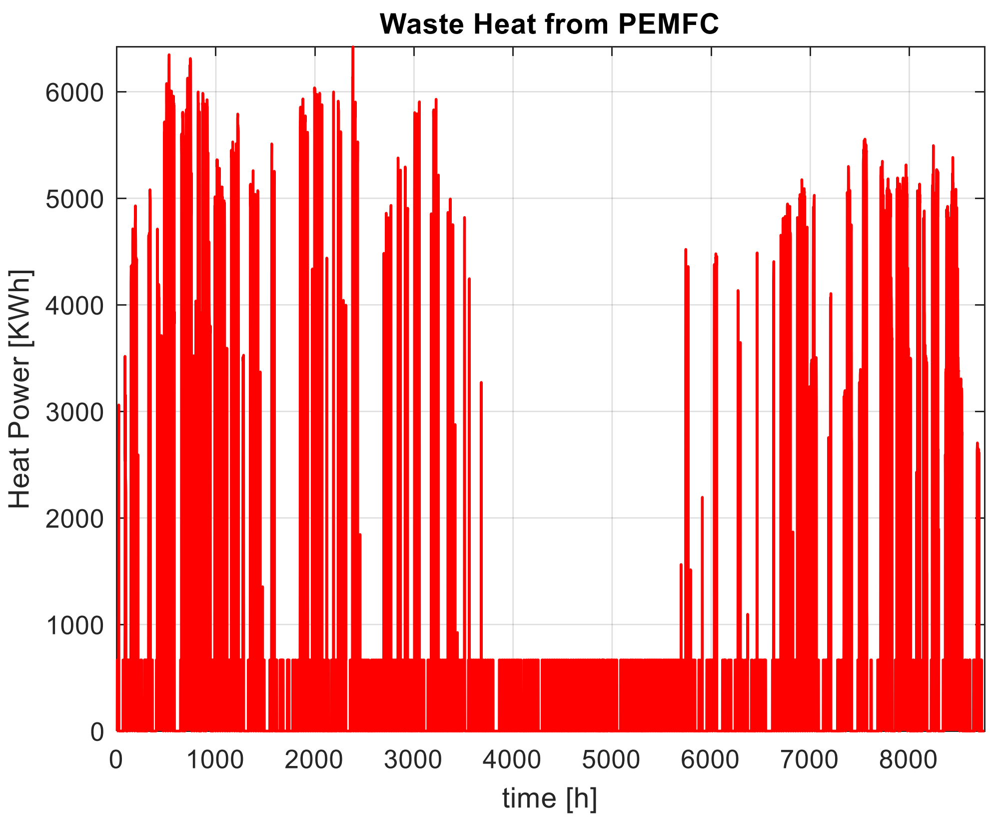

Figure 117 Annual behaviour of the H2 tank state of charge (SOCH). The dotted line indicates the minimum charge level (SOC_h2_min) below which the reservoir cannot be discharged. Reference simulation: SIM_RESTMY_LP_GPS0.

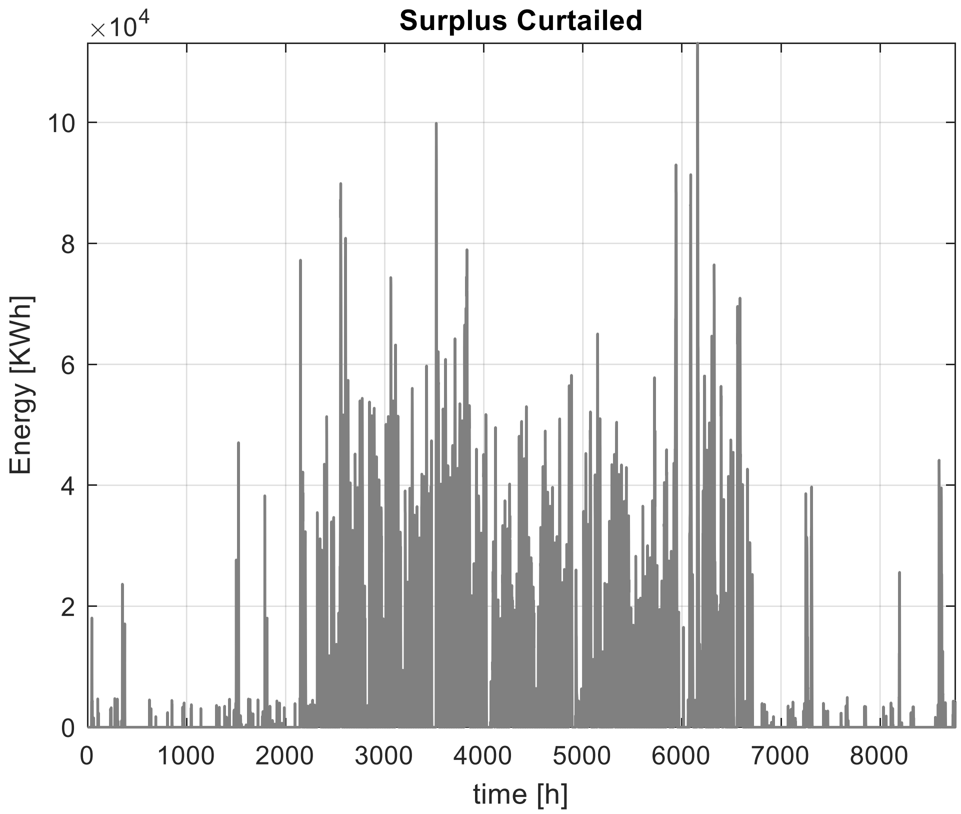

Figure 118 Hourly, annual series of curtailed surplus energy due to lack of grid and storage availability. Reference series: SIM_RESTMY_LF_GPS0.

The shares of the contribution made to the composition of the LCOE of the different components is quite similar to that of the off-grid case of the PPL case. Apart from the different fluctuations between storage and wind power, which represent 2 possible minimum configurations, in fact, no huge variations are observed between the case with and without grid intervention, which is present with 1% at GPS_target 43.52% only because of the costraint to sell and buy back before using the energy produced.

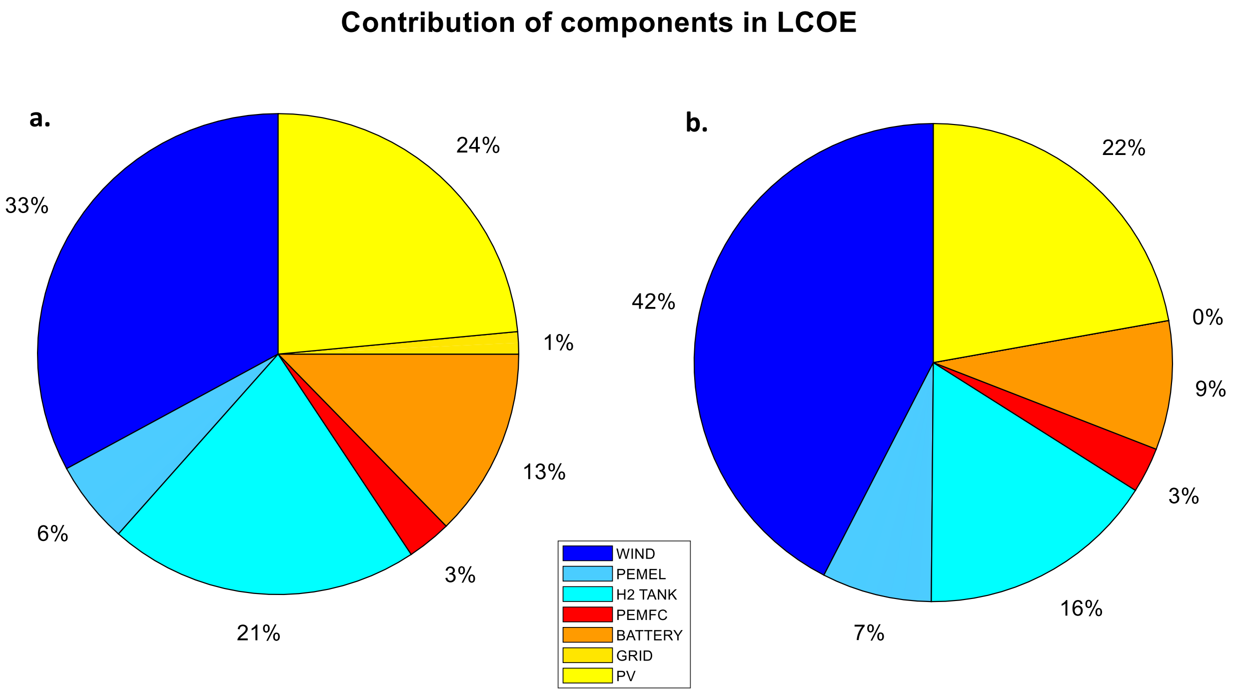

Figure 119 Pie charts showing in relation to 3 different GPS_target values the percentage contributions made by the costs associated with each component in the composition of the LCOE. The graphs refer to the following simulations respectively: a. SIM_RESTMY_LP_GPS20; b. SIM_RESTMY_LP_GPS0;

It should be considered that the economic actor involved in this case is the one defined in the methods section. If the system were to be released from load, the grid would not be a disadvantage, as the system alone would always be in a position to sell energy to the grid. This would lead to a limitation of expenditure, although not by any really significant amount due to the large gap between the maximum grid capacity and the amount of surplus available.

Finally, Figure 120 e Figure 121 give evidence of enormous annual quantity of CO_2 emissions saved in the case of GPS_target=0% both for a European country against Norway but also in the case of service for future load rather than current load. Indeed FPL emissions are an upperbound of those related to PPL.

Table 35 Riassunto dei valori di emissione risparmiati con riferimento ai diversi tipi di inquinanti, ai diversi periodi di carico e alle diverse coordinate geografiche indentificate

	PPL						FPL					
	UE country			Norway			UE country			Nor		
	2014	2015	TMY	2014	2015	TMY	2014	2015	TMY	2014	2015	TMY
CO2	303.29			11.31			1213.177			45.23		
CH4	0.015			89e-5			0.061			0.0036		
N2O	13.06			0.108			52.25			0.436		

In Table 35 values are given not only for CO_2 emissions but also for the other two pollutants listed by the IPCC.

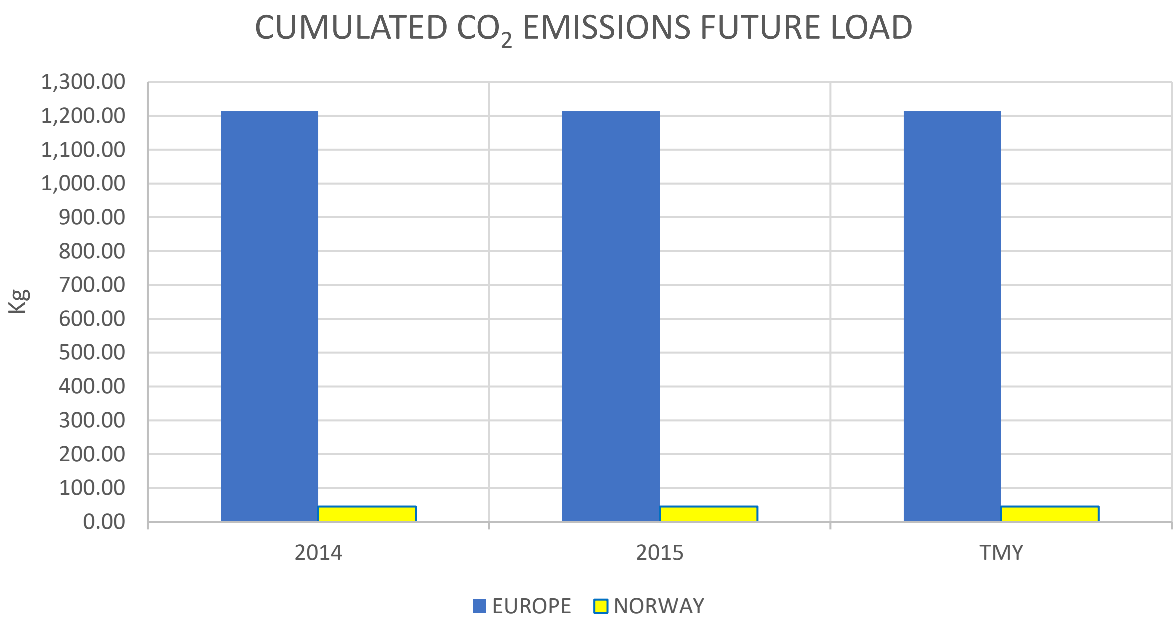

Figure 120 Comparison of the emissions saved in an average European country and in Norway by the installation of the system under study in relation to FPL

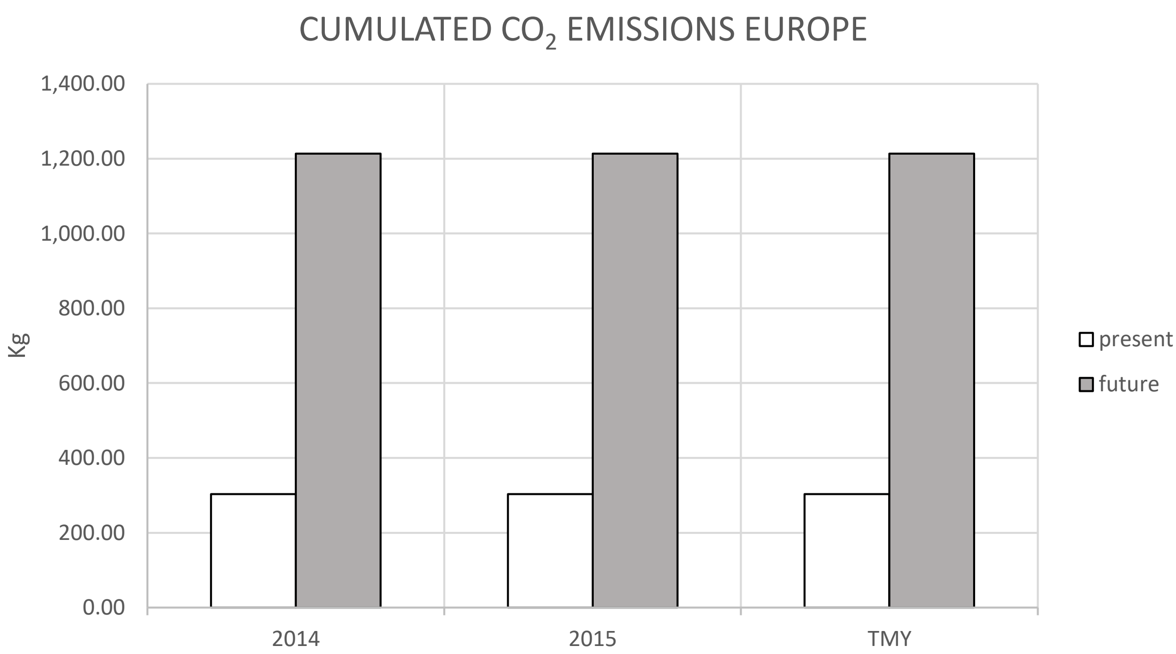

Figure 121 Comparison of the emissions saved in an average European country by the installation of the system under study referred to FPL and PPL

5. CONCLUSIONS

The conclusions related to the study and to the objectives that were set at the beginning of this work are presented below.

The main result that emerges very significantly from the simulations is that the hybrid storage system is much more favourable than one based solely on Li-ion batteries. This is due to 3 main reasons:

- *Storage differentiation related to the characteristics of the storage itself.* In fact, as we have seen, storage based on H_2 production allows the energy produced to be stored and released on a seasonal basis, while the battery has characteristics that allow it to meet a demand for storage or to satisfy part of the DEFICIT in a very rapid and flexible manner. The presence of a seasonal storage type within a system based on RES production is essential to fully exploit the energy produced during the year. Hydrogen storage also has the advantage, compared to other types of seasonal storage, of being much faster in charge and discharge, allowing it to act in synergy with the battery.

- *Aumento del grado di affidabilità.* Increased reliability. The flexibility of the set of components that make up the hydrogen storage complex makes it possible not only to support the battery but even to replace it, delegating to the PEMFC the coverage response in the event of major system oversizing or unforeseen events that do not allow the battery to operate. At the same time, the battery is a reliable and flexible element that can operate autonomously in emergencies, allowing the operator to carry out the appropriate maintenance on the hydrogen system.

- *Reduction of investment cost related to the storage section:* indeed, for high requirements of storage capacity the hydrogen production-based storage guarantees a saving related to the avoided installation of very high capacity battery. This is because, apart for very small sizing, the weight of costs of investment for transformation technologies becomes negligible with respect to that for the tank which is much cheaper of a battery. The reason is that, while PEMEL and PEMC are related only to the entity of the hourly power stocked and changes size principally on the base of the load to be covered, tank is more related to the quantity of surplus available which requires high capacity to be stored. For battery, these 2 tasks that are related to different technologies in H2 storage, are instead co-existent constituting by this way a constraint for the sizing.

The advantage of hydrogen storage emerges above all in cases of low or almost zero dependence on the grid and in cases involving larger order sizes than those required at present.

In addition, despite the large gap between the present and future load size, no substantial energy price increases are evident due to the larger size of the system. It is also remarkable that for solutions involving equal sizing of PEMFC and PEMEC, the shares of LCOE composition linked to storage is practically the same for both H2-Battery hybrid solutions and solutions involving the installation of hydrogen storage only (which confirms what said above considering the medium low size of the plant).

It is also clear that there is an economic advantage in integrating the DEMO system with a pre-existing grid, which makes it possible to reduce the size of the hybrid system so that it can cover the periods of greatest availability of renewable resources. This advantage could also be extended to the case of future load if the sell-buyback mechanism, which causes occupation of the grid that cannot be used for net sales purposes, were to be eliminated.

However, it must be noted that the immaturity of some technologies, especially those related to the hydrogen storage system (PEMEC and PEMFC), as well as the high investments related to the size of the system's production sector, do not allow the generation of LCOE that are competitive on the market compared to those offered by an already built network.

Any considerations regarding the comparison with the alternative solution of expanding the medium distribution network responsible for the bottleneck (already present in the area) are referred to the company Tronder Eenrgi, which for confidentiality reasons could not provide the economic entity of this option.

It would be very important, however, to follow up this preliminary study with a series of studies (which is already happening in part) cocerning modifications of the present one or specifications of it and addressing the following issues:

- Management of waste energy produced by the use of PEMFC and the curtailing of surpluses that cannot be stored or sold to the grid

- Revision of the definition of economic actors in order to decouple load from the production and storage system

- More accurate description and modelling of the network system with the introduction of a local network smaller than the medium-sized distribution network but larger than the one used for internal management of the production and storage system.

- Elimination of the sell-buyback system

- Purchase of the small local distribution network by the system operator in order to avoid costs related to connection fees and/or network use.

- Investigation of the effect of global warming on climate and weather events related to the installation site in order to predict possible changes in the system's producibility. In fact, even if this study shows an increase in the price of energy, certainly attributable to the trend of meteorological phenomena in 2015 compared to 2014, there is no certainty or possibility of demonstrating a relationship between this and global variations in the local climate.

Ultimately, the results on the saving of pollutant and climate-altering emissions make the solution explored in this study of enormous interest for countries with a high density of small population centres in the European area. These are still heavily dependent on both the (sometimes insufficient) national grid and the carbon-rich energy mix for power generation. This is to be added to the fact that the system enters in the type of technologies to which the first step of the European Hydrogen Strategy makes reference to.

BIBLIOGRAPHY

[1] “TA-9-2021-0241_IT”.

[2] “Eolico: mercati, aspetti finanziari, economics.”

[3] “ds_rec_twinpeak_2_mono_series_en”.

[4] “rec_twinpeak_technology_factsheet_en”.

[5] P. Marocco *et al.*, “A study of the techno-economic feasibility of H2-based energy storage systems in remote areas,” *Energy Conversion and Management*, vol. 211, May 2020, doi: 10.1016/j.enconman.2020.112768.

[6] “gen specification v27”.

[7] E. Vartiainen, G. Masson, C. Breyer, D. Moser, and E. Román Medina, “Impact of weighted average cost of capital, capital expenditure, and other parameters on future utility-scale PV levelised cost of electricity,” *Progress in Photovoltaics: Research and Applications*, vol. 28, no. 6, pp. 439–453, Jun. 2020, doi: 10.1002/pip.3189.

[8] Y. T. W. Saputra and I. Garniwa, “Techno-economy study of battery energy storage system for electricity grid peak generation,” in *IOP Conference Series: Earth and Environmental Science*, Apr. 2021, vol. 716, no. 1. doi: 10.1088/1755-1315/716/1/012070.

[9] K. Mongird *et al.*, “Energy Storage Technology and Cost Characterization Report,” 2019.

[10] W. Cole and A. W. Frazier, “Cost Projections for Utility-Scale Battery Storage,” 2030. [Online]. Available: www.nrel.gov/publications.

[11] Tsiropoulos I, Tarvydas D, and Lebedeva N, “Li-ion batteries for mobility and stationary storage applications Scenarios for costs and market growth,” 2018. doi: 10.2760/87175.

[12] A. L. G. Lemence and M. A. M. Tamayao, “Techno-Economic Potential of Hybrid Renewable Energy Systems for Rural Health Units in the Philippines,” *World Medical and Health Policy*, vol. 13, no. 1, pp. 97–125, Mar. 2021, doi: 10.1002/wmh3.388.

[13] M. Alam, K. Kumar, and V. Dutta, “Analysis of solar photovoltaic-battery system for off-grid DC load application,” *International Transactions on Electrical Energy Systems*, vol. 31, no. 1, Jan. 2021, doi: 10.1002/2050-7038.12707.

[14] B. A. Franco, P. Baptista, R. C. Neto, and S. Ganilha, “Assessment of offloading pathways for wind-powered offshore hydrogen production: Energy and economic analysis,” *Applied Energy*, vol. 286, Mar. 2021, doi: 10.1016/j.apenergy.2021.116553.

[15] A. Christensen and A. Co, “Assessment of Hydrogen Production Costs from Electrolysis: United States and Europe.”

[16] J. Hinkley, J. Hayward, R. Mcnaughton, R. Gillespie, M. Watt, and K. Lovegrove, “Cost assessment of hydrogen production from PV and electrolysis Ayako Matsumoto (Mitsui Global Strategic Studies Institute),” 2016.

[17] T. International Renewable Energy Agency, *GREEN HYDROGEN COST REDUCTION SCALING UP ELECTROLYSERS TO MEET THE 1.5°C CLIMATE GOAL H 2 O 2*. 2020. [Online]. Available: www.irena.org/publications

[18] H. Böhm, A. Zauner, D. C. Rosenfeld, and R. Tichler, “Projecting cost development for future large-scale power-to-gas implementations by scaling effects,” *Applied Energy*, vol. 264, Apr. 2020, doi: 10.1016/j.apenergy.2020.114780.

[19] E. Taibi, R. Miranda, W. Vanhoudt, T. Winkel, J.-C. Lanoix, and F. Barth, *Hydrogen from renewable power: Technology outlook for the energy transition*. 2018. [Online]. Available: www.irena.org

[20] F. Dawood, G. M. Shafiullah, and M. Anda, “Stand-alone microgrid with 100% renewable energy: A case study with hybrid solar pv-battery-hydrogen,” *Sustainability (Switzerland)*, vol. 12, no. 5, Mar. 2020, doi: 10.3390/su12052047.

[21] X. Chen *et al.*, “Multi-criteria assessment and optimization study on 5 kW PEMFC based residential CCHP system,” *Energy Conversion and Management*, vol. 160, pp. 384–395, Mar. 2018, doi: 10.1016/j.enconman.2018.01.050.

[22] P. Nagapurkar and J. D. Smith, “Techno-economic optimization and social costs assessment of microgrid-conventional grid integration using genetic algorithm and Artificial Neural Networks: A case study for two US cities,” *Journal of Cleaner Production*, vol. 229, pp. 552–569, Aug. 2019, doi: 10.1016/j.jclepro.2019.05.005.

[23] S. Nasri, S. ben Slama, I. Yahyaoui, B. Zafar, and A. Cherif, “Autonomous hybrid system and coordinated intelligent management approach in power system operation and control using hydrogen storage,” *International Journal of Hydrogen Energy*, vol. 42, no. 15, pp. 9511–9523, Apr. 2017, doi: 10.1016/j.ijhydene.2017.01.098.

[24] S. A. Amirkhalili and A. R. Zahedi, “Techno-economic Analysis of a Stand-alone Hybrid Wind/Fuel Cell Microgrid System: A Case Study in Kouhin Region in Qazvin,” *Fuel Cells*, vol. 18, no. 4, pp. 551–560, Aug. 2018, doi: 10.1002/fuce.201700149.

[25] Iea, “Technology Roadmap Hydrogen and Fuel Cells.” [Online]. Available: www.iea.org/t&c/

[26] A. Körner, “Technology Roadmap Hydrogen and Fuel Cells Technical Annex.”

[27] A. Mayyas and M. Mann, “Emerging manufacturing technologies for fuel cells and electrolyzers,” in *Procedia Manufacturing*, 2019, vol. 33, pp. 508–515. doi: 10.1016/j.promfg.2019.04.063.

[28] N. Himabindu, R. P. Mandi, and H. Santoshkumar, “Modelling and cost optimization of a community microgrid,” *IOP Conference Series: Materials Science and Engineering*, vol. 1114, no. 1, p. 012061, Mar. 2021, doi: 10.1088/1757-899x/1114/1/012061.

[29] F. Dawood, G. M. Shafiullah, and M. Anda, “Stand-alone microgrid with 100% renewable energy: A case study with hybrid solar pv-battery-hydrogen,” *Sustainability (Switzerland)*, vol. 12, no. 5, Mar. 2020, doi: 10.3390/su12052047.

[30] H. Sharma and S. Mishra, “Techno-economic analysis of solar grid-based virtual power plant in Indian power sector: A case study,” *International Transactions on Electrical Energy Systems*, vol. 30, no. 1, Jan. 2020, doi: 10.1002/2050-7038.12177.

[31] T. Sarkar, A. Bhattacharjee, H. Samanta, K. Bhattacharya, and H. Saha, “Optimal design and implementation of solar PV-wind-biogas-VRFB storage integrated smart hybrid microgrid for

ensuring zero loss of power supply probability,” *Energy Conversion and Management*, vol. 191, pp. 102–118, Jul. 2019, doi: 10.1016/j.enconman.2019.04.025.

[32] M. K. Kiptoo, O. B. Adewuyi, M. E. Lotfy, T. Amara, K. V. Konneh, and T. Senjyu, “Assessing the techno-economic benefits of flexible demand resources scheduling for renewable energy–based smart microgrid planning,” *Future Internet*, vol. 11, no. 10, Oct. 2019, doi: 10.3390/FI11100219.

[33] Y. Xiang, H. Cai, J. Liu, and X. Zhang, “Techno-economic design of energy systems for airport electrification: A hydrogen-solar-storage integrated microgrid solution,” *Applied Energy*, vol. 283, Feb. 2021, doi: 10.1016/j.apenergy.2020.116374.

[34] P. Fu, D. Pudjianto, X. Zhang, and G. Strbac, “Integration of hydrogen into multi-energy systems optimisation,” *Energies*, vol. 13, no. 7, 2020, doi: 10.3390/en13071606.

[35] F. A. Alturki and E. M. Awwad, “Sizing and cost minimization of standalone hybrid wt/pv/biomass/pump-hydro storage-based energy systems,” *Energies*, vol. 14, no. 2, Jan. 2021, doi: 10.3390/en14020489.

[36] M. A. Shoeb and G. M. Shafiullah, “Renewable energy integrated islanded microgrid for sustainable irrigation-a Bangladesh perspective,” *Energies*, vol. 11, no. 5, 2018, doi: 10.3390/en11051283.

[37] “PV15_WIND6_S036054421930547X”.

[38] Z. S. Hosseini *et al.*, “Levelized Cost of Energy Calculations for Microgrid-Integrated Solar-Storage Technology,” in *Proceedings of the IEEE Power Engineering Society Transmission and Distribution Conference*, Oct. 2020, vol. 2020-October. doi: 10.1109/TD39804.2020.9300022.

[39] “PV12_S0196890418307003”.

[40] B. Alotri, “Comprehensive cost assessment of present and future energy conversion technologies.”

[41] F. A. Alturki and E. M. Awwad, “Sizing and cost minimization of standalone hybrid wt/pv/biomass/pump-hydro storage-based energy systems,” *Energies*, vol. 14, no. 2, Jan. 2021, doi: 10.3390/en14020489.

[42] B. Alotri, “Comprehensive cost assessment of present and future energy conversion technologies.”

[43] M. K. Kiptoo, O. B. Adewuyi, M. E. Lotfy, T. Amara, K. V. Konneh, and T. Senjyu, “Assessing the techno-economic benefits of flexible demand resources scheduling for renewable energy–based smart microgrid planning,” *Future Internet*, vol. 11, no. 10, Oct. 2019, doi: 10.3390/FI11100219.

[44] C. Dao, B. Kazemtabrizi, and C. Crabtree, “Wind turbine reliability data review and impacts on levelised cost of energy,” *Wind Energy*, vol. 22, no. 12. John Wiley and Sons Ltd, pp. 1848–1871, Dec. 01, 2019. doi: 10.1002/we.2404.

[45] C. Kost, S. Shammugam, V. Jülch, H.-T. Nguyen, and T. Schlegl, “LEVELIZED COST OF ELECTRICITY RENEWABLE ENERGY TECHNOLOGIES,” 2018. [Online]. Available: www.ise.fraunhofer.de

[46] T. Sarkar, A. Bhattacharjee, H. Samanta, K. Bhattacharya, and H. Saha, “Optimal design and implementation of solar PV-wind-biogas-VRFB storage integrated smart hybrid microgrid for ensuring zero loss of power supply probability,” *Energy Conversion and Management*, vol. 191, pp. 102–118, Jul. 2019, doi: 10.1016/j.enconman.2019.04.025.

[47] P. Fu, D. Pudjianto, X. Zhang, and G. Strbac, “Integration of hydrogen into multi-energy systems optimisation,” *Energies*, vol. 13, no. 7, 2020, doi: 10.3390/en13071606.

[48] S. M. Shaahid, L. M. Alhems, and M. K. Rahman, “Techno-economic assessment of establishment of wind farms in different Provinces of Saudi Arabia to mitigate future energy challenges,” *Thermal Science*, vol. 2018, 2019, doi: 10.2298/TSCI171025109S.

[49] “WIND7_S1364032119302515”.

[50] “WIND6_PV15_S036054421930547X”.

[51] Unfccc, “ADOPTION OF THE PARIS AGREEMENT - Paris Agreement text English.”

[52] A. R. Darío Gómez *et al.*, “Chapter 2: Stationary Combustion 2006 IPCC Guidelines for National Greenhouse Gas Inventories 2.1 C H A P T E R 2 STATIONARY COMBUSTION Volume 2: Energy 2.2 2006 IPCC Guidelines for National Greenhouse Gas Inventories Contributing Author.”

[53] J. A. Duffie and W. A. Beckman, *Solar engineering of thermal processes*. Wiley, 2013.

[54] “PEMFC7_S0959652620302729 v”.

[55] “STUDY ON EARLY BUSINESS CASES FOR H2 IN ENERGY STORAGE AND MORE BROADLY POWER TO H2 APPLICATIONS,” 2017.

[56] V. I. Borzenko and D. O. Dunikov, “Feasibility analysis of a hydrogen backup power system for Russian telecom market,” in *Journal of Physics: Conference Series*, Nov. 2017, vol. 891, no. 1. doi: 10.1088/1742-6596/891/1/012077.

APPENDIX A

WIND PRODUCIBILITY CODE

```
ws=xlsread(filename, sheetname, cellsinterval);
P_curve=xlsread(filename, sheetname, cellsinterval);
wsc=P_curve(:,1); %wind speed curve;
P_c=P_curve(:,2); %power curve;
nlws=length(ws);

ii=1;
v_Ps_year_WIND=0.*ws;

for ii=1:nlws

    %% If WS is not in the curve range
    if ws(ii)<wsc(1) || ws(ii)>wsc(end)

        v_Ps_year_WIND(ii)=0;

    %% if we are working at less than max power
    elseif ws(ii)<wsc(15*2+1)

        jj=14*2+1;

        while v_Ps_year_WIND(ii)==0 && jj≥1

            if ws(ii)≥wsc(jj)

                v_Ps_year_WIND(ii)=P_c(jj);

            end

            jj=jj-1;

        end

    %% We are working at max power
    else

        v_Ps_year_WIND(ii)=P_c(15*2+1);

    end

end

save filename
```

APPENDIX B

Here are reported the tables with the main results of the simulation performed:

Table 36 Results from the input meteorological year 2014

GPS TARGET	Grid Share	OPT (2014)							load type
		P_rated_PV [KW]	P_rated_wind [KW]	P_FCnom [KW]	P_ELnom [KW]	E_ACC [KWh]	E_BT [KWh]	LCOE [€/KWh]	
100%	100%	0	0	0	0	0	0	0.0650	PRESENT
100%	100%	0	0	0	0	0	0	0.0650	
90%	90%	1083	0	0	0	0	0	0.0766	
80%	80%	2733	177	0	0	0	0	0.0974	
70%	70%	2991	2404	0	0	0	0	0.1345	
60%	60%	4040	3062	0	0	0	3176	0.1803	
50%	50%	5276	3738	0	0	0	6854	0.2322	
40%	40%	7216	4287	0	0	0	10882	0.2937	
30%	30%	8779	6354	0	0	0	14575	0.3728	
20%	20%	13428	8309	0	0	0	20189	0.5049	
10%	10%	8130	20282	1269	5386	339657	7643	0.6824	
0%	0%	11179	16029	1446	5863	2152924	6955	0.9542	
10%	10%	29330	20153	0	0	0	30000	0.9824	
0%	0%	20574	64638	0	0	0	178589	2.6610	
100%	44%	0	0	0	0	0	0	0.0647	FUTURE
100%	44%	0	0	0	0	0	0	0.0647	
44%	44%	44550	65437	5671	26158	8612343	23499	0.9543	
40%	40%	45312	65351	5653	25711	8600302	22978	0.9543	
30%	30%	47157	63604	5729	23826	8641839	23994	0.9546	
20%	20%	49269	58766	5684	23297	8855793	26611	0.9553	
10%	10%	43360	63018	6000	23095	8637847	32253	0.9545	
0%	0%	52255	56574	5911	23749	8979754	23748	0.9424	

Table 37 Results from the input meteorological year 2015

GPS TARGET	Grid Share	OPT (2015)							load type
		P_rated_PV [KW]	P_rated_wind [KW]	P_FCnom [KW]	P_ELnom [KW]	E_ACC [KWh]	E_BT [KWh]	LCOE [€/KWh]	
100%	100%	0	0	0	0	0	0	0.0650	PRESENT
100%	100%	0	0	0	0	0	0	0.0650	
90%	90%	1179	0	0	0	0	0	0.0779	
80%	80%	2132	613	0	0	0	0	0.0974	
70%	70%	2479	2139	0	0	0	0	0.1239	
60%	60%	3455	3205	0	0	0	1877	0.1652	
50%	50%	4956	3508	0	0	0	5704	0.2156	
40%	40%	6703	3823	0	0	0	10678	0.2777	
30%	30%	9034	5320	0	0	0	15535	0.3655	
20%	20%	11884	9580	0	0	0	22007	0.5175	
10%	10%	10890	13090	1168	5044	874881	10720	0.7146	
0%	0%	11991	19388	1413	7713	2693720	0	1.0823	
10%	10%	17274	17963	0	0	0	45685	0.8980	
0%	0%	90073	30158	0	0	0	130231	2.6646	
100%	44%	0	0	0	0	0	0	0.0647	FUTURE
44%	44%	39999	58467	5668	26426	11090984	37549	1.0510	
40%	40%	47144	52993	5652	19640	11149452	40173	1.0501	
30%	30%	47119	51123	5734	22481	11277559	38312	1.0491	
20%	20%	44781	54997	5664	23605	11174748	35541	1.0489	
10%	10%	41716	52959	5725	22522	11219118	45202	1.0485	
0%	0%	52168	59312	5747	27157	11147256	14390	1.0414	

Table 38 Results from the input meteorological year TMY

GPS TARGET	Grid Share	OPT (TMY)							load type
		P_rated_PV [KW]	P_rated_wind [KW]	P_FCnom [KW]	P_ELnom [KW]	E_ACC [KWh]	E_BT [KWh]	LCOE [€/KWh]	
100%	100%	0	0	0	0	0	0	0.0650	PRESENT
100%	100%	0	0	0	0	0	0	0.0650	
90%	90%	978	0	0	0	0	0	0.0753	
80%	80%	2413	0	0	0	0	0	0.0904	
70%	70%	3089	1479	0	0	0	529	0.1244	
60%	60%	4209	2078	0	0	0	3621	0.1692	
50%	50%	5593	2445	0	0	0	7519	0.2196	
40%	40%	7241	3080	0	0	0	11664	0.2795	
30%	30%	9479	4722	0	0	0	16166	0.3661	
20%	20%	13625	8327	0	0	0	21896	0.5196	
10%	10%	12556	10420	1197	4507	1014142	12077	0.7256	
0%	0%	18634	21203	1436	9735	1282615	15119	1.0625	
10%	10%	23720	12505	0	0	0	43698	0.8798	
0%	0%	15723	32261	0	0	0	228418	2.4163	
100%	44%	0	0	0	0	0	0	0.0647	FUTURE
100%	44%	0	0	0	0	0	0	0.0647	
44%	44%	74445	97000	5755	49662	3656768	61334	1.0566	
40%	40%	78015	86835	5780	40118	4413778	65800	1.0572	
30%	30%	82486	88492	5774	41884	3982254	63231	1.0566	
20%	20%	74058	83118	5816	40000	4748355	73682	1.0582	
10%	10%	68701	85890	5784	40359	5020667	69583	1.0574	
0%	0%	68972	105813	5945	54689	3627153	50013	1.0446	